

Key Technologies on New Energy Vehicles

Shichun Yang

Xinhua Liu

Shen Li

Cheng Zhang

---

# Advanced Battery Management System for Electric Vehicles



华中科技大学出版社  
<http://www.hustp.com>



Springer

# **Key Technologies on New Energy Vehicles**

Key Technologies on New Energy Vehicles publishes the latest developments in new energy vehicles - quickly, informally and with high quality. The intent is to cover all the main branches of new energy vehicles, both theoretical and applied, including but not limited:

- Control Technology of Driving System
- Hybrid Electric Vehicle Coupling Technology
- Cross Disciplinary design optimization technology
- Single and Group Battery Technology
- Energy Management Technology
- Lightweight Technology
- New Energy Materials and Device
- Internet of Things (IoT)
- Cloud Computing
- 3D Printing
- Virtual Reality Technologies

Within the scopes of the series are monographs, professional books or graduate textbooks, edited volumes, and reference works purposely devoted to support education in related areas at the graduate and post-graduate levels.

To submit a proposal or request further information, please contact:

Dr. Mengchu Huang, Senior Editor, Applied Sciences

Email: [mengchu.huang@springer.com](mailto:mengchu.huang@springer.com)

Tel: +86-21-2422 5094

Shichun Yang · Xinhua Liu · Shen Li ·  
Cheng Zhang

# Advanced Battery Management System for Electric Vehicles

Shichun Yang  
School of Transportation Science  
and Engineering  
Beihang University  
Beijing, China

Shen Li  
Department of Mechanical Engineering  
Imperial College London  
London, UK

Xinhua Liu  
School of Transportation Science  
and Engineering  
Beihang University  
Beijing, China

Cheng Zhang  
Institute for Clean Growth and Future  
Mobility  
Coventry University  
Coventry, UK

ISSN 2662-2920

ISSN 2662-2939 (electronic)

Key Technologies on New Energy Vehicles

ISBN 978-981-19-3489-6

ISBN 978-981-19-3490-2 (eBook)

<https://doi.org/10.1007/978-981-19-3490-2>

Jointly published with Huazhong University of Science and Technology Press

The print edition is not for sale in China (Mainland). Customers from China (Mainland) please order the print book from: Huazhong University of Science and Technology Press.

© Huazhong University of Science and Technology Press 2023

This work is subject to copyright. All rights are reserved by the Publishers, whether the whole or part of the material is concerned, specifically the rights of reprinting, reuse of illustrations, recitation, broadcasting, reproduction on microfilms or in any other physical way, and transmission or information storage and retrieval, electronic adaptation, computer software, or by similar or dissimilar methodology now known or hereafter developed.

The use of general descriptive names, registered names, trademarks, service marks, etc. in this publication does not imply, even in the absence of a specific statement, that such names are exempt from the relevant protective laws and regulations and therefore free for general use.

The publishers, the authors, and the editors are safe to assume that the advice and information in this book are believed to be true and accurate at the date of publication. Neither the publishers nor the authors or the editors give a warranty, expressed or implied, with respect to the material contained herein or for any errors or omissions that may have been made. The publishers remain neutral with regard to jurisdictional claims in published maps and institutional affiliations.

This Springer imprint is published by the registered company Springer Nature Singapore Pte Ltd.  
The registered company address is: 152 Beach Road, #21-01/04 Gateway East, Singapore 189721,  
Singapore

# **Committee of Reviewing Editors**

## **Chairman of the Board**

Ouyang Minggao (Tsinghua University)

## **Vice Chairman of the Board**

Wang Junmin (University of Texas at Austin)

## **Members**

Ma Fangwu (Jilin University)

Wang Jianqiang (Tsinghua University)

Ai Xinping (Wuhan University)

Li Keqiang (Tsinghua University)

Yu Zhuoping (Tongji University)

Chen Yong (Hebei University of Technology)

Yin Chengliang (Shanghai Jiao Tong University)

Wang Feiyue (Institute of Automation, Chinese Academy of Sciences)

Deng Weiwen (Beijing University of Aeronautics and Astronautics)

Hua Lin (Wuhan University of Technology)

Wu Chaozhong (Wuhan University of Technology)

Chen Hong (Jilin University)

Yin Guodong (Southeast University)

Huang Yunhui (Huazhong University of Science and Technology)

# **Foreword: New Energy Vehicles and New Energy Revolution**

The past two decades have witnessed the research and development (R&D) and the industrialization of China's new energy vehicles. Reviewing the development of new energy vehicles in China, we can find that the "Tenth Five-Year Plan" is the period when China's new energy vehicles began to develop and our nation started to conduct organized R&D of the electric vehicle technology on a large scale; the "Eleventh Five-Year Plan" is the period when China's new energy vehicles shifted from basic development to demonstration and examination as the Ministry of Science and Technology carried out the key project themed at "energy saving and new energy vehicles"; the period of the "Twelfth Five-Year Plan" is the duration when China's new energy vehicles transitioned from demonstration and examination to the launch of industrialization as the Ministry of Science and Technology organized the key project of "electric vehicles"; the period of the "Thirteenth Five-Year Plan" is the stage when China's new energy vehicle industry realized the rapid development and upgrading as the Ministry of Science and Development introduced the layout of the key technological project concerning "new energy vehicles".

The decade between 2009 and 2018 witnessed the development of China's new energy automobile industry starting from scratch. The annual output of new energy vehicles developed from zero to 1.27 million, while the holding volume increased from zero to 2.61 million, each of which occupied over 53% in the global market and ranked 1st worldwide; the energy density of lithium-ion power batteries had more than doubled and the cost reduced by over 80%. In 2018, 6 Chinese battery companies were among the top 10 global battery businesses, with the first and the third as China's CATL and BYD. In the meanwhile, a number of multinational automobile businesses shifted to develop new energy vehicles. This was the first time for China to succeed in developing high-technology bulk commodities for civic use on a large scale in the world, also leading the trend of the global automobile development. The year of 2020 marked the landmark in the evolution of new energy automobile. Besides, this year was the first year when new energy vehicles entered families on a large scale and the watershed where new energy vehicles shifted from policy-driven to market-driven development. This year also saw the successful wrapping up of the mission in the *Development Plan on Energy Saving and New Energy Vehicle Industry (2012–2020)*

and the official release of *Development Plan on New Energy Vehicle Industry (2021–2035)*. At the end of 2020, in particular, president Xi Jinping proposed that China strove to achieve the goal typified by peak carbon dioxide emissions by 2030 and carbon neutral by 2060, so as to inject great power into the sustainable development of new energy vehicles.

Looking back to the past and looking forward to the future, we can see even more clearly the historical position of the current development of new energy vehicles in the energy and industrial revolution. As is known to us all, each and every energy revolution started from the invention of power installations and transportation vehicles. On the other hand, the progress of power installations and transportation vehicles contributed to the development and exploitation of energy and led to industrial revolution. In the first energy revolution, steam engine was used as the power installation, with coal and train as energy and transportation respectively. As for the second energy revolution, internal combustion engine was taken as the power installation, oil and natural gas as energy, gasoline and diesel as energy carrier, and automobile as the transportation vehicle. At the current stage of the third energy revolution, all kinds of batteries are power installation, the renewable energy as the subject of energy and electricity and hydrogen as energy carrier, and electric vehicles as the means of transportation. In fact, the first energy revolution enabled the UK to outperform Netherlands while the second energy revolution made the USA overtook the UK, both in terms of the economic strength. The present energy revolution may be the opportunity for China to catch up with and surpass other nations. How about the fourth industrial revolution? In my opinion, it is the green revolution based on renewable energy and also the smart revolution on the basis of digital network.

From the perspective of energy and industrial revolution, we can find three revolutions closely related to the new energy vehicles: electrification of power—the revolution of electric vehicles; low-carbon energy—the revolution of new energy; systematic intelligence—the revolution of artificial intelligence (AI).

First, electrification of power and the revolution of electric vehicles.

The invention of lithium-ion battery triggered the technological revolution in the area of storage battery over the past 100 years. Viewed from the development of power battery and power electronic device, the involvement of high specific energy battery and high specific power electric drive system would contribute to the platform development of electric chassis. The volume power of the machine controller based on new-generation power electric technology has more than doubled to 50 kw. In future, the volume power of the high-speed and high-voltage machine can be nearly doubled to 20 kw, and the power volume of the automobile with 100 kw volume power could be no more than 10 L. With the constant decline of the volume of the electric power system, the electrification will lead to the platform and module development of chassis, which will lead to a major change in terms of vehicle design. The platform development of electric chassis and the lightweight of body materials will bring about the diversification and personalization of types of vehicles. Besides, the combination of active collision avoidance technology and body lightweight technology will result in a significant change in automobile manufacturing system. The revolution of power electrification will promote the popularity of new energy electric vehicles and will

eventually contribute to the overall electrification of the transportation sector. China Society of Automobile Engineers proposed the development goals of China's new energy vehicles in the *2.0 Technology Road Map of Energy Saving and New Energy Vehicles*: The sales of new energy vehicles would reach 40% of the total sale of vehicles by 2030; new energy vehicles would become the mainstream by 2035 with its sale accounting for over 50% of the total sale of vehicles. In the foreseeable future, electric locomotives, electric ships, electric planes and other types will become a reality.

Second, low-carbon energy and new energy revolution.

In the *Strategy on Energy Production and Consumption Revolution (2016–2030)* jointly issued by National Development and Reform Commission and National Energy Administration, a target was proposed that the non-fossil energy would account for around 20% of total energy consumption by 2030 and over 50% by 2050. Actually, there are five pillars aimed to realize the energy revolution: firstly, the transformation of renewable resources and the development of photovoltaic and wind power technologies; secondly, the energy system is shifting from centralized to distributed development, turning every building into a micro-power plant; thirdly, the storage of intermittent energy by way of relevant technologies such as hydrogen and battery; fourth, the development of energy (electric power) Internet technology; fifth, enabling electric vehicles to become the end of energy usage, energy storage and energy feedback. In fact, China's photovoltaic and wind power technologies are fully qualified for large-scale distribution, but energy storage remains a bottleneck which needs to be solved by way of battery, hydrogen and electric vehicles. With the large-scale promotion of electric vehicles, along with the mixture of electric vehicles and renewable energy, electric vehicles will become the “real” new energy vehicles utilizing the entire chain of clean energy. In so doing, it could both solve the pollution and carbon emission problems of the vehicle itself, but could also be conducive to the carbon emission reduction of the entire energy system, thus bringing about a new energy revolution for the entire energy system.

Third, intelligent development of system and AI revolution.

Electric vehicles have three attributes of travel tools, energy devices and intelligent terminals. Intelligent and connected vehicles (ICVs) will restructure the industrial chain and value chain of vehicles. Software defines vehicles while data determine value. The traditional vehicle industry will be transformed into a high-tech industry leading the AI revolution. In the meanwhile, let's take a look at the Internet connection and the feature of sharing regarding vehicles, among “four new attributes”, from the perspectives of both intelligent travel revolution and the new energy revolution: for one thing, the connotation of the Internet pays equal attention to the Internet of vehicle information and the Internet of mobile energy. For another, the connotation of sharing lays equal emphasis on sharing travel and energy storage information. And both stationery and running electric vehicles can be connected to the mobile energy Internet, finally realizing a full interaction (V2G, vehicle to grid). As long as the energy storage scale of distributed vehicles is large enough, it will become the core hub of intelligent transportation energy, namely, the mobile energy Internet. Intelligent charging and vehicle to grid will meet the demand of absorbing renewable

energy fluctuations. By 2035, China's inventory of new energy vehicles will reach about 100 million. At that time, the new energy vehicle-mounted battery power will reach approximately 5 billion KWH (kilowatt-hours) with 2.5–5 billion KWH as the charging and discharging power. By 2035, the maximum installed capacity of wind power and photovoltaic power generation will not surpass 4 billion KW. The combination of vehicle-mounted energy storage battery and hydrogen energy could completely meet the demand of load balance.

All in all, with the accumulation of experience over the past two decades, since 2001, China's electric vehicles have "shifted to another path and led in the sector of new energy vehicles" worldwide. At the same time, China could build its advantage in terms of renewable resources with AI leading the world. It can be predicted that the period between 2020 and 2035 will be a new era when the revolution of new energy electric vehicles, the revolution of renewable energy and the revolution of artificial intelligence will leapfrog and develop in a coordinated manner and create a Chinese miracle featuring the strategic product and industry of new energy intelligent electric vehicles. Focusing on one strategic product and sector, such three technological revolutions and three advantages will release huge power, which could help realize the dream of a strong vehicle nation and play a leading role in all directions. With the help of such advantages, China will create a large industrial cluster with the scale of the main industry exceeding 10 trillion yuan and the scale of related industries reaching tens of trillions of yuan. The development of new energy vehicles at a large scale will result in a new energy revolution, which will bring earthshaking changes to the traditional vehicle, energy and chemical industry, thus truly embracing the great changes unseen in a century since the replacement of carriages by vehicles.

The technology revolution of new energy vehicle is advancing the rapid development of related interdiscipline subjects. From the perspective of technical background, the core technology of energy saving and new energy vehicles—the new energy power system technology, remains the frontier technology at the current stage. In 2019, China Association for Science and Technology released 20 key scientific and engineering problems, 2 of them (electrochemistry of high energy and density power battery materials, and hydrogen fuel battery power system) belonging to the scope of new energy system technology; The report of *Engineering Fronts 2019* published by Chinese Academy of Engineering mentioned the power battery 4 times, fuel battery 2 times, hydrogen energy and renewable energy 4 times as well as electricity-driven/hybrid electric-driven system 2 times. Over the past two decades, China has accumulated plenty of new knowledge, new experience, and so many methods during the research and development regarding new energy vehicles. The "research series of key technologies on energy saving and new energy vehicles" are based on Chinese practice and the international frontier, aiming to review China's research and development achievements on energy saving and new energy vehicles, meet the needs of technological development concerning China's energy saving and new energy vehicles, reflect the key technology research trend of international energy saving and new energy vehicles, and promote the transformation and application of key technologies as regards China's energy saving and new energy vehicles. The series involve four modules: vehicle control technology, power battery technology, motor driving

technology as well as fuel battery technology. All those books included in the series are research achievements with the support of National Natural Science Foundation of China (NSFC), major national science and technology projects or national key research and development programs. The publish of the series plays a significant role in enhancing the knowledge accumulation of key technologies concerning China's new energy vehicle, improving China's independent innovation capability, coping with climate change and promoting the green development of the vehicle industry. Moreover, it could contribute to China's development into a strong vehicle nation. It is hoped that the series could build a platform for academic and technological communication and the author and readers could jointly make contributions to reaching the top in the international stage concerning the technological and academic level in terms of China's energy saving and new energy vehicle.

January 2021 (2021年1月)

Ouyang Minggao  
Academician of Chinese Academy of Sciences  
Professor of Tsinghua University (THU)  
Beijing, China

# Preface

In recent years, the electric vehicle industry has developed rapidly with cutting-edge technologies such as 5G, Internet of Things, big data and artificial intelligence. “The new four modernizations of the automobile industry” with electrification, networking, intelligentization and sharing as its core is reshaping the pattern of the automobile industry, among which electrification is the best foundation for all these advanced intelligence technologies.

The popularization of electric vehicles in the world has become an important development trend. The main energy source of electric vehicles is power batteries; available power cells include lead-acid batteries, nickel-cadmium batteries, lithium-ion battery batteries and fuel cells, among which lithium-ion batteries are currently the mainstream power cells and the main object for this book.

Battery management system (BMS) is an indispensable key component of new energy vehicle. Its core functions include data collection, state estimation, balance management, thermal management, communication and fault diagnosis. This book describes the electrochemical model, black box model, equivalent circuit model and other modeling methods, and corresponding parameter identification methods.

In order to make better use of power battery, more and more requirements are put forward for BMS, especially in the aspect of high-precision battery state estimation of full climate, and full lifespan. This book elaborates the SOC estimation methods with model-based estimation methods and data-driven algorithms, combined with simulation cases. SOH estimation methods are introduced from the aspects of direct measurement, indirect analysis, data-driven and multi-scale joint estimation. In addition, the estimation methods of power, energy and safety state are discussed in detail combined with data-driven methods.

The available charge and discharge capacity of a battery pack is determined by the unit with the highest and lowest capacity respectively, and this kind of inconsistency will gradually increase with time accumulation, leading to accelerated aging. This may cause overcharge and overdischarge during cycling, resulting in the risk of thermal runaway safety. Therefore, the charge optimization control algorithm, which aims at the longest cycle life, needs to be implemented with passive equilibrium and the non-destructive active equilibrium. This can reduce the inconsistency, maximize

the energy efficiency of the battery pack and effectively ensure the safety of battery charging and discharging process with thermal management system.

With the deep fusion of technologies such as automobile manufacturing technology and information and communication technology, the automobile industry is accelerating to the direction of “Four modernizations”. At the same time, the on-board electronic systems are becoming more and more complex, it has gradually acquired network communication functions, including communication with other vehicles, infrastructure and access to the Internet. The functional security of the system has been the focus of research in the field of automotive electronic control, and hence, the integration of the battery management system on the vehicle also requires special attention. The modern vehicles have already transformed into a large-scale intelligent mobile terminal. Once the cybersecurity accident happens, it will possibly cause the extremely serious influence to the property security, the personal security and even the national public security.

Digital twin is a technology which integrates multi-physical, multi-scale and multi-disciplinary attributes, with the characteristics of real-time synchronization, faithful mapping and high fidelity, and can realize the interaction and fusion between the physical world and the information world. It can not only realize full lifespan management, but also carry out massive data mining with Internet of things and big data technology. Therefore, the next-generation battery management system based on digital twin will be a promising research direction.

Thanks to the reviewers for their valuable comments on this book. Thanks to the publisher for strong support during the preparation process. Many thanks to the postgraduate students Bin Guo, Xinlei Gao, Jiayuan Lin, Rong He, Yang Hua, Sida Zhou, Xianan Zhou, Zhengjie Zhang, Zuoming Zhang, Zhiwei Fan, Qimeng Gu, Xinnna Jin, Jichong Li, Bin Ma, Lin Li, Rui Cao, Mingyue Wang, Hanchao Cheng, Lisheng Zhang and Hanqing Yu for their contribution in this book.

Due to limited knowledge of authors, mistakes and inappropriateness are unavoidable, criticism is welcome of all readers.

Beijing, China  
February 2022

Shichun Yang

# Contents

## Part I Electric Vehicle and Battery Management

<b>1</b>	<b>Electric Vehicle .....</b>	<b>3</b>
1.1	Background of Electric Vehicle Industry .....	3
1.2	EV Categories .....	4
1.2.1	BEV .....	4
1.2.2	HEV .....	5
1.2.3	FCEV .....	6
1.3	Basics of Vehicle Dynamics .....	8
1.3.1	Vehicle Longitudinal Dynamics .....	8
1.3.2	Vehicle Dynamics Equation .....	10
1.3.3	Vehicle Maximum Speed .....	10
1.3.4	Vehicle's Gradeability .....	11
1.3.5	Vehicle Acceleration Performance .....	12
1.3.6	Vehicle's Power and Energy Requirements .....	12
	References .....	13
<b>2</b>	<b>EV Power Battery .....</b>	<b>15</b>
2.1	Principle and Types of Power Batteries .....	15
2.1.1	Lead-Acid Battery .....	17
2.1.2	Ni–Cd Battery .....	19
2.1.3	Ni–MH Battery .....	19
2.1.4	Lithium–Ion Battery .....	20
2.2	Performance Parameter of Power Battery .....	24
2.2.1	Nominal Parameter .....	24
2.2.2	Electric Parameter .....	26
2.2.3	Other Parameters .....	28
2.3	Development and Trend of Power Battery .....	29
	References .....	31

<b>3 Key Technologies of BMS</b>	33
3.1 Overview of BMS	33
3.1.1 BMS Architecture	33
3.1.2 Sampling Chip	35
3.2 Core Functions of BMS	43
3.2.1 Parameter Collection	44
3.2.2 State Estimation	45
3.2.3 Balance Management	46
3.2.4 Thermal Management	46
3.2.5 Communication	48
3.2.6 Malfunction Diagnosis	49
References	50

## Part II State Estimation Methods

<b>4 Battery Model</b>	55
4.1 Electrochemical Models	56
4.1.1 Pseudo-Two-Dimensional (P2D) Model	56
4.1.2 Single Particle Model (SPM)	60
4.2 Black-Box Model	60
4.3 Equivalent Circuit Model (ECM)	62
4.3.1 Resistance Model	62
4.3.2 RC Model	63
4.3.3 Fractional-Order Model	65
4.4 Parameter Identification	66
4.4.1 Offline Methods	67
4.4.2 Online Parameter Identification Algorithms	73
4.4.3 Perspective of Parameter Identification Algorithms	79
References	79
<b>5 SOC Estimation</b>	81
5.1 SOC Definition	81
5.2 Different Estimation Algorithms	82
5.2.1 Empirical Method	82
5.2.2 Model-Based Methods	85
5.2.3 Data Driven Methods	94
5.3 Case Study	97
5.3.1 Simulation	97
5.3.2 Validation of Accuracy	104
References	108
<b>6 SOH Estimation</b>	111
6.1 SOH Definition	111
6.2 Direct Measurement Method	112

6.2.1	Capacity .....	113
6.2.2	Internal Resistance .....	113
6.2.3	Impedance .....	114
6.2.4	Cycle Number .....	115
6.2.5	Other Methods .....	115
6.3	Indirect Analysis Methods .....	116
6.3.1	Voltage Curve Analysis .....	116
6.3.2	Incremental Capacity Analysis .....	117
6.3.3	Differential Voltage Analysis .....	117
6.3.4	Differential Thermal Voltammetry .....	118
6.3.5	Other Methods .....	121
6.4	Data-Driven Methods .....	121
6.4.1	Empirical Methods .....	121
6.4.2	Sample Entropy .....	122
6.4.3	Other Methods .....	124
6.5	Multiscale Joint Estimation .....	125
6.5.1	Adaptive Method .....	125
6.5.2	Fusion Algorithms .....	125
6.6	Case Study .....	125
6.6.1	Joint Estimation of SOC-SOH .....	125
6.6.2	Accuracy Validation .....	128
6.7	Summary .....	132
	References .....	133
7	<b>SOP Estimation .....</b>	135
7.1	SOP Definition .....	135
7.2	Interpolation Method .....	136
7.3	Model-Based Method .....	137
7.3.1	Equivalent Circuit Model .....	137
7.3.2	Electrochemical Model .....	140
7.3.3	Fusion Model .....	141
7.4	Data-Driven Methods .....	142
7.4.1	BP Neural Networks .....	142
7.4.2	Support Vector Machine .....	144
7.5	Simulation Case Study .....	144
	References .....	146
8	<b>SOE and SOS Estimation .....</b>	149
8.1	State of Energy (SOE) Estimation .....	149
8.1.1	Definition .....	149
8.1.2	Power Integral Method .....	150
8.1.3	OCV Based Method .....	150
8.1.4	Neural Networks .....	151

8.1.5	Model-Based Method .....	151
8.1.6	Simulation Case Study .....	151
8.2	State of Safety (SOS) Estimation .....	155
8.2.1	Thermal Runaway .....	157
8.2.2	Early Warning of Battery Failures .....	158
References .....		160
<b>Part III Control Method</b>		
<b>9</b>	<b>Passive and Active Balancing .....</b>	<b>165</b>
9.1	Battery Pack Inconsistency Analysis .....	165
9.1.1	Production Factor .....	165
9.1.2	Use Factor .....	166
9.1.3	Inconsistency Improvement .....	167
9.2	Balancing Management System .....	168
9.2.1	Balancing System Architecture .....	168
9.2.2	Balancing System Classification .....	168
9.3	Balancing Circuit Topology .....	169
9.3.1	Passive Balancing .....	169
9.3.2	Active Balancing .....	170
9.3.3	Summary of Balancing Topology .....	178
9.4	Balancing Control Strategy .....	178
9.4.1	Balancing Control Variables .....	180
9.4.2	Control Strategy .....	185
9.5	Conclusion .....	186
References .....		187
<b>10</b>	<b>Optimized Charging Management .....</b>	<b>189</b>
10.1	Background .....	189
10.2	Charging Protocol .....	189
10.2.1	Constant Current-Constant Voltage (CC-CV) .....	190
10.2.2	Multi-Stage Constant-Current Charging .....	190
10.2.3	Pulse Charging .....	191
10.3	Model-Based Charging Optimization Method .....	192
10.3.1	To Shorten the Battery Charging Time as the Optimization Goal .....	192
10.3.2	To Extend the Battery Cycle Life as the Optimization Goal .....	193
10.3.3	To Improve Battery Storage Energy as the Optimization Goal .....	194
References .....		194

<b>11 Thermal Management and Thermal Safety .....</b>	<b>197</b>
11.1 The Effect of Temperature on Battery Performance .....	197
11.1.1 Low Temperature .....	197
11.1.2 Higher Temperature .....	198
11.1.3 Temperature Difference .....	199
11.2 Thermal Management Method .....	200
11.2.1 Low Temperature Heating Method .....	200
11.2.2 High Temperature Heat Dissipation Method .....	202
11.3 Thermal Management Control Strategy .....	205
11.3.1 Thermal Model .....	206
11.3.2 Thermal Management Strategy .....	210
References .....	212

## Part IV Functional and Cyber Security

<b>12 Functional Security .....</b>	<b>215</b>
12.1 Introduction of ISO26262 .....	215
12.1.1 Background .....	215
12.1.2 Goals .....	216
12.1.3 Scope and Content .....	216
12.1.4 Automotive Electronics, Electrical Products .....	217
12.1.5 Introduction to the New Edition .....	218
12.2 ASIL Levels .....	218
12.2.1 Hazard Analysis and Risk Assessment .....	219
12.2.2 Examples of Hazard Analysis and Risk Assessment .....	220
12.2.3 ASIL Decomposition Principle .....	223
12.2.4 ASIL Decomposition Example .....	223
12.3 Functional Security Development Process .....	226
12.3.1 Concept Development .....	226
12.3.2 System Level Development .....	228
12.3.3 Hardware Development .....	230
12.3.4 Software Development .....	232
References .....	235
<b>13 Cyber Security .....</b>	<b>237</b>
13.1 Overview of Automotive Cyber Security .....	237
13.2 Cyber Security for In-Vehicle Communication .....	243
13.2.1 In-Vehicle Network .....	244
13.2.2 CAN Bus Communication Protocol .....	244
13.2.3 CAN Bus Cyber Security Vulnerability .....	247
13.2.4 CAN Bus Attack Methods .....	249
13.2.5 CAN Bus Protection Measures .....	250
13.3 Cyber Security for Charging .....	255
13.3.1 The Overall Process of Charging .....	255
13.3.2 Cyber Security Protection During Charging .....	260
13.4 Cyber Security for Remote Communication .....	261

13.4.1	Cyber Security Threats of Remote Communication . . . . .	262
13.4.2	V2C Communication Security Protection Strategy . . . . .	263
13.4.3	Application of FOTA Security Technology in Vehicle System . . . . .	265
References	.....	267

## Part V Application and Perspective

<b>14</b>	<b>Vehicle Applications</b> . . . . .	271
14.1	Composition of Power Battery System . . . . .	272
14.2	Power Battery Pack . . . . .	273
14.3	Lightweight of Battery Pack . . . . .	276
14.3.1	Lightweight Design Approach for Battery Systems . . . . .	276
14.3.2	Trends in Lightweight Battery Systems . . . . .	277
14.4	Application of BMS . . . . .	277
References	.....	278
<b>15</b>	<b>Battery Digital Twin</b> . . . . .	281
15.1	Concept of Digital Twin . . . . .	283
15.1.1	History of Digital Twin . . . . .	283
15.1.2	Different Forms of Digital Twin . . . . .	283
15.1.3	Key Features of Digital Twin . . . . .	286
15.1.4	Meaning of Digital Twin . . . . .	289
15.2	Digital Twin in BMS . . . . .	292
15.2.1	Multi-Scale/Dimension Design of Battery Based on Digital Twin . . . . .	293
15.2.2	Modeling of Battery System Based on Digital Twin . . . . .	296
References	.....	299
<b>16</b>	<b>Cloud Battery Management System</b> . . . . .	301
16.1	Electric and Electronic Architecture . . . . .	301
16.2	Cloud Platform and Service . . . . .	302
16.3	Cloud Battery Management System Framework . . . . .	305
16.3.1	End Sensing . . . . .	305
16.3.2	Edge Computing . . . . .	306
16.3.3	Cloud Computing . . . . .	307
16.3.4	Knowledge Repository . . . . .	307
16.4	Cloud Battery Management System Module and Function . . . . .	308
16.4.1	Cloud Control Method . . . . .	308
16.4.2	Thermal Runaway Early Warning Method . . . . .	309
16.4.3	Cloud Big Data Analysis . . . . .	310
16.4.4	Full Life Cycle Management . . . . .	311
16.5	Future Task and Perspective . . . . .	312
References	.....	313

## About the Authors



**Prof. Shichun Yang** is Dean of School of Transportation Science and Engineering at Beihang University, leading personnel of scientific and technological innovation in the National Ten-thousand Talents Program, leading personnel among the young and middle-aged in the Ministry of Science and Technology, national outstanding scientific and technological worker. He is Vice Chairman of Electric Vehicle Division of National Technical Committee of Automobile Standardization (NTCAS), expert of Road Vehicle Specialized Committee of China Intelligent Transportation System Association (CTTSA), Vice Chairman of SAE Vehicle Safety and Information Security Technical Committee. His research mainly works on scientific and technological research for EV power system safety, high-efficient optimal theory and integrated control. e-mail: [yangshichun@buaa.edu.cn](mailto:yangshichun@buaa.edu.cn)



**Dr. Xinhua Liu** is an Assistant Professor of School of Transportation Science and Engineering at Beihang University, Visiting Lecture of Dyson School of Design Engineering at Imperial College London (UK). Her research interests mainly lie in the interface between electrochemical science and engineering applying a digital process, including designer energy materials for various energy storages; model-driven microstructure optimization for high-performance batteries; cloud control-based battery degradation mechanism, diagnose and battery management system design. e-mail: [liuxinhua19@buaa.edu.cn](mailto:liuxinhua19@buaa.edu.cn)



**Dr. Shen Li** is a Research Associate of Department of Mechanical Engineering at Imperial College London, UK, since 2018. He is also a technical consultant at Imperial Consultants Ltd., UK, since 2021. His research interests include solid mechanics including interfacial contact problem and friction, energy storage including lithium-ion battery simulation using electrochemical model and equivalent circuit model, battery thermal management, degradation, control algorithm and pack-level simulation. e-mail: [shen.li@imperial.ac.uk](mailto:shen.li@imperial.ac.uk)



**Dr. Cheng Zhang** is an Assistant Professor of Institute for Clean Growth and Future Mobility at Coventry University, UK, since 2019. His research interests mainly lie in advanced battery management algorithms, including design of experiment for battery characterization, electrical-thermal-aging simulation of battery systems, model-based real-time parameter and state estimation, and optimal control. e-mail: [ad4275@coventry.ac.uk](mailto:ad4275@coventry.ac.uk)

# **Part I**

## **Electric Vehicle and Battery Management**

# Chapter 1

## Electric Vehicle



### 1.1 Background of Electric Vehicle Industry

The huge energy requirement of the automobile industry cannot be met by the non-renewable petroleum in the long term. With the rapid development of global economy, the problems of energy shortage and environmental pollution are becoming increasing prominent. The transformation of the automobile industry, which currently accounts for a large proportion of the global petroleum consumption and pollutive emissions, is an inevitable trend. New energy vehicles (NEVs) representing the future of the automobile industry are rapidly gaining global influences and market shares (Ehsani et al. 2018).

Transport electrification is one inevitable development trend of the global automobile industry. Many developed countries have published national or regional strategic plans and technical roadmaps to guide the development of NEVs, such as the ‘Guidance for Developing Pure and Hybrid Electric Vehicles’ in Japan, ‘EV Everywhere Grand Challenge Blueprint’ in America and ‘National Electromobility Development Plan’ in Germany (Mohr et al. 2015). Some countries and automobile enterprises have proposed a complete ban on the sale of non-renewable vehicles by 2030 (or shortly after 2030). According to statistics, the number of REVs sold in America in 2018 reached 360,800 with 61% year-on-year growth.

NEVs have become one of the strategic emerging industries in China, as a promising solution to alleviate the pressure of oil requirement, improve the environment, and to realize the strategic restructuring, transformation and upgrading of the automobile industry (Du et al. 2019; Satyendra Kumara and Revankar 2017). The Chinese government attaches great importance to the development of NEV technology and industry, as the General Secretary Xi Jinping pointed out that ‘NEV is the route to transforming China from a big country to a strong country in automobile industry’. The Chinese government has issued several national strategic policies, such as the ‘Energy Saving and New Energy Automobile Industry Development Plan 2012–2020’ and ‘China Manufacturing 2025’ to promote the development of REV

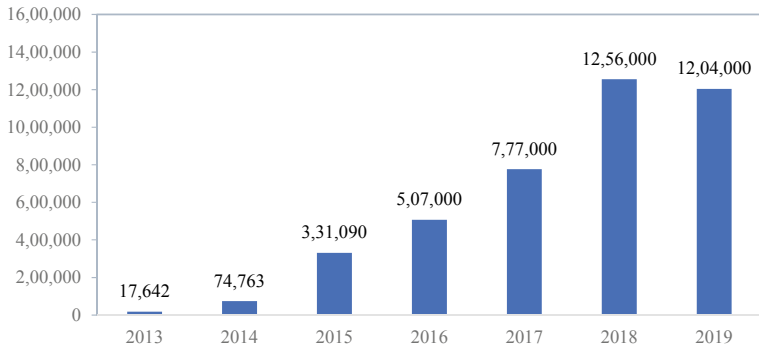


**Fig. 1.1** NEV sales in China from 2013 to 2019

technology and industry. China has become the largest REV market since 2015 for five consecutive years. The number of NEV sales in China are 1.25 million and 1.20 million in 2018 and 2019, respectively. The NEV sales in China from 2013 to 2019 are given in Fig. 1.1.

The Chinese Society of Automotive Engineering issued the new ‘Energy saving and REV technology roadmap’ in Oct 2020 entrusted by the Ministry of Industry and Information Technology of China, which projected that by 2035 the NEV will account for 50% of all new vehicle sales and the inventory of fuel-cell vehicles will reach 1 million.

## 1.2 EV Categories

Electric vehicle (EV) is the product of synthesis and integration of automobile engineering, electric drive, power electronics, automatic control systems, renewable energy and new materials. EV has entered the stage of fast development with rapidly advancing technologies and performance indicators. The scale of the EV industry has been growing rapidly. There are several different EV categories, including battery electric vehicle (BEV), hybrid electric vehicle (HEV) and fuel cell electric vehicle (FCEV).

### 1.2.1 BEV

BEVs use the rechargeable batteries as the sole power source, such as lead acid batteries, Ni–Cd batteries and lithium ion batteries (LIB). The vehicle is driven by electric motor powered by the onboard energy storage system.

The structure of the BEV consists of the onboard energy storage system, powertrain system, chassis, vehicle body and auxiliary systems. The powertrain system includes motor, traction control system and transmission system.

The key technologies for BEV development include the powertrain system, steering system, suspension system, auxiliary systems, propulsion system and the vehicle control systems. Battery, motor and transmission system are the three most critical components of the BEV.

The transmission system of an EV transfers the motor's output torque to the driving shaft. When electric motors are used to drive the vehicle, most parts of the conventional transmission system of internal combustion engine (ICE) vehicles become redundant. Because electric motors can start under load, EVs do not need the clutches of traditional ICE vehicles. Because the rotation direction of the electric motor can be changed by circuit control, and the reverse gear in the transmission of ICE becomes obsolete. EVs with stepless motor speed control do not need a gearbox, and the electric wheel drive in EVs makes the transmission differential unnecessary.

The power batteries used in EVs mainly include lead-acid batteries, LIBs and Ni-MH batteries. Among them, Ni-MH batteries are only used in Toyota's non-plug-in hybrids and are not suitable as the solo power source. LIB is the most widely used power battery in EVs. There are many different LIB chemistries. At present, the mature LIB chemistries mainly include ternary lithium batteries and LiFePO<sub>4</sub> batteries, which are two mainstream batteries in the EV market. At present most major car companies have rolled out their own pure electric passenger car and electric cars.

Motor is one of the most critical parts in the EV. DC motors have long been used as driving motors for EVs because the batteries provide DC power. Many EVs adopt the DC drive system due to the mature technology. However, traditional DC motors have some disadvantages, such as the increased volume and inertia of the rotor due to the armature winding, the limited scope of working environment of the mechanical commutator, lower efficiency compared with other types of motors, and the high maintenance requirement. In order to enhance the EV performance, the motor needs to have a wide range of speed regulation, high speed, high start torque, small volume, small mass, high efficiency and dynamic braking and energy generative feature. At present, DC motors have been mostly replaced by AC motors, permanent magnet motors and switched reluctance motors.

### 1.2.2 HEV

HEV uses a combination of on-board consumable fuel and rechargeable energy storage device as the power source. According to the power system structure, it can be categorized as series hybrid electric vehicle (SHEV), parallel hybrid electric vehicle (PHEV) and series-parallel combined hybrid electric vehicle (CHEV). The onboard energy storage system e.g., the batteries, still cannot meet the energy/power requirements of certain vehicles, e.g., heavy-duty vehicles, and the hybrid powertrain

can significantly enhance the vehicle's driving range and power capacity (Sabri et al. 2016; Husain 2011; Zhang and Liu 2012; Chen et al. 2014).

The degree of hybridization  $H$  of a HEV is defined as the percentage of electrical system power  $P_{\text{elec}}$  in the total system power  $P_{\text{total}}$ . According to the degree of hybridization, the HEVS can be categorized as low hybridization, mild hybridization, moderate hybridization, strong hybridization and plug-in HEV.

Low hybridization (also known as micro hybrid): the traditional engine starter is replaced by a belt starter generator (BSG) system. The motor with small power capacity cannot start the vehicle alone. Therefore, the engine power is needed to start the vehicle. Generally, the rate of fuel saving is about 5% ~ 10% under urban driving conditions.

Mild hybridization: integrated starter motor (ISG) is used. The start and stop of the engine can be controlled by the motor. Energy can be recovered during vehicle braking or downhill driving. The degree of hybridization is generally less than 20%. A representative model is the General Motors hybrid pickup truck.

Moderate hybridization: the ISG system is adopted with high voltage motor. The hybridization degree can reach 30%. The fuel saving rate can reach 20–30% under urban driving conditions. This technology is mature and is widely used. Examples include Honda Insight, Accord, and Civic models.

Heavy hybridization (also known as full hybrid power, strong hybrid power): high voltage motor at 272–650 V is adopted, and the degree of hybridization can reach more than 50%. The fuel saving rate can reach 30–50% under urban circulation conditions. With the advancing motor and battery technology, heavy hybridization system has gradually become the mainstream HEV. One example is Toyota Prius HEV.

Plug-in HEV: the external power grid can be used to charge the onboard energy storage device. Generally, plug-in HEVs have on-board charger, which can be plugged to domestic power source. PHEV can drive in pure electric mode, and switch to hybrid mode when the battery power reaches low level. According to the power-train architecture, PHEV mainly include SHEV and CHEV. The SHEV is mainly driven by the onboard energy storage system with long pure electric driving range, while the CHEV is mainly driven by hybrid power with relatively short pure electric driving range. A diversity of PHEV models exists in the market.

### **1.2.3 FCEV**

FCEV uses either a single power source of fuel cells or a hybrid power source combining fuel cells with rechargeable energy storage system. Currently, the fuel cells adopted in EVs are generally hydrogen fuel cell. FCEVs can use pure hydrogen or hydrogen produced by other fuels as the hydrogen sources. Hydrogen fuel cell is an energy conversion device that converts the chemical energy of hydrogen and oxygen (or air) into electric energy through electrochemical reaction. No harmful substances will be produced during the reaction. It has advantages of high efficiency,

zero emission and low noise, etc. Therefore, FCEV represents a promising developing trend for the automobile industry from the perspective of energy efficiency and environmental friendliness. It is also of great significance for stabilizing national and global energy supply, improving energy structure and developing low-carbon transportation.

The development of FCEV can be divided into four main stages: concept design and principle verification before 2000, key technology research and demonstration during 2000–2010, commercial application and demonstration in specific fields from 2010 to 2015, and finally entering commercialization stage after 2015.

In 2015, Toyota introduced the Mirai fuel cell sedan and began selling it in Japan, the United States and Europe. Currently, the Mirai has a driving range of 500 km, a top speed of 200 km/h and 0–100 km/h in 9 s. The fuel replenishment only takes 5 min. In 2016, Honda launched Clarity, a FCEV equipped with a 70Mpa high-pressure hydrogen storage tank. The driving range is more than 700 km, and refuel takes only about 3 min. In 2018, Hyundai launched its fuel cell SUV, the NEXO, with a range of 800 km. In the same year, Mercedes-Benz released the GLC fuel cell hybrid sedan in Germany, with a top speed of 160 km/h and a range of 478 km under the comprehensive NEDC driving condition.

China has also made great progress in fuel cell reactor technology, key materials, infrastructure and other aspects. In 2016, SAIC released Roewe 950 fuel cell hybrid sedan with a maximum driving range of 430 km. The vehicle can start at -20°C ambient temperature. In 2017, SAIC launched FCV80, a fuel cell hybrid bus, which uses 35Mpa high-pressure hydrogen storage system, with a driving range up to 500 km and fuel replenishment in about 5 min. In addition, other Chinese automobile enterprises such as Yutong Bus, Zhongtong Bus and Dongfeng Automobile, have also launched fuel cell bus products.

At present, the bottlenecks of FCEV development include not only the low durability of fuel cells, the high cost / low performance of key materials and critical components, but also the limited coverage of hydrogen supply stations. According to incomplete statistics, by 2017, there are only about 100 public hydrogen refueling stations in Japan, 14 in South Korea, 69 in the United States, 56 in Germany and 15 in China.

China has identified FCEV as a key future-oriented technology to realize its strategic goals of clean, low-carbon and efficient development. It plans to deploy 5000 FCEVs as demonstration projects in the public service fleet in specific regions by 2020, and 50,000 FCEVs by 2025. FCEV will be commercialized on a large scale in the fields of private passenger vehicles and large commercial vehicles, and the number is expected to reach 1 million by 2030.

## 1.3 Basics of Vehicle Dynamics

### 1.3.1 Vehicle Longitudinal Dynamics

The schematic diagram of forces on vehicle is shown in Fig. 1.2.

The traction force on the vehicle is generated by the power devices and transmitted to the driving wheel via the transmission. The acceleration of the vehicle can be calculated according to Newton's second law,

$$\frac{dv}{dt} = \frac{\Sigma F_t - \Sigma F_r}{\delta M} \quad (1.1)$$

where  $V$  is the speed;  $\Sigma F_t$  is the total traction force;  $\Sigma F_r$  is the sum of resistances;  $M$  is the mass of the vehicle;  $\delta$  is the rotational inertia coefficient to transform the inertia of the rotating parts into the equivalent translational mass. The resistances on the moving vehicle usually include air resistance  $F_w$ , rolling resistance  $F_r$ , and climbing resistance  $F_g$ .

The air resistance  $F_w$  can be expressed as

$$F_w = \frac{1}{2} \rho A_f C_D (v - v_w)^2 \quad (1.2)$$

where  $C_D$  is the drag coefficient,  $v_w$  is the component of wind speed in the direction of vehicle movement.  $v_w$  is positive when it is in the same direction with the vehicle speed.

When the vehicle runs on paved road, the rolling resistance  $F_r$  mainly comes from the hysteresis of tire material, which can be calculated as follows,

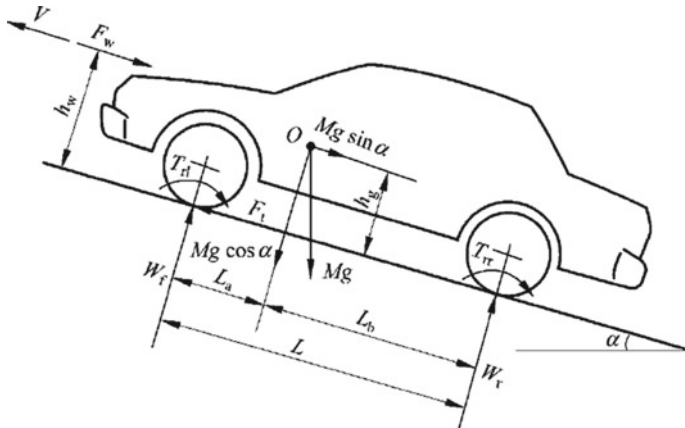


Fig. 1.2 Schematic diagram of forces on vehicle

**Table 1.1** Typical values of rolling resistance coefficient

Road condition	Rolling resistance coefficient
Asphalt or cement concrete	0.013
Compacted gravel pavement	0.02
Gravel road	0.025
Unpaved road	0.05
Farmland	0.1–0.35
Truck tires on concrete or asphalt	0.006–0.01
Wheel on a railroad track	0.001–0.002

$$F_r = Mg f_r \cos \alpha \quad (1.3)$$

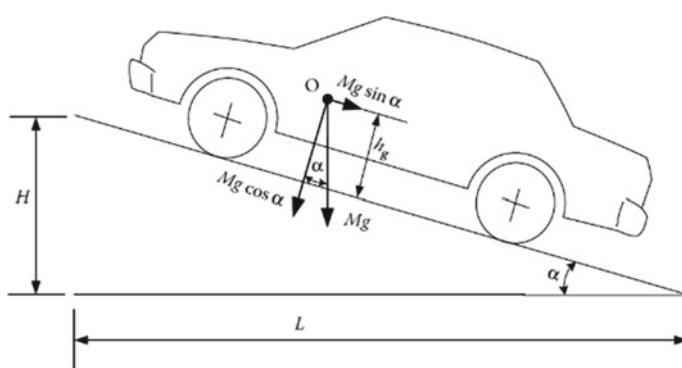
where  $f_r$  is the rolling resistance coefficient and  $\alpha$  is the slope of the ground, as shown in Fig. 1.2.

The rolling resistance coefficient  $f_r$  depends on the material, structure, temperature, inflation pressure, surface geometry of the tire and the material, roughness of the road and whether there is liquid on the road. The typical values of  $f_r$  on various types of roads are given in Table 1.1. Researchers have developed new tires in recently years with  $f_r < 0.01$  to reduce the energy consumption of the vehicle.

When the vehicle is on a slope, its gravity will produce a downhill force component, which is the climbing resistance,

$$F_g = Mg \sin \alpha \quad (1.4)$$

when slope angle is small,  $\sin \alpha$  can be approximated by the value of slope as shown in Fig. 1.3,

**Fig. 1.3** Schematic diagram of climbing resistance

$$i = \frac{H}{L} = \tan \alpha \approx \sin \alpha \quad (1.5)$$

Sometimes the rolling resistance of the tire and the climbing resistance together is called road resistance,

$$F_{rd} = F_r + F_g = Mg(f_r \cos \alpha + \sin \alpha) \quad (1.6)$$

When the slope angle  $\alpha$  is small, the road resistance can be approximated as follows,

$$F_{rd} = F_r + F_g = Mg(f_r + i) \quad (1.7)$$

### 1.3.2 Vehicle Dynamics Equation

The forces on the vehicle are shown in Fig. 1.2, including the traction forces on the front and rear tires ( $F_{tf}$ ,  $F_{tr}$ ), rolling resistance on the front and rear tires ( $F_{rf}$ ,  $F_{rr}$ ), air resistance  $F_w$  and climbing resistance  $F_g$ . The longitudinal dynamics equation of vehicle is

$$M \frac{dV}{dt} = (F_{tf} + F_{tr}) - (F_{rf} + F_{rr} + F_w + F_g) \quad (1.8)$$

where  $dV/dt$  is the vehicle's acceleration,  $M$  is the vehicle's mass.

### 1.3.3 Vehicle Maximum Speed

Vehicle performance is usually described in terms of maximum speed, gradability and acceleration performance. It is generally assumed that the maximum traction of a vehicle on the road is subject to the maximum torque of the power plant and not to the adhesion of the road.

The maximum vehicle speed is defined as the constant cruising speed the vehicle can maintain on a flat road surface under full power output (engine throttle fully open or motor's full power output). The maximum speed depends on the traction forces and resistance on the vehicle or the maximum speed of the power plant and the transmission ratio. The balance between traction and resistance can be expressed as:

$$\frac{T_p i_g i_0 \eta_t}{r_d} = Mg f_r \cos \alpha + \frac{1}{2} \rho_a C_D A_f v^2 \quad (1.9)$$

where  $T_p$  is the output torque of the power plant,  $i_g$  is the transmission ratio, and  $i_g = N_{in}/N_{out}$  ( $N_{in}$  is the input speed and  $N_{out}$  the output speed).  $i_0$  is the transmission ratio of the main gear reducer, and  $\eta_t$  is the transmission efficiency from the power system to the driving wheel.

It is worth noting that for some vehicles, the maximum speed depends on the maximum speed of the power plant. In this case, the maximum speed is expressed as:

$$v_{\max} = \frac{\pi n_{p\max} r_d}{30 i_0 i_{g\min}} \text{ (m/s)} \quad (1.10)$$

where  $n_{p\max}$  and  $i_{g\min}$  stand for the maximum speed of the motor and the minimum transmission ratio.

### 1.3.4 Vehicle's Gradeability

The gradeability is generally defined as the maximum slope that a vehicle can climb at a constant speed. For heavy goods vehicles or off-road vehicles, the gradeability is generally defined as the maximum slope that vehicle can climb in full speed range. When a vehicle travels at a constant speed on a slope with small angle, its traction force and resistance force are balanced as follows,

$$\frac{T_p i_0 i_g \eta_t}{r_d} = M g f_r + \frac{1}{2} \rho_a C_D A_f v^2 + M g i \quad (1.11)$$

Therefore, the slope value can be expressed as

$$i = \frac{T_p i_0 i_g \eta_t / r_d - M g f_r - \frac{1}{2} \rho_a C_D A_f v^2}{M g} = d - f_r \quad (1.12)$$

where

$$d = \frac{F_t - F_w}{M g} = \frac{T_p i_0 i_g \eta_t / r_d - \frac{1}{2} \rho_a C_D A_f v^2}{M g} \quad (1.13)$$

When the slope is steep, the gradeability can be calculated as follows,

$$\sin \alpha = \frac{d - f_r \sqrt{1 - d^2 + f_r^2}}{1 + f_r^2} \quad (1.14)$$

### 1.3.5 Vehicle Acceleration Performance

The acceleration performance of a vehicle is generally defined as the acceleration time and the acceleration distance required for the vehicle to accelerate from zero to a certain speed on a flat road. According to Eqs. 1.1–1.8, the acceleration equation of the vehicle can be obtained,

$$a = \frac{dv}{dt} = \frac{F_t - F_f - F_w}{M\delta} = \frac{T_p i_0 i_g \eta_t / r_d - Mg f_r - \frac{1}{2} \rho_a C_D A_f v^2}{M\delta} = \frac{g}{\delta} (d - f_r) \quad (1.15)$$

Therefore, the acceleration time  $t_a$  and acceleration distance  $S_a$  from low speed  $v_1$  to high speed  $v_2$  can be calculated as follows,

$$t_a = \int_{v_1}^{v_2} \frac{M\delta}{T_p i_0 i_g \eta_t / r_d - Mg f_r - \frac{1}{2} \rho_a C_D A_f v^2} dv \quad (1.16)$$

$$S_a = \int_{v_1}^{v_2} \frac{M\delta v}{T_p i_0 i_g \eta_t / r_d - Mg f_r - \frac{1}{2} \rho_a C_D A_f v^2} dv \quad (1.17)$$

### 1.3.6 Vehicle's Power and Energy Requirements

The vehicle's output power demand is the sum of drag power and vehicle acceleration power as follows,

$$P_e = \frac{v}{\eta_t} \left( F_f + F_w + F_g + M_v \delta \frac{dv}{dt} \right) \quad (1.18)$$

or alternatively

$$P_e = \frac{v}{1000 \eta_t} \left( Mg f_r \cos \alpha + \frac{1}{2} \rho_a C_D A_f v^2 + Mg \sin \alpha + M \delta \frac{dv}{dt} \right) \quad (1.19)$$

The energy requirements of the vehicle over a time period can be expressed as follows,

$$E_t = \int_{t_0}^{t_1} P_e dt \quad (1.20)$$

## References

- Chen Z, Mi C, Xu J, Member S (2014) Energy management for a power-split plug-in hybrid electric vehicle based on dynamic programming and neural networks. *IEEE Trans Veh Technol* 63:1567–1580
- Du ZL, Lin BQ, Guan CX (2019) Development path of electric vehicles in China under environmental and energy security constraints. *Resour Conserv Recycl* 143:17–26
- Ehsani M, Gao Y, Longo S et al (2018) Modern electric, hybrid electric, and fuel cell vehicles. CRC Press, Boca Raton
- Husain I (2011) Electric and hybrid vehicles: design fundamentals. CRC Press, Florida
- Mohr SH, Wang J, Ellem G, Ward J, Giurco D (2015) Projection of world fossil fuels by country. *Fuel* 141:120–135
- Sabri MFM, Danapalasingam KA, Rahmat MF (2016) A review on hybrid electric vehicles architecture and energy management strategies. *Renew Sustain Energy* 53:1433–1442
- Satyendra Kumara M, Revankar ST (2017) Development scheme and key technology of an electric vehicle: An overview. *Renew Sustain Energy Rev* 70:1266–1285
- Zhang Y, Liu HP (2012) Fuzzy multi-objective control strategy for parallel hybrid electric vehicle. *IET Electr Syst Transp* 2:39

# Chapter 2

## EV Power Battery



Power battery is widely used in energy storage system. The batteries performances affect the performances and market recognition of new energy vehicles. The requirements on batteries include safety, energy density, power density, efficiency, maintenance level, management, cost, ambient condition and environmentally friendly issue. Electric vehicle is limited by travel mileague which is determined by energy density. For hybrid electric vehicle, power density is the primary factor (Xiong et al. 2018; Goodenough and Park 2013; Deng et al. 2020; Senyshyn et al. 2015; Han et al. 2019; Lu et al. 2013).

At present, lead-acid, Ni-MH and lithium-ion batteries are common in electric vehicles. The energy density of lithium-ion batteries is the highest among the three types. Furthermore, the lithium-ion battery becomes the research focus due to its high power density, low self-discharge rate, weak memory effect and environmentally friendly issue. lithium-ion batteries are applied in electric vehicles, hybrid electric vehicles and fuel cell vehicles.

### 2.1 Principle and Types of Power Batteries

There are many varieties of power batteries. As electrochemical energy storage system, lead-acid, Ni-MH, Ni-Cd and lithium-ion batteries are applied in electric vehicles. Lead-acid batteries were used in electric vehicles in early stages. There were breakthroughs on the development of Ni-MH batteries in 1980s, and Ni-MH batteries were industrialized. The high performances of lithium-ion batteries further promote the development of electric vehicles.

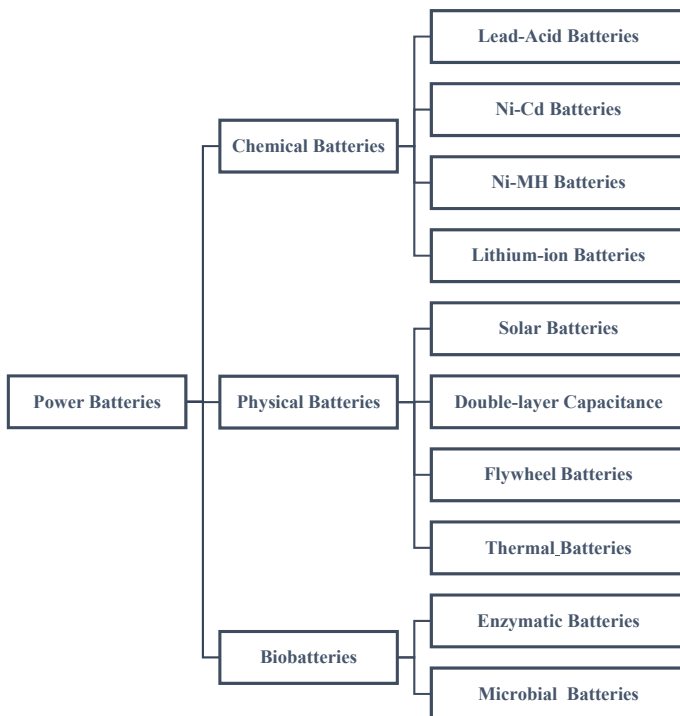


**Fig. 2.1** Common types of power batteries

There were several rounds of major improvements for power batteries. As shown in Fig. 2.1, batteries can be classified into three types: chemical batteries, physical batteries and biobatteries. Chemical batteries are common in electric vehicles.

The characteristics of power batteries are shown in Fig. 2.2 (Ma et al. 2014). The area represents the range of volume energy density and mass energy density. The batteries performances are determined by chemistries, structures and fabrication.

Main features of the power batteries are shown in Table 2.1 (Feng et al. 2018). Although lead-acid, Ni–Cd and Ni–MH batteries are safe and with low cost, their energy density is low and are detrimental to environment. Therefore, these batteries can not meet the demand on electric vehicle batteries.

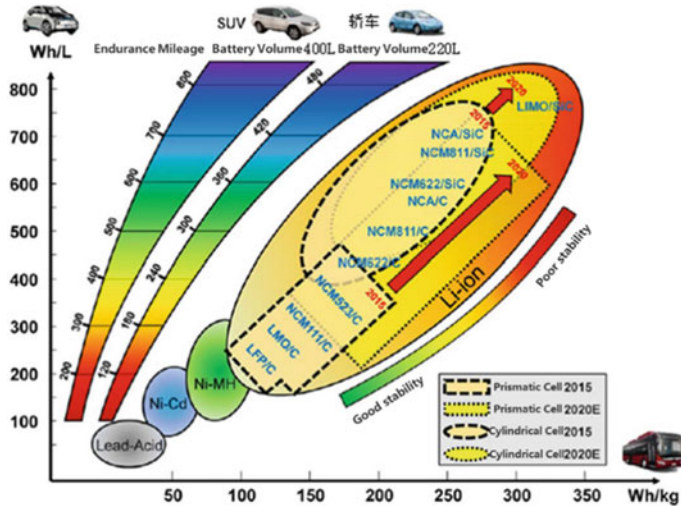


Fig. 2.2 Application status of vehicle power batteries

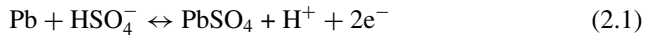
### 2.1.1 Lead-Acid Battery

Since the invention of lead-acid batteries 160 years ago, they are still applied in electric vehicles till now.  $\text{PbO}_2$  and  $\text{Pb}$  are usually used as cathode and anode materials for lead-acid batteries. The  $\text{H}_2\text{SO}_4$  solution is chosen as electrolyte.

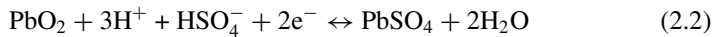
While the cell is in discharge, electrons are released from anode and  $\text{PbSO}_4$  is formed. After receiving electrons,  $\text{Pb}^{4+}$  from cathode becomes  $\text{Pb}^{2+}$  and form  $\text{PbSO}_4$ .  $\text{H}_2\text{SO}_4$  concentration decreases and  $\text{PbSO}_4$  concentration increases. Potential voltage keeps decreasing.

In charge process,  $\text{PbSO}_4$  from cathode reacts with  $\text{H}_2\text{O}$  and forms  $\text{PbO}_2$ .  $\text{Pb}^{2+}$  becomes  $\text{Pb}$  on anode.  $\text{H}_2\text{SO}_4$  concentration increases. Potential voltage keeps rising.

Reaction in anode:



Reaction in cathode:



Overall reaction:

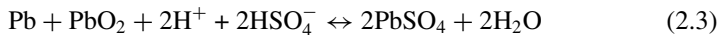


**Table 2.1** Application status of main power batteries

	Lead-acid battery	Ni-Cd battery	Ni-MH battery	Lithium-ion battery
Mass energy density (Wh/kg)	33~42	50~80	70~95	118~250
Volume energy density (Wh/L)	60~110	50~150	140~300	250~693
Mass power density (W/kg)	180	200	200~300	200~430
Volumetric power density (W/L)	450	200	300	800
Self-discharge (month)	<5%	10%	20%	<5%
Operating temperature (°C)	-10~50	-20~50	-20~60	-20~60
Cycle life	>300	>800	>800	>1000
Environmental impact	Heavy metal pollution	Heavy cadmium pollution	Heavy metal pollution	Relatively low
Safety	★★★★★	★★★★★	★★★★★	★★★★☆
Production cost	★★☆☆☆	★★☆☆☆	★★★★★	★★★★★

Valve regulated lead-acid (VRLA) is a type of lead-acid batteries that doesn't require maintenance. There are two types of VRLA: gelled electrolyte (GEL) and absorbent glass mat (AGM) batteries.

The reaction under condition of O<sub>2</sub> is:



### **2.1.2 Ni–Cd Battery**

Ni–Cd battery has been developed for over a century. It was widely applied due to its high capacity, easy maintenance, low cost and simple fabrication. It can be categorized as pocket type plate, sintered plate and fiber plate.

Ni–Cd battery is a kind of alkaline battery since KOH solution is used as electrolyte. The cathode material is NiOOH and anode material is Cd. The chemical reaction is:



During discharge, Cd is oxidized into Cd(OH)<sub>2</sub>. NiOOH is reduced into Ni(OH)<sub>2</sub> with H<sub>2</sub>O released from electrolyte. H<sub>2</sub>O is generated in charge process. There is memory effect for Ni–Cd battery, i.e., the unavailable capacity for Ni–Cd battery is reduced when Ni–Cd is always not fully discharged.

Cd is poisonous and accumulates in organism. It will circulate in food chain and can be dangerous to human.

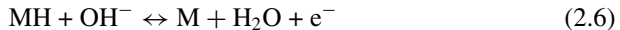
### **2.1.3 Ni–MH Battery**

Ni–MH battery is designed based on Ni–Cd battery, but there are improvements on memory effect and metal pollution.

Ni–MH battery is also alkaline battery because it uses KOH as electrolyte. The cathode material is Ni(OH)<sub>2</sub>/NiOOH. Anode material is M/MH<sub>x</sub>. M/MH<sub>x</sub> contains types such as AB<sub>2</sub> (TiMn<sub>2</sub>), AB<sub>5</sub> (LaNi<sub>5</sub>), AB (TiFe) and A<sub>2</sub>B (Mg<sub>2</sub>Ni). M/MH<sub>x</sub> will expand during storing hydrogen and shrink while realizing hydrogen. M/MH<sub>x</sub> is both electrically and thermally conductive but weak in mechanical characteristics.

Chemical reactions in Ni-MH are:

Reaction in anode:



Reaction in cathode:



Overall reaction:



$\text{H}_2\text{O}$  and  $\text{OH}^-$  are only involved in charge transfer and not in chemical reaction. Therefore, KOH concentration will keep constant during charge and discharge processes.

### 2.1.4 Lithium–Ion Battery

Compared with lead-acid, Ni–Cd and Ni-MH batteries, lithium–ion batteries support higher C rate, higher energy density and longer cycling lifetime.

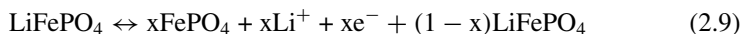
Lithium–ion battery is composed of electrodes, separator, electrolyte and casing. Common cathode material includes:  $\text{LiFePO}_4$ ,  $\text{LiMn}_2\text{O}_4$  and NCM. Anode material is based on carbon, silicon and lithium titanate.

During charge process, Lithium–ion ( $\text{Li}^+$ ) is delithiated from lattice of cathode material, migrated through electrolyte to anode material and intercalated into anode lattice. Electrons are transferred into negative by external circuit. During discharge process,  $\text{Li}^+$  is delithiated from anode lattice and transferred to cathode material lattice through electrolyte.  $\text{Li}^+$  is transferred between anode and cathode during charge and discharge, therefore it is also called ‘walking chair battery’.

#### 2.1.4.1 Lithium Iron Phosphate Battery

$\text{LiFePO}_4$  lattice is in olivine structure as shown in Fig. 2.3.

Capacity density of  $\text{LiFePO}_4$  is 170mAh/g. Due to the two-phase delithiation reaction, the voltage potential is stable. The reaction is:



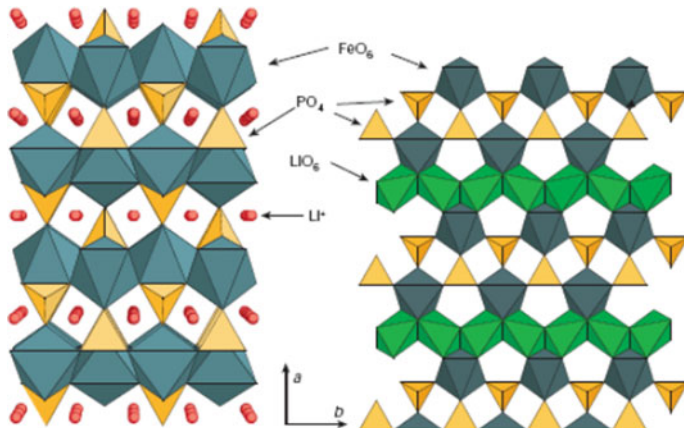


**Fig. 2.3** Diagram of  $\text{LiFePO}_4$  crystal structure

$\text{LiFePO}_4$  is widely applied in electric vehicles especially buses due to its safety, low cost and eco-friendly behavior. However, the charge rate is low and performance is poor in low temperature. Voltage plateau is low in charge and discharge processes.

#### 2.1.4.2 Lithium Manganate Battery

The structure of  $\text{LiMn}_2\text{O}_4$  is spinel as shown in Fig. 2.4.

Reaction in anode:

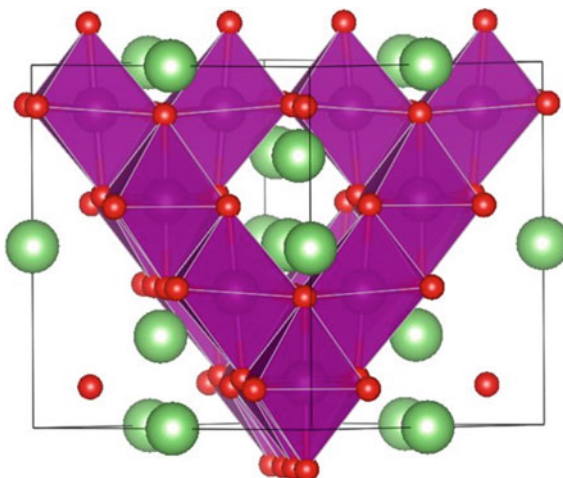
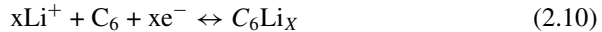


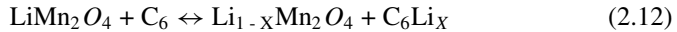
**Fig. 2.4** Diagram of  $\text{LiMn}_2\text{O}_4$  crystal structure (Green-Li, Red-O)



Reaction in cathode:



Overall reaction:



$\text{LiMn}_2\text{O}_4$  battery is applied due to its abundancy, low cost, safety and eco-friendly behavior. However, the performances in cycling at high temperature are poor and capacity loss is obvious.

#### 2.1.4.3 NCM Battery

In NCM battery, NCM and NCA are used as cathode materials. The energy density is higher than  $\text{LiFePO}_4$  battery.

NCM material can be denoted as  $\text{LiNi}_x\text{Co}_y\text{Mn}_z\text{O}_2$ , where  $x + y + z = 1$ . According to the ratio, NCM battery can be categorized as NCM333 (1:1:1), NCM523 (5:2:3), NCM622 (6:2:2) and NCM811 (8:1:1), etc. NCM with Ni content  $< 60\%$  is conventional NCM material. NCM with Ni content  $> 60\%$  is Ni-rich ternary material. NCA belongs to Ni-rich ternary material.

$\text{LiNi}_x\text{Co}_y\text{Mn}_z\text{O}_2$  is hexagonal crystal lattice, which can be regarded as combination of laminar  $\text{LiMn}_2\text{O}_4$  and  $\text{LiMO}_2$  (M can be Ni, Co and Mn). Valences of Co and Mn are +3 and +4, respectively. When  $x:z = 1:1$  (NCM333 or NCM424), valence of Ni is +2, and NCM is symmetric. When  $x:z \neq 1:1$  (NCM523 or NCM622), Ni valence is combination of +2 and +3, and NCM is unsymmetric.

The thermal stability, capacity retention and capacity density of NCM material are shown in Fig. 2.5 (Xiong and Shen 2019).

#### 2.1.4.4 Lithium Titanate Battery

Lithium titanate material includes  $\text{Li}_4\text{TiO}_4$ ,  $\text{Li}_2\text{TiO}_3$ ,  $\text{Li}_4\text{Ti}_5\text{O}_{12}$  and  $\text{Li}_2\text{Ti}_3\text{O}_7$ .  $\text{Li}_4\text{Ti}_5\text{O}_{12}$  (LTO) is in spinel structure with safety, reliability and cycling stability, which has been applied in electric vehicles.

Structure of  $\text{Li}_4\text{Ti}_5\text{O}_{12}$  is shown in Fig. 2.6.

There is little volume change for lithium titanate during charge and discharge, therefore it is also called zero-strain material. Compared with graphite material in anode, voltage plateau of lithium titanate is 1.5 V vs.  $\text{Li}/\text{Li}^+$ . Therefore, lithium plating is avoided in anode, which makes lithium titanate battery safer.

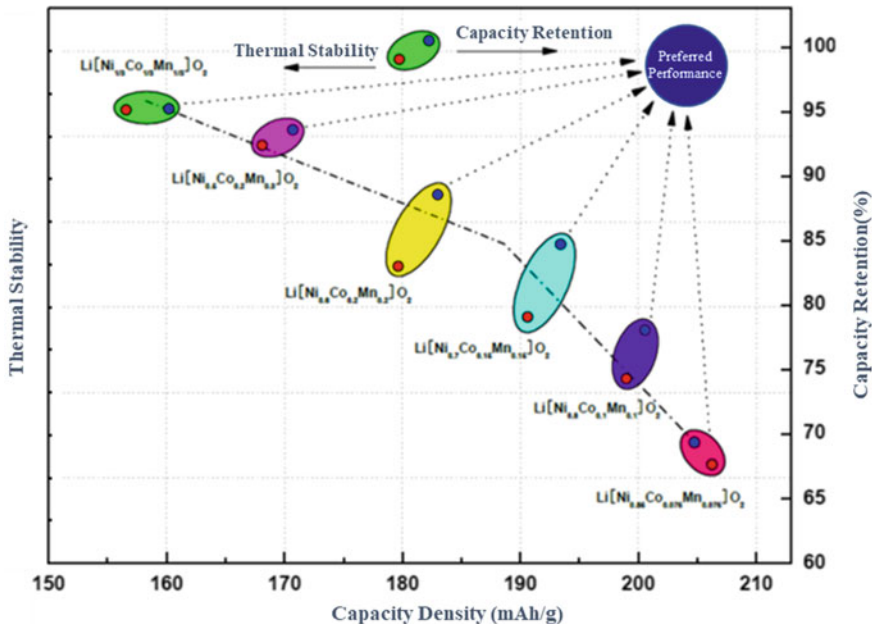


Fig. 2.5 Performance diagram of ternary materials with different components

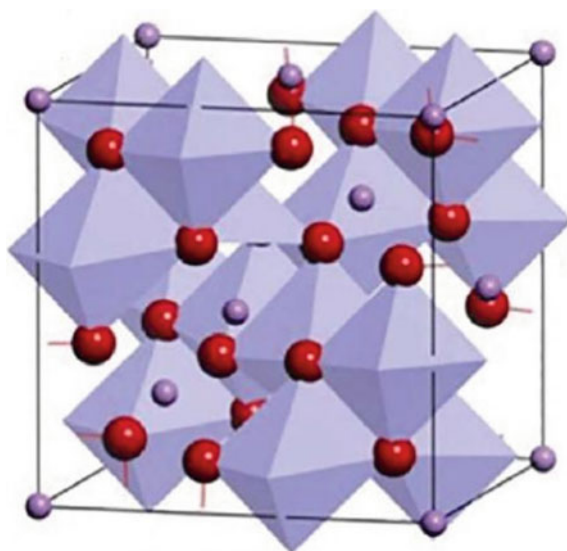


Fig. 2.6 Diagram of  $\text{Li}_4\text{Ti}_5\text{O}_{12}$  crystal structure

LTO battery supports fast charging with charge rate reaching 10 or 20 °C under wide range of working temperature. However, the voltage plateau is low and energy density is also low.

## 2.2 Performance Parameter of Power Battery

### 2.2.1 Nominal Parameter

#### 2.2.1.1 Battery Capacity

Capacity is the available charge from a battery under certain discharge condition. Capacity is denoted as  $C$  and with unit Ah. Capacity is categorized as theoretical capacity, rated capacity and practical capacity.

Theoretical capacity is the total charge under the condition that all active materials are reacted. Theoretical capacity is denoted as  $C_T$ . Theoretical capacity can be calculated by mass of active material according to Faraday law as:

$$Q = nF \frac{m}{M} \quad (2.13)$$

where  $Q$  is charge in reaction in unit (Ah),  $n$  denotes gained or lost electrons,  $m$  is mass of active material in unit (g),  $F$  is Faraday constant and  $M$  is molar mass in unit (g/mol).

Theoretical capacity can be calculated by:

$$C_T = 26.8n \frac{m_0}{M} \quad (2.14)$$

where  $m_0$  is mass of electrodes in reaction.

Rated capacity is the lowest available capacity from a battery under certain condition (e.g. temperature, cutoff voltage and charge rate) when the battery is fabricated.

Practical capacity is the real charge under certain discharge condition and is denoted as  $C_P$ . Practical capacity is time integral of discharge current:

$$C_P = \int_{t_0}^{t_{cut}} i(t) dt \quad (2.15)$$

where  $t_0$  is the initial time,  $t_{cut}$  is the time when battery reaches cutoff voltage and  $i(t)$  is discharge current during discharge.

Under constant current discharge, the practical capacity is measured as:

$$C_P = IT \quad (2.16)$$

where  $I$  is constant discharge current and  $T$  is the time period before cutoff voltage is reached.

Since the current is determined by the current rate, suffix  $C$  shows the current rate the battery is discharged at.

Due to the internal resistance, active material is not fully reacted. Therefore, the practical capacity and rated capacity are always lower than theoretical capacity.

When battery is discharged at a high current rate, polarization becomes aggressive and voltage lowers down quickly, practical capacity of the battery is low. When current rate is low, polarization is weak and voltage lowers down slowly, practical capacity of the battery is high, even higher than rated capacity.

### 2.2.1.2 Battery Voltage

Electromotive force is an important index showing the discharge ability of battery. It is also called as equilibrium potential which is the difference of voltage potential between positive and negative. Electromotive force is usually denoted as  $E$ :

$$E = \psi_+ - \psi_- \quad (2.17)$$

where  $\psi_+$  is positive potential at equilibrium and  $\psi_-$  is negative potential at equilibrium.

Open circuit voltage is voltage potential difference between positive and negative when there is no flowing current. Open circuit voltage is denoted as  $U_{ocv}$ . Open circuit voltage is determined by active material, electrolyte, concentration and temperature etc. and is irrelevant of battery structure and size. Open circuit voltage is usually lower than electromotive force.

Working voltage is voltage potential difference when battery is under load and denoted as  $U_{cc}$ . When battery is in discharge, working voltage is lower than open circuit voltage and electromotive force due to polarization resistance and Ohmic resistance:

$$U_{cc} = E - IR_i = E - I(R_\Omega + R_f) \quad (2.18)$$

where  $R_i$  is battery internal resistance,  $R_\Omega$  is Ohmic internal resistance and  $R_f$  is polarization resistance.

Working voltage is affected by discharge time, discharge current, working temperature and cutoff voltage.

Rated voltage is used to differentiate batteries of different chemistries. Rated voltage for lead-acid, Ni-Mh, LFP and LTO batteries can be different.

Discharge cutoff voltage is the lowest working voltage that is still suitable for discharge. Discharge cutoff voltage is affected by form factors and working condition. When battery is discharged below cutoff voltage, battery may be destroyed and accident may happen.

Similar to discharge cutoff voltage, maximum voltage when a battery is in charge is charge cutoff voltage.

## **2.2.2 *Electric Parameter***

### **2.2.2.1 Internal Resistance**

Internal resistance is the resistance in current when batter is in use. It includes Ohmic resistance  $R_\Omega$  and polarization resistance  $R_f$ .

Ohmic resistance is from electrodes materials, electrolyte, separator and contact resistance of all components. Ohmic resistance is related with temperature, capacity, degradation, size, structure and assembly.

Polarization is the phenomenon when electrode potential deviates from equilibrium potential as current flows through electrode. Polarization resistance is generated from electrochemical reactions from anode and cathode. Polarization resistance contains electrochemical polarization resistance and concentration polarization resistance. Polarization resistance is affected by current, temperature, active material and fabrication etc. Electrochemical polarization and concentration polarization will increase with current density and can even cause passivation on electrodes interfaces which increases resistance. Under low temperature, electrochemical polarization and ion diffusion is weak and polarization is increased.

### **2.2.2.2 Discharge/Charge Current**

Discharge/charge current significantly affect the battery performances. Discharge/charge current is usually denoted by rate.

Discharge/charge rate is the rate between discharge/charge current and rated capacity. For example, the C rate for 2 A current in a 10 Ah cell is 0.2 C. Similarly, the C rate for 15 A current in a 10 Ah cell is 1.5 C.

Hour rate is the hours used in the full discharge of a cell at certain current. For example, hour rate for 10 A current in a cell with 50 Ah rated capacity is 5 h. The lower hour rate is, the higher the current is.

Suffix of the capacity is used to show the C rate, because the practical capacity is affected by current rate. To present capacity in a rigorous way, capacity should be given along with the C rate.

### 2.2.2.3 Energy

Battery converts chemical energy into electricity. Battery energy is calculated by the charge that battery can provide externally with unit Wh. The chemical energy in the electrochemical system can be calculated by Gibbs free energy.

The battery theoretical energy  $W_T$  is the maximum work battery does under isothermal pressure condition, and is written as:

$$W_T = -\Delta G = nFE \quad (2.19)$$

The battery practical energy  $W_A$  is the energy that battery exerts under certain working condition. It can be calculated by the integral of current and terminal voltage product, which is written as:

$$W_A = \int U(t)I(t)dt \quad (2.20)$$

In the practical application of electrical vehicle, practical energy can be estimated by the product of capacity and rated voltage. The estimated energy is written as:

$$W_A = C_R U_R \quad (2.21)$$

Energy density is the energy per volume or mass.

The specific energy or mass energy density is the energy per mass. It is the rate between energy and mass  $m$ . The unit of specific energy is Wh/kg. The specific energy is written as:

$$W' = \frac{W}{m} \quad (2.22)$$

The volumetric energy density is the battery energy per volume. It is the rate between battery energy and battery volume  $V$ . The unit of volumetric energy density is Wh/L. The volumetric energy density is calculated by:

$$W' = \frac{W}{V} \quad (2.23)$$

### 2.2.2.4 Power

Battery power  $P$  is the battery output energy in unit time. The unit of battery power is W or kW.

Battery power density is the output power for unit volume or mass of battery.

Mass power density is the rate between power and mass  $m$ . The unit of mass power density is W/kg. Mass power density is calculated by:

$$P' = \frac{P}{m} \quad (2.24)$$

The volumetric power density is power in unit volume. It is the rate between power and volume  $V$ . The unit of volumetric power density is W/L. The volumetric power density is calculated by:

$$P' = \frac{P}{V} \quad (2.25)$$

## 2.2.3 Other Parameters

### 2.2.3.1 Lifetime

Battery lifetime includes cycling lifetime and calendar lifetime.

Cycling lifetime is the maximum cycling number when the capacity reaches cutoff value under certain cycling condition. A cycle involves a charge and a discharge process. Cycling lifetime is affected by charge/discharge rate, depth of discharge and temperature etc.

Calendar lifetime is the time period when capacity is reduced to certain value since the battery capacity is fabricated. There are dry storage and wet storage ways. In wet storage way, battery is stored with electrolyte inside and the lifetime is shorter than that in dry storage.

### 2.2.3.2 Self Discharge

Self discharge is the capacity loss from unexpected chemical reaction. Self discharge arises from thermodynamic instability of electrodes and their redox reactions.

There are reversible and irreversible capacity loss in self discharge. In reversible self discharge, the lost capacity can be recovered during the recharging process. While in irreversible self discharge, capacity can not be recovered.

Self discharge is affected by electrode materials, fabrication process, storage temperature and storage period etc. Self discharge rate is used to describe the rate of self discharge capacity loss and is written as:

$$R_{sd} = \frac{C_0 - C(T)}{C_0 T} \quad (2.26)$$

where  $T$  is storage time,  $C_0$  is initial capacity and  $C(T)$  is remaining capacity at time  $T$ .

## 2.3 Development and Trend of Power Battery

As energy storage system, the performances of power battery determine market acceptance. Energy density is a primary factor for electric vehicle as it limits the mileages of electric vehicles. Power density is dominating in hybrid electric vehicles. Although lead-acid batteries are cheap, their energy and power density are lower than other battery types and there are metal contamination issues for lead-acid batteries. The energy density and power density of Ni–Cd batteries are higher than that of lead-acid batteries. However, the application of Ni–Cd batteries is limited by Cd pollution and memory effect. The cycling lifetime and energy density are low for Ni–MH batteries. Until now, lithium-ion batteries are promising energy storage solutions as they perform well in terms of energy density, power density and lifetime.

As shown in Fig. 2.7, there are mainly three types of lithium-ion batteries according to the geometry: prismatic cell, cylindrical cell and pouch cell. lithium-ion battery is composed of anode, cathode, separator, electrolyte, current collector and casing. The anode material includes LCO, LFP, LMN, NMC and NCA, to name a few. Cathode material includes graphite, LTO and silicon carbon composites, silicon and silicon alloy. Electrolyte is composed of high concentration organic solvent, lithium salt and additives. Organic solvent can be PC, EC and EMC, etc. Lithium salt involves



**Fig. 2.7** Main packaging forms of lithium-ion batteries

$\text{LiPF}_6$  and  $\text{LiPF}_4$ . Separator material is PP, PE, double-layer PP/PE and triple-layer PP/PE/PP membrane.

Cathode material is the most expensive above all the components in lithium-ion batteries. The comprehensive performance of lithium-ion batteries is better than other types of batteries. lithium-ion batteries are applied in electric vehicles and hybrid electric vehicles. Potentially lithium-ion batteries are promising solution of energy storage.

For power batteries, there are requirements such as safety, lifetime, energy density, power density, maintenance, cost and environmental issue. The cost, lifetime, charge rate and safety limits the development of lithium-ion batteries and these are the key research aspects.

Compared with laptop, cell phone and UPS, the working condition for lithium-ion batteries in electric vehicles is more complex. For example, the wider working temperature range, drive cycle and high C rate discharge/charge are challenging issues. High temperature accelerates the side reactions and degradation and causes safety issues such as thermal runaway. Low temperature is detrimental to battery performances and causes short circuits due to pierced separator in lithium plating degradation mode. The requirement on safety for power battery is higher than electronic devices. Safety issues from electrochemical, mechanical and environmental aspects are to be studied.

Power battery lifetime includes cycling lifetime, working lifetime and calendar lifetime. Cycling lifetime is the cycle numbers before capacity is lowered down to certain value (e.g. 80% of rated capacity) under certain working conditions such as discharge current, temperature and cutoff voltage. Working lifetime is the battery lifetime under certain working conditions. Calendar lifetime is the time period from the manufacturing to failure. How to improve lifetime under complicated working conditions is the research issue.

The battery system with high energy density is being promoted by the demand on longer mileages. More research aspects involve cathodes materials with high Ni purity, silicon materials of anodes, solid electrolyte, lithium-sulphur battery, lithium-air battery, sodium-air battery. Performances of energy density, power density, stability, safety and lifetime are considered in the design of lithium-ion batteries.

Until now, the geometry of lithium-ion batteries has not been unified. Therefore, the many choices of varieties and sizes increase the cost in research and are detrimental to mass production such as platform production and modular production and optimization for second-use of batteries. Standardization of lithium-ion battery geometry is to be developed.

## References

- Deng L, Wu F, Gao X, Wu W (2020) Development of a LiFePO<sub>4</sub>-based high power lithium secondary battery for HEVs applications. *Rare Met* 39:1457–1463
- Feng X, Ouyang M, Liu X et al (2018) Thermal runaway mechanism of lithium ion battery for electric vehicles: a review. *Energy Storage Mater* 10:246–267
- Goodenough JB, Park K (2013) ChemInform abstract: the Li-ion rechargeable battery: a perspective. *ChemInform* 44:1167–1176
- Han X, Lu L, Zheng Y, Feng X, Li Z, Li J, et al (2019) A review on the key issues of the lithium ion battery degradation among the whole life cycle. *eTransportation* 1:100005
- Ma H, Fa A, Mohameda (2014) Hybrid electric vehicles and their challenges: a review. *Renew Sustain Energy* 29:135–50
- Lu L, Han X, Li J et al (2013) A review on the key issues for lithium–ion battery management in electric vehicles. *J Power Sources* 226:272–288
- Senyshyn A, Mühlbauer MJ, Dolotko O, Ehrenberg H (2015) Low-temperature performance of Li-ion batteries: the behavior of lithiated graphite. *J Power Sources* 282:235–240
- Xiong R, Shen W (2019) Advanced battery management technologies for electric vehicles. Wiley, Chichester
- Xiong R, Chen H, Wang C, Sun F (2018) Towards a smarter hybrid energy storage system based on battery and ultracapacitor - a critical review on topology and energy management. *J Clean Prod* 202:1228–1240

# Chapter 3

## Key Technologies of BMS



### 3.1 Overview of BMS

The main differences between traditional fuel vehicles and electric vehicles are that electric vehicles are powered by batteries. Power batteries are the indispensable parts of electric vehicles. Battery Management System (BMS) is the core technique for battery packs. BMS is designed to improve safety, reliability of batteries, increase discharge rate, extend lifetime and prolong mileages. BMS is a significant connection of battery pack, whole vehicle system and motor. BMS optimize the power and mileage for electric vehicle since single cell has limited capacity and voltage. Battery packs are composed of battery cells in series or in parallel. BMS monitors battery modules and manages batteries according to battery parameters such as current, voltage, internal resistance and capacity. BMS conducts calculation, gives order, executes and gives warning. For battery modules of low performances, BMS is important. Therefore, BMS is studied by researchers around the world. Although single cells have different form factors and performances, they have similar functions.

The framework of BMS is shown in Fig. 3.1 (Xiong et al. 2020; Liu et al. 2019; Rao and Wang 2011; Li et al. 2016a).

#### 3.1.1 BMS Architecture

According to the framework, there are centralized and distributed BMS.

In centralized BMS, central control unit and data acquisition unit form the managing units and collect basic information such as voltage, current and temperature. The collected data is analyzed in processor. Centralized BMS is of low cost, compact structure and reliability and is common in small battery systems with low capacity, voltage and volume.

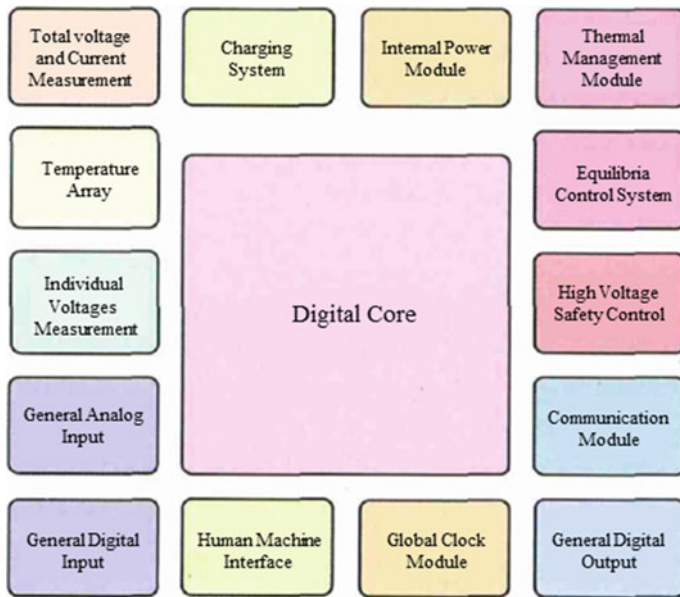


**Fig. 3.1** BMS software and hardware framework for vehicle

Distributed BMS conducts management in module and pack levels. Slave board detects voltage and temperature and conducts management. Motherboard estimates states of battery system, conducts management on switches, temperature, running, charging, diagnosis and communication. A typical distributed BMS framework is shown in Fig. 3.2.

The working principle of BMS is: data acquisition units collect battery states and these information are processed and analyzed by control units. Commands and communications are made according to the analysis results.

BMS hardware is designed based on the functionalities demanded on battery system and whole vehicle. The common functions include sampling (of voltage, current and temperature), charging port detection (CC and CC2), charging wake up (CP and A+), relays control, states diagnosis, insulation detection, voltage interlocking, collision detection, CAN communication and data storage.

Main controller acquires information from controller and high-voltage controller, analyzes and controls battery states, conducts troubleshooting and provides solutions.

High-voltage controller collects real-time battery voltage and current, provides accurate data for calculating SOC and SOH and realizes precharge and insulation.

Slave controller collects cell information of voltage, temperature, SOC and SOH and provide feedback. Slave controller also conducts passive balancing to minimize inhomogeneity of cells. Communications between sampling chip and main chip are conducted by CAN and daisy chain. CAN is more stable but the cost is high considering power chips and isolation circuits. In principle, daisy chain is SPI communication. Cost of daisy chain is low but stability is worse than CAN. Limited by the

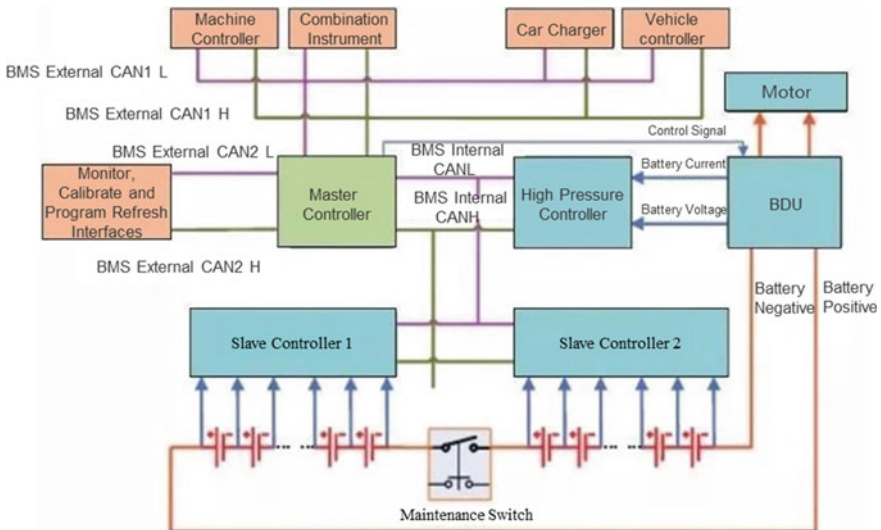


**Fig. 3.2** Schematic diagram of BMS distributed architecture

cost, manufacturers are considering daisy chain more. Communication stability can be enhanced by implementing more daisy chains.

### 3.1.2 Sampling Chip

BMS designs are more based on integrated data acquisition chips and application schemes from IC manufacturers. The main companies for BMS design include: Maxim, Linear Technology (owned by ADI), Intersil, TI, ADI, NXP and Infineon.

#### 3.1.2.1 Maxim Solution

Maxim product series schemes include 12 cells. Maxim battery monitor (MAX172XX series), protector (DS277X series) and battery selector (MAX1538) prolong battery lifetime efficiently and improve safety and reliability of battery system. High-voltage devices help to realize low-carbon schemes and minimize geometry, cost and design complexity of BMS. The schematic of Maxim product is shown in Fig. 3.3.

Features of Maxim products:

1. Simplification on battery pack design. 12 monitoring channels. Capacitor isolation SMBus communication with fewer units and lower cost. Serial cells up

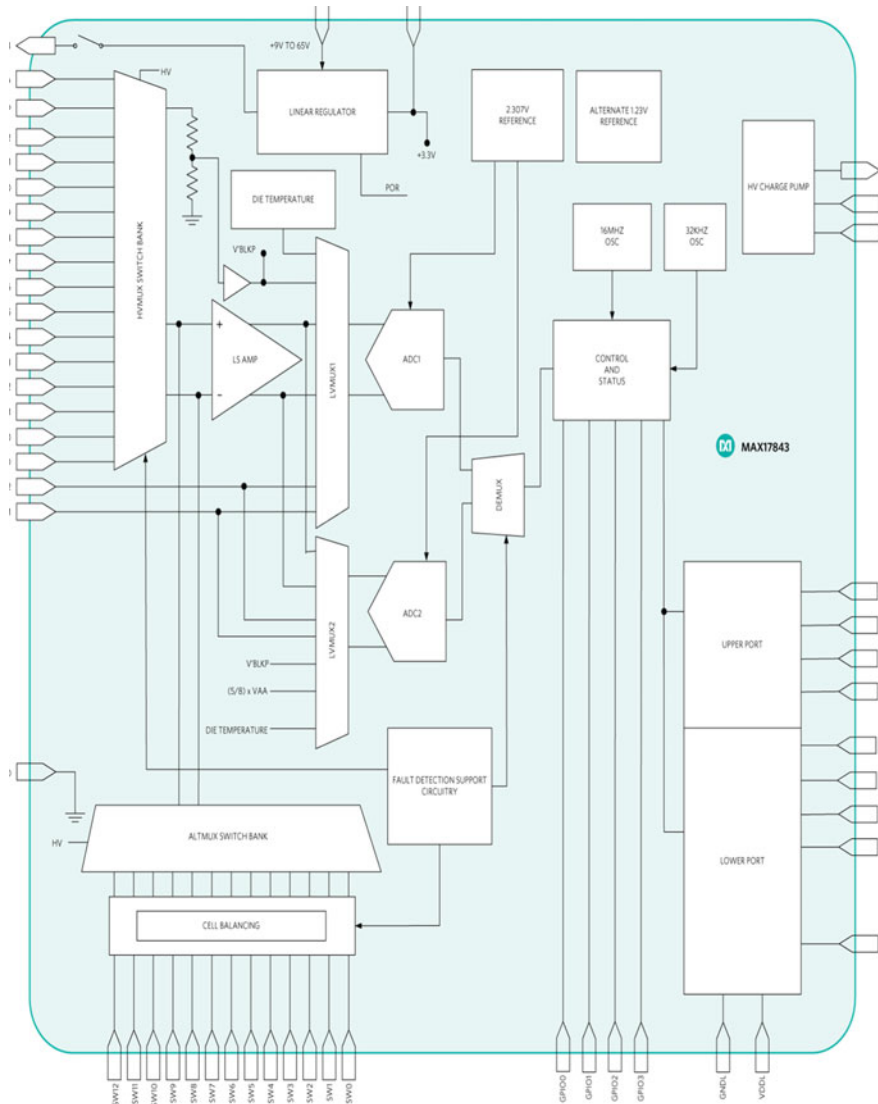


**Fig. 3.3** Maxim solution application diagram

- to 31 cells. Up to 372 cells monitored. Low-cost capacitor isolation between battery packs.
2. High voltage and small BiCMOS with ESD protection ( $\pm 2$  kV for human safety). Hot swapping. AEC-Q100 passed in wide working temperature range with reliability.
  3. Consideration of voltage from 12 channels and one high-voltage switch with fault tolerance. High-speed 12-bit ADC. Two-phase scanning with correction

on acquired data. Simultaneous voltage measurement with high accuracy and fast speed: voltage of 120 cells is measured within 10  $\mu$ s.  $\pm 0.25\%$  error in rated working temperature range.  $\pm 20$  mV error in AEC-Q100 type 2 temperature range.

4. Reduced power consumption by 10 times with 100 $\mu$ A in working mode and prolonged battery lifetime. Unique internal switches lower down power consumption (1 $\mu$ A current drain) so that battery can maintain for several years.
5. For electric vehicle application, configuration and self diagnosis modes are implemented, which is important for safety monitoring. The Maxim series can work under extreme environments such as magnetic field and transient noise. High current, strip line and onboard monitoring are used in IC testing for reliability. Open and short circuit on pin can be diagnosed and FMEA standard is passed.

### 3.1.2.2 Linear Technology Solution

Linear technology monitors multiple cells and supports high voltage monitoring. 12-bit ADC, accurate voltage reference, multiplexer of high voltage input and a serial interface are implemented inside. All these units are connected to monitor each cell without using optical coupler equipment or optical isolator.

LTC6804-1/LTC6804-2 is designed for vehicle or transportation. AEC-Q100 is sealed inside. The framework is shown in Fig. 3.4.

Features of Linear technology products:

1. Voltage of 12 cells in series monitored. Stacked structure supports hundreds of cells.
2. isoSPITM input inside, fast communication speed 1Mbps, 100 m single twisted pair, low EMI sensitivity and radiation.
3. Error within 1.2 mV. All measurements made in 290  $\mu$ s. Simultaneous voltage and current measurement.
4. Programed third order filter with incremental 16-bit ADC.
5. For system of ISO26262 standard. Passive balancing using timer.
6. 5 general digital I/O or simulation input. Temperature sensor input. One I2C or SPI controller.
7. 4 $\mu$ A current at sleep mode.

### 3.1.2.3 Intersil Solution

ISL78600 monitors up to 12 cells in series. It supports accurate monitoring, battery balancing and diagnosis. There are three modes: manual control mode, timing balancing mode and automatic balancing mode. The end of automatic mode indicates that charge transfer has reached the value calculated by micro-precessor. The framework is shown in Fig. 3.5.

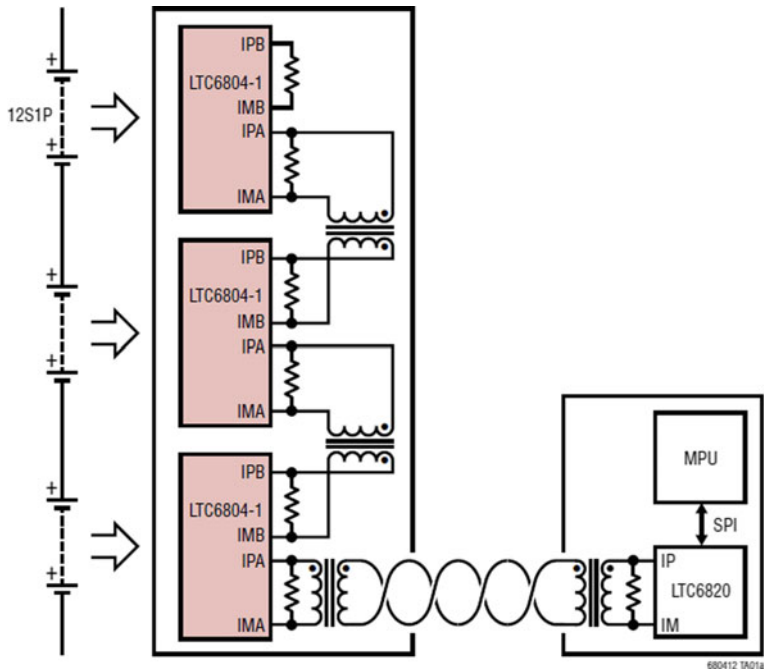


**Fig. 3.4** Linear technology solution application diagram

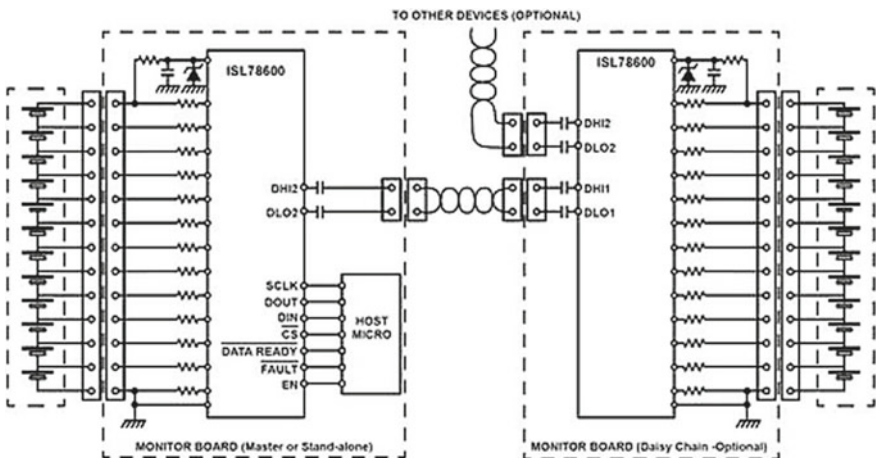


**Fig. 3.5** Intersil BMS solution diagram

The solution of HEV/EV follows ISO26262 (ASIL) standard. Internal error diagnosis is conducted. Several external errors can also be detected such as: circuit failure, over voltage, under voltage, temperature and balancing.

Intersil BMS provides accuracy that is high enough in charging process to prolong mileages and lithium-ion battery lifetime. Each chip adopts 14-bit data converter that considers temperature effects. 12 channels are scanned in 250  $\mu$ s. To improve stability, communication of noise cancelling and fault tolerance abilities are realized. The differential daisy chain structure connects stacked battery packs using cheap twisted pair and it avoids hot swap and high transient voltage. Intersil solution significantly reduces the cost of BMS. ISL78600 supports 2.5 MHz SPI or 400 kHz I2C ports for connection with micro-controller. The temperature range is  $-40$  to  $+105$   $^{\circ}$ C.

### 3.1.2.4 TI Solution

TI monitors and protects 3–16 cells and has other functions of external IC. Key parameters such as voltage, current and temperature are collected by monitor and then transferred to micro-controller. Simple diagnosis (over potential) and advanced diagnosis (more index) are conducted by protector. The errors include over voltage, under voltage, over current and short circuiting. TI solution also approves and identifies battery packs and components (such as charging cable and printer cartridge). External IC improves battery pack capacity by techniques such as active balancing technique (ACB). The framework is shown in Fig. 3.6.

The energy transferring efficiency reaches 87% for DC-DC active balancing. EM1410 is composed of 5 core chips and 5 powering chips. The main chip EMB1432 is AFE chip with 14 channels. EMB1428 is controller chip with 7 channels. EMB1499 is voltage controller chip with 7 channels. These chips are used to conduct balancing bi-directionally, control 14 cells in series and reach 60 V voltage. It provides 5 V balancing voltage and 750 V output voltage and passes AECQ-100 standard for vehicle.

### 3.1.2.5 ADI Solution

AD7280A implemented all functions for monitoring stacked lithium-ion batteries. Voltage can be added to multiple circuits. ADC measuring channel can be used for management of up to 6 cells.  $\pm 3$  ppm internal reference voltage is provided with accuracy of  $\pm 1.6$  mV. ADC resolution is 12-bit and it only takes 7  $\mu$ s to convert 48 units. The framework is shown in Fig. 3.7.

AD7280A is powered by single VDD with 8–30 V voltage range and 33 V maximum rated voltage. There are 6 differential simulation channel inputs. Input signal is 1–5 V (VIN (+) to VIN (-)). 6 stacked cells in series are allowed. 6 ADC input channels are implanted for temperature measurement and system diagnosis. Relays can be progressed according to different application requirements. Real-time

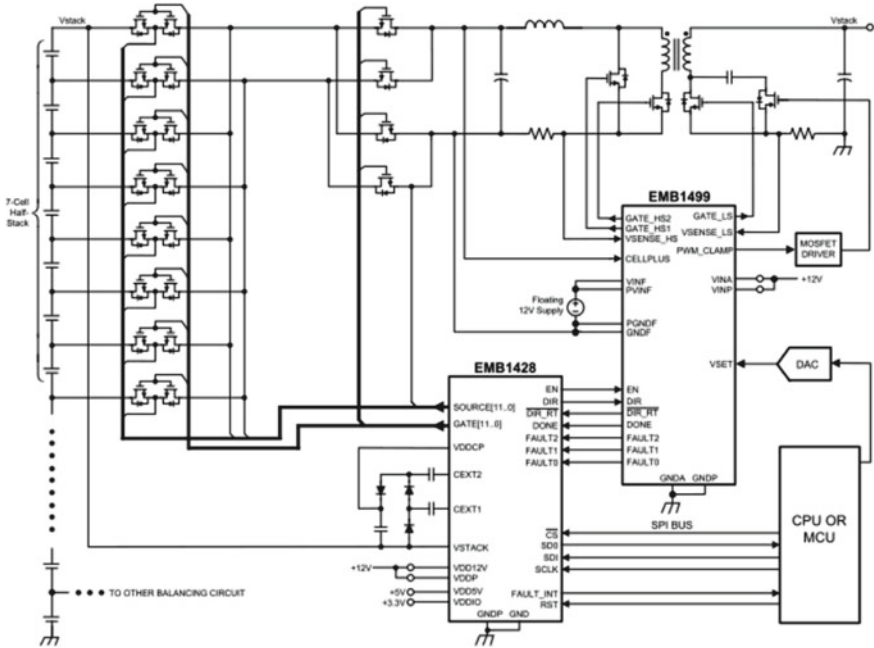


**Fig. 3.6** TI BMS solution diagram

notification is supported for monitoring of ADC input. Balancing output controls external FET transistor and all cells can discharge. For self testing, a known voltage can be imposed on ADC. In daisy chains, up to 8 devices can be stacked and no extra isolation is needed. Only one power pin is needed with power consumption of 6.5 mA and transferring speed is 1MSPS.

### 3.1.2.6 NXP Solution

MC33771 includes main functions including measuring current and voltage. The accuracy is 2 mv within 65  $\mu$ s, which qualifies ISO 26262 ASIL-C standard. Implanted function testing and diagnosis make the product pass ISO 26262 ASIL-C standard. No external circuit is needed. Stable adaptor used for daisy chain differential transceiver. Voltage of 3750 V is isolated. Communication speed reaches 2 Mbps and no CAN is used. The same adaptor with voltage isolation function is connected with dual SPI input of MCU. Less material is needed with robust isolation function qualified for ASIL-C standard. The framework is shown in Fig. 3.8.

MC33771 and MC33664 communication units prolong the battery lifetime. Daisy chain is used in controllers and the expensive CAN is avoided. Micro-controller, adaptor and CAN isolation layers are not required. Cost is lowered down and design process is simplified.

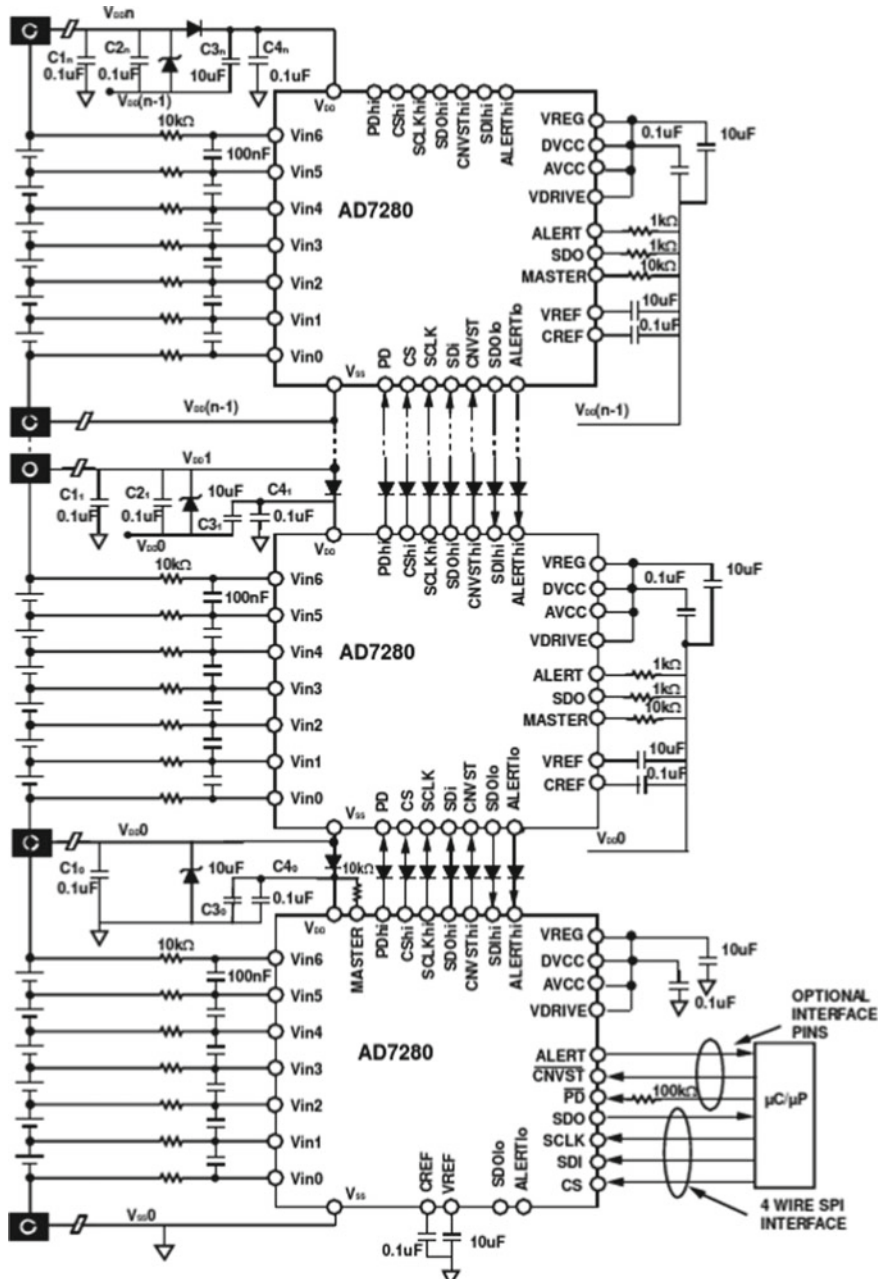


Fig. 3.7 AD7280A application diagram

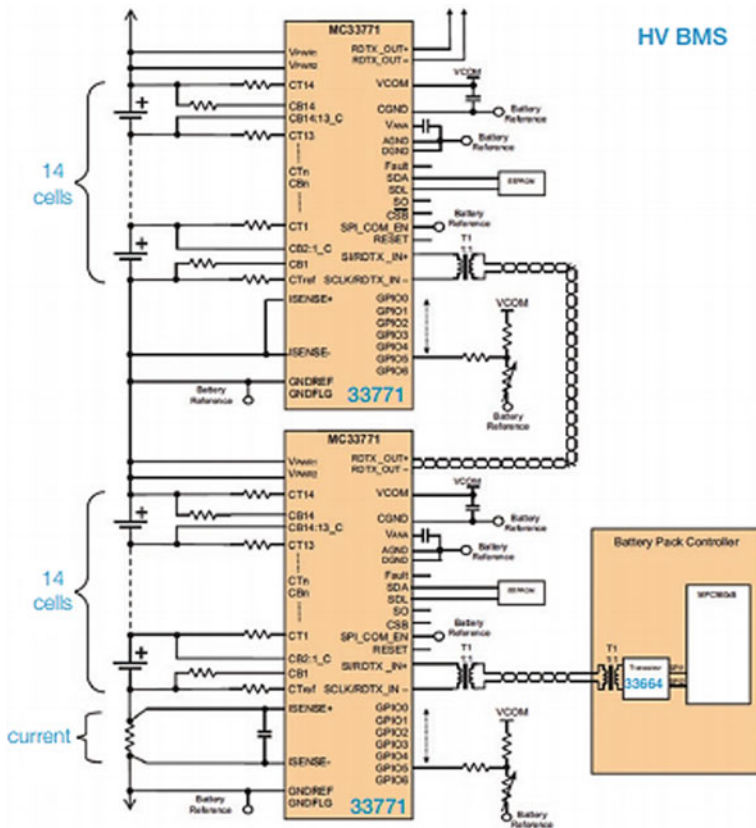


Fig. 3.8 NXP application diagram

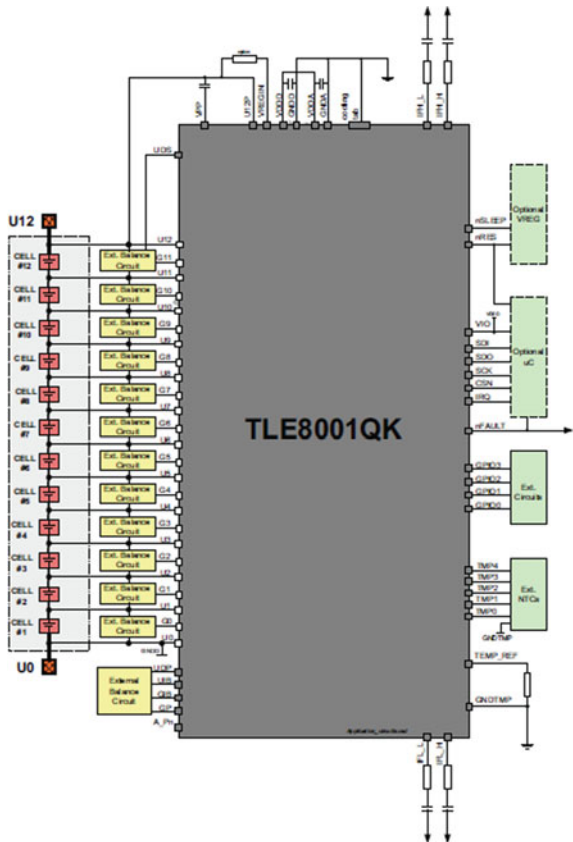
### 3.1.2.7 Infineon Solution

As one of the leading companies in semi-conductor industry, Infineon releases BMS chip TLE8001. The framework is shown in Fig. 3.9.

Main features:

1. 12 cells in series monitored;
2. 12 ADC monitoring all voltage. Filters implanted with 13-bit resolution;
3. 5 temperature sensor branches;
4. Internal temperature sensor;
5. Supports passive and active balancing;
6. Integrated MOSFET with low resistance;
7. High-speed differential COM (IBCB);
8. Wide cover on diagnosis and protection;
9. Allows random connection of all cells;
10. Low standby current;

**Fig. 3.9**  
TLE8001 application  
diagram



11. AEC-Q100 passed;
12. Two independent internal voltage sources. Double monitoring on each unit. Safety standard ISO26262.

## 3.2 Core Functions of BMS

The main functions required in BMS standard released by International Electro Commission (IEC) in 1995 include: SOC display, temperature information, high temperature alarm, electrolyte information, performance anomaly warning, degradation information and crucial data recording.

Power battery is developed along with electric vehicles. The standard requirement of BMS is increased as well. BMS on electric vehicle is complicated. BMS is designed according to different batteries. Main functions of BMS include: data collecting,

state estimation, balancing, thermal management, discharge/charge management, communication and alarming.

BMS also covers voltage control and charge management. BMS is activated by 12 V voltage of hard wire or CAN conducted by VCU. After BMS self-diagnosis is completed, high-voltage command is released from VCU. Relays are closed by BMS control and high voltage is turned on. To turn off the high voltage, 12 V voltage from VCU will call BMS. CP or A+ signal is used in plug-in situation. There are slow charging and fast charging modes. In slow charging mode, AC is transformed into DC and charged into batteries. Procedures are easy and charging time is long. In fast charging mode, DC from charging pile is charged into batteries and 1C and higher C rates are applied. Fast charging is called by A+ signal. The procedure of fast charging is complicated and over charging and temperature should be controlled to avoid accelerated degradation.

### **3.2.1 Parameter Collection**

There are many parameters to describe battery performances, such as voltage, capacity, internal resistance, temperature and current. Voltage provides reference for over charge and over discharge. Terminal voltage is used in SOC estimation. Current can also be used in judging over charge and over discharge and SOC estimation. Temperature significantly affects capacity, voltage, internal resistance, discharge/charge rate, lifetime, safety and inhomogeneity.

Collection of necessary data is the basic for BMS so that batteries are managed effectively and lifetime is prolonged. Data accuracy, sampling rate and filtering are important. Sampling rate frequency should be higher than 1/s considering the voltage, current and temperature changing rate. Basic measurements for BMS include voltage, current and temperature information and insulation diagnosis are required for the whole system especially high-voltage system. High voltage interlock loop (HVIL) diagnosis is conducted to check the feedback in the high-voltage system. Safety schemes are in action when feedback loop is broken.

Information on battery voltage, current, charging state, insulating resistance and switches are collected by main controller. Slave controller collects real-time voltage and temperature and upload them. CAN and daisy chain are used to communicate between sampling chips and main chips. Compare with daisy chain, CAN is more stable but more expensive considering power chips and isolating circuits. In principle, daisy chain is SPI communication. Daisy chain is less expensive and less stable. More companies are adopting daisy chain with the reduced cost and improved performances.

### 3.2.2 State Estimation

Battery states include state of charge (SOC), state of health (SOH), state of power (SOP), state of safety (SOS) and state of energy (SOE). SOC describes the available capacity. SOH shows the battery health state and is calculated by capacity or resistance change. SOP shows the peak power in a time period. SOE shows the ratio of remnant energy and rated energy. Safety of battery is estimated by SOS.

SOC is one of the most important parameters of BMS and provides the reference on charge/discharge and balancing controlling. SOH provides information on usage, maintenance and economy. SOS, SOF and SOE describe the battery from the aspects of safety, function and energy, respectively. The relation of all states is shown in Fig. 3.10. SOC is the basic of BMS, and SOC is affected by SOH. SOP is determined by SOC, SOH and SOS. SOE is affected by SOC, SOH, temperature and future working conditions. All these states can not be easily estimated due to the non-linearity in battery behaviors. Conventional SOC estimation methods include: OCV, internal resistance and Ah counting. More methods are developed such as fuzzy logic model, self-adaptive neural model, Kalman Filter, linear regression and impedance spectra method. Ah counting is common and can be combined with other methods such as resistance and OCV. The combined methods have higher accuracy than Ah counting method. The framework of BMS estimation methods is shown in Fig. 3.10 (Lu et al. 2013; Deng et al. 2016; Li et al. 2016b).

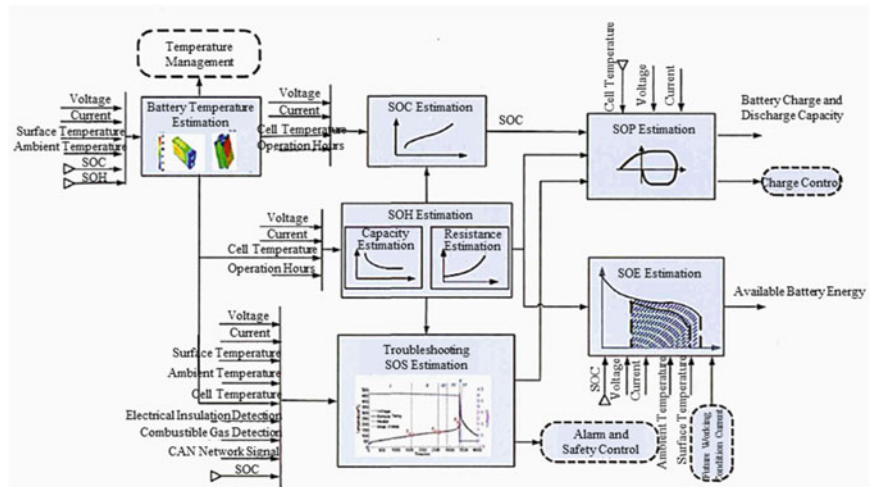


**Fig. 3.10** BMS state estimation algorithm framework

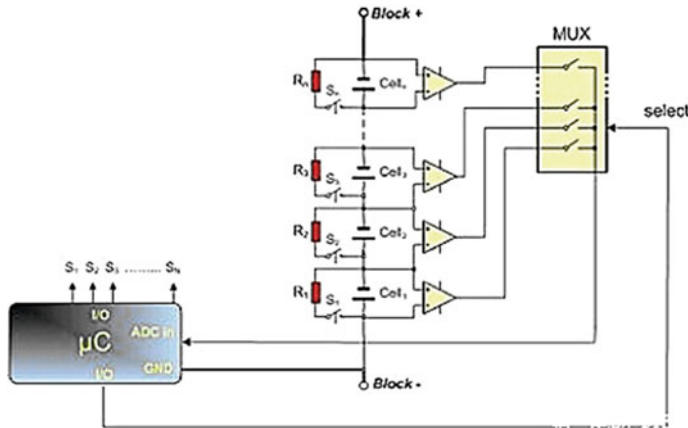


**Fig. 3.11** Schematic diagram of passive balancing circuit

### 3.2.3 Balance Management

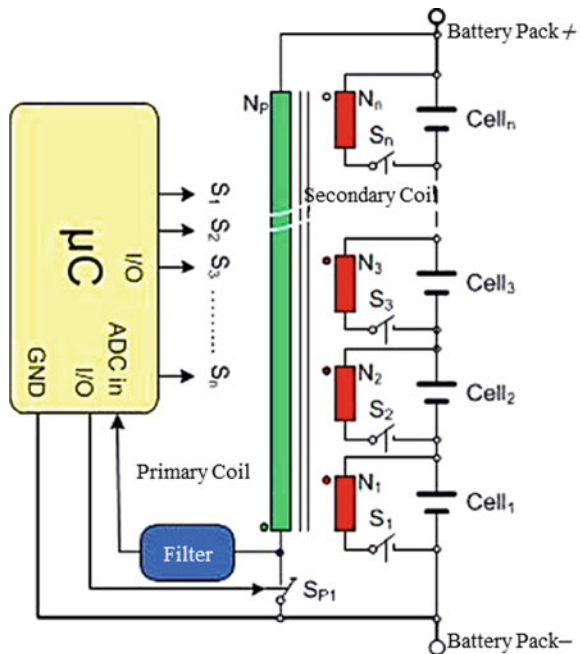
Battery cells are different due to the differences made in manufacturing process. There are differences in capacity, internal resistance, self-discharge rate and charging rate. Due to the cell differences, capacity and lifetime of battery pack are reduced. The inhomogeneities and consequent lifetime within the battery packs will deteriorate with time under temperature and vibration condition. Battery balancing management is designed to reduce the deterioration (Xiong et al. 2017; Lin et al. 2017; Bergveld et al. 2002).

Passive balancing scheme and active balancing scheme are as schematically shown in Figs. 3.11 and 3.12, respectively. In passive balancing scheme, the remnant capacity is released through resistance. The circuit is simple and reliable with low cost. However, the battery efficiency is lowered down and the generated heat in passive balancing is detrimental to battery pack. In active balancing scheme, the over-charge can be transferred to cell of high capacity. The efficiency of battery pack is higher than in passive balancing but the circuits are more complex and less reliable with higher cost.

### 3.2.4 Thermal Management

TMS is one of the most important components of BMS. TMS maintains the battery temperature in a suitable temperature range by close loop of heat conducting media, measuring and controlling units and temperature controlling devices. As a result, the performances and lifetime are improved. TMS functions include cooling, preheating and balancing. For cooling, battery is effectively cooled when battery temperature is

**Fig. 3.12** Schematic diagram of active balancing circuit



high to avoid thermal runaway. For preheating, battery is heated to improve performances and safety under low temperature. Cooling and preheating are designed to respond to the external working condition. For balancing, temperature inhomogeneity is reduced within the cell to avoid degradation at hotter place.

There are air cooling, liquid cooling and cooling using PCM. Air cooling and liquid cooling are commonly applied. The schematic of air cooling is shown in Fig. 3.13. Air is used as heat conducting media. The structure is simple and light. Ventilation efficiency is high even with hazardous gas with low cost and no leaking

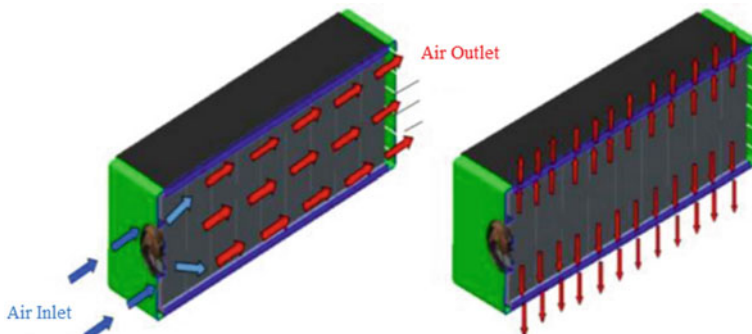
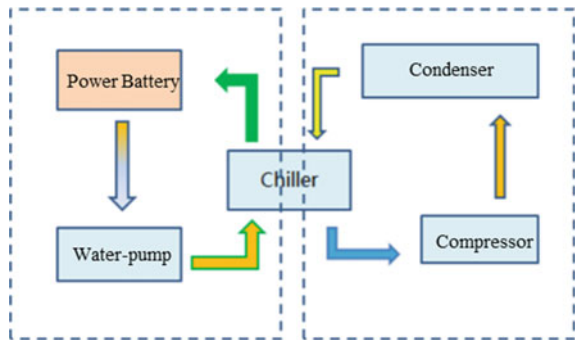


**Fig. 3.13** Schematic diagram of battery air cooling

**Fig. 3.14** Schematic diagram of battery liquid cooling



danger. However, the convection heat coefficient is low. The schematic of liquid cooling is shown in Fig. 3.14. The generated heat is rejected through liquid to reduce temperature. The heat convection coefficient is higher than that in air cooling. In liquid cooling, temperature and temperature gradient are eliminated efficiently. However, liquid cooling system is heavy and design is complex. Maintenance cost is high and there is leaking danger. There are requirements on sealing, mechanical strength, vibration and lifetime.

### 3.2.5 Communication

Data communication is one of the most significant parts of BMS. Apart from the real-time communication between motherboard and slave board, there are communication inputs to BMS from vehicle controller, charging controller, DCDC, dashboard, gateway and motor etc. Until now, CAN is adopted for external communication. CAN and daisy chain are adopted for internal communication. CAN is robust but its cost is high. Daisy chain is not suitable for long-range communication and is applied more in HEV. CAN is applied more on bus. Wireless communication or power line carrier can be made on intelligent battery modules. Both ways reduce BMS space and reduce the complexity of internal circuits. However, the reliability and anti-interference ability are worse than CAN.

Until now, CAN is adopted commonly. Therefore, power system is connected to external communication system (vehicle and charger) through CAN. CAN is a serial communication way that supports distributed control or real-time control. Communication media can be twisted pair, coaxial cable or optical fiber. CAN conducts long-range reliable communication under magnetic field with low cost. CAN is invented by BOSCH in 1980s and it is a communication protocol designed to exchange data between controllers and actuators. In network of CAN, any node can send message to other nodes. Network nodes are prioritized according to the urgency of real-time requests. 8b short frame structure is used in data link layer for easy correction.

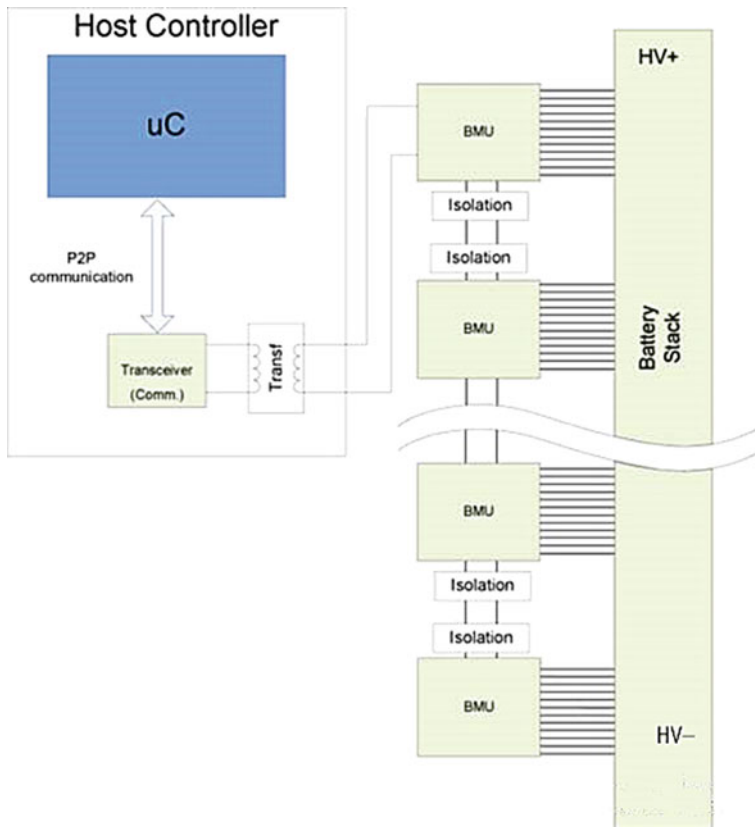


**Fig. 3.15** BMS daisy chain communication framework

Twisted pair and optical fiber are adopted with 1 Mb/s speed and 110 nodes. Service address is abandoned. High fault tolerance and reliability are realized.

BMS daisy chain communication framework is shown in Fig. 3.15. Each BMU has an input port and an output port. These I/O ports are connected to each other. BMU #N – 1 sends data to BMU #N which sends its data to BMU #N + 1. Compared with CAN, if somewhere is disconnected in daisy chain, data will still be communicated. However, workload and power of BMU is high.

### 3.2.6 Malfunction Diagnosis

Battery malfunction includes sensor malfunction, error of actuators (e.g. switch, fan, pump and heater), network error and other errors in hardware and softwares. The battery cell error includes overpotential (overcharge), undervoltage (overdischarge),

**Table 3.1** Malfunction classification

Status classification	Malfunction situation	Treatment measures
Level I malfunction	Does not affect the operation of the entire vehicle, may affect the life of the power system, or may fail in the future	Remind the vehicle driver or management personnel to pay attention, do not need to understand or take measures in detail. The power system needs maintenance
Level II malfunction	Affect the operation of the whole vehicle, and safety accidents may occur	Send an alarm signal to the vehicle controller, send a strong current signal through the battery failure redundant protection through line, and trip the strong current relay to avoid the expansion of the battery pack failure

overcurrent, ultrahigh temperature, short circuiting, electrolyte leaking and insulator failure. BMS performs diagnosis on error type based on the collected data and alarm in early stage.

The malfunctions of battery system are classified according to different battery behaviors. BMS and VCU respond by taking different precautions, giving warnings and even cutting voltage. For example, the errors can be classified into class I and class II (Table 3.1). Class II is serious error. In this error, requests of cutting voltage are made through CAN. In some BMS strategies, if controller does not respond for a certain time period, BMS will be forced to powered off for safety. Class I error is warning error. When class I error is indicated through CAN, main controller will adjust controlling parameters to reduce the workload on batteries and reduce current and power to avoid damaging batteries.

## References

- Bergveld HJ, Kruijt WS, Notten PHL (2002) Battery management systems. Springer, Netherlands
- Deng Z, Yang L, Cai Y et al (2016) Online available capacity prediction and state of charge estimation based on advanced data-driven algorithms for lithium iron phosphate battery. Energy 112:469–480
- Li J, Han Y, Zhou S (2016a) Advances in battery manufacturing, services, and management systems. Wiley, Hoboken
- Li Y, Chattopadhyay P, Xiong S et al (2016b) Dynamic data-driven and model-based recursive analysis for estimation of battery state-of charge. Appl Energy 184:266–275
- Lin C, Yu Q, Xiong R et al (2017) A study on the impact of open circuit voltage tests on state of charge estimation for lithium-ion batteries. Appl Energy 205:892–902
- Liu KL, Li K, Peng Q et al (2019) A brief review on key technologies in the battery management system of electric vehicles. Front Mech Eng 14(1):47–64
- Lu L, Han X, Li J et al (2013) A review on the key issues for lithium-ion battery management in electric vehicles. J Power Sources 226:272–288
- Rao Z, Wang S (2011) A review of power battery thermal energy management. Renew Sustain Energy Rev 15(9):4554–4571

- Xiong R, Cao J, Yu Q et al (2017) Critical review on the battery state of charge estimation methods for electric vehicles. *IEEE Access: Pract Innov Open Solutions* PP(99):1
- Xiong R, Pan Y, Shen WX et al (2020) Lithium–ion battery aging mechanisms and diagnosis method for automotive applications: recent advances and perspectives. *Renew Sustain Energy Rev* 131

## **Part II**

# **State Estimation Methods**

# Chapter 4

## Battery Model



Lithium ion batteries (LIBs) have become the favorite choice as the power sources for electric vehicles (EVs) due to the advantages such as long service life, high energy and power density and environmental friendliness, etc. The operating conditions of the LIBs in EVs vary with the environment, and the BMS is key to ensuring system safety, longevity and high efficiency.

LIBs show highly nonlinear dynamics, and the battery performance and ageing process depend on the operating conditions, such as temperature, C-rate, depth of discharge and cycle number. A battery model is required to capture accurately the battery dynamics and the ageing process.

The battery model used in EVs needs to meet several requirements due to the computational and memory constraints of the onboard BMS, including ease of parametrization, reliable parameter identification, accurate model parameters and high computational efficiency, etc. The widely used battery models include electrochemical models, equivalent circuit models (ECMs) and black-box models, as shown in Fig. 4.1.

Electrochemical models are derived from the chemical/electrochemical laws and the transport equations governing the battery's internal reaction process. The model uses coupled partial differential equations with boundary conditions to explain the dynamic mass transport process between the battery's positive and negative electrodes. The model has high accuracy at the expense of high computational complexity. It is difficult to implement electrochemical models in real-time in the onboard BMS. Therefore, researchers have proposed many simplified models.

Equivalent circuit models (ECMs) use electrical elements, such as resistors, capacitors and voltage source to simulate the terminal voltage-current dynamics of the battery. The dependency of the battery's properties on the operating condition, e.g., temperature, is usually captured by linear time-varying parameters. Although the model accuracy is low compared with the electrochemical models, the ECMs have several advantages, including simple model structure, ease of parametrization and real-time implementation. The ECMs have been widely used for model-based battery

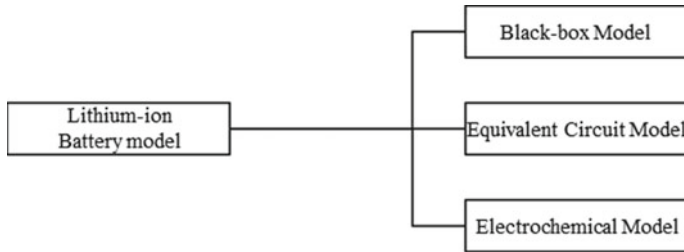


**Fig. 4.1** Different types of battery models

state estimation and real-time control and simulation. Fractional order ECMs have also been proposed recently, e.g., using constant-phase elements to replace the RC networks, in order to improve the model accuracy.

Black-box models capture the battery dynamics using linear or nonlinear mapping techniques, while a prior knowledge of battery mechanics is not required for the model development. However, the model performance depends strongly on the quality of the training data set. Therefore, it is challenging to improve the generalization performance of black-box models.

Model parametrization is an essential step of model development for lithium ion batteries. The parameter identification algorithm has a strong impact on the model accuracy and reliability. Model parameters can be identified offline or online. Look-up tables are usually used in the offline parameter identifications to describe the parameter dependency on the operating conditions. The test data collection can be time-consuming because the battery dynamics depend on many factors, such as battery temperature and ageing conditions. On the other hand, the online parameter identification algorithms can adapt and update the model parameters in real-time according to the time-varying environment and operating conditions, which can facilitate industrial implementation. The popular parameter identification algorithms for battery models include Kalman filter and Least Squares methods, etc.

## 4.1 Electrochemical Models

### 4.1.1 Pseudo-Two-Dimensional (P2D) Model

Electrochemical models describe the battery dynamics using the physical principles that govern the battery's internal reactions. The model can capture the distribution of lithium ion concentration and the reaction rate and distribution profiles. Therefore, electrochemical models have been widely used for analyzing the battery performance and physical properties. Electrochemical models usually involve coupled nonlinear equations, and the computational expense is high. Doyle et al. (1993) and Newman

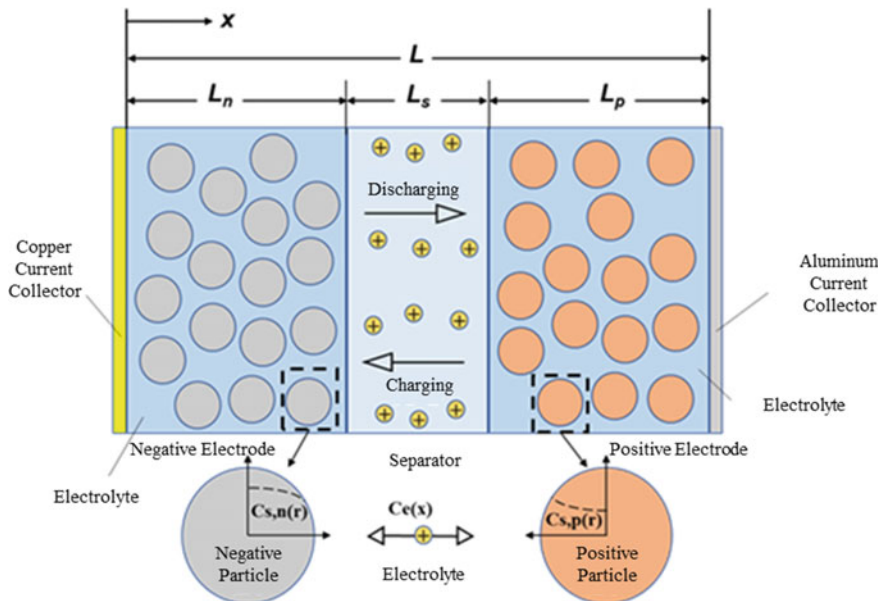


**Fig. 4.2** Illustration of the P2D model

et al. (2003) first proposed the classic pseudo-two-dimensional (P2D) model based on the porous electrode theory and concentrated solution theory.

In the P2D model, the battery is represented with a sandwich structure, which consists of the negative and positive electrodes (with current collectors), separator and electrolyte, as shown in Fig. 4.2 (Jokar et al. 2016; Dao et al. 2012). The electrodes are represented by a group of sphere particles immersed in the electrolyte. The P2D model can capture the dynamic intercalation and de-intercalation process of lithium ion at the solid–liquid interface and the concentration of lithium ion in the thickness direction ( $x$ ) of the electrode and the radial direction ( $r$ ) of the particles.

The Fick's second law is used in the P2D model to describe the diffusion process and the concentration profile of lithium ions in the electrode particles. The concentration distribution of lithium ion in the electrolyte and separator is governed by the charge conservation and mass conservation laws. The Ohm's law governs the potential profile in the solid phase, and the potential in the liquid phase is calculated using the Krichhoff's law and Ohm's law. The reaction dynamics at the solid–liquid interface are described by the Butler-Volmer equation.

Therefore, the model consists of the diffusion and potential equations in the solid and liquid phases, charge conservation equation and the Butler-Volmer equation. The concentrations of lithium ion in the time and spatial dimensions (e.g., thickness direction of the electrode and radial direction of the particles) are captured. These equations are summarized in Table 4.1.

**Table 4.1** A list of the P2D model equations (Zhang et al. 2000; Doyle et al. 1996; Fuller et al. 1994; Rahman et al. 2016; Shen and Li 2016)

Phase	Control equation	Explanation
Positive electrode	$\frac{\partial C_{s,p}(x,t)}{\partial t} = D_{sp} \frac{\partial}{\partial x} \left( \rho^2 \frac{\partial C_{s,p}(x,t)}{\partial r} \right)$	Li <sup>+</sup> concentration in solid phase
	$\varepsilon_p \frac{\partial C_{e,p}(x,t)}{\partial t} = \frac{\partial}{\partial x} \left( D_{eff,p} \frac{\partial C_{e,p}(x,t)}{\partial x} \right) + a_p(1-t_+)J_p(x,t)$	Li <sup>+</sup> concentration in liquid phase
	$\sigma_{eff,p} \frac{\partial^2 \phi_{s,p}(x,t)}{\partial x^2} = a_p F J_p(x,t)$	Potential equation
	$-\sigma_{eff,p} \frac{\partial \phi_{s,p}(x,t)}{\partial x} - \kappa_{eff,p} \frac{\partial \phi_{e,p}(x,t)}{\partial x} + \frac{2k_{eff,p}RT}{F} (1-t_+) \frac{\partial \ln C_{e,p}}{\partial x} = I$	
	$J_p(x,t) = K_p \left( c_{s,p,\max} - c_{s,p,surf} \right)^{0.5} c_{e,p}^{0.5}$ $\times \left[ \exp\left(\frac{0.5F\mu_{s,p}(x,t)}{RT}\right) - \exp\left(-\frac{0.5F\mu_{s,p}(x,t)}{RT}\right) \right]$	B-V equation
	$\mu_{s,p}(x,t) = \phi_{s,p}(x,t) - \phi_{e,p}(x,t) - U_p$	Overpotential
	$V_{cell}(t) = \phi_{s,p}(0,t) - \phi_{s,n}(L,t)$	Terminal voltage
	$\varepsilon \frac{\partial C_e(x,t)}{\partial t} = \frac{\partial}{\partial x} \left( D_{eff} \frac{\partial C_e(x,t)}{\partial x} \right)$	Li <sup>+</sup> concentration in solid phase
	$-\kappa_{eff} \frac{\partial \phi_e(x,t)}{\partial x} + \frac{2k_{eff}RT}{F} (1-t_+) \frac{\partial \ln C_e}{\partial x} = I$	Potential equation
	$\frac{\partial C_{s,n}(x,t)}{\partial t} = \frac{D_{sn}}{\rho^2} \frac{\partial}{\partial r} \left( \rho^2 \frac{\partial C_{s,n}(x,t)}{\partial r} \right)$	Li <sup>+</sup> concentration in solid phase
Separator	$\varepsilon_n \frac{\partial C_{e,n}(x,t)}{\partial t} = \frac{\partial}{\partial x} \left( D_{eff,n} \frac{\partial C_{e,n}(x,t)}{\partial x} \right) + a_n(1-t_+)J_n(x,t)$	Li <sup>+</sup> concentration in liquid phase
	$\sigma_{eff,n} \frac{\partial^2 \phi_{e,n}(x,t)}{\partial x^2} = a_n F J_n(x,t)$	Potential equation
	$-\sigma_{eff,n} \frac{\partial \phi_{s,n}(x,t)}{\partial x} - \kappa_{eff,n} \frac{\partial \phi_{e,n}(x,t)}{\partial x} + \frac{2k_{eff,n}RT}{F} (1-t_+) \frac{\partial \ln C_{e,n}}{\partial x} = I$	
	$J_n(x,t) = K_n \left( c_{s,n,\max} - c_{s,n,surf} \right)^{0.5} c_{e,n}^{0.5} \times \left[ \exp\left(\frac{0.5F\mu_{s,n}(x,t)}{RT}\right) - \exp\left(-\frac{0.5F\mu_{s,n}(x,t)}{RT}\right) \right]$	B-V equation
Negative electrode	$\mu_{s,n}(x,t) = \phi_{s,n}(x,t) - \phi_{e,n}(x,t) - U_n$	Over-potential
		(continued)

**Table 4.1** (continued)

Phase	Control equation	Explanation
	$V_{\text{cell}}(t) = \phi_{\text{s,p}}(0, t) - \phi_{\text{s,n}}(L, t)$	Terminal voltage

The P2D model complexity and computational expense are very high, making it unsuitable for onboard BMS applications. To solve this problem, researchers have proposed battery models with reduced complexity.

#### 4.1.2 Single Particle Model (SPM)

The single particle model (SPM) was proposed by Zhang et al. in 2000 to simplify the P2D model, as shown in Fig. 4.3.

In the SPM, each electrode is represented by a single sphere particle, neglecting the concentration difference of lithium ion and potential difference at different locations along the thickness direction of the electrode. The computational expense of the SPM is significantly reduced compared with the P2D model, making it suitable for online estimation of battery states.

Similar to the SPM model, researchers have proposed multiple-particle models, which use multiple particles with different radiuses to represent the electrode to study the battery characteristics.

## 4.2 Black-Box Model

Black-box models have been used for simulating the behaviors of the lithium ion battery, which is a highly complex and highly nonlinear electrochemical system. Black-box models use linear or nonlinear mapping functions to capture the battery characteristics, and the knowledge of the physical principles of the battery is not required for model development. As a result, the model lacks physical interpretation. However, black-box models show high flexibility in terms of the model structure and parametrization. Currently, the widely used black-box models for lithium ion batteries include neural-networks (NN) and support vector machine (SVM).

NN can simulate the biological process in human brains. The NN model needs to be trained to capture the battery characteristics. The model consists of input layer, hidden layer and the output layer, and each layer includes a number of neurons. Each neuron is connected with the neurons of the previous layer through weight factors. The weight factors are optimized during the model training procedure to generate

**Fig. 4.3** Battery SPM

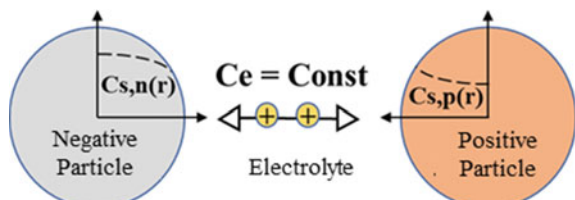
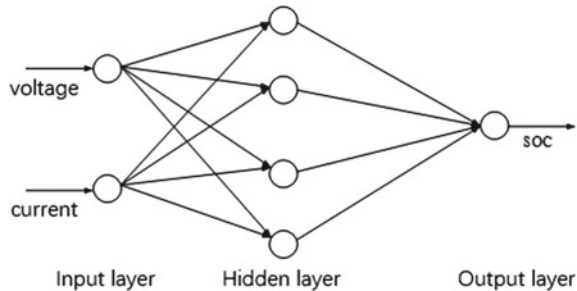


**Fig. 4.4** Battery SOC estimation using Neural Networks



the expected output. The classic NN model is shown in Fig. 4.4 for SOC estimation. Other types of NNs, including the feedforward NN and deep-learning NN, have also been used for battery models.

The existing NN models are mainly used in big-data analytic systems while data are collected from real-world vehicles. The developed model can capture the static and dynamic characteristics of the battery in real-time operations. The performance of the NN models depends strongly on the training data set. The model can achieve high accuracy within the range of the training data set. However, the generalization performance cannot be guaranteed, and the model accuracy can degrade significantly outside the range of the training data set.

The SVM method is based on the statistic learning theory. The algorithm aims to find the hyperplane that is furthest from the data samples. It has advantage in terms of sparsity and robustness. The proper choice of the kernel functions according to the modelling objective is important for the model performance, which is also challenging when implementing the algorithm. The SVM can be used as a classifier in the BMS to categorize the individual cells in a battery module according to their charging/discharging capacities to identify and separate the strong and weak cells, which is of high importance to the state estimation of the battery pack/module. The conventional SVM is an offline modeling method and relies on the offline selection and adaption of the kernel functions, making it difficult for real-time implementation in the onboard BMS systems in EVs.

Long short-term memory (LSTM) neural network is an improved recurrent neural network (RNN) architecture with long/short-term memory gates, as shown in Fig. 4.5. The LSTM has a memory unit which encapsulate the notion of forgetting part of the stored old information and adding new information. The LSTM NN models have been used for battery SOC and SOH estimation. However, the estimation performance depends strongly on the training data set. The LSTM NN can also suffer from over-fitting as other NN methods. Further, the model performance also depends on adjustable parameters, which results in poor generalization capability for different battery chemistries, or even under different operating conditions for the same battery type.

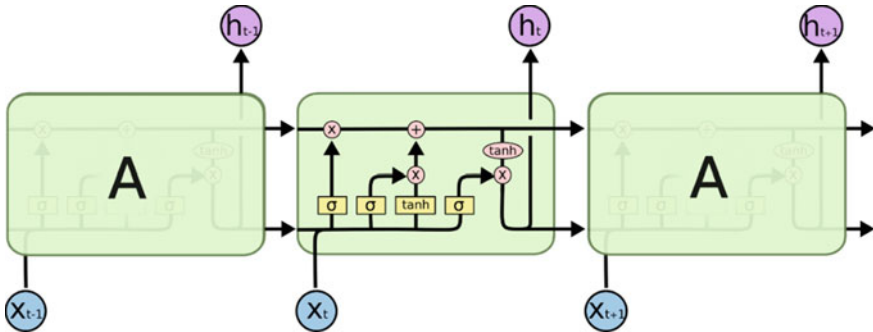


**Fig. 4.5** Illustration of the LSTM Neural Networks

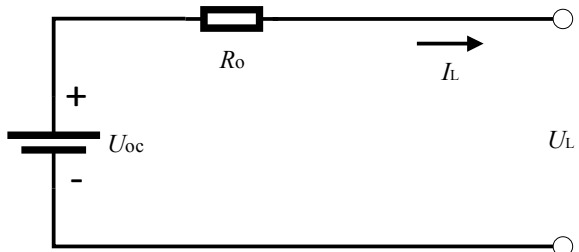
### 4.3 Equivalent Circuit Model (ECM)

ECM uses electrical elements, such as voltage source, resistors and capacitors, etc., to simulate the battery's terminal behavior. The advantages of ECM include the simple model structure, low number of parameters and low computational expense, which facilitates onboard implementation in the BMS. The widely used ECMS include the resistance model, RC model, the PNGV model and fractional order ECMS.

#### 4.3.1 Resistance Model

The resistance model is the simplest ECM, which consists of an ideal voltage source  $U_{oc}$  and a series resistor  $R_o$ , as shown in Fig. 4.6.  $U_L$  and  $I_L$  represent the battery's terminal voltage and current, respectively.  $U_{oc}$  and  $R_o$  are in turn the open-circuit voltage and the internal resistance of the battery. Both  $U_{oc}$  and  $R_o$  depend on the battery SOC, SOH and temperature.

**Fig. 4.6** Battery resistance model



### 4.3.2 RC Model

The RC model of lithium ion batteries uses RC networks in addition to the resistance model. This can improve the model accuracy under dynamic operating conditions. The model equations can be put in state-space form. The widely used RC models include the Thevenin model (with 1 RC network) and the DP model (with 2 RC networks), as shown in Fig. 4.7.

The Thevenin model can capture the battery's internal polarization overpotential. However, the model accuracy is low at the end of discharge. To address the problem, the DP model can be used with the two RC networks to represent the concentration polarization and electrochemical polarization process, respectively, as shown in Fig. 4.7, where  $R_{p1}$  and  $R_{p2}$  stand for the resistance of the electrochemical and concentration polarization, respectively, and  $C_{p1}$  and  $C_{p2}$  are used to capture the dynamics of the polarization process.

The model equations are given in Eq. (4.1) according to the Kirchhoff's law,

$$\begin{cases} U_o = R_o i_t \\ i_t = U_p / R_p + C_p dU_p / dt \\ U_t = U_{OCV} - U_p - U_o \end{cases} \quad (4.1)$$

The above equation can be discretized as follows,

$$\begin{bmatrix} SOC(k+1) \\ U_P(k+1) \end{bmatrix} = \begin{bmatrix} 1 & 0 \\ 0 & e^{-T_s/R_p C_p} \end{bmatrix} \begin{bmatrix} SOC(t) \\ U_P(t) \end{bmatrix} + \begin{bmatrix} -\frac{\eta T_s}{Q_c} \\ R_p (1 - e^{-T_s/R_p C_p}) \end{bmatrix} * I_k + w_k \quad (4.2)$$

And the terminal voltage is

$$U_t(k) = U_{ocv}(SOC) - U_p - R_o I_k + v_k \quad (4.3)$$

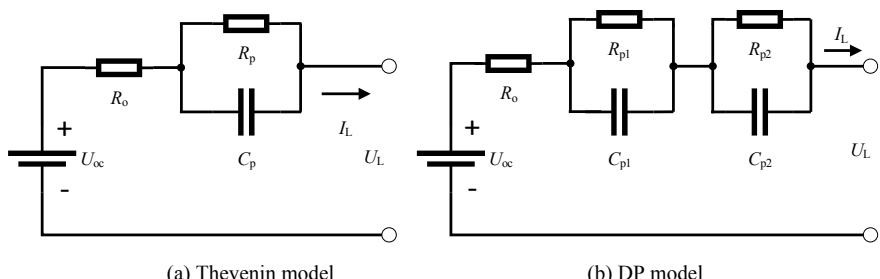


**Fig. 4.7** Battery RC models

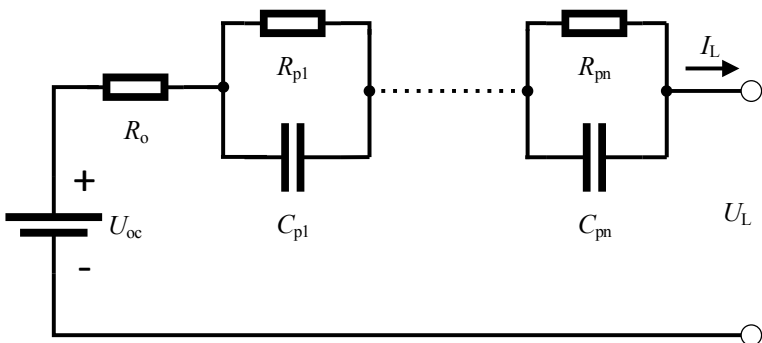
where,  $\mathbf{x}_k = [SOC \ U_p]^T$  is the state,  $\mathbf{u}_k = I_k$  is the input current,  $z_k = U_t(k)$  is the output voltage.  $w_k$  and  $v_k$  are the process and measurement noises, respectively. The covariance matrix of  $w_k$  and  $v_k$  are in turn  $\mathbf{Q}$  and  $\mathbf{R}$ .

More than two RC networks can be used in the ECM, leading to the n-th order RC model (usually,  $n \leq 4$ ), as shown in Fig. 4.8.

The PNGV model uses an additional capacitor based on the Thevenin model, as shown in Fig. 4.9 which can capture the potential change due to the accumulation of load current to improve the model accuracy. It can also take into consideration the polarization effect of the battery's reaction.

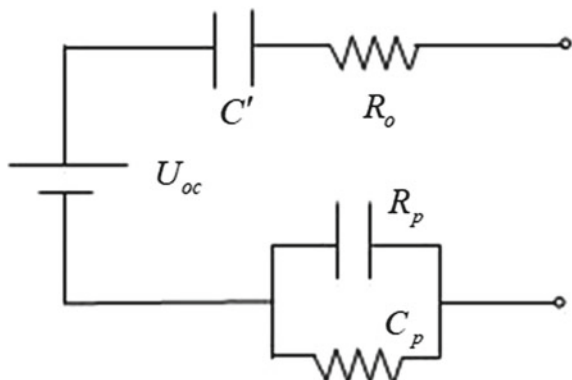
The inconsistency of the battery's OCV after charging and discharging can be described using a hysteresis element, as shown in Fig. 4.10.

The model accuracy depends on the parameters. However, these model parameters change with the battery's ageing, which can reduce the model accuracy if this effect is not taken into consideration.



**Fig. 4.8** Battery ECM with n RC networks

**Fig. 4.9** PNGV model



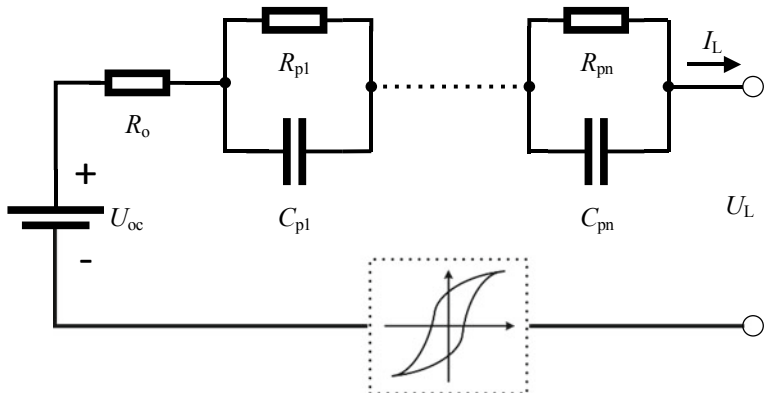


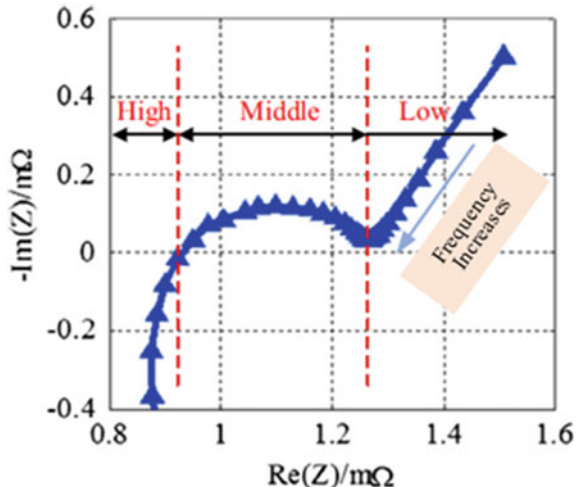
**Fig. 4.10** Battery OCV considering the OCV hysteresis

#### 4.3.3 Fractional-Order Model

The battery's frequency-domain electrochemical impedance spectroscopy (EIS) is measured using low-amplitude sine wave current excitation at a range of frequencies. EIS is a useful method for battery characterization. The Nyquist plot of a battery's EIS is shown in Fig. 4.11. The intersection point between the EIS curve and the real axis stands for the ohmic resistance; the semi-circle at middle frequency represents charge transfer process and the SEI layer effect; the low frequency part is due to the diffusion process of the lithium ions.

The fractional order model uses constant phase element (CPE) to replace the RC networks in the ECM in order to fit to the EIS curve, as shown in Fig. 4.12, where  $R_o$

**Fig. 4.11** Illustration of the battery EIS curve



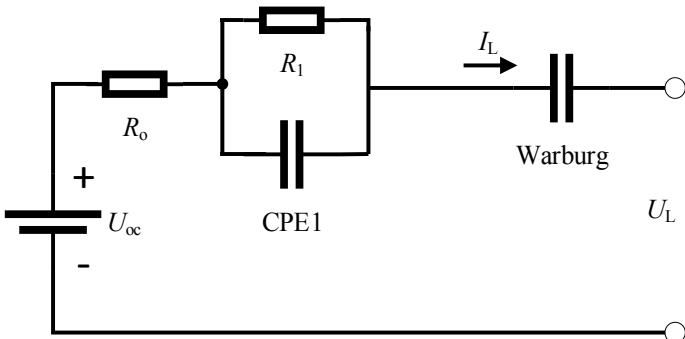


**Fig. 4.12** Battery fractional-order model

is the ohmic resistance.  $R_1$  and CPE1 in parallel are used to describe the polarization effect, and the diffusion effect is captured by the Warburg element.

The parameter identification of the fractional order model depends on the frequency-domain EIS data, which are generally obtained using electrochemical workstation. Researchers have also proposed to identify parameters of the fractional order model from time-domain test data using least squares method.

#### 4.4 Parameter Identification

Although the ECM can capture the battery characteristics with desirable accuracy under dynamic current load condition, the model performance depends significantly on the identified parameters. A poorly parametrized model can lead to large prediction error under certain operating conditions, especially outside the scope of the training data set. Since ECM is widely used for battery state estimation, a low model accuracy will also reduce the accuracy of the model-based state estimation. The state estimation results can fluctuate or even diverge. Therefore, the parameterization procedure is very important for the model's practical application.

Take the first order ECM as an example. The battery OCV can be characterized experimentally. The other parameters, i.e., the RC values, need to be identified by curve fitting techniques. There are offline and online parameter identification methods. The offline methods use optimization algorithms to find the optimal parameters within a wide parameter space that minimize a cost function. The root mean square error of the model's voltage prediction is usually used as the cost function. The popular offline parameter identification methods include the least squares method and intelligent optimization algorithms. On the other hand, for online parameter identification methods, the model parameters are usually formulated as the time-varying states of a linear system, which are tracked in real-time using online adaptive algorithms, such as the recursive least squares method and dual-Kalman filter method.

This section presents a summary of the commonly used parameter identification methods for battery models, with an analysis of the pros and cons of each method and the suitable application condition. The prospects of the parameter identification algorithms are also discussed.

#### 4.4.1 Offline Methods

##### 4.4.1.1 Least Squares Method

The parameter identification assumes that the system states are known, which is the inverse problem of state estimation where the model parameters are known. The least squares method is the fundamental algorithm for parameter identification with a long history and wide range of practical applications. Gauss proposed the least squares algorithm in 1975 to estimate the unknown parameters from observation data by minimizing the weighted root mean square error between the model's prediction and the measurements. The inverse of the measurement covariance is usually used as the weight. The least squares method has advantages of clear interpretability and simple implementation. It has been widely used for parameter identification of static and dynamics linear and nonlinear systems. The algorithm is illustrated in Fig. 4.13 using a single input single output (SISO) system as the example, where  $u(k)$  is the input and  $z(k)$  is the output. Both  $u(k)$  and  $z(k)$  are measurable. The model equations are given as follows.

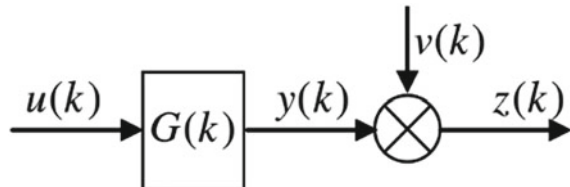
$$z(k) = y(k) + v(k) \quad (4.4)$$

$$\begin{aligned} & a_0y(k) + a_1y(k-1) + a_2y(k-2)K a_n y(k-n) \\ & = b_0u(k) + b_1u(k-1) + b_2y(k-2)K b_m y(k-m) \end{aligned} \quad (4.5)$$

Let  $a_0 = 1$  and  $m = n$ . From Eq. (4.2),

$$y(k) + \sum_{i=1}^n a_i y(k-i) = \sum_{i=0}^n b_i u(k-i) \quad (4.6)$$

**Fig. 4.13** The single-input-single-output system



The z-transfer function from  $u(k)$  to  $y(k)$  in the discrete time domain can then be obtained,

$$G(z) = \frac{y(z)}{u(z)} = \frac{b_1 z^{-1} + b_2 z^{-2} + K b_n z^{-n}}{1 + a_1 z^{-1} + a_2 z^{-2} + K a_n z^{-n}} \quad (4.7)$$

If the measurement noises are taken into consideration,

$$z(k) = - \sum_{i=1}^n a_i y(k-i) + \sum_{i=1}^n b_i u(k-i) + v(k) \quad (4.8)$$

Let  $(k)$  denote the  $k$ -th time step, and  $z(k)$  as the  $k$ -th noisy observation.  $y(k)$  and  $u(k)$  are in turn the true values of the  $k$ -th output and input.  $v(k)$  is a zero-mean random noise. Let  $h(k) = [-y(k-1), -y(k-2), \dots, y(k-n), -u(k-1), -u(k-2), \dots, -u(k-n)]$  and  $\theta = [a_1, a_2, \dots, a_n, b_1, b_2, \dots, b_n]^T$ .

From Eq. (4.8)

$$z(k) = h(k)\theta + v(k) \quad (4.9)$$

where  $\theta$  is the parameter vector to be identified. Let  $k = 1, 2, \dots, m$ . Equation (4.9) can be reformulated as

$$Z_m = \begin{bmatrix} z(1) \\ z(2) \\ M \\ z(m) \end{bmatrix} \quad (4.10)$$

$$H_m = \begin{bmatrix} h(1) \\ h(2) \\ M \\ h(m) \end{bmatrix} = \begin{bmatrix} -y(0) & K & -y(n-1) & u(0) & K & u(1-n) \\ -y(1) & K & -y(n-2) & u(1) & K & u(2-n) \\ M & M & M & M & M & M \\ -y(m-1) & K & -y(m-n) & u(m-1) & K & u(m-n) \end{bmatrix} \quad (4.11)$$

$$\theta_m = [a_1 K a_n \ b_1 K b_n]^T \quad (4.12)$$

$$V_m = [v(1) \ v(2) \ K \ v(m)]^T \quad (4.13)$$

$$Z_m = H_m \theta_m + V_m \quad (4.14)$$

where  $Z_m$  is the output vector,  $H_m$  the input matrix,  $\theta$  the parameter vector, and  $V_m$  stands for the measurement errors.

The least squares method then finds the optimal values of  $\theta$  which minimizes the root mean square error between the model's prediction and the measurements, as

follows.

$$\min J(\hat{\theta}) = \min \left[ \left( Z_m - H_m \hat{\theta} \right)^T \left( Z_m - H_m \hat{\theta} \right) \right] \quad (4.15)$$

$$\frac{\partial J}{\partial \theta} \Big|_{\theta=\hat{\theta}} = -2H_m^T \left( Z_m - H_m \hat{\theta} \right) = 0 \quad (4.16)$$

$$H_m^T H_m \hat{\theta} = H_m^T Z_m \quad (4.17)$$

When the number of measurements is higher than the number of parameters, i.e., the input matrix is column full-rank and  $H_m^T H_m$  is full rank. There is then a unique solution to Eq. (4.12), which is the optimal parameter estimation,

$$\hat{\theta} = (H_m^T H_m)^{-1} H_m^T Z_m \quad (4.18)$$

#### 4.4.1.2 Simulated Annealing Algorithm

The intelligent parameter identification algorithms rely on the optimization theory, which searches for the optimal or sub-optimal parameters in a large parameter space. Among the different kinds of intelligent optimization algorithms including simulated annealing algorithm, particle swarm algorithm, ant colony algorithm, artificial immune algorithm and the Bat algorithm etc., the simulated annealing algorithm and particle swarm algorithm are widely used in engineering applications. The simulated annealing algorithm is a meta-heuristic optimization algorithm inspired by the annealing process during the industrial metallurgical processes. When the metal changes from liquid to solid state as the temperature drops, the system tends to converge spontaneously to the point with the lowest internal energy. During the state updating process, according to the Metropolis principle, when the internal energy of the new system state is lower than the original state, the new state will be accepted. Otherwise, the probability of accepting the new state follows a probability distribution, as follows,

$$p = \exp \left( -\frac{E_x - E_{x_0}}{T} \right) \quad (4.19)$$

where  $p$  is the probability;  $E$  the system internal energy; and  $T$  is the temperature. In this section, the root mean square error (RMSE) is selected as the fitting function. When  $E_{x_0} < E_x$ , the new state is accepted.

$$p(x \rightarrow x_0) = \begin{cases} 1 & E_{x_0} < E_x \\ \exp \left( -\frac{E_{x_0} - E_x}{T} \right) & E_{x_0} \geq E_x \end{cases} \quad (4.20)$$

Under each annealing temperature, iterative searches for the new states will be performed until the algorithm converges or the limit of iteration is reached. Next, the annealing temperature is updated as follows,

$$T_{\text{new}} = K \cdot T \quad (4.21)$$

where  $T_{\text{new}}$  is the new temperature, and  $K$  is the annealing rate.

Therefore, the algorithm simulates the annealing process. Under every annealing temperature, iterative searches are conducted to find the optimal solution. The cost function, usually the RMSE or the largest error, represents the system's internal energy, which is used to calculate the chance of accepting the new solution. According to the Metropolis principle, the probability of accepting new solution drops with the temperature, as it is shown in Eq. (4.20). It indicates that at high temperature the algorithms can search a large parameter space; while at low temperature, the convergence rate increases. Therefore, a high initial temperature and low temperature decaying rate can be used in order to ensure a wide searching scope. However, this will reduce the convergence rate. Further, the computational expense is high because of the many iterations under each annealing temperature.

The Simulated Annealing algorithm can be summarized as follows.

Step 1: Set the initial temperature, search for the global equilibrium state using the Monte Carlo algorithm.

Step 2: For each iteration, evaluate the cost function at the updated state, and decide whether to accept the new state according to the Metropolis principle (Fig. 4.14).

Step 3: Perform iterations under each temperature until the algorithm converges or the number of iterations reaches the set limit.

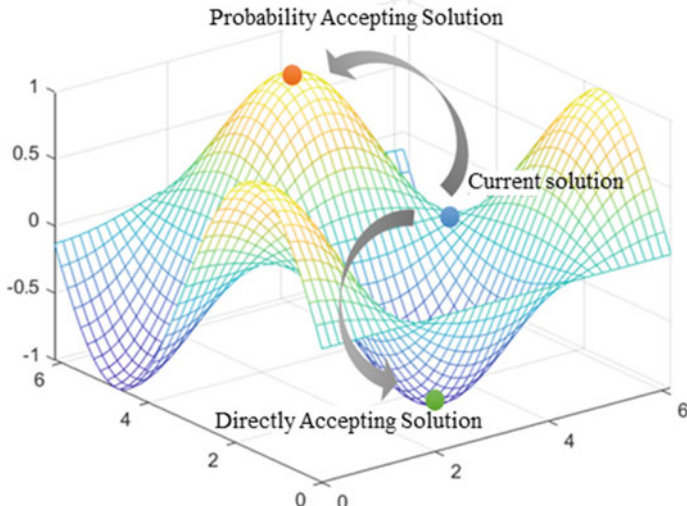


**Fig. 4.14** Illustration of the Metropolis Principle

#### 4.4.1.3 Particle Swarm Optimization Algorithm

The Particle Swarm algorithm simulates the predatory process of bird flock. If one bird in the flock finds food in one location, the others bird will change their current flying direction towards the new location. The particle swarm algorithm simulates this process by representing each bird as a particle. The position and velocity of each particle stands for the location and flying direction of the bird. The food location for each bird is defined as the individual optimum, and the best food location in the whole flock is the global optimum. These particles are initialized with random positions and velocities. The velocities of the particles are then adjusted towards the individual optimum and global optimum. The position and velocity of each particle, as well as the individual optimum and global optimum, are updated after each iteration (Fig. 4.15). The velocity updating equation is given as follows,

$$\mathbf{v}_{k+1} = \omega \mathbf{v}_k + c_1 r_1 [\mathbf{p}_k - \mathbf{x}_k] + c_2 r_2 [\mathbf{g}_k - \mathbf{x}_k] \quad (4.22)$$

where  $\omega$  is the inertia weight,  $c_1$  and  $c_2$  are the learning coefficients.  $r_1$  and  $r_2$  are random numbers between 0 and 1.  $v$  is the velocity of the particle,  $x$  is the current position,  $p$  is individual optimum, and  $g$  is the global optimum. The position is updated as follows,

$$\mathbf{x}_{k+1} = \mathbf{x}_k + \mathbf{v}_k \quad (4.23)$$

The convergence rate of the particle swarm algorithm is high. However, the searching scope is relatively small, which is usually limited to the scope of initialization. Therefore, one way to improve the algorithm performance is to enhance the searching capability in large scope.

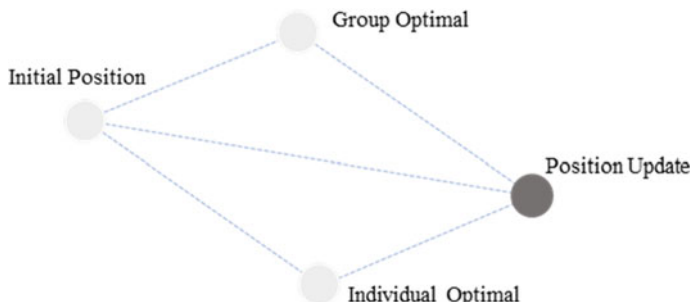


**Fig. 4.15** Illustration of the position updating rule of particle swarm algorithms

#### 4.4.1.4 Genetic Algorithm

Genetic algorithm reflects the natural selection process where the fittest individuals are selected for reproduction of the next generation. The algorithm uses a group of particles as feasible solutions to evaluate the cost function at each iteration, and the best solutions will be selected to produce the particles in the next iteration through evolution and mutation.

According to the principle of genetics, the fittest individuals can be found using the natural selection process. These individuals can then reproduce the next generation. This keeps the useful information of the previous generation, while eliminating the unfitting ones, in order to approach the optimum.

Evolution and mutation are important to the genetic algorithm. Evolution stands for the selection process where the fittest solutions in the previous generation are selected to pass their information to the next generation. Mutation stands for the process where information changes randomly from generation to generation, including large variation (e.g., gene mutation) and small variation (e.g., chromosome crossover between individuals), etc. The gene mutation rate is usually low (about 1%), while the chromosome crossover rate is high (usually larger than 10%). The procedure of the genetic algorithms is illustrated in Fig. 4.16.

When the genetic algorithm is used for the parameter identification of battery models, the particle set represent the parameter searching scope, and each individual

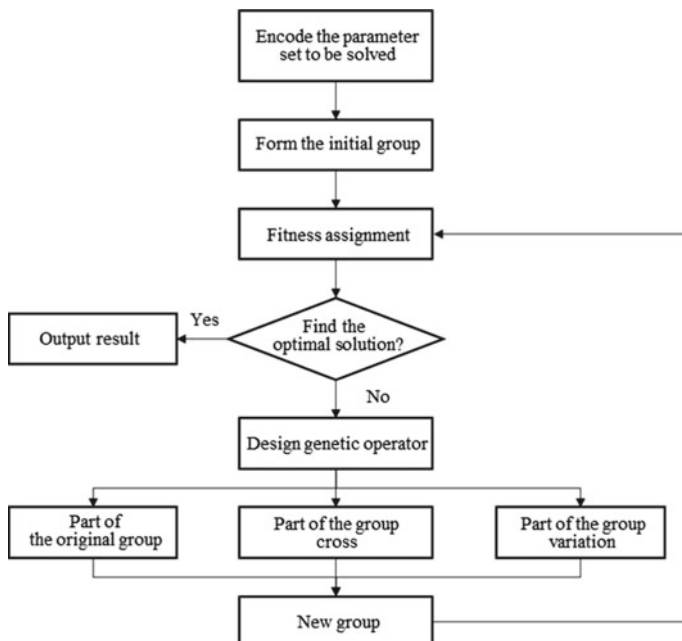


**Fig. 4.16** Implementation procedure of genetic algorithm

particle stands for a feasible solution of the model parameters. The voltage RMSE or the extreme voltage error is usually used as the cost function to evaluate the fitness of the solutions. The optimal solution is the parameter set that can best fit the voltage curve.

Generally, the model cannot fit the battery's voltage curve perfectly, and the algorithm usually terminates when the maximum iteration number is reached. Therefore, the convergence of GA depends on the iteration number and the distribution of the initial particles. Further, the mutation rate can vary at different stages of the model training procedure. In the initial stage, a high mutation rate can be used to increase the searching scope, while at the later stage, a lower mutation rate can increase the convergence rate. Therefore, the algorithm performance can be improved by optimizing the mutation rule and the probability of evolution to improve the accuracy of the parameter identification.

#### 4.4.2 Online Parameter Identification Algorithms

##### 4.4.2.1 Recursive Least Squares

The Least Squares (LS) method requires a large amount of data in order to improve the accuracy of the identified parameters. The parameters are obtained after processing the batch data. This leads to high storage and computational expense for the onboard system. Therefore, the LS method is not suitable for online parameter identification.

The recursive least squares (RLS) method is developed for online parameter identification. The RLS method updates the parameters at current step  $\hat{\theta}(m+1)$  based on the previous parameter set  $\hat{\theta}(m)$  using the latest measurements. The parameters are thus updated in a recursive way until the accuracy requirement is met.

Let the parameters at time step  $m+1$  as

$$\hat{\theta}_{m+1} = (H_{m+1}^T H_{m+1})^{-1} H_{m+1}^T Z_{m+1} \quad (4.24)$$

Let  $P_m = (H_m^T H_m)^{-1}$ , then Eq. (4.24) can be reformulated as

$$\hat{\theta}_{m+1} = P_{m+1} \left[ \begin{array}{c|c} H_m^T & h^T(m+1) \end{array} \right] \left[ \begin{array}{c} Z_m \\ z_{m+1} \end{array} \right] = P_{m+1} H_m^T Z_m + P_{m+1} h^T(m+1) z_{m+1} \quad (4.25)$$

$$P_{m+1} = (H_{m+1}^T H_{m+1})^{-1} = \left( \left[ \begin{array}{c|c} H_m^T & h^T(m+1) \end{array} \right] \left[ \begin{array}{c} Z_m \\ z_{m+1} \end{array} \right] \right)^{-1} \quad (4.26)$$

The recursive calculation of  $P$  is given as follows,

$$P(m+1) = \left[ 1 - \frac{P(m)h(m+1)h^T(m+1)}{1 + h^T(m+1)P(m)h(m+1)} \right] P(m) \quad (4.27)$$

And the parameters  $\theta$  can be updated as follows,

$$\hat{\theta}_{m+1} = \hat{\theta}_m + \frac{P(m)h(m+1)}{1 + h^T(m+1)P(m)h(m+1)} (z(m+1) - h^T(m+1)\hat{\theta}_m) \quad (4.28)$$

The updating equations of RLS consists of Eq. (4.27) and (4.28).  $\hat{\theta}(m)$  is the parameter set at time step  $m$ ,  $h^T(m+1)\hat{\theta}_m$  is the prediction of the output at time step  $m+1$ , and  $z(m+1)$  is the measurement at step  $m+1$ . The prediction error is also called innovation.  $\frac{P(m)h(m+1)}{1 + h^T(m+1)P(m)h(m+1)}$  is the gain matrix. There are usually two ways of selecting the initial parameters of  $\hat{\theta}(m)$  and  $P(m)$ :

1. Let  $\hat{\theta}(0)$  equal zero, or a low value, and  $P(0) = \alpha E$ , where  $\alpha$  is a large number ( $10^5$ – $10^{10}$ );
2. Use the first  $L$  measurements to estimate the  $\hat{\theta}(L)$  and  $P(L)$  by least squares method, and  $L < m$ . Then start the recursive estimation from step  $L+1$ .

#### 4.4.2.2 Kalman Filter

The Kalman filter algorithm is a time-domain recursive estimator based on the generalized Least Squares method. The system equations are in the state-space form, and the parameters are solved recursively. Therefore, there is no need to store the past measurements, making it suitable for real-time implementation, especially in onboard systems with limited storage and computational resources.

The Kalman filter is the minimum covariance state estimator for the stochastic state-space system. It works in a prediction-correction iteration as follows,

$$\text{State estimation} = \text{State prediction} + \text{Kalman filter gain} \times \text{innovation} \quad (4.29)$$

For a discrete-time linear system,

$$\hat{x}(k|k-1) = F_{k-1}\hat{x}(k-1) \quad (4.30)$$

$$Z(k) = H_k\hat{x}(k) \quad (4.31)$$

The implementation procedure of the Kalman filter algorithm can be summarized as follows,

Initialization	$\hat{x}_0 = E[x_0]$
	$P_0 = E[(x_0 - \hat{x}_0)(x_0 - \hat{x}_0)^T]$

(continued)

(continued)

Prediction	
State prediction	$\hat{x}(k k-1) = \mathbf{F}_{k-1}\hat{x}(k-1)$
Prediction covariance matrix	$\mathbf{P}(k k-1) = \mathbf{F}_{k-1}\mathbf{P}(k-1)\mathbf{F}_{k-1}^T + \mathbf{Q}_{k-1}$
Correction	
Gain	$\mathbf{G}_k = \mathbf{P}(k k-1)\mathbf{H}_k^T(\mathbf{H}_k\mathbf{P}(k k-1)\mathbf{H}_k^T + \mathbf{R}_k)^{-1}$
State correction	$\hat{x}(k) = \hat{x}(k k-1) + \mathbf{G}_k(\mathbf{Z}_k - \mathbf{H}_k\hat{x}(k k-1))$
Correction covariance matrix	$\mathbf{P}(k) = (\mathbf{I} - \mathbf{G}_k\mathbf{H}_k)\mathbf{P}(k k-1)$

This Kalman filter in the above table only works for discrete-time linear systems with Gaussian noises. For nonlinear systems with non-Gaussian noises, various nonlinear Kalman filters have been proposed, including the Extended Kalman filter, Unscented Kalman filter and Cubature Kalman filter.

The nonlinear Kalman filter is derived based on the Bayesian theory. However, it is difficult to directly calculate the high-dimensional integral of nonlinear functions. The Cubature Kalman filter replaces the integral of nonlinear function with cubature calculation of a multidimensional geometry. It has high computational efficiency and high numerical accuracy and has been widely used in practical applications.

The classic Kalman filter is only applicable to linear systems, and the estimation accuracy will reduce for nonlinear systems. The Bayes estimation is a widely used method for the state estimation of nonlinear systems. The system states are estimated as the expected value of a stochastic variable with a probability density function, which can be calculated using nonlinear integral method.

There are two assumptions about the system:

**Assumption 1** The system is represented as a Markov process, i.e., the current state only depends on the state of the previous one step.

**Assumption 2** The probability density of one-step-ahead prediction of the states and the likelihood probability density follow Gaussian distribution.

Based on the Bayesian theory, the state estimation problem is formulated as follows. The current state to be estimated follows a probability distribution which depends on the past system states and measurements.

$$\begin{cases} x \sim p(x_k|x_1, x_2, \dots, x_{k-1}, z_1, z_2, \dots, z_{k-1}) \\ z \sim p(z_k|z_1, z_2, \dots, z_{k-1}, x_1, x_2, \dots, x_{k-1}, x_k) \end{cases} \quad (4.32)$$

According to Assumption 1, the previous information has no influence on the future states. Therefore, the above equation can be simplified as

$$\begin{cases} x \sim p(x_k|x_{k-1}) \\ z \sim p(z_k|x_k) \end{cases} \quad (4.33)$$

Therefore, the one-step-ahead prediction of the current state (a prior prediction) is given below,

$$p(\mathbf{x}_k|z_{k-1}) = \int p(\mathbf{x}_k|\mathbf{x}_{k-1})p(\mathbf{x}_{k-1}|z_{k-1})d\mathbf{x}_{k-1} \quad (4.34)$$

According to Bayesian theory,

$$p(x_k|z_k) = \frac{p(z_k|x_k)p(x_k|z_{k-1})}{p(z_k|z_{k-1})} \quad (4.35)$$

where  $p(z_k|z_{k-1}) = \int p(z_k|\mathbf{x}_k)p(\mathbf{x}_k|z_{k-1})d\mathbf{x}_k$ , and  $p(x_k|z_{k-1})$  is the prior information, and  $\frac{p(z_k|x_k)}{p(z_k|z_{k-1})}$  is the likelihood function.

Therefore, there are two function integrals, i.e., the one-step-ahead prediction and the state correction.

According to Assumption 2, the system probability density function is Gaussian. For the nonlinear system model,

$$\begin{cases} x_k = f(x_{k-1}, w_k) \\ z_k = h(x_k, v_k) \end{cases} \quad (4.36)$$

From Eq. (4.34), the one-step ahead prediction is

$$x_{k|k-1} = \int f(x_{k-1}, w_k)N(x_{k-1}, P_{k-1})dx_{k-1} \quad (4.37)$$

From Eq. (4.35), the observation equation is

$$z_{k|k-1} = \int h(x_{k|k-1}, w_k)N(x_{k|k-1}, P_{k|k-1})dx_{k|k-1} \quad (4.38)$$

The above integral equation is of Hammerstein type. According to the integral theory, there are various numerical methods for solving the integral equation. However, the computational expenses can be too high for online implementations. The Gaussian integral formula is the widely used method to simplify the calculation,

$$\mathbf{x}_{k|k-1} = \sum_{i=1}^L \omega_i f(\xi_i) \quad (4.39)$$

This method simplifies the integral of nonlinear function using a weighted sum of function evaluations. Therefore, there is no need to solve the function integral, nor to calculate the partial differentiation (e.g., the extended Kalman filter). It only needs to calculate the function values at some Sigma points. This can significantly reduce the computational expense, which is useful for battery's SoC estimation.

The extended Kalman filter (EKF) was proposed for estimating the states of a nonlinear system. The EKF linearized the nonlinear function using first order Taylor approximation and the Jacobean matrix is calculated. However, the approximation accuracy can be low, because only first order approximation is used. Therefore, this method has low accuracy for highly nonlinear systems. Further, the EKF is based on the KF theory for linear systems, and therefore it also assumes that the noises follow Gaussian distribution. The estimation accuracy can be improved by approximating the probability density function rather than linearizing the nonlinear functions. The widely used methods include the unscented Kalman filter (UKF), cubature Kalman filter (CKF) and integral on sparse grids, etc.

The UKF method uses sampling technique known as the unscented transformation (UT), which captures the nonlinear system properties using the statistic characteristics of the samples. The UKF method can effectively solve the nonlinear estimation problem. However, the unscented Kalman filter uses empirical equations to approximate the complex probability distribution, which can lead to poor estimation performance under certain working conditions.

Cubature Kalman filter (CKF) is developed following rigorous mathematic derivation, which guarantees the accuracy and stability of the estimator. Therefore, the CKF method is superior to other nonlinear Kalman filters in terms of several performance indexes. The Hammerstein-type integral can be formulated as follows when the probability density function is Gaussian,

$$\int_{\mathbb{R}^n} g(\mathbf{x}) N(\mathbf{x}; \mathbf{x}, \mathbf{P}_x) d\mathbf{x} = \frac{1}{\sqrt{\pi^n}} \int_{\mathbb{R}^n} g(\sqrt{2\mathbf{P}_x} \mathbf{x} + \mathbf{x}) e^{-\mathbf{x}\mathbf{x}^T} d\mathbf{x} \quad (4.40)$$

There is a unique property of this formulation. Let  $\mathbf{x} = r\mathbf{y}$ , and  $\mathbf{y}^T \mathbf{y} = 1$ , i.e., the set of vectors  $\mathbf{y}$  constitute the surface of a unit sphere  $S_n = \{\mathbf{y} | \mathbf{y}^T \mathbf{y} = 1\}$ .  $r$  is the radius of the sphere. Then according to the integral formula under the spherical coordinates

$$d\mathbf{x} = r^{n-1} dr d\sigma(\mathbf{y}) \quad (4.41)$$

Equation (4.40) can be

$$I = \int_0^\infty \int_S g(r\mathbf{y}) r^{n-1} e^{-r^2} d\sigma(\mathbf{y}) dr \quad (4.42)$$

The equation is transformed to the volume calculation of a geometry in the multi-dimensional space. Therefore, the method is termed as cubature method. According to the triple integral method, Eq. (4.42) can be calculated using one surface integral and one definite integral.

$$S(r) = \int_S g(r\mathbf{y})d\sigma(\mathbf{y}) \quad (4.43)$$

$$R = \int_0^\infty S(r)r^{n-1}e^{-r^2}dr \quad (4.44)$$

Equation (4.44) can be further simplified using different methods. The surface integral on the sphere can be calculated as follows using third-order polynomial approximation,

$$S_3(r) = \frac{A_n}{2n} \sum_{i=1}^n (\mathbf{g}(r\mathbf{e}_i) + \mathbf{g}(-r\mathbf{e}_i)) \quad (4.45)$$

The corresponding radial integral is

$$\begin{cases} r_1 = \sqrt{\frac{n}{2}} \\ w_{r,1} = \frac{1}{2}\Gamma\left(\frac{n}{2}\right) \end{cases} \quad (4.46)$$

Combining Eqs. (4.45) and (4.46), the surface-radial integral of the sphere is

$$\begin{aligned} \int_{R^n} \mathbf{g}(\mathbf{x}) e^{-\mathbf{x}\mathbf{x}^T} d\mathbf{x} &= \sum_{j=1}^{w_r} \sum_{i=1}^{w_s} w_{r,j} w_{s,j} \mathbf{g}(r_j \mathbf{y}_i) \\ &= \frac{\sqrt{\pi^n}}{2n} \sum_{i=1}^n \left( \mathbf{g}\left(\sqrt{\frac{n}{2}}\mathbf{e}_i\right) + \mathbf{g}\left(-\sqrt{\frac{n}{2}}\mathbf{e}_i\right) \right) \end{aligned} \quad (4.47)$$

Next, the one-step ahead prediction of the system states can be calculated as follows using the cubature formula,

$$\mathbf{x}_{k|k-1} = \sum_{i=1}^L \frac{1}{L} (f(\bar{\mathbf{x}} + \sqrt{n\mathbf{P}_x}\mathbf{e}_i) + f(\bar{\mathbf{x}} - \sqrt{n\mathbf{P}_x}\mathbf{e}_i)) \quad (4.48)$$

Therefore, the CKF method is derived based on the cubature formula. The integral of nonlinear function is approximated using the function evaluation at the Sigma points. This approximation method has high accuracy because of the three-order polynomial approximation.

#### 4.4.2.3 Particle Filter

Particle filter uses the Monte Carlo sampling method to solve the complex nonlinear integral equation, while the Kalman filter is based on the Bayesian theory. The implementation procedure of particle filter includes Monte Carlo sampling, sequential importance sampling and re-sampling etc. The advantage of particle filter is the high accuracy, especially for highly nonlinear systems. However, the computational expense is high, and the online implementation is difficult.

#### 4.4.3 Perspective of Parameter Identification Algorithms

The parameter identification of the battery model is an optimization problem. The existing global optimization algorithms have high arithmetic complexity and high spatiotemporal complexity, making them unsuitable for real-time implementation in the embedded systems of onboard BMS. On the other hand, the online identification algorithms, such as the Kalman filter algorithm and the Least Squares method, are vulnerable to disturbances and noises, which can cause low accuracy. Therefore, the development of new parameter identification algorithms involves a trade-off between complexity and accuracy. The algorithm accuracy can be sacrificed in order to reduce the computational expense in order to facilitate onboard and online implementation in the BMS of EVs.

## References

- Dao T, Vyasarayani CP, Mcphee J (2012) Simplification and order reduction of lithium-ion battery model based on porous-electrode theory. *J Power Sources* 198:329–337
- Doyle M, Fuller TF, Newman J (1993) Modeling of galvanostatic charge and discharge of the lithium polymer insertion cell. *J Electrochem Soc* 140(6):1526–1533
- Doyle M, Newman J, Gozdz AS, Schmutz CN, Tarascon JM (1996) *J Electrochem Soc* 143:1890–1903
- Fuller T, Doyle M, Newman J (1994) *J Electrochem Soc* 141:1–10
- Jokar A, Rajabloo B, Desilets M et al (2016) Review of simplified Pseudo-two-Dimensional models of lithium-ion batteries. *J Power Sources* 327:44–55
- Newman EJ, Thomas KE, Hafezi H et al (2003) Modeling of lithium-ion batteries. *J Power Sources* 119–121:838–843
- Rahman MA, Anwar S, Izadian A (2016) Electrochemical model parameter identification of a lithium-ion battery using particle swarm optimization method. *J Power Sources* 307:86–97
- Shen WJ, Li HX (2016) Parameter identification for the electrochemical model of Li-ion battery. In: Proceedings of 2016 international conference on system science and engineering (ICSSE). IEEE, Puli, pp 1–4
- Zhang D, Popov BN, White RE (2000) Modeling lithium intercalation of a single spinel particle under potentiodynamic control. *J Electrochem Soc* 147(3):831–838

# Chapter 5

## SOC Estimation



### 5.1 SOC Definition

Battery state of charge (SOC) is the ratio between the battery's remaining charge and the total charge capacity. The SOC is not directly measurable. It can be calculated under a fixed discharge rate according to the 'Battery Test Procedure for Electric Vehicle' by the Advanced Battery Consortium of America, as in Eq. (5.1)

$$SOC(t) = SOC(0) - \int_0^t \frac{\eta_i i(t)}{Q_N} dt \quad (5.1)$$

where  $SOC(0)$  is the initial SOC,  $Q_N$  is the battery capacity (Ampere hour, Ah),  $\eta$  is the coulombic efficiency.  $i$  is the current (positive for charging).

SOC is important for proper battery utilization in order to prevent over-charge and over-discharge, etc. Because of the high importance, the battery SOC estimation algorithm is a key to BMS. It is essential to keep track of the battery SOC in real-time. Although the SOC is not directly measurable, it is closely related with the battery's voltage, current and temperature etc. Therefore, the SOC is usually estimated using these measurable signals in practical applications. There are various SOC estimation algorithms, and the applicability depends on the available signal measurements, the battery chemistry, characteristics and the operating conditions.

There are no standard test specification and procedure, or standard data set for battery SOC characterization, which is a challenge for the development and validation of accurate estimation algorithms. Further, because of the effect of ageing and battery imbalance on the SOC accuracy, it is difficult to guarantee long-term accuracy.

The real-time estimation of SOC is critical for EVs. First, the accurate SOC estimation can protect the battery from abuse conditions such as over-charge and over-discharge. This can help optimize the battery utilization to reduce cost. For example, if the SOC estimation is lower than the actual value, the user will need to

charge the battery more than required. It can also cause over-charge during charging, which will accelerate the ageing process. On the other hand, if the SOC estimation is higher than the actual value, the battery won't be fully charged, which reduces the driving range. Second, the SOC estimation is important for other BMS functions. For example, the SOC is used with other battery parameters to estimate the vehicle's remaining driving range. The SOC is a key parameter for vehicle control, such as the energy management system. Therefore, accurate SOC estimation is key to both the battery safety and the performance of the vehicle (Lu et al. 2013; Deng et al. 2016, 2020; Xiong et al. 2017).

## 5.2 Different Estimation Algorithms

The study of SOC estimation algorithm can date back to 1938, almost at the same time with the invention of rechargeable batteries. Heyer demonstrated a device for estimating the battery's remaining charge using the voltage measurement alone in 1938. Because the SOC estimator was used as indicator for battery replacement, the accuracy requirement was low. With the advance of the battery technology and the expanding of the application range, the operating conditions become more and more complex, and the accuracy requirement increases as well. As a result, the SOC estimation algorithms become more complex (Lin et al. 2017; Liu et al. 2014; Ji et al. 2020; Xiong et al. 2018; Zhang et al. 2015; Yang et al. 2017).

The battery shows highly nonlinear dynamics which are affected by many factors, such as the current profile, voltage level, relaxation effect, temperature, C-rate, cycle time and ageing status, etc. These factors have influences on the SOC estimation. Therefore, the accurate SOC estimation is a challenge for the BMS in EVs. The existing estimation methods can be categorized in three groups, i.e., the empirical methods, model-based methods and data-driven methods, as shown in Fig. 5.1. The empirical methods are usually based on the coulombic counting method or other experimental characterization techniques. The model-based method is based on a battery model to describe the battery dynamics, such as the equivalent circuit model or the electrochemical model. The data-driven methods do not involve the physical interpretation of the battery properties, and the input–output relationship is learned directly from test data during model training.

### 5.2.1 Empirical Method

#### 5.2.1.1 Open-Circuit Voltage (OCV) Method

The OCV method is one of the first SOC estimation algorithms, and it is one of the simplest for implementation. OCV is battery's steady state voltage after resting for a long time, e.g., 4 h. The OCV is close to the battery's electromotive force.

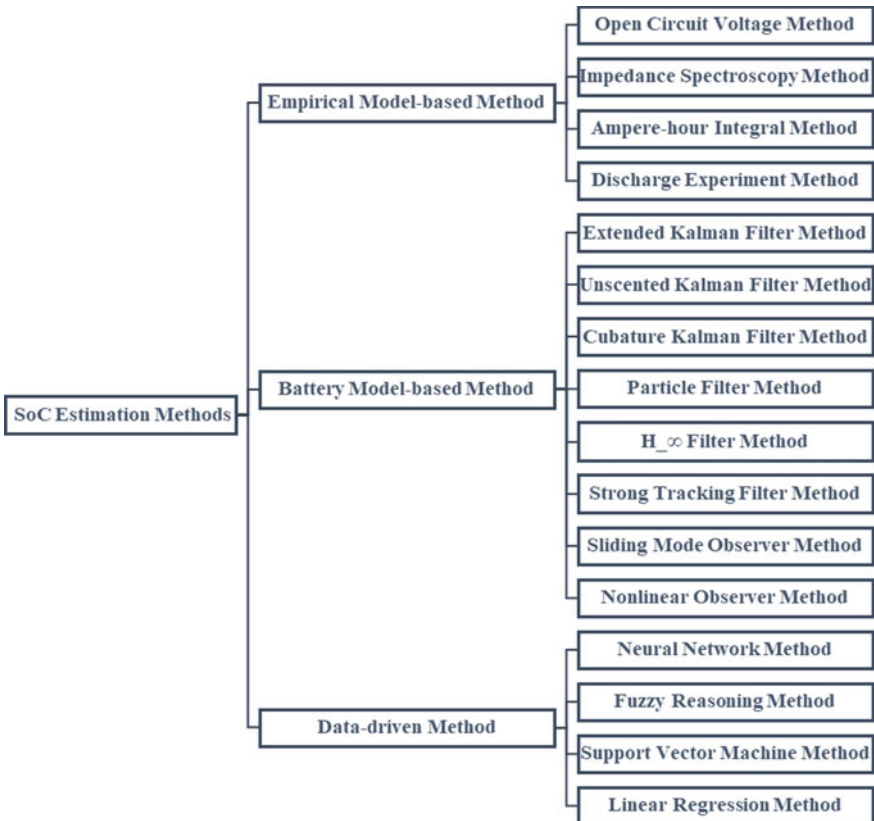


**Fig. 5.1** Classification of SOC estimation methods

According to electrochemical theory, there is a well-defined relationship between the SOC and the electromotive force, and this relationship is almost independent from temperature and current rates. Therefore, the battery SOC can be estimated using this relationship. The OCV-SOC relationship is usually characterized first and stored in the onboard microprocessor as a look-up table. Next, when the battery is rested for a long time and the voltage reaches equilibrium state, the OCV can be measured. Then the SOC value can be obtained using the look-up table. This advantages of the OCV method include simplicity, ease of implementation, and the applicability to many battery chemistries. However, there is an obvious disadvantage, i.e., the battery has to rest for a sufficiently long time for the voltage to stabilize. The length of the rest period is a trade-off between time and estimation accuracy. Therefore, it cannot be used under current load or during the relaxation period where the voltage keeps changing. Therefore, the OCV method cannot be used alone for SOC estimation, and it is usually used in combination with other estimation methods that can work under dynamics current load.

The underload voltage curve has also been used for SOC estimation. However, this method only works under constant current operating conditions.

### 5.2.1.2 Ah-Integral Method

The Ah-integral method was originally proposed by Fingers et al. in one patent. It is a coulombic counting method, as shown in Eq. (5.2). Here, the battery is considered as energy storage device whose dynamic properties are ignored. The SOC (the remaining charge) is calculated by integrating the input and output charge. Because of the simplicity and ease of implementation, the Ah integral method is now widely used in BMS applications.

$$SOC = SOC_0 + \frac{1}{C} \int_{t_0}^t \eta I dt \quad (5.2)$$

The Ah integral method has two disadvantages. First, it depends on a known initial SOC. The accurate initial SOC can be difficult to obtain. For example, due to battery ageing and capacity reduction, the battery cannot be fully charged. As a result, the estimation of the initial SOC after a full-charge operation can be higher than the actual value. This initial error can increase with battery usage and ageing. Second, the Ah integral method is an open loop method which is vulnerable to current measurement errors. The SOC estimation error caused by the current sensor bias will increase with time due to the accumulation effect of the integral. Further, it is difficult to use the Ah integral method when the environment temperature is too high, or the load current is highly fluctuating.

Therefore, the Ah integral method is usually used in combination with the OCV method in practical applications. The OCV method is used for calibration of the SOC value after the battery rests for a long period (e.g., parking overnight), while the Ah integral method is used for SOC estimation under current load and during the relaxation period. This combination of the Ah integral with the OCV method is a popular solution for practical implementation especially when the onboard computational power is limited.

### 5.2.1.3 Discharge Test Method

A full discharge test is the most reliable method for SOC characterization. This method usually uses constant current discharge, and it is not suitable for dynamic load profiles. It is usually used for battery characterization in laboratory to study the battery properties. There are two disadvantages: (1) the test time is long; (2) the battery is under constant-current discharge, and thus cannot be used for work.

### 5.2.2 Model-Based Methods

There are generally two types of model-based SOC estimation methods, the Kalman filter method and the state observer method. The Kalman filter method is a widely used SOC estimation algorithm which relies on the advanced microprocessors used in the BMS. This battery dynamics are described using a state-space model, and the system states (including the SOC) are estimated in real-time using the Kalman filter method. Various Kalman filter algorithms, including EKF, UKF, Adaptive Kalman Filter (AKF) and Dual Extended Kalman Filter (DEKF), etc., have been used for SOC estimation based on different battery models. The first step is to develop the battery state-space model, followed by parametrization. The Kalman filter based SOC estimation algorithm is suitable for all battery chemistries. The algorithm also offers an estimation of the SOC error and the confidence interval. The method is applicable under highly dynamic current profiles.

The observer-based methods are similar to the Kalman filter methods. The battery dynamics are first described using a state-space model, and the state observer can then be designed using control theory which guarantees stability and convergence. The battery dynamics are generally simplified as a linear model to reduce the complexity, and the model structure is selected to ensure the observability of the SOC. The design of the observer involves a good understanding of the relevant control theories. The widely used observers include robust filter and sliding mode observer, etc. The computational expense of the observer-based methods is lower than the Kalman filter methods, and the robustness of the observer can be enhanced. The SOC estimation accuracy is highly relevant with the model accuracy.

#### 5.2.2.1 EKF

The Kalman filter is a minimum-covariance state estimator based on the recursive least square method for SOC estimation. It is an optimal estimator for linear systems with Gaussian noises. This method considers the battery as a system with current input and voltage output, and the battery SOC is one of the system states. The SOC estimation works in a prediction-correction iteration. The model's voltage prediction is compared with the measurement and the modelling error is used as feedback to update the SOC estimation. This iterative calculation has a low requirement for onboard storage and computation, making it suitable for practical BMS. Because of the nonlinear dynamics of the battery, the extended Kalman filter and unscented Kalman filter are usually needed for SOC estimation. The nonlinear system is linearized using the Taylor series method in the EKF method.

For a nonlinear discrete-time system, the state equation and the output equations are given as follows,

$$\begin{cases} \text{State Equation: } x_k = f(x_{k-1}, u_{k-1}) + \omega_{k-1} \\ \text{Observation Equation: } y_k = h(x_k, u_k) + v_k \end{cases} \quad (5.3)$$

where  $x_k \in R^n$  is the system state vector,  $u_k$  is the system input,  $y_k \in R^m$  is the measurement vector.  $\omega_k$  and  $v_k$  represent the process and measurement noise, respectively.  $f(x_k, u_k)$  and  $g(x_k, u_k)$  stand for the nonlinear state equation and output equation, respectively.

Linearize the two nonlinear functions using first-order Taylor series,

$$\begin{cases} f(x_k, u_k) \approx f(\hat{x}_k, u_k) + \frac{\partial f(x_k, u_k)}{\partial x_k} \Big|_{x_k=\hat{x}_k} (x_k - \hat{x}_k) \\ g(x_k, u_k) \approx g(\hat{x}_k, u_k) + \frac{\partial g(x_k, u_k)}{\partial x_k} \Big|_{x_k=\hat{x}_k} (x_k - \hat{x}_k) \end{cases} \quad (5.4)$$

where  $\hat{x}_k$  is the estimated value of  $x_k$ . Denote  $\hat{A}_k = \frac{\partial f(x_k, u_k)}{\partial x_k} \Big|_{x_k=\hat{x}_k}$  and  $\hat{C}_k = \frac{\partial g(x_k, u_k)}{\partial x_k} \Big|_{x_k=\hat{x}_k}$ , and substitute into Eq. (5.3), yielding:

$$\begin{cases} x_k \approx A_{k-1}x_{k-1} + f(\hat{x}_{k-1}, u_{k-1}) - A_{k-1}\hat{x}_{k-1} + \omega_{k-1} \\ y_k \approx C_k x_k + h(\hat{x}_k, u_k) - C_k \hat{x}_k + v_k \end{cases} \quad (5.5)$$

The iteration procedure of the EKF algorithm is given as follows from Eqs. (5.6) to (5.11), where  $\hat{x}_{k|k-1}$  is the prediction value of the states,  $\hat{x}_{k|k}$  is the final state estimation after correction.  $K_k$  is the gain matrix;  $P_{k|k}$  is the covariance matrix of state estimation and  $P_{k|k-1}$  is the covariance matrix of the state prediction.

The initial conditions are:

$$\hat{x}_{0|0} = E(x_0), \quad P_{0|0} = \text{var}(x_0) \quad (5.6)$$

The one-step ahead prediction is as follows,

$$\hat{x}_{k|k-1} = f(\hat{x}_{k-1|k-1}, u_{k-1}) \quad (5.7)$$

And the covariance matrix of the state prediction is:

$$P_{k|k-1} = A_{k-1}P_{k-1|k-1}A_{k-1}^T + Q_{k-1} \quad (5.8)$$

The gain matrix can be calculated as follows,

$$K_k = P_{k|k-1}C_k^T(C_k P_{k|k-1}C_k^T + R_k)^{-1} \quad (5.9)$$

After obtaining the latest measurement, the state estimation is updated as follows,

$$\hat{x}_{k|k} = \hat{x}_{k|k-1} + K_k [y_k - g(\hat{x}_{k|k-1}, u_k)] \quad (5.10)$$

And the covariances matrix of the estimated states is

$$P_{k|k} = (I - K_k C_k) P_{k|k-1} \quad (5.11)$$

The SOC estimation is achieved by repeating Eqs. (5.6) to (5.11) at each time step.

### 5.2.2.2 Unscented Kalman Filter

The EKF is based on the Kalman filter by linearizing the original nonlinear system using the first-order Taylor series approximation. However, this approximation induces model error, because the higher order terms of the Taylor series are neglected, and the model error can lead to divergence of the estimation. Further, the Jacobian matrix needs to be updated at every iteration of the EKF, thus increasing the computational expense. Finally, the solution for the linearized system is only a local optimum for the original nonlinear system, and the local optimum can only approach the global optimum when the state equation and the observation equation are both continuous with weak nonlinearity.

To address the above disadvantages of the EKF algorithm, the unscented Kalman filter (UKF) was proposed for state estimation of nonlinear systems based on an unscented transformation. Instead of linearizing the nonlinear system, the UKF method uses a group of particles to approximate the probability density distribution of the system states. These particles are carefully designed to improve the approximation accuracy. The UKF method can reduce the model error caused by the linearization step in the EKF, and it also avoids the calculation of the Jacobian matrix, which reduces the computational expense.

The unscented transform is key to the UKF. The unscented transform uses the statistics of a group of particles to approximate the probability distribution of the states after a nonlinear transformation. These particles are first selected so that their statistic properties (mean and variance) follow a known probability distribution. The new values of these particles after the nonlinear transformation are then used to approximate the probability distribution of the new states.

The implementation of the UKF method is given in Fig. 5.2,

#### (1) Initialization

$$\hat{x}_0 = E(x_0) \quad P_0 = \text{var}(x_0) \quad (5.12)$$

#### (2) State prediction

Apply unscented transform to the state estimation results in the previous step to generate  $2n + 1$  Sigma points, as shown in Eq. (5.13). Then use these Sigma points to predict the state value at the next step. The mean values of the new states are then updated as in Eq. (5.14).

$$\left\{ \begin{array}{l} x_{k-1}^i = \hat{x}_{k-1}, i = 0 \\ x_{k-1}^i = \hat{x}_{k-1} + (\sqrt{(n + \lambda) P_{k-1}})_i, i = 1, \dots, n \\ x_{k-1}^i = \hat{x}_{k-1} - (\sqrt{(n + \lambda) P_{k-1}})_{i-n}, i = n + 1, \dots, 2n \end{array} \right. \quad (5.13)$$

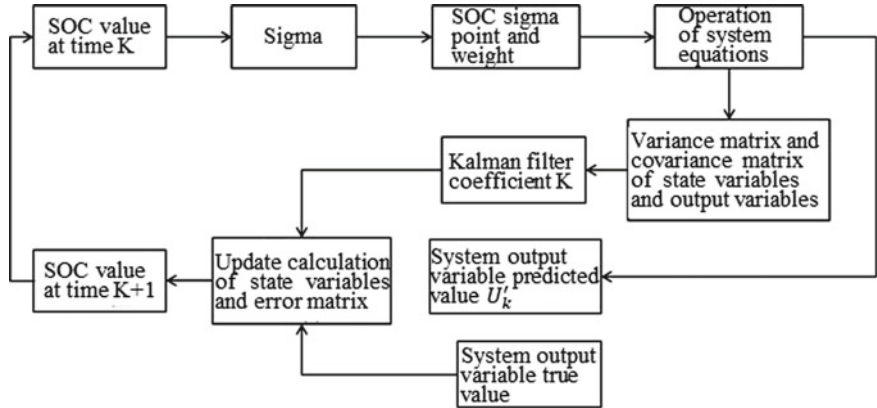


**Fig. 5.2** Implementation procedure of UKF

$$\begin{aligned} x_{k|k-1}^i &= f(x_{k-1}^i, u_{k-1}) \\ \hat{x}_{k|k-1} &= \sum_{i=0}^{2n} \omega_m^i x_{k|k-1}^i \end{aligned} \quad (5.14)$$

(3) The covariance matrix of the states is

$$P_{x,k|k-1} = \sum_{i=0}^{2n} \omega_c^i [x_{k|k-1}^i - \hat{x}_{k|k-1}] [x_{k|k-1}^i - \hat{x}_{k|k-1}]^T + Q_k \quad (5.15)$$

(4) The prediction of the output is

$$y_{k|k-1}^i = h(x_{k|k-1}^i, u_k) \quad \hat{y}_{k|k-1} = \sum_{i=0}^{2n} \omega_m^i y_{k|k-1}^i \quad (5.16)$$

(5) The covariance matrix of the output prediction

$$\begin{aligned} P_{yy,k} &= \sum_{i=0}^{2n} \omega_c^i [y_{k|k-1}^i - \hat{y}_{k|k-1}] [y_{k|k-1}^i - \hat{y}_{k|k-1}]^T + R_k \\ P_{xy,k} &= \sum_{i=0}^{2n} \omega_c^i [x_{k|k-1}^i - \hat{x}_{k|k-1}] [y_{k|k-1}^i - \hat{y}_{k|k-1}]^T \end{aligned} \quad (5.17)$$

(6) The Kalman filter gain is

$$K_k = P_{xy,k} / P_{yy,k} \quad (5.18)$$

(7) Correction of the new states and the covariance matrix,

$$\begin{aligned}\hat{x}_{k|k} &= \hat{x}_{k|k-1} + K_k(y_k - \hat{y}_{k|k-1}) \\ P_{x,k|k} &= P_{x,k|k-1} - K_k P_{yy,k} K_k^T\end{aligned}\quad (5.19)$$

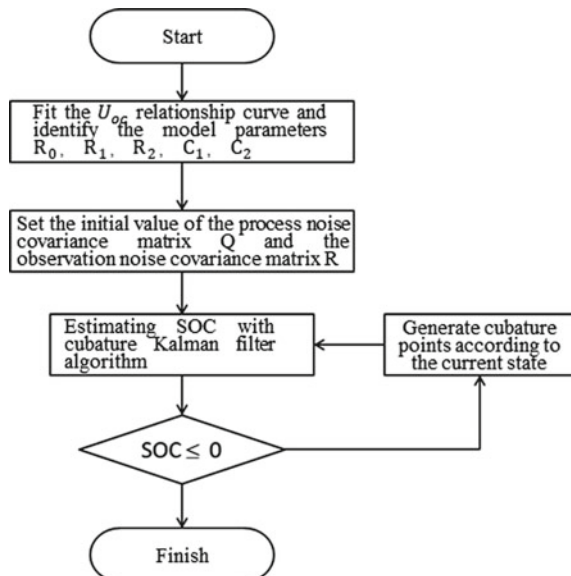
When using the UKF method for SOC estimation, after the initialization step, the SOC prediction and correction procedure will be conducted in every time step. The Kalman filter gain is also updated using the covariance matrixes. Owing to the feedback mechanism of the prediction-correction scheme, the SOC estimation will gradually converge to the actual value as time goes by, even with a large initial SOC error.

### 5.2.2.3 Cubature Kalman Filtering

The Cubature Kalman filter (CKF) method is a recently proposed nonlinear state observer method through rigorous mathematic derivation. The CKF method uses the third-order cubature formula to numerically solve the Gaussian-weighted integral. It inherits the advantage of high computational efficiency of the cubature integral method to approximate high-dimensional integral equation. Many studies have validated the high accuracy of the CKF method.

The implementation procedure of the CKF method for SOC estimation is given in Fig. 5.3.

**Fig. 5.3** Implementation procedure of UKF for SoC estimation



### 5.2.2.4 Particle Filter

The particle filter (PF) is based on the Monte Carlo method for state estimate. The probability distribution of the states is represented using a weighted set of particles. The weights of these particles can be adjusted using the sequential importance sampling method. The original function integral in the Bayesian filter is then simplified by a weighted mean of the function evaluations at the particles, and the covariance of the estimated states are minimized. The original PF method developed in 1970s have limitations such as high computational expense and particle degeneracy problem. The particle degeneracy problem is solved by Gordon, Salmond and Smith using the resampling technique, and the problem of high computational expense is overcome by the recent development of microprocessor technology. As the result, the PF filter algorithm has made new development and become the new research hotspot. There is no limitation on the noise statistics when applying the PF, and it is suitable for highly nonlinear systems. The PF method has been widely used nowadays in visual tracking and target identification.

The implementation procedure of the PF algorithm for battery SOC estimation is given in Fig. 5.4. First, the battery state-space model is developed in the discrete-time domain, and the battery SOC is one of the system states. The battery terminal voltage is the output.

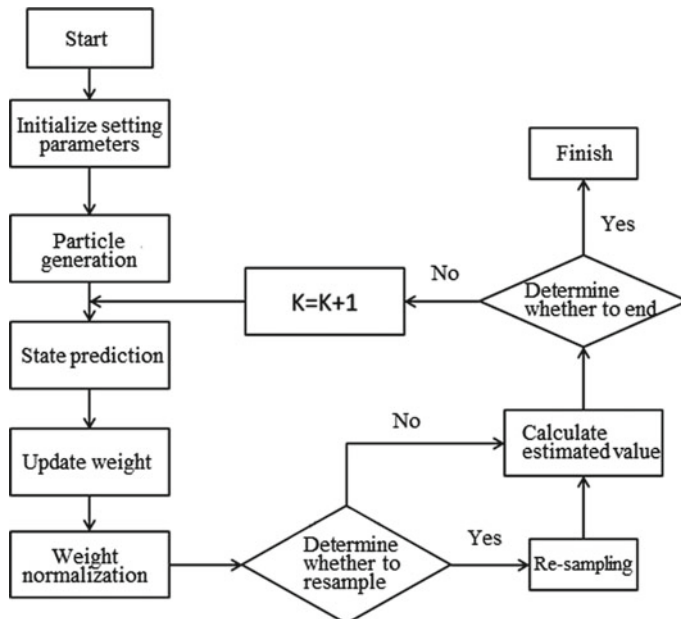


**Fig. 5.4** Implementation procedure of the PF

$$\begin{aligned}x_{k+1} &= f(x_k, i_k, w_k) = x_k - \frac{n_i k \Delta t}{\eta_i \eta_T \eta_n Q_n} + \omega_k \\y_{k+1} &= f(y_k, i_k, v_k) = K_0 - R i_k - K_2 x_k + K_3 \ln(x_k) \\&\quad + K_4 \ln(1 - x_k) + v_k\end{aligned}\tag{5.20}$$

where  $w_k$  is the process noise, and  $v_k$  is the measurement noise. Let  $w_k \sim N(0, Q)$  and  $v_k \sim N(0, R)$ .  $\Delta t$  is the sampling period.

(1) Initialization at  $k = 0$ :

Generate  $N$  particles  $\{x_{0,i}\}$  according to the initial probability distribution  $P(x_0)$

(2) State prediction

Use the set of particles  $\{x_{0,i}\}$  and the state equation, generate the new set of particles for the next iteration.

(3) Weight calculation and normalization

Use the system output equation and the new particle set  $\{x_{0,i}\}^+$  to generate the prediction of the system output. When the new measurement (i.e., the battery terminal voltage) becomes available, compare the predictions with the measurement. The weights of the new particles can then be calculated using the voltage prediction error,

$$W_i = \frac{1}{\sqrt{2\pi R}} e^{-\frac{(y_k - y_{i,k})^2}{2R}}\tag{5.21}$$

The weights are then normalized as follows,

$$W_i^* = W_i \left/ \sum_1^N W_i \right.\right.\tag{5.22}$$

(4) Resampling

During the resampling procedure, the particles with high weights have a higher chance to be kept and the particles with low weights are more likely to be deleted. The weights of the new particle after resampling are all reset at  $1/N$ , and the state estimation  $\bar{x}_k$  is the weighted sum of the particles,

$$\bar{x}_k = \sum_{i=1}^N w_k(i) x_k(i)\tag{5.23}$$

The implementation procedure of the PF algorithm with sequential importance sampling is explained as follows,

① Prediction

Generate new particles from the particles in the previous step,

$$x_k(i) \sim p(x_k|x_{k-1}(i)) (i = 1, 2 \dots N) \quad (5.24)$$

② Update

Calculate the importance weights of the particles, followed by normalization,

$$w_k(i) = \frac{w_k^*(i)}{\sum_{i=0}^N w_k^*(i)} \quad (5.25)$$

③ State estimation

$$\bar{x}_k = \sum_{i=1}^N w_k(i) x_k(i) \quad (5.26)$$

④ Resampling

Calculate the number of effective particles  $\hat{N}_{eff} = 1 / \sum_{i=1}^N (\hat{w}_k^i)^2$ . If  $\hat{N}_{eff} < N_{thr}$ , where  $N_{thr}$  is the threshold value, then perform the resampling procedure to get the new set of particles.

The resampling step can introduce an extra random covariance. Therefore, the resampling is conducted after the filtering step when the sample set can represent the posterior distribution. In order to prevent the problem of particle depletion caused by resampling, an extra parameter  $\alpha$  can be used according to the Genetic algorithm,

$$w_t^{(i)} = (w_{t-1}^i)^\alpha \cdot \frac{p(Z_t|X_t^{(i)}) p(X_t^{(i)}|X_{t-1}^{(i)})}{q(X_t^{(i)}|X_{t-1}^{(i)}, Z_t)} \quad (5.27)$$

where  $0 < \alpha < 1$  is the coefficient to adjust the effect of the previous weight.

The recursive estimation of the system states  $x_k$  is achieved by repeating Eq. (5.24)–(5.27).

### 5.2.2.5 $H_\infty$ Observer

The EKF algorithm has been widely used in practical applications. However, the estimation accuracy of EKF is low for highly nonlinear systems. The EKF offers high accuracy only when the noise statistics are known a prior. If this information is not available, the implementation of EKF needs careful tuning, such as increasing the covariance matrix of the process noise, increasing the weight of the real-time measurement and reducing the weight of the one-step ahead prediction. This filter

tuning can be useful, but it is difficult to find the optimal parameters. Further, the EKF performance can degrade or even diverge when the noises are biased or non-Gaussian. These disadvantages have limited the practical applications of the EKF. The  $H_\infty$  filter was proposed to address this problem. A prior knowledge of the noise statistics is not required in the  $H_\infty$  filter, and the noises are assumed to be bounded random signal.

The  $H_\infty$  filter is designed to minimize the worst-case estimation error caused by the process noise, measurement noise and the initial state error, and it can be used as the optimal estimator under significant system uncertainty. The  $H_\infty$  filter can achieve high estimation accuracy with noisy measurements, and it has high robustness against system and measurement uncertainties. Because of the highly dynamic current profiles for EV driving, the performance of the  $H_\infty$  filter can be superior to that of EKF for SOC estimation.

The implementation procedure of the  $H_\infty$  filter is given as follows,

$$\hat{x}_{k+1,k} = f(\hat{x}_k, u_k) \quad (5.28)$$

$$\hat{x}_{k-1} = \hat{x}_{k+1,k} + K_{k+1}(y_{k+1} - g(\hat{x}_{k+1,k}, u_{k+1})) \quad (5.29)$$

$$K_{k+1} = P_{k+1} \hat{C}_{k+1} \left[ I + \hat{C}_{k+1} P_{k+1} \hat{C}_{k+1}^T \right]^{-1} \quad (5.30)$$

$$\hat{z}_{k+1,k} = L_{k+1} \hat{x}_{k+1} \quad (5.31)$$

where  $K_{k+1}$  is the gain matrix and  $L_{k+1}$  is the output matrix. The other parameters are similar to that of the EKF. The nonlinear battery model is usually linearized first, and the  $H_\infty$  filter is then applied to the obtained linear time-varying battery model.

### 5.2.2.6 State Observer

State observers are developed after the Kalman filter algorithm. In fact, Kalman filter is also a state observer method, where the states are estimated by comparing the model's prediction and the measurements. The advantage of the Kalman filter family is that there is a standard procedure for the filter design and iterative implementation. Once the state-space model is developed, the user only needs to specify the initial state and the covariance matrix of the noises. On the other hand, the design of the state observer relies on control theory for parameter tuning to guarantee the stability of the filter, which is more complicated than the design of Kalman filter. The advantages of state observers include high robustness and low computational expense, because the feedback gain of the state observer can be constant while the gain is calculated iteratively for Kalman filter. The widely used state observers include linear observer, PI observer and sliding-mode observer.

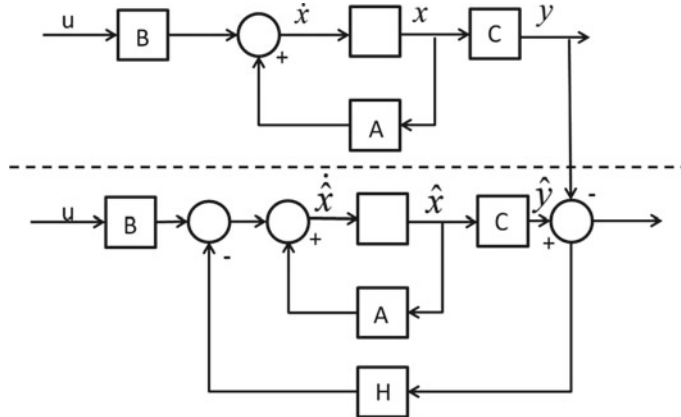


**Fig. 5.5** Principle of the state observer

The structure of the observer is given in Fig. 5.5, while the different types of observers mainly differ in the design of the feedback gain, i.e., the  $H$  matrix. These observer methods are suitable for SOC estimation in electric vehicles under dynamic current load owing to the high stability and high robustness. The state observer can achieve accurate SOC estimation even with modelling error. In contrast, the Kalman filter can suffer from divergence problems because of modelling errors and measurement noises.

### 5.2.3 Data Driven Methods

#### 5.2.3.1 Neural Networks

Neural networks model is inspired by the neurological behavior of humans for information processing. This modelling method is well suited for capturing complex and nonlinear dynamics. For example, the battery thermal behavior shows high nonlinearity and high complexity, which is difficult to describe using conventional methods. Therefore, researchers have developed battery thermal model using neural networks. The development of neural networks model does not need a prior knowledge or empirical equations of the system behavior. The relationship between the system input and output is learned directly from the training data set. The model diagram is shown in Fig. 5.6, which consists of the input layer, hidden layer and output layer. The number of neurons of each layer can be adjusted according to the requirements, and parallel computation techniques can be applied for model training. Neural networks have been used for battery SOC estimation. The battery current rate, temperature and terminal voltage are usually used as the inputs, and the SOC as the output. A high SOC estimation accuracy can be achieved if the model is properly trained.

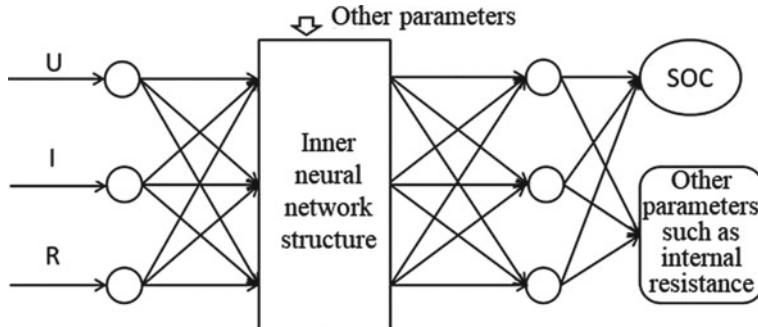


**Fig. 5.6** SoC estimation using neural networks

The advantages of the neural networks based SOC estimation include the high accuracy for capturing nonlinear dynamics and the wide applicability to many different types of batteries. One disadvantage is that the model training process involves a large amount of test data, high computational expense and long training time. Further, it is difficult to take into consideration the time-varying battery parameters caused by ageing. The model's SOC prediction performance depends on the quality of the training data, and it is difficult to predict the generalization performance of the neural networks in operating conditions that are not covered by the training data set. Therefore, the practical implementation of the neural networks model in industrial BMS is still challenging.

### 5.2.3.2 Support Vector Machine

Support vector machine (SVM) was proposed by Vapnik et al. in 1990s based on the statistical learning theory. It is developed as a classification algorithm using a limited number of samples. The SVM uses kernel functions to map the input to a high dimensional space, and then finds the optimal separation hyperplane. The method adopts the principle of structure risk minimum and trades off between error rate and model complexity to improve the learning and generalization performance. The SVM method can achieve good statistical performance with a small set of training samples. The training data set is critical to the development and training of the SVM algorithm. The diagram of a simple linear SVM is illustrated in Fig. 5.7. The SVM method can be used for SOC estimation in the BMS application.

### 5.2.3.3 Deep-Learning Neural Networks

Deep-learning neural networks (DNN) is a new machine learning algorithm, which can be used for SOC estimation. The DNN can directly map the inputs (voltage, current and temperature, etc.) to SOC estimation without using a battery model or

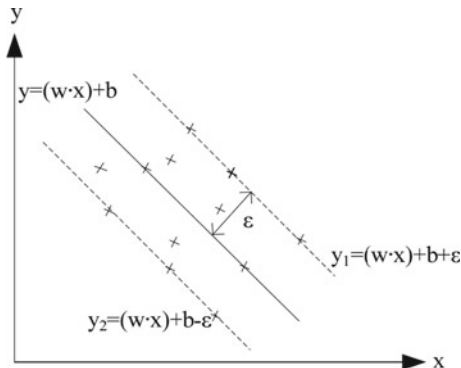


**Fig. 5.7** Linear SVM

a Kalman filter or an observer. The weights of the DNN can be optimized using the training data set. The physical mechanism of the battery is not required for the development of DNN model, which is advantageous because the battery internal dynamics is highly complex (Fig. 5.8).

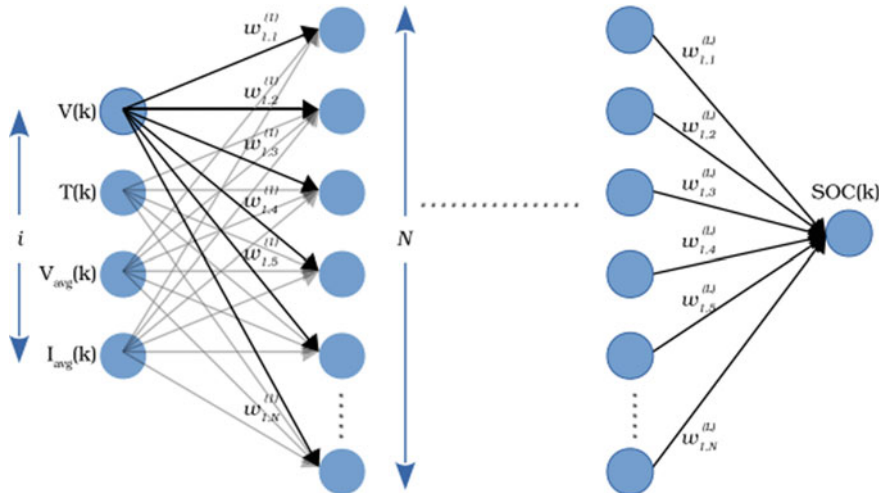


**Fig. 5.8** Model structure of DNN

## 5.3 Case Study

This case study uses the Kalman filter for battery SOC estimation based on a Thevenin model. The model parameters are identified using experimental data. The model and Kalman filter are implemented in Matlab, and various operation conditions are studied.

### 5.3.1 Simulation

#### (1) Parameter identification

The development of battery model always involves a trade-off between accuracy and complexity. After comparing different battery models, the Thevenin model, as shown in Fig. 4.7a, is selected because of its high accuracy for capturing the battery's voltage profile and ease of industrial implementation. The model parameters are also easy to identify.

The model equations are given as follows,

$$\begin{cases} \dot{U}_p = -\frac{U_p}{C_p R_p} + \frac{I_L}{C_p} \\ U_t = U_{oc} - U_p - I_L R_o \end{cases} \quad (5.32)$$

where  $R_o$  is the Ohmic resistance,  $R_p$  is the polarization resistance and  $C_p$  is the polarization capacitance.  $U_p$  is the polarization voltage, and  $U_{oc}$  is the open-circuit voltage.  $I_L$  is the load current (charging current is positive).

The equation is discretized as follows assuming constant signals between samples.

$$U_{P,k} = \exp(-\Delta t/\tau)U_{P,k-1} + R_p I_{L,k-1} [1 - \exp(-\Delta t/\tau)] \quad (5.33)$$

The model parameters are identified using the least squares method introduced in the previous section, and the battery is tested using the pulse current. All tests are conducted inside a thermal chamber. The detailed test procedure is as follows,

- (1) fully charge the battery using the constant current constant voltage (CCCV) procedure, and then rest for an hour.
- (2) Discharge the battery at 1C until the SOC is reduced by 10%.
- (3) Rest for one hour, and record the battery's voltage during relaxation.
- (4) Repeat step (2) and (3), until the battery reaches end of discharge.
- (5) Identify the model parameters under each SOC level using the least squares method.

The above test and parameter identification procedure is repeated under different chamber temperatures.

The battery voltage is shown in Fig. 5.9,

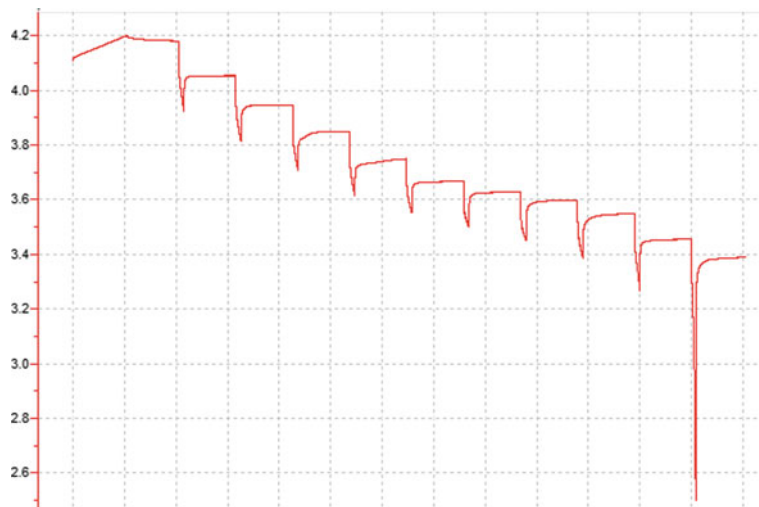


**Fig. 5.9** Battery voltage profile in one test

The voltage response of the model after parameter identification is shown in Fig. 5.10 in comparison with the measurements. As it can be seen, the model accuracy is high, and the correlation index is 0.988 between the measurements and the mode output. The identification results of the model parameters, including the resistance and capacitance, etc., are given in Fig. 5.11.

The identification results show that the battery resistance is almost constant between 10 and 90% SOC, while noticeable resistance increase can be seen at the two ends of SOC range. The polarization resistance varies more noticeably, especially

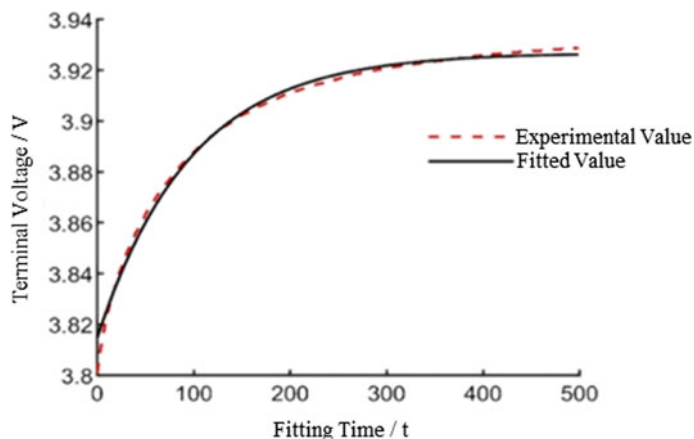
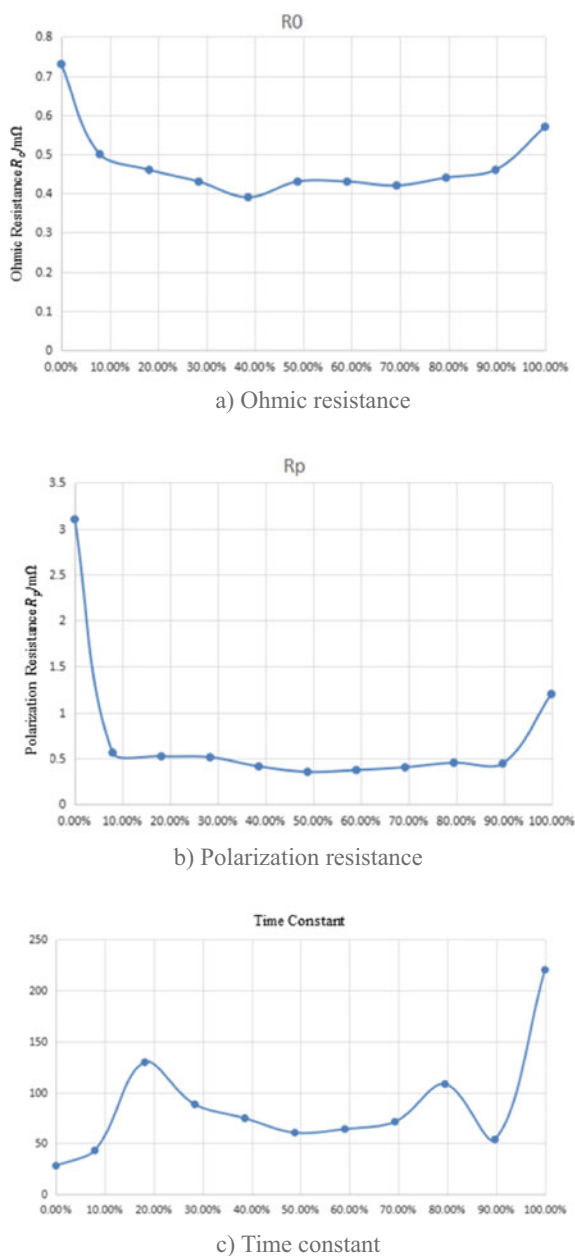


**Fig. 5.10** Comparison between the model's voltage prediction and the measurements

**Fig. 5.11** Model parameter identification results



under low SOC level. The time constant is reduced at low SOC, which is probably caused by the rapid OCV drop.

## (2) Model development

Assuming constant current during sampling period, the system equations of the Thevenin model can be discretized as follows,

$$U_{p,k} = e^{(-\Delta t/\tau)} U_{p,k-1} + R_p I_{t,k-1} [1 - e^{(-\Delta t/\tau)}] \quad (5.34)$$

The battery SOC is calculated by the Ah integral method,

$$z_k = z_{k-1} - I_{t,k} \Delta t / C_n \quad (5.35)$$

where  $z_k$  is the SOC value at step  $k$ .  $\Delta t$  is the sampling time, and  $C_n$  is the nominal capacity of the battery at current temperature.

The polarization voltage and the battery SOC are the system states, and the battery terminal voltage is the system output. The system state equation and the observation equation are given as follows,

$$\begin{cases} \begin{bmatrix} U_{p,k} \\ z_k \end{bmatrix} = \begin{bmatrix} e^{-\Delta t/\tau} & 0 \\ 0 & 1 \end{bmatrix} \begin{bmatrix} U_{p,k-1} \\ z_{k-1} \end{bmatrix} + \begin{bmatrix} (1 - e^{-\Delta t/\tau}) R_p \\ -\Delta t / C_n \end{bmatrix} I_{t,k} + \omega_{1,k-1} \\ U_{t,k} = \begin{bmatrix} -1 & \frac{dU_{oc}}{dz} \end{bmatrix} \begin{bmatrix} U_{p,k} \\ z_k \end{bmatrix} - I_{t,k} R_o + v_{1,k} \end{cases} \quad (5.36)$$

Denote  $x$  as the system states, i.e.,  $x = [U_p \ z]^T$ . The first step of Kalman filter implementation is the initialization of the system states and the covariance matrix. The initialization does not change the following calculation. Therefore, the initial states can be set at zero.

$$\hat{x}_{0|0} = E(x_0), \ x_{0|0} = 0 \quad (5.37)$$

The state prediction equation is given as follows,

$$\hat{x}_{k|k-1} = \begin{bmatrix} e^{-\Delta t/\tau} & 0 \\ 0 & 1 \end{bmatrix} \hat{x}_{k-1|k-1} + \begin{bmatrix} (1 - e^{-\Delta t/\tau}) R_p \\ -\Delta t / C_n \end{bmatrix} I_{L,k} \quad (5.38)$$

and the covariance matrix is

$$P_{k|k-1}^x = \begin{bmatrix} e^{-\Delta t/\tau} & 0 \\ 0 & 1 \end{bmatrix} P_{k-1|k-1}^x \begin{bmatrix} e^{-\Delta t/\tau} & 0 \\ 0 & 1 \end{bmatrix}^T + Q_{k-1}^x \quad (5.39)$$

where  $Q$  is the covariance of the process noise.

The Kalman filter gain is calculated as follows,

$$\begin{aligned} K_k^x &= P_{k|k-1}^x C_k^{xT} \left( C_k^x P_{k|k-1} C_k^{xT} + R_k^x \right)^{-1} \\ &= P_{k|k-1}^x \left[ -1 \frac{dU_{oc}}{dz} \right]^T \left\{ \left[ -1 \frac{dU_{oc}}{dz} \right] P_{k|k-1} \left[ -1 \frac{dU_{oc}}{dz} \right]^T + R_k^x \right\}^{-1} \end{aligned} \quad (5.40)$$

where  $R$  is the covariance matrix of the measurement noise.

The state estimation prediction can be corrected after obtaining the latest measurement,

$$\hat{x}_{k|k} = \hat{x}_{k|k-1} + K_k^x \left[ U_{t,k} - \left( \left[ -1 \frac{dU_{oc}}{dz} \right] \hat{x}_{k|k-1} - I_{t,k} R_o \right) \right] \quad (5.41)$$

and the updated covariance matrix is

$$P_{k|k}^x = (I - K_k^x C_k^x) P_{k|k-1}^x = \left( I - K_k^x \left[ -1 \frac{dU_{oc}}{dz} \right] \right) P_{k|k-1}^x \quad (5.42)$$

The EKF procedure for SOC estimation thus includes an iterative calculation of Eqs. (5.39) to (5.42). In the dual-EKF algorithm, the battery capacity reduction is estimated together with the SOC. The estimation of SOC and battery capacity can be executed at different timescales to improve the algorithm's stability and to reduce the computational cost.

The battery model and state estimation scheme are implemented in Matlab, including the input layer, the Ah-counting module, the SOC estimation module and the output layer.

### (1) Input layer

The input layer includes the current, voltage, temperature input signals, as shown in Fig. 5.12. Four different test profiles are included in the input layer:

- RT\_130AH\_110 stands for 110 A constant current discharge;
- RT\_130AH\_120A stands for 120 A constant current discharge;
- RT\_130AH\_charge stands for CCCV full charge;
- RT\_130AH\_DST is the dynamic discharge profile for DST test.

Temp stands for the temperature input. Each test profile consists of the current profiles and time stamps and the initial SOC (SOC\_0). The data can be imported from Excel file.

### (2) Ah integral module

The Ah integral module (Ah\_integral) is used to validate the performance of the EKF estimation, as shown in Fig. 5.13. The initial SOC of the Ah-counting module is set to the correct value, i.e., SOC\_0.

### (3) State estimation module

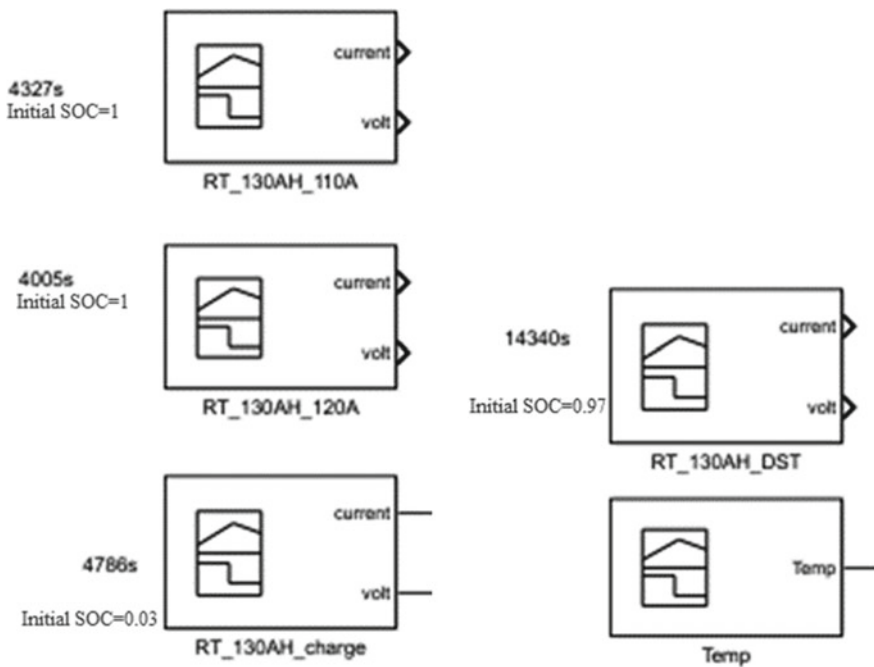


Fig. 5.12 Input layer

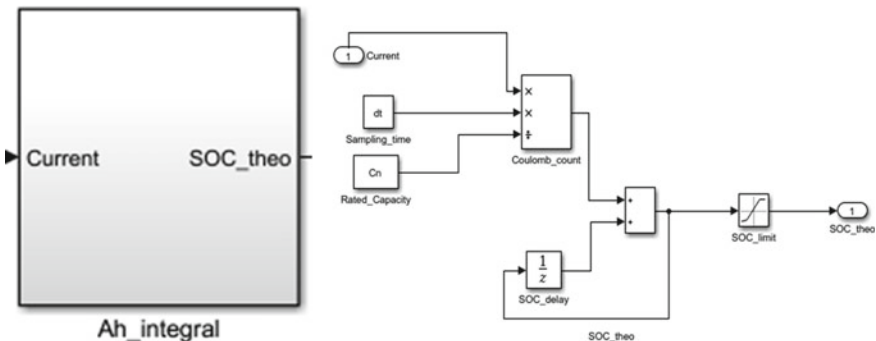
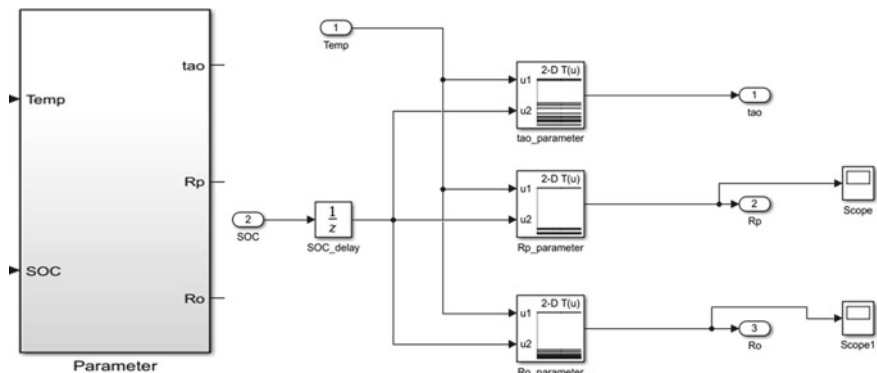


Fig. 5.13 Ah integral module

### ① Parameter identification

The identified model parameters (time constants, polarization resistance and capacitance) and the parameter dependency on temperature and SOC are stored in lookup tables. The real-time parameters are obtained using linear interpolation method (Fig. 5.14).

### ② SOC estimation module using EKF



**Fig. 5.14** Parameter identification module

The SoC estimation module using the EKF algorithm is implemented in Simulink using the above equations, as shown in Fig. 5.15.

### ③ Output layer

The output layer includes SOC estimation results and the estimation error, as shown in Fig. 5.16.

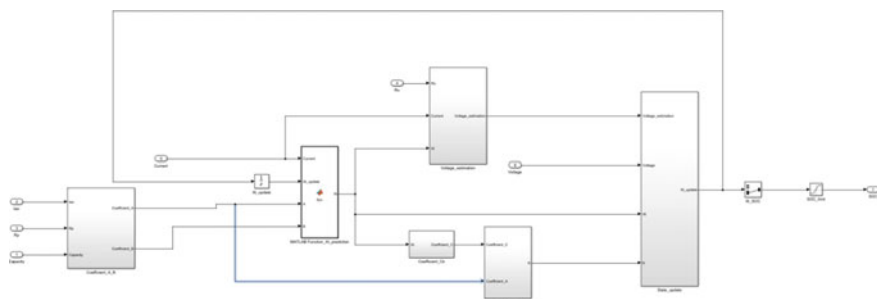
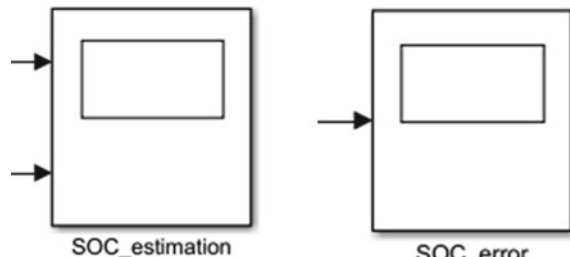


**Fig. 5.15** EKF module

**Fig. 5.16** Output layer



### 5.3.2 Validation of Accuracy

#### (1) Constant current load condition

The constant current load profile is used to simulate the operating condition of the battery under charging or when the EV is in constant-speed cruise mode. The SOC estimation error under constant current load needs to be validated first, because the battery parameters under constant current may be different from the identified parameters using the current pulses.

The model's voltage output is compared with the measurements under 125 A charge/discharge at 45°C. The test starts with constant current discharge, followed by rest period and then the CCCV charge procedure. Figure 5.17 shows that the model accuracy is high, which validated the effectiveness of the parameter identification algorithm.

The SOC estimation results under this working condition are shown in Fig. 5.18, along with the estimation error. The results show that the SOC estimation accuracy is high for discharging and rest period, while the error increases during the charging period (error peaks at around 50% SOC). The SOC error is limited within 3% through the full test.

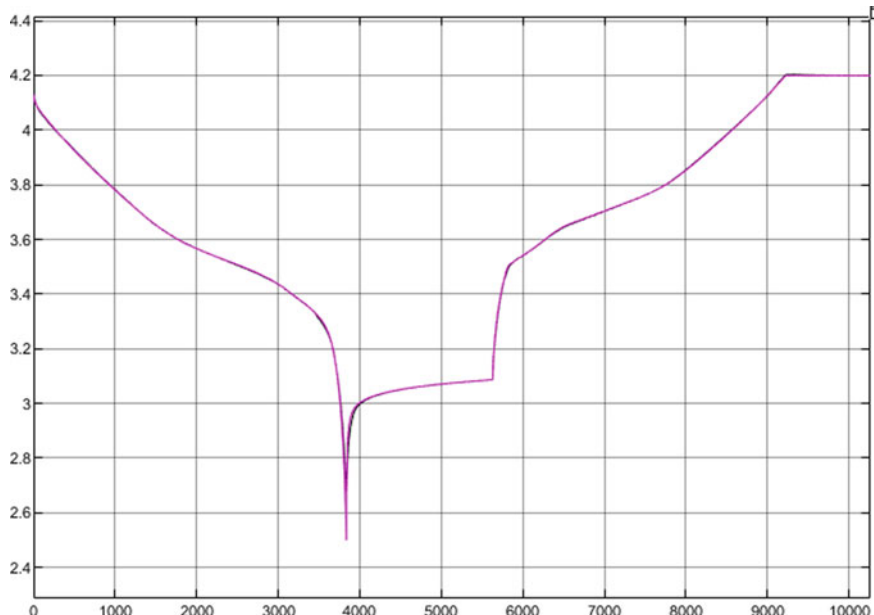


Fig. 5.17 Modelling results under constant current load (45 °C, 125 A)

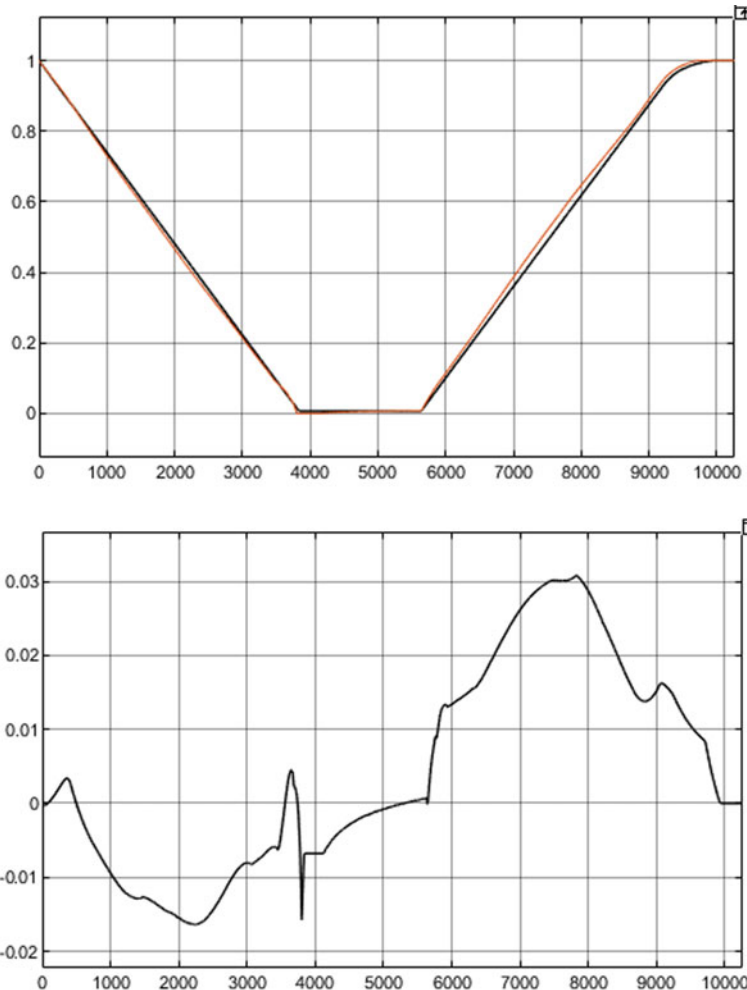
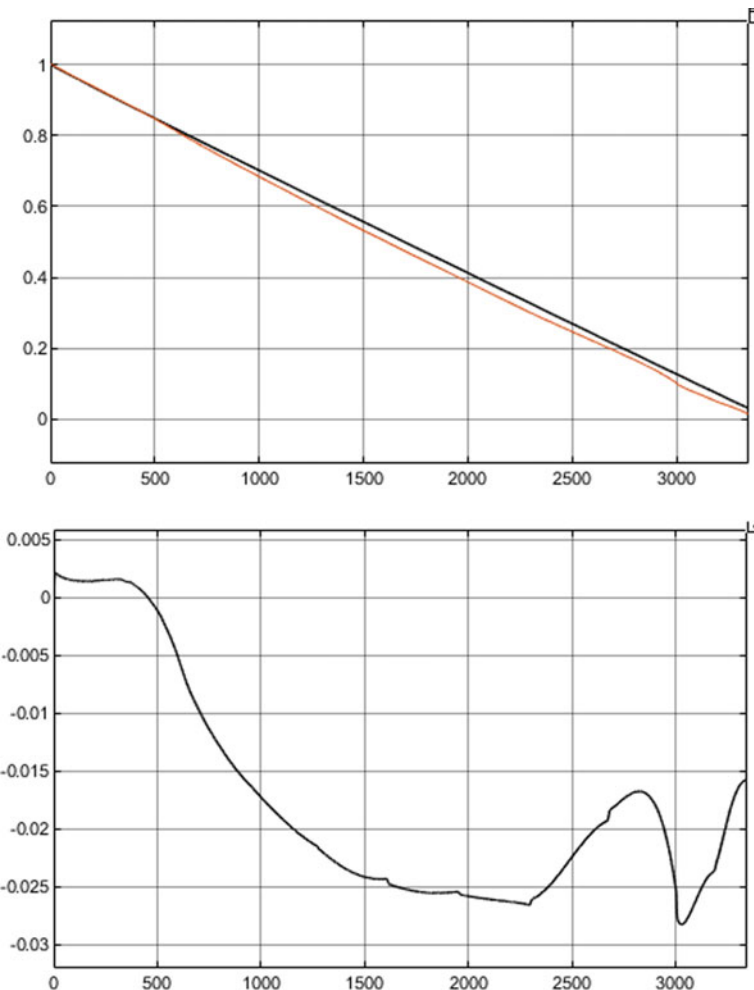


Fig. 5.18 SOC estimation results and errors (45 °C, 125 A)

The constant current test is repeated under low temperatures. The SOC estimation results at  $-10^{\circ}\text{C}$  are shown in Fig. 5.19. The SOC estimation error is limited within 3%, indicating a high performance of the state estimation.

## (2) Validation under dynamic current profile

The accuracy of the battery model and the state estimation algorithm are validated further under dynamic current load. The current profile is obtained from the vehicle's real-world driving test. The battery is then tested in laboratory using the dynamic current profile. The validation results under  $-10^{\circ}\text{C}$  are



**Fig. 5.19** SOC estimation results and errors ( $-10^{\circ}\text{C}$ , 125 A)

shown in Fig. 5.20. As it is shown, the estimation accuracy is high, and the error is limited within 2%.

### (3) Convergence study

The above validation is conducted under ideal conditions, i.e., correct initial SOC and battery capacity. In practice, the estimation accuracy will be influenced by wrong initializations. Suppose there is a 10% initial SOC error. The estimation results under the constant current discharge load at  $45^{\circ}\text{C}$  is shown in Fig. 5.21. As it is shown, the SOC estimation gradually converges to the

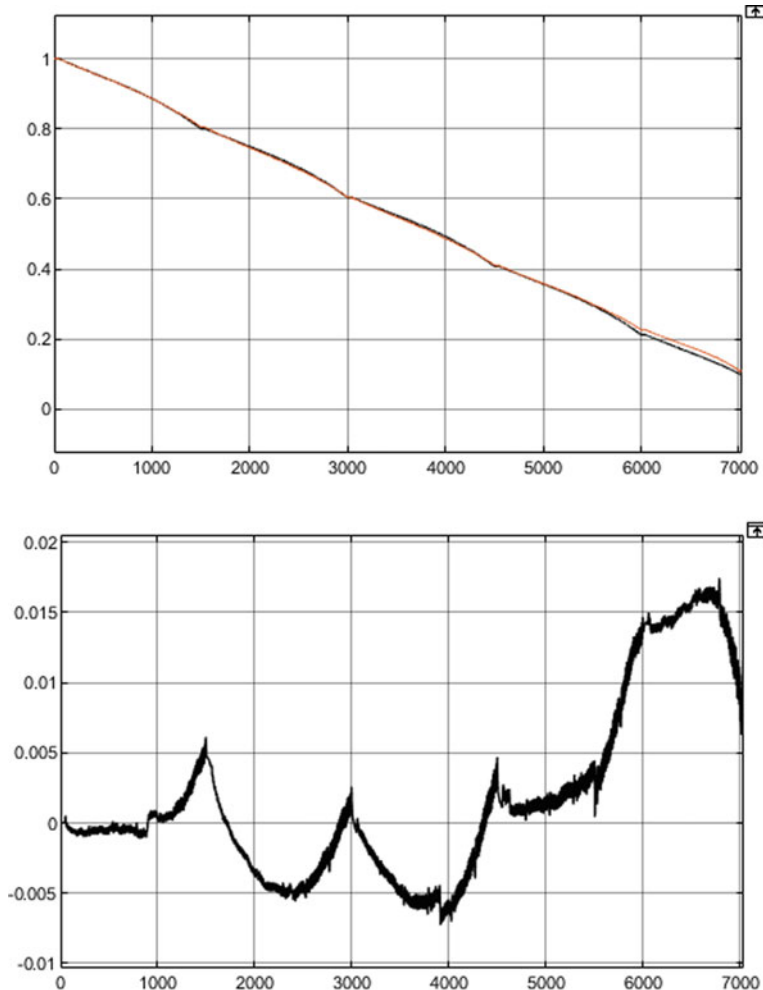


**Fig. 5.20** SOC estimation results and estimation error under dynamics current profile

correct value. After 1000 s (SOC at 70%), the SOC error is reduced to below 2%. Similar results are obtained under dynamic current profiles. Therefore, these experimental results have verified the effectiveness of the proposed SOC estimation algorithm to correct the initial error.

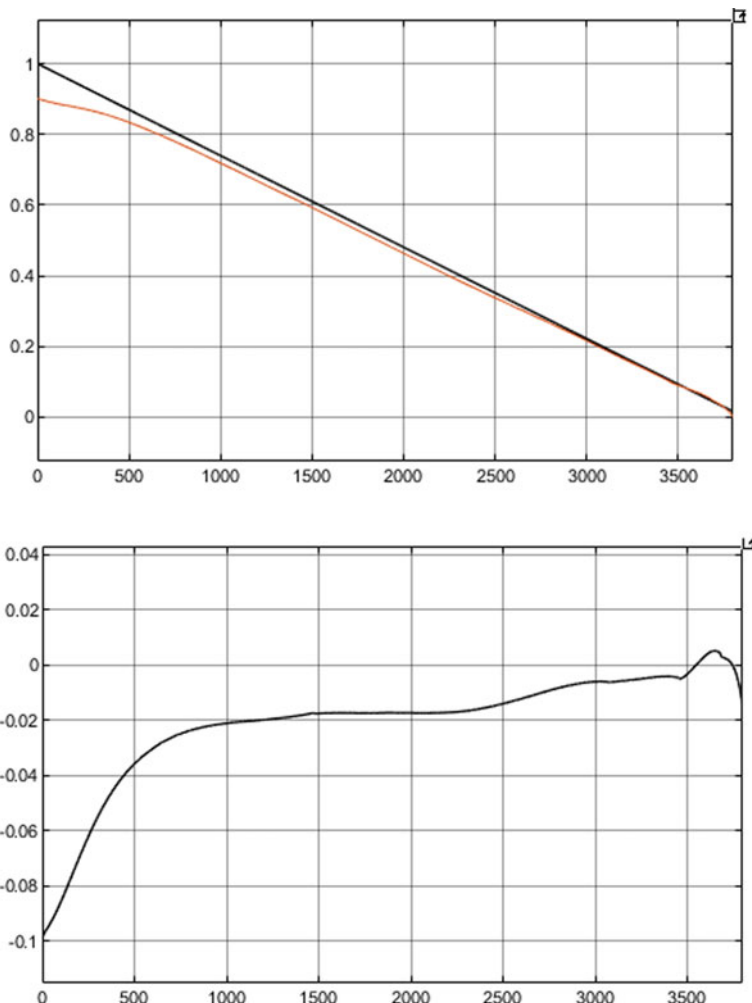


**Fig. 5.21** SOC estimation results (45 °C, 125 A constant current discharge)

## References

- Deng Z, Yang L, Cai Y et al (2016) Online available capacity prediction and state of charge estimation based on advanced data-driven algorithms for lithium ion phosphate battery. *Energy* 112:469–480
- Deng LZ, Wu F, Gao XG, Wu WP (2020) Development of a LiFePO<sub>4</sub>-based high power lithium secondary battery for HEVs applications. *Rare Met* 39(12):1457–1463
- Ji YR, Weng ST, Li XY, Zhang QH, Gu L (2020) Atomic-scale structural evolution of electrode materials in Li-ion batteries: a review. *Rare Met* 39(3):205–217
- Lin C, Yu Q, Xiong R et al (2017) A study on the impact of open circuit voltage tests on state of charge estimation for lithium-ion batteries. *Appl Energy* 205:892–902

- Liu S, Jiang J, Shi W, Ma Z, Guo H (2014) State of charge and peak power estimation of NCM/Li<sub>4</sub>Ti<sub>5</sub>O<sub>12</sub> battery using ic curve for rail tractor application. In: IEEE transportation and electrification conference and Expo, ITEC Asia-Pacific 2014—Conference Proceedings, pp 1–3
- Lu L, Han X, Li J et al (2013) A review on the key issues for lithium-ion battery management in electric vehicles. *J Power Sources* 226:272–288
- Xiong R, Tian J, Shen W, Sun F (2018) A novel fractional order model for state of charge estimation in lithium ion batteries. *IEEE Trans Veh Technol* 68(5):4130–4139
- Xiong R, Cao J, Yu Q et al (2017) Critical review on the battery state of charge estimation methods for electric vehicles. *IEEE Access: Practical Innovations, Open Solutions* PP(99):1
- Yang R, Xiong R, He H, Mu H, Wang C (2017) A novel method on estimating the degradation and state of charge of lithium-ion batteries used for electrical vehicles. *Appl Energy* 207:331–340
- Zhang C, Wang LY, Li X, Chen W, Yin GG, Jiang J (2015) Robust and adaptive estimation of state of charge for lithium-ion batteries. *IEEE Trans Industr Electron* 62(8):4948–4957

# Chapter 6

## SOH Estimation



### 6.1 SOH Definition

The battery energy and power capacities will decrease with ageing. The ageing indicator, state of health (SOH), is of great significance to the battery safety, the EV's performance and the user's driving experience. Once the SOH drops below a threshold value, the battery needs to be retired from EV to prevent safety hazards.

The widely used SOH definition is the ratio of the current capacity to the nominal capacity, under a specified test condition (CCCV fully charge followed by a constant current discharge at a fixed rate). The failure of battery is defined in the test procedure (USABC battery characterization protocol) when the battery capacity reaches 80% of the nominal capacity. Then the battery is no longer suitable for EV usage and needs replacement. The SOH can also be defined using other measurable performance parameters, such as the internal resistance or impedance. The battery's capacity and resistance, which determine the battery's energy and power capacities, are widely used for SOH estimation in practical applications (Waag et al. 2013).

- (1) SOH definition using capacity is given as follows,

$$SOH = \frac{Q_{\text{aged}}}{Q_{\text{new}}} \quad (6.1)$$

where  $Q_{\text{aged}}$  is the current capacity, and  $Q_{\text{new}}$  is the nominal capacity at beginning of life.

- (2) SOH definition using resistance is as follows,

$$SOH = \frac{R_{\text{EOL}} - R}{R_{\text{EOL}} - R_{\text{new}}} \quad (6.2)$$

where  $R_{\text{EOL}}$  is the battery resistance at end of life,  $R_{\text{new}}$  is the resistance at beginning of life, and  $R$  is the current resistance.

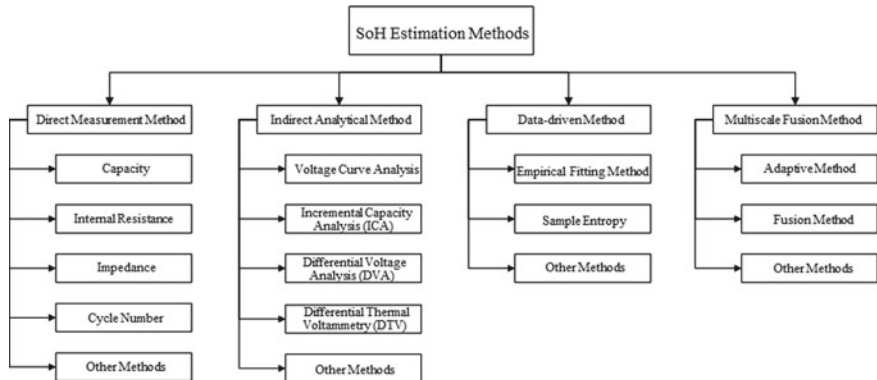


**Fig. 6.1** Classification of SOH estimation methods

Battery is a highly complex system and the ageing process can be even more complex. The battery's capacity/power degradation is the result of complicated electrochemical processes including multiple ageing mechanism and interactions. It is usually very difficult to separate and study an individual ageing mechanism, because these various ageing mechanisms are coupled and happen at the same timescale. Therefore, battery ageing study is very challenging.

The ageing mechanisms for the anode and cathode of the battery are different. The anode ageing is mainly caused by the growth of solid electrolyte interface (SEI), which leads to resistance increase. The lithium plating at the anode caused by fast charging at low temperature can lead to fast degradation of the battery's capacity and power. The cathode performance decreases with storage time and cycling operations due to structural cracking, chemical decomposition and dissolution, etc. The electrolyte decomposition is another cause to battery ageing.

There are various tools and methods for SOH estimation to predict the battery's service life. These methods are classified into four groups here: direct measurement methods, indirect analytical methods, data-driven methods and multiscale fusion methods, as shown in Fig. 6.1.

## 6.2 Direct Measurement Method

Battery capacity measurement is the mostly widely used method to characterize the battery's SOH. Other widely used SOH indicators include ohmic resistance, impedance, cycle number and fault detection etc.

### 6.2.1 Capacity

The driving range of battery-powered EVs is determined by the battery capacity. The capacity measurement is the widely used method for SOH estimation.

This method is the simplest and most accurate for SOH estimation. Firstly, the battery is fully charged following the specified charging procedure, such as the CCCV protocol. Then it is fully discharged under a fixed rate till end of discharge (e.g., using a cut-off voltage threshold). The battery capacity is then obtained by calculating the discharge capacity in Ampere hour. Then the SOH can be obtained as the ratio between the current capacity and the nominal capacity. The disadvantage of this method is that it cannot be applied when the battery is under dynamic current load in EVs. This method is usually used in laboratory estimation of the battery's capacity.

### 6.2.2 Internal Resistance

The battery's power capacity depends on the internal resistance, which can be calculated using the instantaneous voltage drop when a pulse current is applied. The internal resistance is also widely used for SOH estimation.

The main internal resistance of the battery includes the ohmic resistance and the polarization resistance. Studies have shown that the ohmic resistance is closely relevant with the SOH while the polarization resistance is relatively independent from SOH. The ohmic resistance consists of the resistance of the current collectors, electrode material, electrolyte and separator. The voltage response of a battery under pulse discharge is shown in Fig. 6.2. When the EV brakes or accelerates, the battery load is similar to a pulse. The ohmic resistance is calculated using the instantaneous voltage drop as follows,



**Fig. 6.2** Battery voltage dynamics under charge/discharge current pulses

$$R_o = \frac{\Delta U}{\Delta I} \quad (6.3)$$

where  $\Delta U$  is the voltage drop, and  $\Delta I$  is the change of current. The resistance can vary with the current rate and the width of the pulse.

Because of the complex internal electrochemical reactions of the battery, the ohmic resistance measurement can also vary with the battery's operating conditions, such as the depth of discharge, temperature and SOC etc. (Jürgen et al. 2011).

### 6.2.3 Impedance

Electrochemical impedance spectroscopy (EIS) is a popular nondestructive method for battery characterization and parameter identification. The test covers a wide frequency range from  $\mu$ Hz to MHz. EIS test is widely used to study the battery's internal electrochemical properties, such as the reaction dynamics at the electrode–electrolyte interface, the electrode impedance and the (de)intercalation of ions in the electrode.

The EIS measurement is an important tool for battery SOH characterization. The battery's overall impedance consists of ohmic resistance, charge transfer and diffusion impedance. The battery's internal properties at different frequency ranges can be revealed by the EIS measurements, e.g., the inductive effect at high frequency due to the porous electrode structure, the ohmic resistance at moderate frequency and the capacitive effect at low frequency due to ion diffusion. The moderate-frequency ohmic resistance increase noticeably with ageing, as shown in Fig. 6.3, which can be used for SOH estimation. The EIS measurements can also be used for parameter

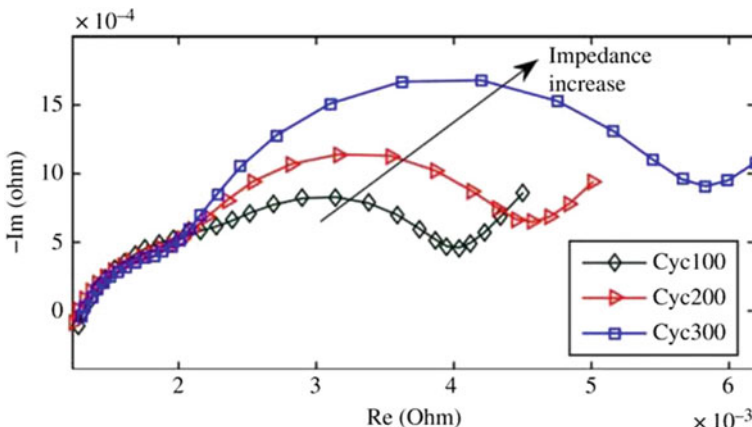
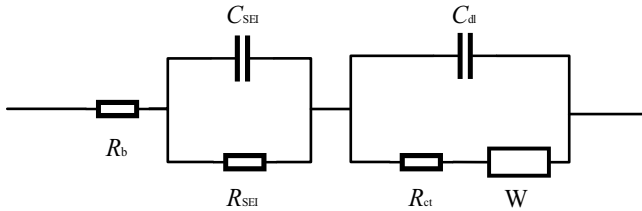


**Fig. 6.3** Battery EIS measurements after different numbers of cycles (Waag et al. 2014)



$R_b$ —Ohmic resistance,  $R_{SEI}$ —SEI resistance,  $C_{SEI}$ —SEI capacitance,  $R_{ct}$ —charge transfer resistance,  $C_{dl}$ —double layer capacitance,  $W$ —Warburg impedance.

**Fig. 6.4** Battery EIS measurements and the frequency-domain equivalent circuit model

identification of the equivalent circuit model in Fig. 6.4, which enables a quantitative analysis and diagnosis of the internal ageing mechanisms.

#### 6.2.4 Cycle Number

The battery's total cycle number during its service life is an important indicator for cell selection. The battery's SOH can be estimated using the number of cycles the battery has experienced and the total cycle number specified by the cell manufacture, as follows,

$$SOH = \frac{N_T - N_E}{N_T} \times 100\% \quad (6.4)$$

where  $N_T$  is the total cycle number specified by manufacture,  $N_E$  is the equivalent full cycles the battery has run through. A fully discharge of the battery from 100% SOC is equivalent to one full cycle. The number of partial charging/discharging cycles can be converted to equivalent full cycle using a conversion coefficient, which is usually calibrated experimentally.

#### 6.2.5 Other Methods

The battery SOH can be characterized using destructive methods to disassemble the battery to enable a direct observation of the ageing conditions of the battery internal components. There are two popular disassembly methods. One is the half-cell test using the harvested battery material, and the other is direct observation of the battery components using Scanning Electron Microscope, Transmission Electron Microscope, X-ray Diffraction, X-ray Photoelectron Spectroscopy, Infrared Spectroscopy and Gas Chromatography etc. These methods are usually applied only in laboratories.

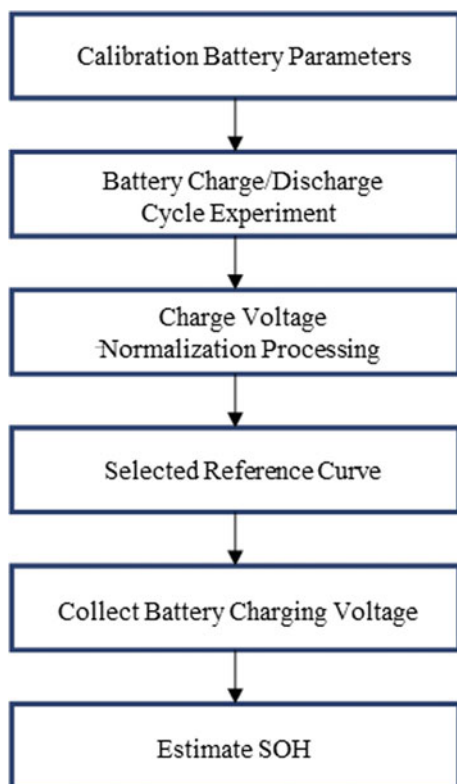
### 6.3 Indirect Analysis Methods

The indirect analysis methods for SOH estimation generally rely on health indicators that are related with the battery's capacity or resistance. These indicators are usually identified by analyzing the battery's operation data at different life stages.

#### 6.3.1 Voltage Curve Analysis

When the battery ages, the voltage curve under large charge/discharge current changes noticeably. This effect can be used for SOH estimation. Because the discharge current profile of the battery in EV depends on the driver's maneuver which is not controllable by the onboard BMS, the charging voltage curve is usually used for SOH estimation. The offline characterization data of the charging voltage curve of the battery at different ageing levels are normalized and stored. Next, the battery's real-time voltage curve under charging is compared with the history data for onboard SOH estimation. The procedure is shown in Fig. 6.5.

**Fig. 6.5** The procedure of voltage curve analysis method for SOH estimation



### 6.3.2 Incremental Capacity Analysis

The incremental capacity analysis (ICA) is a useful method for SOH estimation and ageing diagnosis without disassembling the battery. During the battery's charging/discharging process, the voltage curve is divided into segments using constant voltage grids (grid size  $\Delta V$ ). The incremental capacity for each voltage segment is calculated by integral of the corresponding current ( $\Delta Q$ ). The incremental capacity (IC) curve,  $\Delta Q/\Delta V$  versus voltage, can then be obtained. The advantage of the IC curve analysis is that the stageing effect on the original voltage curve caused by electrode phase changes is transformed into more identifiable peaks and valleys on the IC curve. It increases the sensitivity of the curve change to the ageing. The shift of the peaks and valleys on the IC curve at different ageing levels can then be used for ageing diagnosis of the battery. In this way, the battery's internal ageing status (shift of electrode stageing) can be estimated using the external measurement signals, the voltage and capacity. The IC curve is usually obtained at low charging current, e.g., C/20, for ageing diagnosis. In practical application, larger current can be used, such as C/3.

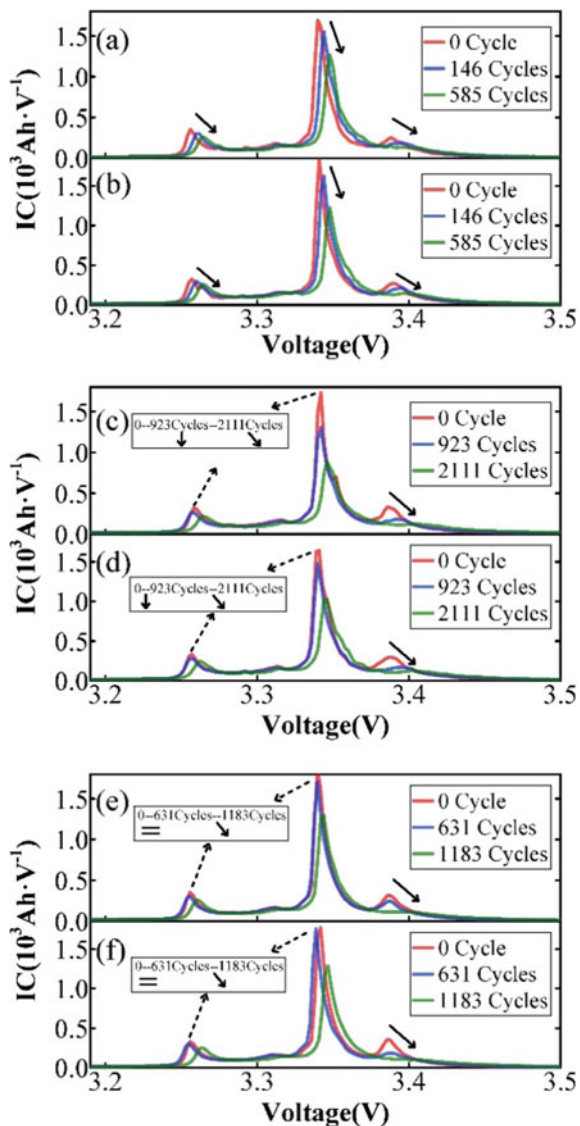
Loss of lithium inventory (LLI) and loss of active material (LAM) are the two main causes to battery ageing. The LAM can be further attributed to the anode ( $LAM_{NE}$ ) and cathode ( $LAM_{PE}$ ). Figure 6.6 shows that the peaks on the IC curve shift to right with reduced magnitude as the battery ages due to LLI and LAM. Therefore, these evolving peaks can be used for SOH estimation (Jiang et al. 2018).

### 6.3.3 Differential Voltage Analysis

The differential voltage analysis (DVA) is another widely used method for battery SOH estimation. It relies on the analysis of the evolving differential voltage (DV) curve,  $\Delta V/\Delta Q$  versus voltage, with ageing. The peaks on the DV curve are caused by the effect of electrode's phase change during charging/discharging. The distance between two peaks on the DV curve stands for the capacity between the two phase-change points. These values can be used for analyzing the battery's capacity loss and LAM.

The DV curve obtained from the charging data of LiFePO<sub>4</sub>-graphite cell is shown in Fig. 6.7 (Han et al. 2014). The DV curve are divided into three segments by the two peaks. The capacities for the segments are denoted in turn as  $Q_A$ ,  $Q_B$  and  $Q_C$ . These various capacity values can be related with the battery's internal ageing mechanisms.

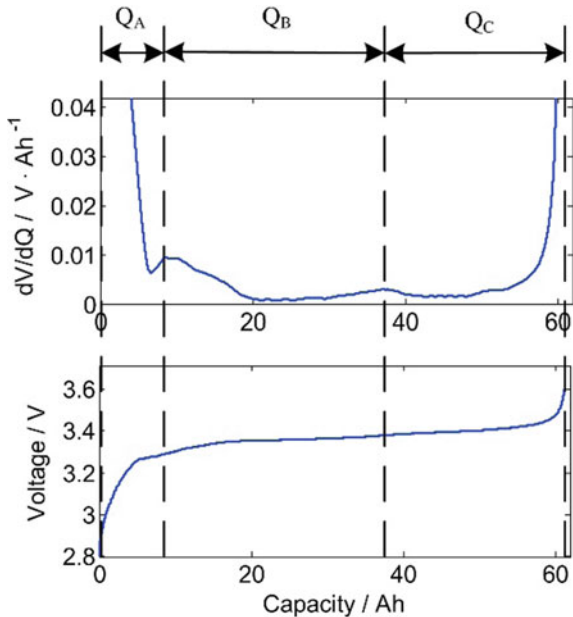
**Fig. 6.6** IC curve of LiFePO<sub>4</sub> cells at different ageing levels (Jiang et al. 2018)



### 6.3.4 Differential Thermal Voltammetry

The differential thermal voltammetry (DTV) method studies the entropy change of the battery by analyzing the battery's surface temperature under constant-current charging/discharging operations. The DTV method can be used for SOH estimation, because the changing rate of the battery's enthalpy and entropy depends on the

**Fig. 6.7** Battery voltage and DVA curve of LiFePO<sub>4</sub> cell under 1/3C constant current charging at 25 °C (Han et al. 2014)



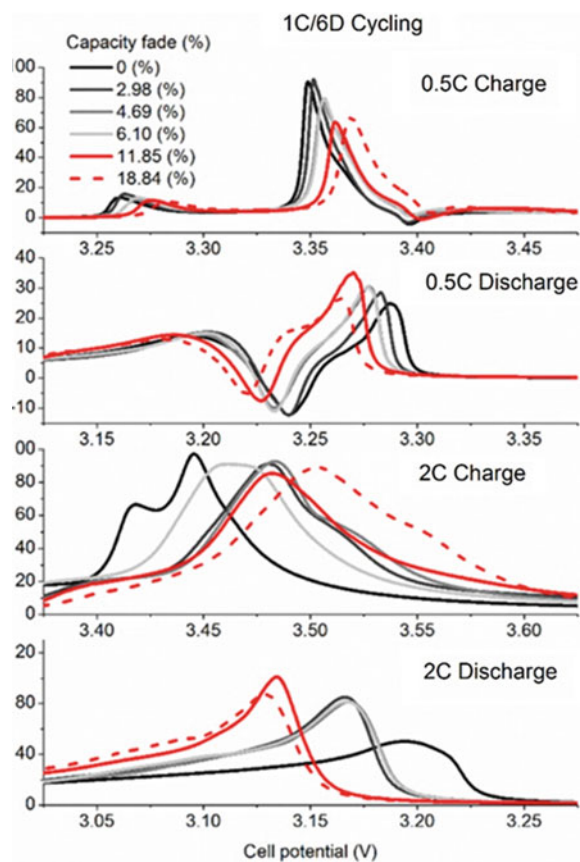
degradation mechanisms. The DTV method is a novel technique for battery diagnosis (Merla et al. 2016). The DTV method relies only on the battery's voltage and temperature signals, and the battery's surface temperature can be measured by thermocouples or thermal imaging camera. The partial derivative of the temperature against voltage is used in DTV analysis,

$$DTV = \frac{dT}{dt} \left/ \frac{dV}{dt} \right. = \frac{dT}{dV} \quad (6.5)$$

where  $T$  is the temperature,  $V$  is the battery voltage and  $t$  is time. The features of the DTV versus voltage curve are then used for battery's ageing diagnosis.

Similar to the IC and DV curves, peaks on the DTV curve are also related to the (de)intercalation of ions into the electrode, because the stageing effect has a noticeable influence on the voltage curve and the changing rate of entropy. The analysis of the evolving peaks on the DTV curve can be supplementary to the IC and DV analysis. Further, the DTV method doesn't require a constant-temperature operating condition. On the contrary, the dynamic temperature is used for battery diagnosis.

**Fig. 6.8** DTV curves of a LiFePO<sub>4</sub>-graphite battery under different charging/discharging currents at different ageing stages (Shibagaki et al. 2018)



The DTV curves of a LiFePO<sub>4</sub>-graphite battery under different charging/discharging currents at different ageing stages are shown in Fig. 6.8. The peaks on the DTV curves represent the region where the voltage changes slowly and the battery produces a lot of heat. The transition between peaks are caused by fast voltage change due to one electrode going through stageing transition. This is similar to the ICA method. The major difference between the ICA and the DTV methods is that the DTV curve has negative peaks. This is because when the heat absorption of the battery's endothermic reactions is significantly higher than the heat generation from exothermic reactions, the battery's temperature will drop, leading to a negative peak in the DV curve. The negative peak will disappear at high current. This is because the heat absorption is proportional to current, while the heat generation is proportional to the square of current. Further, when the current changes direction, the entropy change will generate heat, leading to the positive peak in the DV curve. As shown in Fig. 6.8, as the battery ages, the peaks shift towards higher voltage under charging. Under discharging, the peaks shift towards lower voltage. This is caused by the resistance increase due to degradation which

increases the battery's internal over-potential. Therefore, the battery's SOH can be estimated using these locations, magnitudes and width of the peaks.

### 6.3.5 *Other Methods*

The battery's mechanical properties also change during the ageing process, such as modulus and density distribution. Ultrasonic detection is the simple and widely used method for Non-Destructive Evaluation and Structural Health Monitoring. The stimulation, propagation and signal reception of mechanical stress wave in the material is used for continuous and real-time monitoring of the mechanical properties to evaluate the structure integrity and to detect internal defects. Ultrasonic detection has been used for monitoring the battery's modulus and density evolution for SOH estimation (Ladpli et al. 2018). Further, the relationship between the battery's mechanical stress change and the battery capacity and resistance has also been used for SOH estimation (Cannarella and Arnold 2014).

## 6.4 Data-Driven Methods

Because of the high complexity of the battery's internal reactions and the high uncertainties of the operating condition, it is challenging to develop accurate physics-based dynamic models of the battery. The advantage of data-driven method is that the physical interpretation of the battery's properties is not required. The data-driven models are developed using the battery's historical data for model training. However, the disadvantage of the data-driven methods is that the experimental data collection can be time-consuming and costly particularly for ageing tests which can take months or a couple of years.

### 6.4.1 *Empirical Methods*

The empirical fitting method captures the relationship between battery degradation and the external operating conditions by learning from the experimental data rather than interpreting the internal ageing mechanism. This method can offer accurate SOH estimation under the support of large amount of test data of the battery. The experiments can be conducted under normal operating conditions or accelerated ageing conditions such as high temperature. Test of accelerating ageing can save time, but the ageing test under normal operating conditions can be more representative of the ageing process of the battery in real-world applications. The SOH evolution is usually described using the Arrhenius equation or polynomials for data fitting, and

the selection of the function depends on the battery electrochemical properties and the fitting accuracy.

### (1) Arrhenius equation

The Arrhenius equation is widely used in empirical methods for SOH estimation. The Arrhenius equations describes the relationship between reaction rate and temperature and activation energy, as follows,

$$k = A \exp\left(-\frac{E_a}{RT}\right) \quad (6.6)$$

where  $k$  is the reaction rate,  $R$  is the molar gas constant.  $T$  is the temperature (unit: K) and  $E_a$  is the activation energy.  $A$  is a constant coefficient. The influence of the other factors, such as DOD, SOC, C-rate, cycle number and Ah throughput, on the ageing rate can be captured by modifying the equation as follows (Bloom et al. 2001):

$$Q = B \exp\left(-\frac{E_a}{RT}\right) t^z \quad (6.7)$$

where  $B$  is the coefficient,  $t$  is time,  $z$  is the power coefficient. These parameters can be varied under different operating conditions to improve the fitting accuracy.

### (2) Polynomial equation

Although the temperature dependency of the ageing processes of many batteries follow the Arrhenius equation, for some batteries the Arrhenius law doesn't apply. A more flexible function base can then be used, such as polynomials, to fit the ageing trend. The polynomial equations have been used to capture the time-dependency of the battery's calendar life (Waag et al. 2013).

## 6.4.2 Sample Entropy

Sample entropy was proposed by Richman et al. (2004) to assess the complexity of time-series signals. The procedure of implementation is as follows,

Analysis object: the time series of  $N$  data samples  $\{x(n)\} = x(1), x(2), \dots, x(N)$ .

**Step 1:** denote a set of  $m$ -dimension vectors,  $\mathbf{X}_m(1), \dots, \mathbf{X}_m(N-m+1)$ , where  $\mathbf{X}_m(i) = \{x(i), x(i+1), \dots, x(i+m-1)\}$ ,  $1 \leq i \leq N-m+1$ , i.e., the  $i$ -th vector  $\mathbf{X}_m(i)$  consists of  $m$  continuous values of  $x$  starting from time step  $i$ .

**Step 2:** define the distance between two vectors  $\mathbf{X}_m(i)$  and  $\mathbf{X}_m(j)$ ,  $d[\mathbf{X}_m(i), \mathbf{X}_m(j)]$ , as the maximum absolute value of the elements of the difference between the two vectors, i.e.,

$$d[\mathbf{X}_m(i), \mathbf{X}_m(j)] = \max_{k=0, \dots, m-1} (|x(i+k) - x(j+k)|) \quad (6.8)$$

**Step 3:** for each vector,  $\mathbf{X}_m(i)$ , count the number of other vectors whose distance from  $\mathbf{X}_m(i)$  is smaller than  $r$ , and denote this number as  $B_i$ . Further for  $1 \leq i \leq N - m$ , let

$$B_i^m(r) = \frac{1}{N - m - 1} B_i \quad (6.9)$$

**Step 4:** denote  $B^{(m)}(r)$  as

$$B^{(m)}(r) = \frac{1}{N - m} \sum_{i=1}^{N-m} B_i^m(r) \quad (6.10)$$

**Step 5:** increase the vector dimension to  $m + 1$ , and denote the number of vectors whose distance from  $\mathbf{X}_{m+1}(i)$  is smaller than  $r$  as  $A_i$ . Calculate  $A_i^m(r)$  as follows,

$$A_i^m(r) = \frac{1}{N - m - 1} A_i \quad (6.11)$$

**Step 6:** define  $A^{(m)}(r)$  as

$$A^{(m)}(r) = \frac{1}{N - m} \sum_{i=1}^{N-m} A_i^m(r) \quad (6.12)$$

Therefore,  $B^{(m)}(r)$  is the probability of two  $m$ -dimension vectors having distance smaller than  $r$ , and  $A^{(m)}(r)$  the probability of two  $(m + 1)$ -dimension vectors having distance smaller than  $r$ . The sample entropy can then be calculated as follows,

$$\text{SampEn } (m, r) = \lim_{N \rightarrow \infty} \left\{ -\ln \left[ \frac{A^m(r)}{B^m(r)} \right] \right\} \quad (6.13)$$

When  $N$  is a finite value, the following approximation can be used,

$$\text{SampEn } (m, r, N) = -\ln \left[ \frac{A^m(r)}{B^m(r)} \right] \quad (6.14)$$

The sample entropy method has been used for battery ageing diagnosis as it can capture the fluctuation and complex evolution of the voltage curve. This method is usually combined with other ageing diagnosis algorithms to improve the effectiveness and accuracy.

### 6.4.3 Other Methods

There are other data-driven method for battery diagnosis, including artificial neural network (ANN), Ordinary Least Squares Regression, Support Vector Machine (SVM), Fuzzy logic and Gaussian process regression, etc.

(1) ANN

The ANN algorithm is inspired by the biological neural networks that constitute animal brains. The ANN has become widely used for modeling complex and unknown systems. One advantage of the ANN method for SOH estimation is its ability to process data with nonlinear correlation. Another advantage is the generalization capability to many battery types, because the physical properties of the battery is not required for the model development. the main disadvantage is the high computational expense, making it difficult for onboard implementation in industrial BMS.

(2) SVM

The SVM method is based on statistical theory and uses the principle of structural risk minimization. The kernel functions are used to map the inputs to a high-dimensional space, where the optimal linear decision function is constructed. The algorithm can avoid curse of dimension while obtaining the global optimal solution. The generalization performance is high. The SVM method has been widely used for classification and regression study, i.e., Support Vector Classification and Support Vector Regression (SVR). The SVR based battery SOH estimation requires low computational time while offering high accuracy. The SVM method is suitable for model training using small set of samples. However, the implementation complexity is high for large data set. The algorithm performance is sensitive the selection of the kernel functions and model parameters, and the uncertainty and trust region of the prediction results are not available. Therefore, the SVM method is usually used in combination with other algorithms.

(3) Fuzzy logic

The fuzzy logic method uses a set of fuzzy rules to process data to develop models for nonlinear and complex systems. Uncertainties of environment and fuzziness of information can be effectively captured by the fuzzy logic method. The measurement data can be categorized as fuzzy set and crisp set. The fuzzy logic method is very useful for SOH estimation. However, it requires a large amount of data and high computational expense. A deep understanding of the battery's properties is also helpful to derive the fuzzy rules.

(4) GPR

The GPR method captures the system dynamics by learning from historical data. The advantage of GPR method is that the algorithm provides a confidence interval of the prediction, i.e., the prediction is probabilistic. The method is suitable for modelling high-dimension nonlinear systems (Liu et al. 2013).

## 6.5 Multiscale Joint Estimation

### 6.5.1 Adaptive Method

The adaptive methods have been widely used for SOH estimation, which relies on the battery's electrical properties, such as resistance, impedance and OCV. These signals need to be directly measurable or can be estimated in real-time. The adaptive algorithms don't require a large amount of offline experimental tests for battery characterization. However, the online adaptive estimation requires high computational expense, making the onboard implementation difficult. The Kalman filter method is widely used for estimation of the battery's parameters and states. Other popular estimation algorithms include EKF, UKF, PF, and Adaptive Extended Kalman Filter, Adaptive Unscented Kalman Filter and Adaptive Particle Filter, etc. Nonlinear observer algorithms including Luenberger observer, PI observer, H-inf observer and sliding mode observer, have also been used for the estimation of the model parameters and states.

### 6.5.2 Fusion Algorithms

These various algorithms introduced in the previous sections can be combined for SOH estimation. Each individual algorithm has its specific advantages and limitations and suitable operating conditions. Therefore, the combination of more than one algorithm can meet the system requirements under a wide range of operating conditions. The SOH estimation using fusion method can address the problems of low accuracy and low reliability and reduce false rate of each individual algorithm. Other advantages of the fusion method include the ease of implementation in real-time onboard controller. Therefore, the fusion methods have good prospect of application and have attracted more and more attention (Andre et al. 2013; Li and Xu 2015).

## 6.6 Case Study

### 6.6.1 Joint Estimation of SOC-SOH

A simulation case study of joint estimation of SOC and SOH is presented in this section. The DEKF method is used here, with one filter for the estimation of the battery capacity. Assuming constant current between samples, the Thevenin model can then be discretized as follows,

$$U_{p,k} = e^{(-\Delta t/\tau)} U_{p,k-1} + R_p I_{t,k-1} [1 - e^{(-\Delta t/\tau)}] \quad (6.15)$$

The SOC is calculated using the Ah counting method,

$$z_k = z_{k-1} - I_{t,k} \Delta t / C_n \quad (6.16)$$

where  $z_k$  is the SOC value at time step k,  $\Delta t$  is the sampling time and  $C_n$  the battery's nominal capacity under current temperature.

Because the battery capacity varies slowly with time, the capacity estimation problem is formulated as follows,

$$\begin{cases} C_k = C_{k-1} + \omega_{2,k-1} \\ d_k = z_k - z_{k-1} + \frac{\eta I_t \Delta t}{C_k} + v_{2,k} \end{cases} \quad (6.17)$$

where  $C_k$  is the battery capacity, considered as a slow-varying system state here.  $z_k$  is the SOC output from the EKF estimation;  $d_k$  is the system output, and the expected value of  $d_k$  is zero.

First, initialize the system state and the covariance matrix. The initialization won't affect the subsequent calculation. Therefore, the initial state is set to be the expected value and the covariance matrix set to zero.

$$\hat{C}_{0|0} = E(C_0), \quad P_{0|0}^C = 0 \quad (6.18)$$

The state prediction equation of the battery's capacity is given as follows,

$$\hat{C}_{k|k-1} = \hat{C}_{k-1|k-1} \quad (6.19)$$

and the covariance matrix is

$$P_{k|k-1}^C = P_{k-1|k-1}^C + Q_{k-1}^C \quad (6.20)$$

where Q is the covariance of the process noise.

The Kalman filter gain is

$$\begin{aligned} K_k^C &= P_{k|k-1}^C C_k^{CT} (C_k^C P_{k|k-1}^C C_k^{CT} + R_k^C)^{-1} \\ &= P_{k|k-1}^C \left( -\frac{\eta I_t \Delta t}{C_{k|k-1}^2} \right) \left( -\frac{\eta I_t \Delta t}{C_{k|k-1}^2} P_{k|k-1} \left( -\frac{\eta I_t \Delta t}{C_{k|k-1}^2} \right)^T + R_k^C \right)^{-1} \end{aligned} \quad (6.21)$$

where R is the covariance matrix of the measurement noise.

Finally, the correction of battery capacity is

$$\hat{C}_{k|k} = \hat{C}_{k|k-1} + K_k^C \left[ 0 - \left( \hat{z}_{k|k} - \hat{z}_{k-1|k-1} + \frac{\eta I_{t,k} \Delta t}{\hat{C}_{k|k-1}} \right) \right] \quad (6.22)$$

and the covariance matrix is updated as follows

$$P_{k|k}^C = (I - K_k^C C_k^C) P_{k|k-1}^C = \left( I - K_k^C \left( -\frac{\eta I_t \Delta t}{C_{k|k-1}^2} \right) \right) P_{k|k-1}^C \quad (6.23)$$

The real-time estimation of the battery capacity is achieved by repeating Eqs. (6.19) to (6.23).

Based on the above analysis, the multiple time-scale joint-estimation method of SOC and SOH is implemented in Matlab. The capacity estimation is normalized to the capacity at 25 °C, i.e., the latest capacity is first estimated, then divided by the battery capacity at 25 °C. The whole model consists of Observation\_equation module, Coefficient\_C module, Covariance and Kalman gain module and State\_update module, as shown in Figs. 6.9, 6.10, 6.11 and 6.12.

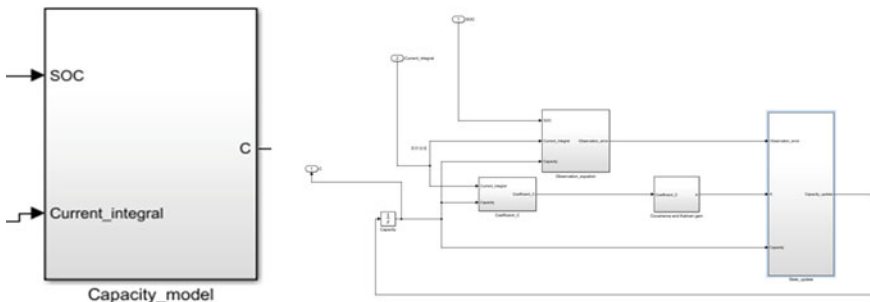


**Fig. 6.9** Capacity estimation module

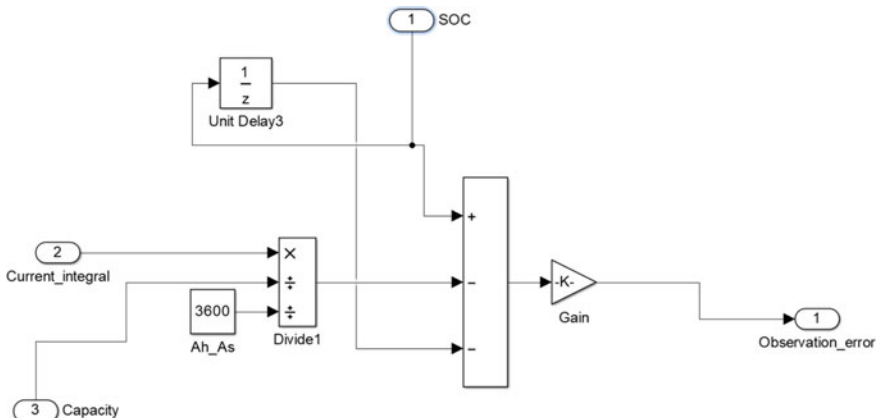


**Fig. 6.10** Observation\_equation module

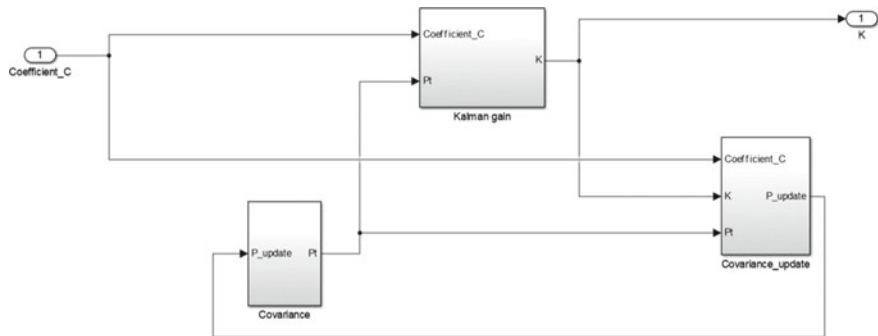


**Fig. 6.11** Covariance and Kalman gain module

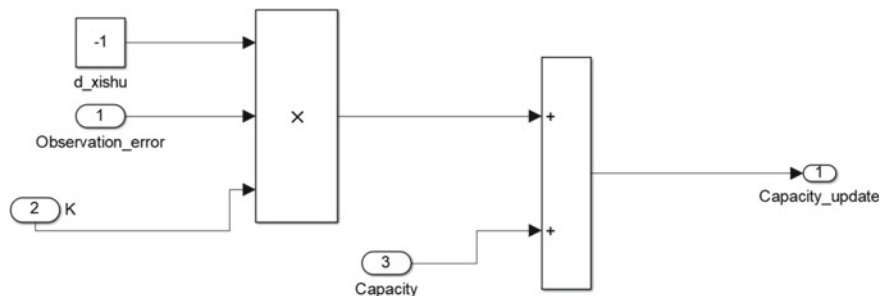


**Fig. 6.12** State\_update module

### 6.6.2 Accuracy Validation

#### (a) Constant current operating condition

The constant current can be used to simulate the battery's operating condition under charging or when the EV is in constant-speed cruise driving mode. Further, because the model parameters identified under other current profiles (such as pulse discharge) may be different from the parameters under constant current, the model error can increase. This makes accurate SOH estimation challenging. Therefore, it is necessary to validate the estimation performance under constant current conditions.

The model's voltage predictions in comparison with the measurements are shown in Fig. 6.13 under 125 A charging and discharging at 45 °C. The test starts from constant current discharge, followed by a rest period and then a CCCV charging operation. The model performance is validated as it can be seen in Fig. 6.13 where the model output matches the measurements with high accuracy. This also verifies the performance of the parameter identification algorithm.

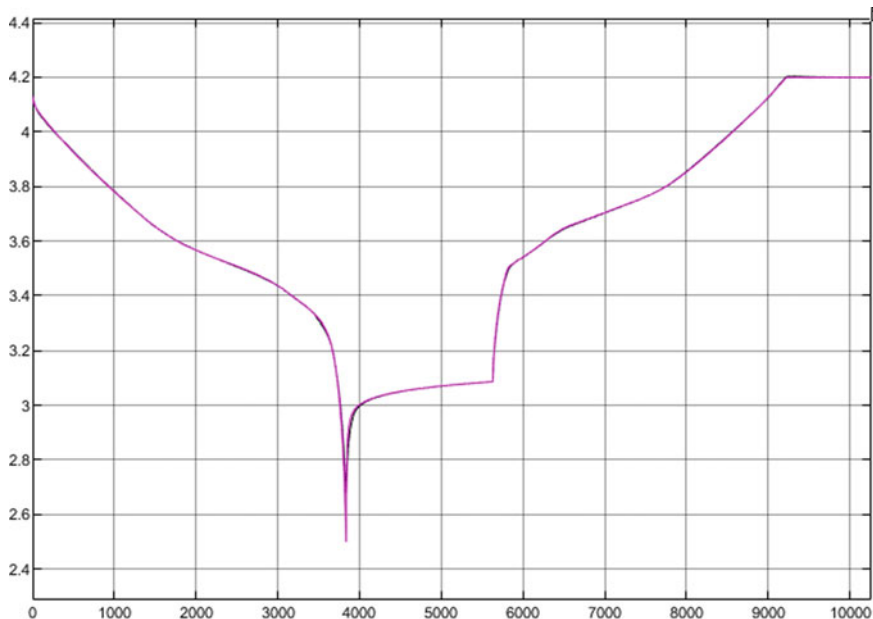


**Fig. 6.13** Model accuracy validation under 125 A charging and discharging at 45 °C

The results of capacity estimation under this operating condition are given in Fig. 6.14. The maximum capacity estimation error is limited under 1.2 Ah (less than 1% error). It has verified the accuracy of the capacity estimation algorithm.

Another validation is conducted at  $-10^{\circ}\text{C}$  under constant current operating condition. The capacity estimation results are given in Fig. 6.15. The maximum error is only 0.6 Ah (less than 0.5% error), which verifies the high accuracy of the estimation algorithm.

(b) Dynamic current operating condition

A dynamic current profile is used to further validate the reliability of the estimation algorithm. The driving profile is part of the BYD test procedure. The estimation results are given in Fig. 6.16. The maximum error is 2 Ah, less than 1.6%.

(c) Convergence analysis

These above two validation case studies are conducted with ideal initial condition. In practice the estimation performance can be affected by the initialization error. The effect of initial error is analyzed in this case study. The initial capacity guess is set at 135 Ah with 5Ah error. The estimation results under constant current load profile are shown in Fig. 6.17, which shows that the estimation gradually converges to the correct value, although the convergence rate is slow. The stable value of the capacity estimation can be verified by analyzing the

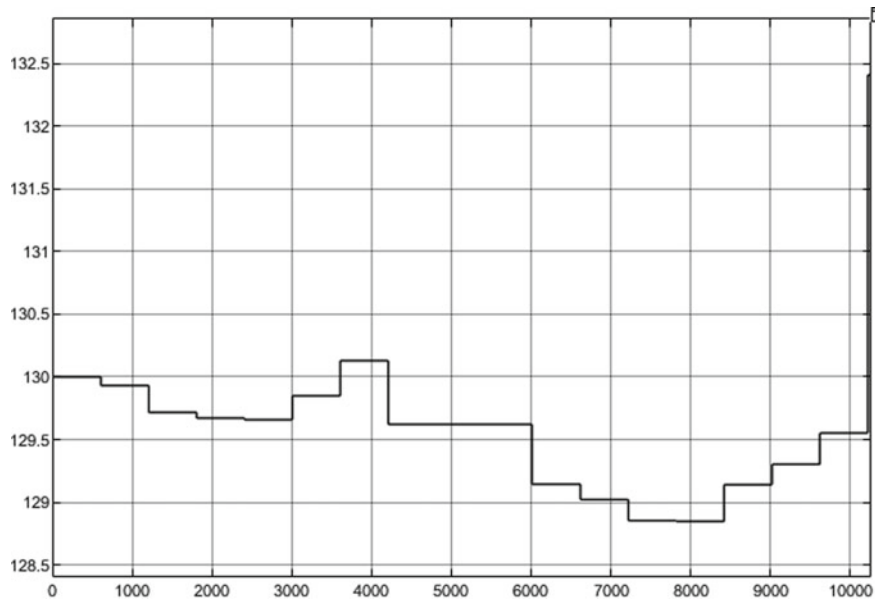


Fig. 6.14 Capacity estimation results at 45 °C under 125 A charging and discharging

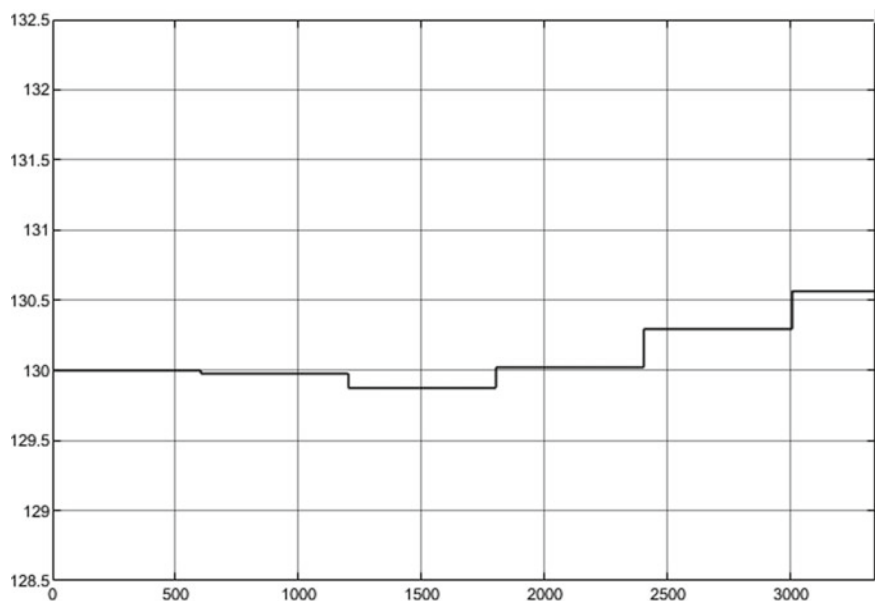


Fig. 6.15 Capacity estimation results at -10 °C under 125 A charging and discharging

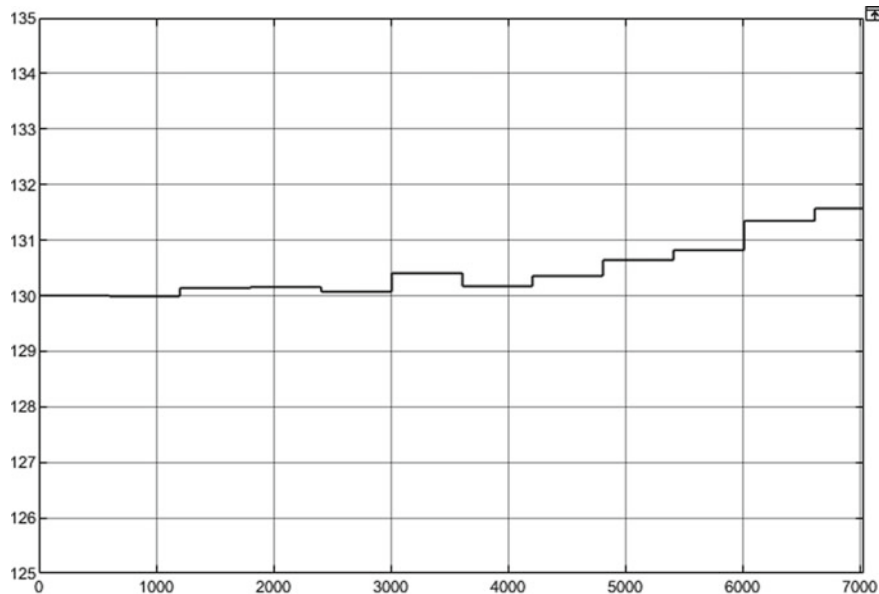


Fig. 6.16 Capacity estimation results (DST)

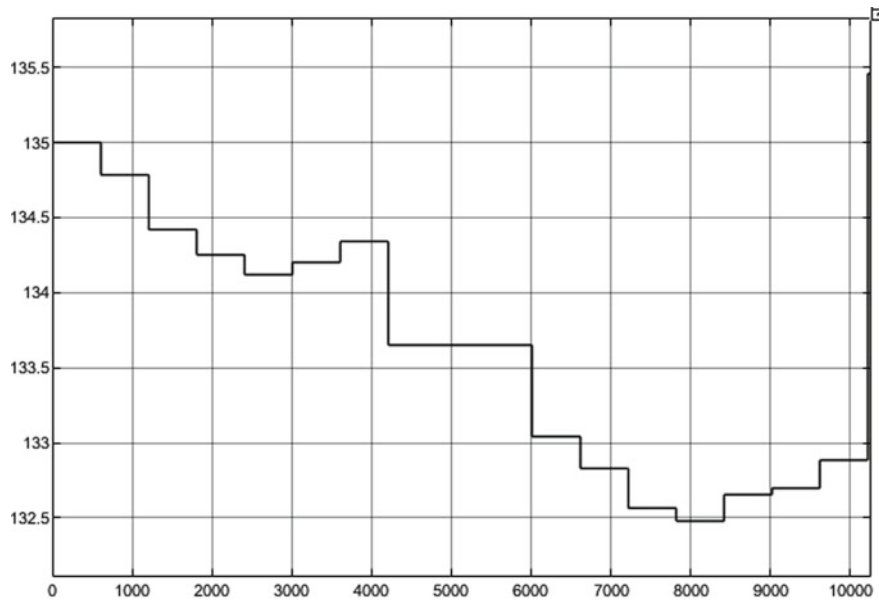
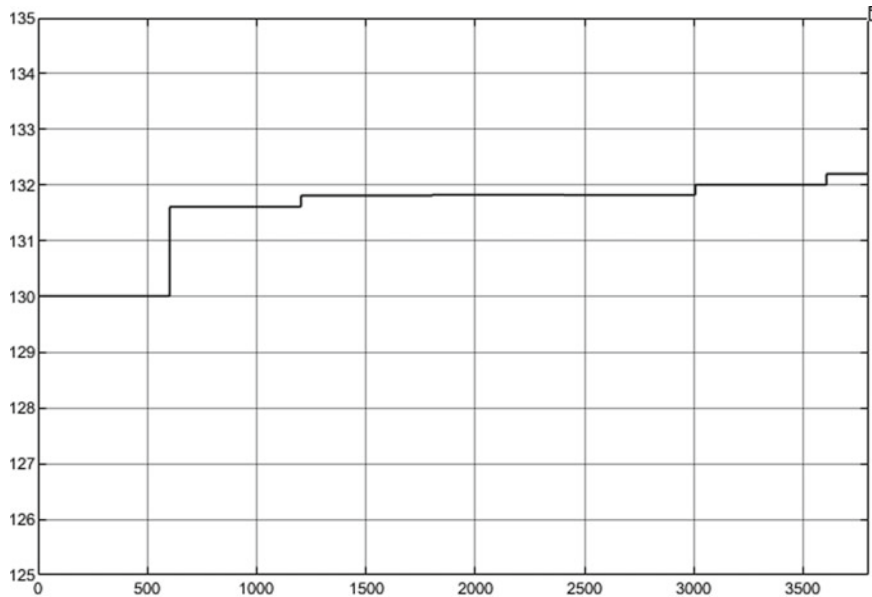


Fig. 6.17 Capacity estimation results at 45 °C under 125 A discharge with initial capacity error



**Fig. 6.18** Capacity estimation results at 45 °C under 125 A discharge with initial SOC error

following a few cycles. The updated battery capacity can then be sent to the battery SOC estimation module.

- (d) The impact of SOC estimation error on the capacity estimation

Because the battery SOC and SOH are estimated together, the estimation error of the SOC has an influence on the capacity estimation results. This case study considers a 10% SOC estimation error and the capacity estimation results are given in Fig. 6.18. The maximum error is 2 Ah. Although the error increases by 1.6 Ah compared with that without SOC estimation error, the error is still within 1.5%.

## 6.7 Summary

Although there is not yet an ideal solution for SOH estimation that can meet the various requirements for different applications, a combination of methods can be used according to the requirements and the available data. For example, on the premise of a large amount of data and the availability of simple algorithms, the combination of the diagnostic techniques, such as ICA and DVA, and the data-driven method can be good choice. If big data is not available, then a combination of the ICA/DVA method with the adaptive model algorithms can be feasible, because the adaptive learning from data can improve the estimation accuracy.

The future perspective of SOH estimation research can have three focuses. The first is to develop simplified model with high accuracy and high robustness against uncertainties that are inevitable in practical applications. The second is SOH estimation at module/pack level considering cell imbalance. The third is to improve the algorithms' generalization capability to different types of battery chemistries, geometry, operating conditions and ageing mechanisms, to facilitate implementation in a wide range of applications.

## References

- Andre D, Appel C, SOCzka-Guth T et al (2013) Advanced mathematical methods of SOC and SOH estimation for lithium-ion batteries. *J Power Sources* 224:20–27
- Bloom I, Cole BW, SOHn JJ et al (2001) An accelerated calendar and cycle life study of Li-ion cells. *J Power Sources* 101(2):238–247
- Cannarella J, Arnold CB (2014) State of health and charge measurements in lithium-ion batteries using mechanical stress. *J Power Sources* 269:7–14
- Han X, Ouyang M, Lu L et al (2014) A comparative study of commercial lithium ion battery cycle life in electrical vehicle: ageing mechanism identification. *J Power Sources* 251:38–54
- Jiang Y, Jiang JC, Zhang CP et al (2018) State of health estimation of second-life LiFePO<sub>4</sub> batteries for energy storage applications. *J Clean Prod* 205:754–762
- Jürgen R, Buchholz M, Meiler M et al (2011) State-of-health monitoring of lithium-ion batteries in electric vehicles by on-board internal resistance estimation. *J Power Sources* 196(12):5357–5363
- Ladpli P, Kopsaftopoulos F, Chang FK (2018) Estimating state of charge and health of lithium-ion batteries with guided waves using built-in piezoelectric sensors/actuators. *J Power Sources* 384:342–354
- Li F, Xu J (2015) A new prognostics method for state of health estimation of lithium-ion batteries based on a mixture of Gaussian process models and particle filter. *Microelectron Reliab* 55(7):1035–1045
- Liu D, Pang J, Zhou J et al (2013) Prognostics for state of health estimation of lithium-ion batteries based on combination Gaussian process functional regression. *Microelectron Reliab* 53(6):832–839
- Merla Y, Wu B, Yufit V et al (2016) Novel application of differential thermal voltammetry as an in-depth state-of-health diagnosis method for lithium-ion batteries. *J Power Sources* 307:308–319
- Richman JS, Lake DE, Moorman JR (2004) Sample entropy. *Methods Enzymol* 384:172–184
- Shibagaki T, Merla Y, Offer GJ (2018) Tracking degradation in lithium iron phosphate batteries using differential thermal voltammetry. *J Power Sources* 374:188–195
- Waag W, Käbitz S, Sauer DU (2013) Experimental investigation of the lithium-ion battery impedance characteristic at various conditions and ageing states and its influence on the application. *Appl Energy* 102:885–897
- Waag W, Fleischer C, Sauer DU (2014) Critical review of the methods for monitoring of lithium-ion batteries in electric and hybrid vehicles. *J Power Sources* 258:321–339

# Chapter 7

## SOP Estimation



### 7.1 SOP Definition

State of power (SOP) is an important parameter for EVs, especially hybrid EVs, for safety control and regenerative braking. SOP represents the battery's peak power capacity within a time window. The accurate SOP estimation is important for optimizing the power management of the vehicle while ensuring battery safety during acceleration, regenerative braking and climbing (Farnann and Sauer 2016; Bhattacharya and Bauer 2012; Larry et al. 2012).

Lithium ion batteries can be divided into two groups, i.e., power batteries and energy batteries. Energy batteries are usually used in pure-electric passenger vehicles or buses, while power batteries are usually used in the hybrid and plug-in hybrid electric cars which have a high power requirement because of the limited space and high C-rate requirements. The engines in hybrid EVs usually work in a constant-output mode, while the battery provide or absorbs the additional instantaneous power during starting, acceleration or brake. Therefore, the vehicle's acceleration and braking performance depends on the battery SOP, which further affects the battery safety and reliability. According to the Partnership for a New Generation of Vehicle, PNGV, issued by the Department of Energy in America, the power capacity of the battery is an important performance index.

The BMS cannot measure the battery's real-time internal electrochemical operating statuses, and there exists estimation errors of the battery parameters and states. The battery's SOP is also dependent on many factors, such as temperature, SOC, ageing, and the internal resistance etc., and the dependency is difficult to quantify. As a result, the real-time estimation of SOP is challenging. The exiting work on the battery's SOP can be generally divided into two groups, the SOP characterization methods and the SOP prediction methods. The SOP prediction methods include interpolation methods, model-based methods and data-driven methods, as shown in Fig. 7.1 (Sun et al. 2014; Feng et al. 2015; Malysz et al. 2015; Liu et al. 2019; Lu et al. 2013; Lai et al. 2020; Lin et al. 2020).

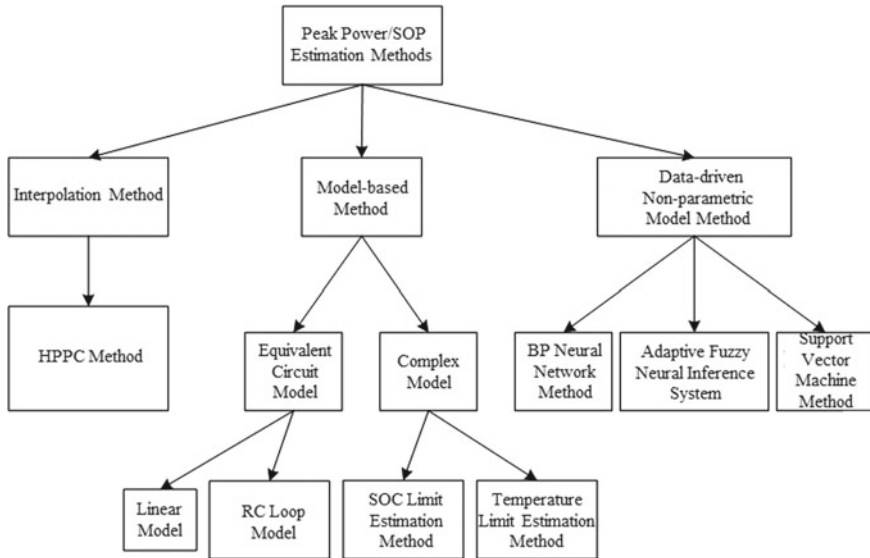


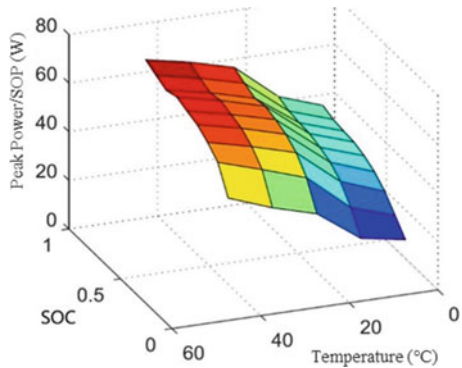
**Fig. 7.1** Classification of SOP estimation methods

## 7.2 Interpolation Method

The HPPC method for SOP characterization is widely used in practice due to its ease of implementation. The method was proposed by Idaho National Engineering and Environmental Laboratory. A 10 s pulse is used to charging/discharge the battery at different SOC levels within the safe range of voltage. The battery maximum power capacity at the corresponding SOC level is obtained when the voltage at the end of the 10 s pulse reaches the voltage limit ( $V_{\min}$  at discharging and  $V_{\max}$  at charging). A 1 h rest period is applied before the pulse test to allow the battery to reach electrochemical and thermal equilibrium. The test is repeated under different temperature levels to characterize the temperature dependency of SOP. The battery's SOP at different SOC and temperatures can then be obtained and stored as a 2D map as shown in Fig. 7.2.

The advantage of the HPPC method is ease of implementation. However, it requires a high experimental effort to characterize the dependency of the SOP on the battery states, including SOC, temperature and especially ageing. Moreover, because of the complexity and nonlinearity of the battery dynamics, the SOP also depends on the load current history, e.g., the battery's internal polarization over-voltage under current load. The battery's internal potential buildup affects the SOP, yet it is not considered in the HPPC method. Ageing effect is not considered in the HPPC test, either. This will reduce the estimation accuracy of the HPPC method.

**Fig. 7.2** SOP map versus temperature and SOC by HPPC tests



### 7.3 Model-Based Method

The model-based method calculates the battery SOP using a battery model and the voltage limits. The models include equivalent circuit model, electrochemical model and model-fusion methods.

#### 7.3.1 Equivalent Circuit Model

The equivalent circuit model (ECM) uses electrical elements such as resistors, capacitors and inductors to describe the battery's equilibrium and dynamic behaviors of the terminal voltage. ECMs have been widely used for online parameter and state estimation. Among the different types of ECMs, the resistor model and the RC network model have been used for SOP estimation.

The resistor model consists of only the OCV and the internal resistance, as shown in Fig. 4.6. The model can capture the instantaneous voltage change as the current jumps. The model structure is simple, and the computational expense is low.

The resistor value can be obtained by applying a pulse current test, as follows,

$$R_0 = \frac{dV}{I} \quad (7.1)$$

where  $dV$  is the instantaneous voltage change, and  $I$  is the current pulse. The test needs to repeat under different SOC and temperature levels. Finally, the battery power capacity can be calculated as follows,

$$\begin{cases} P_{\min}^{chg} = U_{\max} \times \frac{U_{OCV} - U_{\max}}{R_{chg}} \\ P_{\max}^{dis} = U_{\min} \times \frac{U_{OCV} - U_{\min}}{R_{dis}} \end{cases} \quad (7.2)$$

where positive power stands for discharging and negative power stands for charging.

Although the resistor model can capture the instantaneous voltage change, the polarization effect of the internal voltage drop is neglected. Therefore, the SOP estimation accuracy is low under dynamic current load profiles. The ECM with RC networks can be used to address this problem.

In addition to the internal resistor, RC networks can be added to the ECM to capture the polarization voltage of the battery under current load, which increases the model accuracy for voltage prediction. Based on the voltage limits, the battery's power capacity can be calculated using recursive methods, such as the EKF, DEKF, AEKF and AUKF methods. The widely used RC-ECMs include the Thevenin model, the PNGV model and the 2 RC model.

The Thevenin model and the 2RC model are shown in Fig. 4.7. The Thevenin model can capture the battery's nonlinear dynamics with high accuracy and low computational expense. Therefore, the model has been widely used in BMS. The 2RC model can capture the battery's internal polarization effect at different timescales, which increases the model accuracy under a wide range of operating conditions. However, the parametrization and computational complexity of the 2RC model is higher than the Thevenin model, making online parameter tracking difficult. The PNGV model is shown in Fig. 4.9, which captures not only the polarization effect, but also the voltage drop induced by the accumulation of current. The model accuracy is high at expense of higher computational complexity.

The model equations of the Thevenin model are given as follows,

$$\begin{cases} \dot{U}_p = -\frac{U_p}{C_p R_p} + \frac{I_L}{C_p} \\ U_t = U_{OC} - U_p - I_L R_0 \end{cases} \quad (7.3)$$

If the current keeps constant within a time period of  $\Delta t$ , the voltage response can be calculated as follows,

$$\begin{cases} U_{p,k+1} = \exp(-\Delta t/\tau) U_{p,k} + R_p I_L [1 - \exp(-\Delta t/\tau)] \\ U_{t,k+1} = U_{OC,k+1} - I_{L,k+1} R_0 - U_{p,k+1} \end{cases} \quad (7.4)$$

The system states include the polarization voltage and the SOC, as follows,

$$\begin{cases} \begin{bmatrix} U_{p,k+1} \\ z_{k+1} \end{bmatrix} = \begin{bmatrix} \exp(-\frac{\Delta t}{\tau}) & 0 \\ 0 & 1 \end{bmatrix} \begin{bmatrix} U_{p,k} \\ z_k \end{bmatrix} + \begin{bmatrix} R_p (1 - \exp(-\frac{\Delta t}{\tau})) \\ \frac{\eta \Delta t}{C} \end{bmatrix} I_{L,k} + \omega_k \\ U_{t,k+1} = \begin{bmatrix} -1 & \frac{dU_{OC}}{dz} \end{bmatrix} \begin{bmatrix} U_{p,k+1} \\ z_{k+1} \end{bmatrix} + [-R_0] I_{L,k} + v_k \end{cases} \quad (7.5)$$

where  $\Delta t$  is the sampling period,  $z_k$  is the SOC at time step  $k$ .  $\eta$  is the coulombic efficiency.  $C$  is the battery's nominal capacity.  $\omega_k$  and  $v_k$  are the process and measurement noises, respectively.

After specifying the voltage upper and low limits, the battery's peak current at the next time step can be calculated as follows,

$$\begin{cases} I_{\max}^{dis} = \frac{U_{OC}(z_k) - U_{p,k} \exp(-\frac{\Delta t}{\tau}) - U_{t,\min}}{\frac{\eta \Delta t}{C} \frac{dU_{OC}(z)}{dz} + R_p (1 - \exp(-\frac{\Delta t}{\tau})) + R_0} \\ I_{\min}^{chg} = \frac{U_{OC}(z_k) - U_{p,k} \exp(-\frac{\Delta t}{\tau}) - U_{t,\max}}{\frac{\eta \Delta t}{C} \frac{dU_{OC}(z)}{dz} + R_p (1 - \exp(-\frac{\Delta t}{\tau})) + R_0} \end{cases} \quad (7.6)$$

A continuous peak current is needed during vehicle acceleration, climbing and braking because these operations cannot complete within one sampling time. The continuous peak current is the maximum current that the battery can deliver for a period of e.g.,  $L * \Delta t$ . The voltage response can be calculated as follows,

$$\begin{cases} U_{p,k+L} = (\exp(-\Delta t/\tau))^L U_{p,k} + R_p I_L \sum_{j=0}^{L-1} \left( \exp\left(\frac{-\Delta t}{\tau}\right) \right)^{L-1-j} [1 - \exp(-\Delta t/\tau)] \\ U_{t,k+L} = U_{OC}(z_{k+L}) - I_{L,k+1} \left( R_0 + R_p \left( 1 - \exp\left(\frac{-\Delta t}{\tau}\right) \right) \right. \\ \left. \times \sum_{j=0}^{L-1} \left( \exp\left(\frac{-\Delta t}{\tau}\right) \right)^{L-1-j} \right) - U_{p,k} \left( \exp\left(\frac{-\Delta t}{\tau}\right) \right)^L \end{cases} \quad (7.7)$$

The continuous peak current during the time window of  $L * \Delta t$  can be obtained,

$$\begin{cases} I_{\max,L}^{dis} = \frac{U_{OC}(z_k) - U_{p,k} \left( \exp\left(-\frac{\Delta t}{\tau}\right) \right)^L - U_{t,\min}}{\frac{\eta L \Delta t}{C} \frac{dU_{OC}(z)}{dz} + R_p (1 - \exp(-\frac{\Delta t}{\tau})) \sum_{j=0}^{L-1} \left( \exp\left(\frac{-\Delta t}{\tau}\right) \right)^{L-1-j} + R_0} \\ I_{\min,L}^{chg} = \frac{U_{OC}(z_k) - U_{p,k} \left( \exp\left(-\frac{\Delta t}{\tau}\right) \right)^L - U_{t,\max}}{\frac{\eta L \Delta t}{C} \frac{dU_{OC}(z)}{dz} + R_p (1 - \exp(-\frac{\Delta t}{\tau})) \sum_{j=0}^{L-1} \left( \exp\left(\frac{-\Delta t}{\tau}\right) \right)^{L-1-j} + R_0} \end{cases} \quad (7.5.8)$$

If  $L = 1$ , this continuous peak current equals the next-step peak current. The peak power (SOP) can be obtained by multiplying the peak current and the voltage values:

$$\begin{cases} P_{\min}^{chg} = \max \left( P_{\min}, \left( U_{OC}(z_{k+L}) - U_{p,k} \left( \exp\left(-\frac{\Delta t}{\tau}\right) \right)^L \right. \right. \\ \left. \left. - I_{\min}^{chg} \left( R_p \left( 1 - \exp\left(-\frac{\Delta t}{\tau}\right) \right) \sum_{j=0}^{L-1} \left( \exp\left(\frac{-\Delta t}{\tau}\right) \right)^{L-1-j} + R_0 \right) \right) I_{\min}^{chg} \right) \\ P_{\max}^{dis} = \min \left( P_{\max}, \left( U_{OC}(z_{k+L}) - U_{p,k} \left( \exp\left(-\frac{\Delta t}{\tau}\right) \right)^L \right. \right. \\ \left. \left. - I_{\max}^{dis} \left( R_p \left( 1 - \exp\left(-\frac{\Delta t}{\tau}\right) \right) \sum_{j=0}^{L-1} \left( \exp\left(\frac{-\Delta t}{\tau}\right) \right)^{L-1-j} + R_0 \right) \right) I_{\max}^{dis} \right) \end{cases} \quad (7.9)$$

The SOP estimation is usually conducted in combination with the SOC estimation. The implementation procedure is shown in Fig. 7.3. The RC ECM-based SOP estimation has high accuracy under dynamic operating load conditions. Other advantages include the real-time implementation, and the flexibility of the prediction time-length. The model accuracy depends on the model parameters. The model

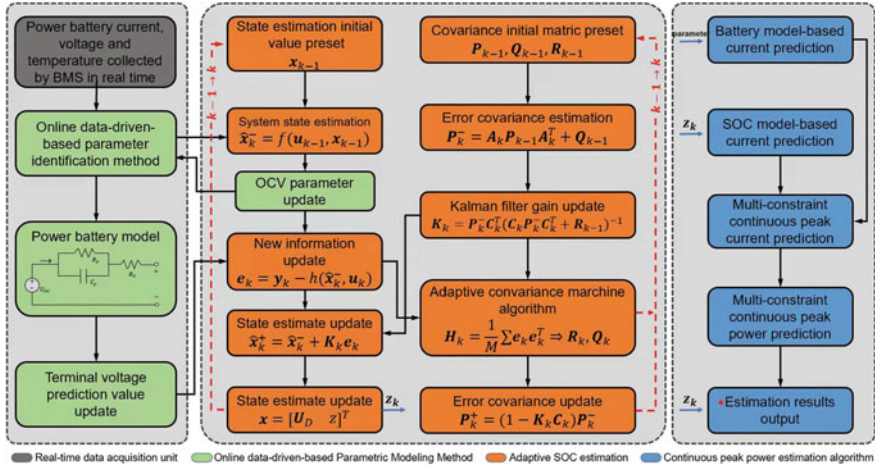


**Fig. 7.3** Joint estimation of SOP and SOC based on ECM

accuracy can be further improved by taking into consideration of the influence of temperature and ageing on the model parameters, which will lead to more accurate SOP estimation.

### 7.3.2 Electrochemical Model

The P2D model is the mostly widely used electrochemical model to describe the battery's internal reaction dynamics. The model considers the battery physical structure including the current collectors, electrodes and the separator, as shown in Fig. 4.2. Each electrode zone consists of both the solid electrode and the liquid electrolyte. The solid electrode is represented using sphere particles at micrometer scale, and the mass transfer process in the electrode is described as the diffusion of the ions inside the particles. During discharging, the ions de-intercalate from the negative electrode and then move through the electrolyte to intercalate into the positive electrode. The reverse reactions occur during charging. The electrochemical reactions at the solid–liquid interface are described using the Butler–Volmer equation. The terminal voltage is the potential difference between the positive and negative electrodes.

It is assumed that the battery's power is limited by the speed of ions diffusion from inside the electrode to the particle surface. Therefore, the battery's instantaneous SOP depends on the ion concentration at the electrode surface. The P2D model can capture the dynamics of the ion concentration at the electrode surface for SOP estimation. The influence of temperature and battery ageing can also be integrated into the P2D model. The P2D model has high physical interpretation and accuracy. However, the model complexity is high, and the model parameters are difficult to obtain. The

parameter uncertainty is high, and therefore it is difficult to guarantee the model accuracy under wide range of operating conditions.

### 7.3.3 Fusion Model

The ECM-based SOC estimation method only considers the voltage limits, while the SOC and temperature limits are neglected. The limits on SOC, temperature and other manufacture specifications (such as C-rate) can be taken into consideration using the fusion method to increase the SOP accuracy and the battery safety.

#### 7.3.3.1 SOC Limits

SOC constraints can be used when estimating the SOP. When the battery SOC is close to the maximum SOC,  $SOC_{\max}$ , the charging current should be limited. Similarly, when the SOC is close to the minimum SOC,  $SOC_{\min}$ , the discharge current needs to be constrained.

$$SOC(t + \Delta t) = SOC(t) - \eta \frac{i(t)\Delta t}{C} \quad (7.10)$$

where  $\eta$  is the coulombic efficiency,  $C$  is the battery's nominal capacity. The charging current is negative and discharge current is positive.  $\Delta t$  is the sampling time.

The maximum current considering the SOC limits can be calculated as follows,

$$\begin{cases} I_{\min}^{-chg} = \frac{SOC(t) - SOC_{\max}}{\eta \Delta t / C} \\ I_{\max}^{-dis} = \frac{SOC(t) - SOC_{\min}}{\eta \Delta t / C} \end{cases} \quad (7.11)$$

This method is usually applied in combination with the voltage limit method, i.e., the peak currents need to meet both SOC and voltage constraints.

#### 7.3.3.2 Temperature Limits

High temperature (e.g., over 45 °C) leads to accelerated battery ageing. Therefore, the temperature limits need to be considered when calculating the SOP. When the battery temperature is close to the upper limits, the battery power should be constrained. The lumped thermal model of the battery is given below,

$$I_k^2 R + T_{\text{avg,batt}} \frac{dU}{dT} I_k + h_w S(T_{\text{amb}} - T_{\text{avg,batt}}) - C_p m \frac{T_{k+L} - T_k}{L \Delta T} = 0 \quad (7.12)$$

where  $R$  is the battery's total internal resistance,  $T_{\text{avg, batt}}$  and  $T_{\text{amb}}$  are the battery temperature and the ambient temperature, respectively.  $C_p$  is the thermal capacity,  $m$  is the battery mass,  $h_w$  is thermal exchange coefficient,  $S$  is the total surface area. Using Eq. (7.12) and the battery's temperature upper limit, the maximum current can be obtained. The method can improve the the battery's thermal safety and reduce the risk of over-temperature and thermal runaway.

## 7.4 Data-Driven Methods

The data-driven methods can extract system properties directly from data using statistic theory, data mining and pattern recognition theory. The widely used methods include neural networks, regression analysis, genetic algorithms, Bayesian theory, support vector machine etc. The data-driven methods have been used for prediction, evaluation, scheduling, monitoring, decision making and optimization. The data-driven method can be used to extract useful information and build system models by processing the historical data. The advantage of the data-driven methods is that a detailed understanding of the physics is not required, making it suitable to model complex and unknown systems. The battery's SOP estimation based on data-driven methods ignores the battery's internal physical processes, and directly learns the relationship between the inputs (current, SOC, temperature, etc.) and the output (power capacity). It generally requires a large amount of data for algorithm training.

### 7.4.1 BP Neural Networks

The BP neural network is a multilayer feedforward network consisting of input layer, hidden layers and the output layer, as shown in Fig. 7.4. The inputs can include the voltage, current, temperature, SOC etc. The output is the battery SOP. The weights between layers can be optimized by back-propagation of the output error using the gradient method.

The number of the hidden layers can be adjusted according to the requirements. The inputs are usually normalized before feeding to the network. The weights for the neural nodes are optimized generally iteratively until the output accuracy is satisfactory (Fig. 7.5).

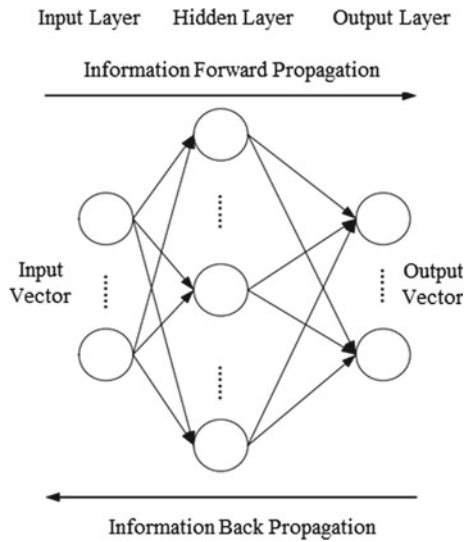


**Fig. 7.4** BP Neural Networks

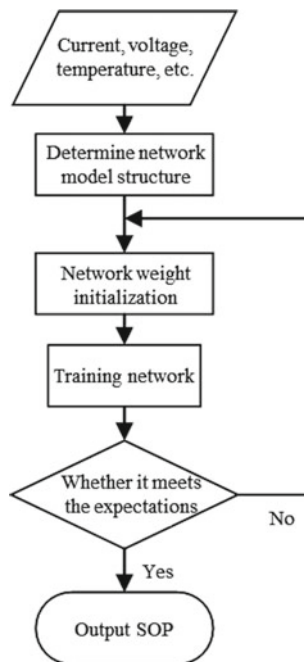


**Fig. 7.5** Procedure for SOP estimation using BP neural networks

### 7.4.2 Support Vector Machine

The SVM method is a machine learning algorithm based on the statistical theory. It is suitable for system modelling from a small data set. The algorithm has high generalization capability and robustness. The performance of SVM depends on five key elements: the kernel function  $g$ , the number of support vectors, the non-zero Lagrange multiplier, the bias term  $b$  and the penalty parameter  $c$ . The kernel function  $g$  and the penalty parameter  $c$  need to be specified first. Then the other parameters can be optimized by solving a quadratic programming problem. The kernel function  $g$  can be adjusted iteratively. The SVM model can be optimized using battery test data for SOP estimation.

## 7.5 Simulation Case Study

The SOP is estimated in this case study using the model-based method introduced in Sect. 7.3.1 based on the Thevenin model. The SOC and temperature constraints are taken into consideration, as shown in Fig. 7.6.

The three modules at the left hand side in Fig. 7.6 are in turn the voltage limits, SOC limits and temperature limits. The time duration of the pulse current is 30 s. The peak current and peak power estimation results are given in Figs. 7.7 and 7.8 respectively.

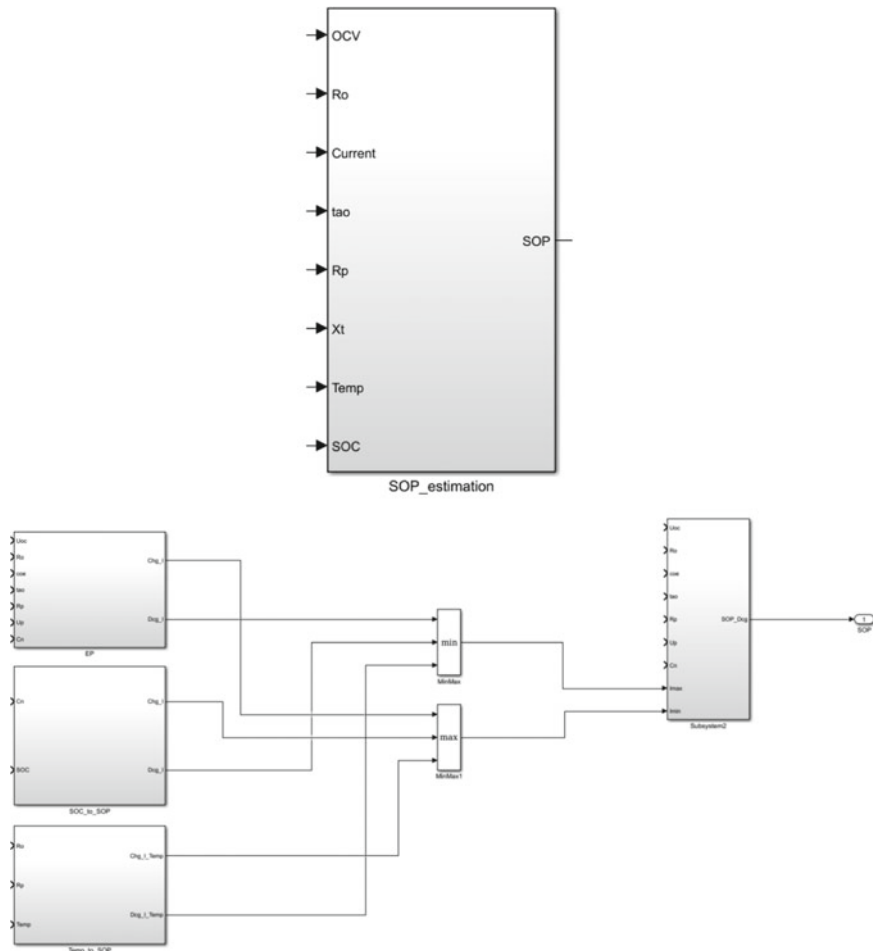


**Fig. 7.6** SOP estimation using fusion method

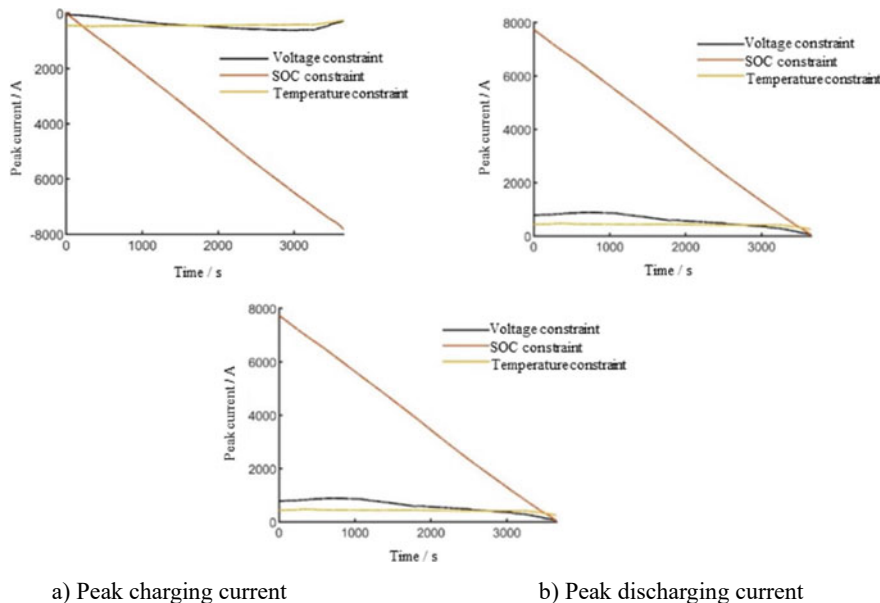


**Fig. 7.7** 30-s peak current for charging and discharging

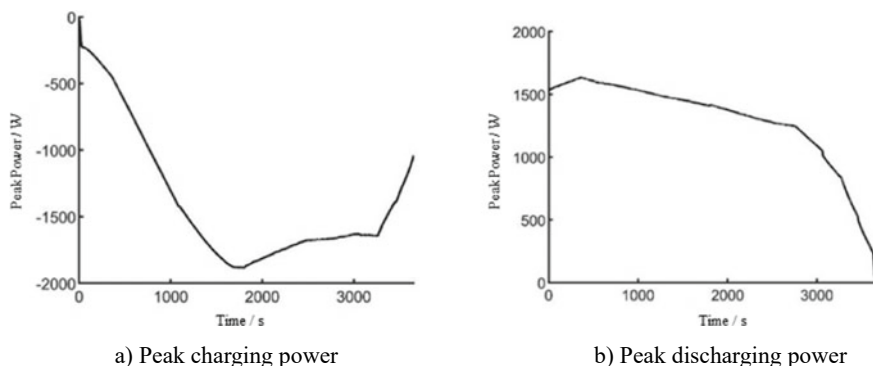


**Fig. 7.8** 30-s peak power for charging and discharging

## References

- Bhattacharya S, Bauer P (2012) Requirements for charging of an electric vehicle system based on state of power (SOP) and state of energy (SOE). In: 2012 7th international power electronics and motion control conference (IPEMC), vol 1, pp 434–438
- Farmann A, Sauer DU (2016) A comprehensive review of on-board State-of-Available-Power prediction techniques for lithium-ion batteries in electric vehicles. *J Power Sources* 329:123–137

- Feng T, Yang L, Zhao X, Zhang H, Qiang J (2015) Online identification of lithiumion battery parameters based on an improved equivalent-circuit model and its implementation on battery state-of-power prediction. *J Power Sources* 281:192–203
- Lai X, He L, Wang S et al (2020) Co-estimation of state of charge and state of power for lithium-ion batteries based on fractional variable-order model. *J Clean Prod* 255
- Larry W, Phillip J, Kollmeyer J, Jahns TM, Lorenz RD (2012) Implementation of online battery state-of-power and state-of-function estimation in electric vehicle applications. In: Energy conversion congress and exposition (ECCE), pp 1819–1826
- Lin P, Jin P, Hong J et al (2020) Battery voltage and state of power prediction based on an improved novel polarization voltage model. *Energy Rep* 6:2299–2308
- Liu K, Li K, Peng Q et al (2019) A brief review on key technologies in the battery management system of electric vehicles. *Front Mech Eng* 14(1):47–64
- Lu L, Han X, Li J et al (2013) A review on the key issues for lithium-ion battery management in electric vehicles. *J Power Sources* 226:272–288
- Malysz P, Ye J, Gu R, Yang H, Emadi A (2015) Battery state-of-power peak current calculation and verification using an asymmetric parameter equivalent circuit model. *Veh Technol IEEE Trans PP(99):1–1.*
- Sun F, Xiong R, He H (2014) Estimation of state-of-charge and state-of-power capability of lithium-ion battery considering varying health conditions. *J Power Sources* 259:166–176

# Chapter 8

## SOE and SOS Estimation



### 8.1 State of Energy (SOE) Estimation

#### 8.1.1 Definition

SOC is usually used to predict the remaining energy of the battery. However, the battery's remaining energy depends on the load current profile, which is not considered by the SOC indicator. Further, the high energy loss due to the battery's internal heat generation at high current cannot be captured by the SOC indicator. Therefore, Mamadou et al. proposed a new indicator, state of energy (SOE) (Cummings and Swartz 2017), to represent the battery's remaining energy. The SOE is the ratio between the battery's remaining energy to the nominal energy.

$$SOE = \frac{E_{remaining}}{E_{rated}} \quad (8.1)$$

where  $E_{rated}$  is the nominal energy.  $E_{rated}$  is the total output energy of the battery from fully charged state to end of discharge at a specific current rate.  $E_{remaining}$  is the battery's remaining energy, which is the total energy output of the battery from current state to end of discharge at the specific current rate (Li et al. 2017a, 2021; Zhang et al. 2015). The test conditions can be specified by the cell manufacture or according to the user's requirements.

The accurate estimation of the battery's SOE is important for predicting the remaining driving range, which is important to release the 'range anxiety' of electric vehicles (Li et al. 2017b; Zheng et al. 2016; Ma and Zhang 2020; Liu et al. 2014). Further, the accurate estimation of SOE is key to energy management of the vehicle, especially hybrid electric vehicles, to optimize the power scheduling and to prolong

the driving range. The widely used SOE estimation methods include power integral method, OCV method, neural networks and model-based methods (Feng et al. 2018; Xia et al. 2014; Wang et al. 2021; Plett 2006).

### 8.1.2 Power Integral Method

According to the definition, SOE can be calculated using the power integral method (Guenther et al. 2013; Lai et al. 2018), given the initial value and the current and voltage signals,

$$SOE = SOE_0 + \frac{\int_0^t \eta_{ED} \cdot I \cdot V \cdot d\tau}{\eta_E \cdot E_N} \quad (8.2)$$

where  $SOE_0$  is the initial SOE.  $\eta_{ED}$  is the power efficiency between discharging and charging.  $I$  is the current (unit: A). The positive current is charging here.  $V$  is the battery's terminal voltage (unit: V).  $t$  is time (unit: s).  $\eta_E$  is the nominal power efficiency, and  $E_N$  is the nominal energy (unit: Wh).

The power integral method is simple to implement. However, given the accurate initial value  $SOE_0$ , it can only maintain high SOE estimation accuracy for a short period in practical applications. This is because it is an open loop method which is vulnerable to measurement errors of the voltage and current signals. The accumulation of error due to the integral operator can lead to estimation divergence. Further, it is difficult to obtain an accurate initial SOE. Therefore, the SOE method needs to be combined with other estimation methods for accurate initialization and regular calibration.

### 8.1.3 OCV Based Method

The battery needs to rest for long period to reach equilibrium to enable the OCV measurement, which can then be used for SOE estimation. However, when the battery is under load, it is difficult to obtain the OCV. Therefore, the OCV based method can only be used when there is a long resting period. The OCV method is usually used to calibrate the power integral method.

### 8.1.4 Neural Networks

The SOE can be estimated using data-driven neural networks method that can learn the relationship between system input and outputs from historical data. However, the training of the neural networks requires a large amount of test data, and the model performance depends on the parameter identification result.

### 8.1.5 Model-Based Method

These model-free methods for SOE estimation have advantages such as low complexity and ease of implementation. However, the estimation accuracy is limited, and the data-driven model requires a lot of test data which is time consuming. Model-based method for SOE estimation can be applied to a wide range of operating conditions. The development of a battery model with low complexity and high accuracy, which is key to SOE estimation in real-time implementations, requires a deep understanding of the battery properties. In addition to the model, an estimation algorithm with high robustness to measurement noises and modelling errors is also required. Further, a low computation expense is desired for onboard implementation. The battery models suitable for SOE estimation include the electrochemical model, thermal model, coupled model and performance model, as shown in Table 8.1. The performance model further includes simplified electrochemical model, equivalent circuit model and neural networks, etc. Among these different types of battery models, the equivalent circuit model has been widely used in BMS, because of the simple structure, low computational expense and ease of parametrization.

### 8.1.6 Simulation Case Study

A model-based SOE estimation algorithm is presented in this section. The ECM is used, and the model parameters are obtained using the PSO method. The SOE is estimated using the unscented Kalman filter algorithm.

#### 8.1.6.1 Battery Model

The battery system consists of  $n$  cells in series. For each cell, a Thevenin model is used to describe the voltage dynamics, as shown in Fig. 8.1. The model equations are given as follows,

$$\begin{cases} U_p^i = -\frac{1}{R_p^i C_p^i} U_p^i - \frac{1}{C_p^i} I_b \\ U_t^i = U_{OCV}^i - R_0^i I_b - U_p^i \end{cases} \quad (i = 1, 2, \dots, n) \quad (8.3)$$

**Table 8.1** Battery models for SOE estimation

	Principle	Application	Limitations
Electrochemical model	Electrochemical theory	Description of the internal electrochemical reactions	High complexity
Thermal model	Thermal dynamics theory	Battery heat generation and dissipation; thermal management system	High complexity
Coupled model	Electrochemical-thermal theory	Coupled electrochemical-thermal properties	High complexity
Performance model	Model simplification, curve fitting	Terminal voltage-current dynamics, power efficiency, battery management system	Battery management system, electric vehicles

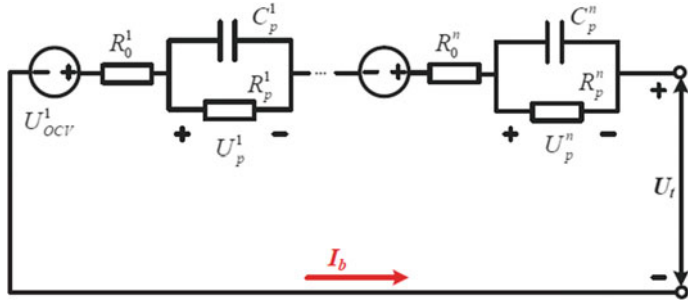


**Fig. 8.1** Equivalent circuit model of the battery system

where  $U_p$  is the voltage across the RC networks,  $U_t$  is the terminal voltage.  $I_b$  is the current. The relationship between OCV and SOC is given as follows,

$$U_{ocv}(z) = K_0 + K_1 z + K_2 z^2 + K_3/z + K_4 \ln(z) + K_5 \ln(1-z) \quad (8.4)$$

where  $z$  stands for SOC,  $K_i$  ( $i = 0, 1, \dots, 5$ ) are the coefficients.

Let  $\alpha_p = \exp(-\Delta t / R_p C_p)$ , Eq. (8.3) can be discretized as follows,

$$\begin{cases} \begin{pmatrix} z_{k+1}^i \\ U_{p,k+1}^i \\ U_{t,k}^i \end{pmatrix} = \begin{pmatrix} 1 & 0 \\ 0 & \alpha_p^i \\ U_{OCV,k}^i - U_{p,k}^i - I_{L,k} R_{0,k}^i + v_k \end{pmatrix} \begin{pmatrix} z_k^i \\ U_{p,k}^i \\ U_{t,k}^i \end{pmatrix} - \begin{pmatrix} -\frac{\Delta t}{C_a} \\ (1 - \alpha_p^i) R_{p,k}^i \\ I_{L,k} \end{pmatrix} I_{L,k} + \omega_k \\ (i = 1, 2, \dots, n) \end{cases} \quad (8.5)$$

where  $C_a$  is the maximum capacity,  $\Delta t$  is the sampling time.  $\omega$  and  $v$  are in turn the process and measurement noise.

### 8.1.6.2 SOE Definition

The SOE definition used here is

$$\text{SOE} = \frac{E_{rem}}{E_{ava}} \quad (8.6)$$

where  $E_{rem}$  is the remaining energy, and  $E_{ava}$  is the maximum available energy.

Since the battery module consists of  $n$  individual cells, the remaining energy,  $E_{rem}$ , is defined as the sum of available energy of all cells from current state to end of discharge (the low SOC limit,  $SOC_{t_1}^i$ ); the battery's charging energy capacity ( $E_{chge}$ ) is the sum of charged energy of all cells from current state to fully charged state (defined as  $SOC_{t_2}^i$ ). The battery's available energy is the sum of  $E_{rem}$  and  $E_{chge}$ , as follows,

$$E_{rem} = \sum_{i=1}^n \int_{SOC_{t_1}^i}^{SOC_{t_2}^i} C_a^i U_{OCV}^i(SOC) dSOC \quad (8.7)$$

$$E_{chge} = \sum_{i=1}^n \int_{SOC_t^i}^{SOC_{t_2}^i} C_a^i U_{OCV}^i(SOC) dSOC \quad (8.8)$$

$$E_{ava} = E_{rem} + E_{chge} \quad (8.9)$$

where the superscript  $i$  stands for the  $i$ -th cell in the series.

### 8.1.6.3 SOE Estimation

The PSO method is used here for the parameter identification. Let  $E = U_t - U_{OCV}$ , then Eq. (8.5) can be reformulated in frequency domain as

$$E(s) = I_L(s) \left( R_0 + \frac{R_p}{1 + R_p C_p} \right) \quad (8.10)$$

After discretization, we obtain

$$E_k^i = \alpha_1^i I_{b,k} + \alpha_2^i E_{t,k-1}^i + \alpha_3^i I_{L,k-1} \quad (8.11)$$

where

$$\begin{cases} \alpha_1^i = R_0^i \\ \alpha_2^i = \alpha_p^i \\ \alpha_3^i = (1 - \alpha_p^i) R_p^i - \alpha_p^i R_p^i \end{cases} \quad (8.12)$$

Then the battery parameters are optimized using the PSO method. Because these parameters vary slowly, there is no need to use adaptive algorithms to track the parameters continuously, which can reduce the computational expense to facilitate onboard implementation. The model parameters can be updated after a fixed time interval (e.g., several weeks).

Next, the UKF method is used for SOE estimation.

A Li(Ni<sub>1/3</sub>Co<sub>1/3</sub>Mn<sub>1/3</sub>)O<sub>2</sub> cell is used here. The nominal capacity is 38 Ah. The voltage limits are 4.2 V and 2.7 V for charging and discharging, respectively. The estimation results are given as follows under NEDC and drive cycle operating conditions (Figs. 8.2, 8.3, 8.4 and 8.5).

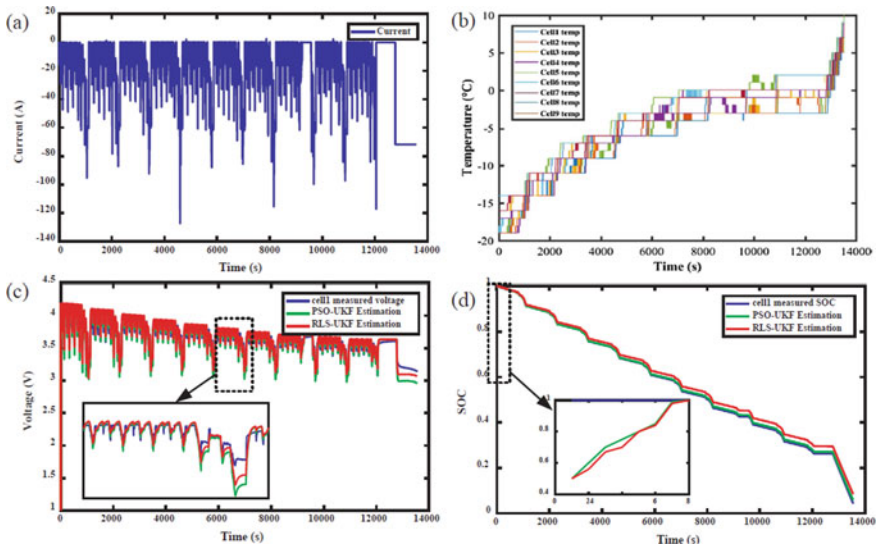


**Fig. 8.2** NEDC load profile: **a** NEDC current; **b** battery temperature; **c** voltage prediction of cell 1; **d** SOC estimation of cell 1

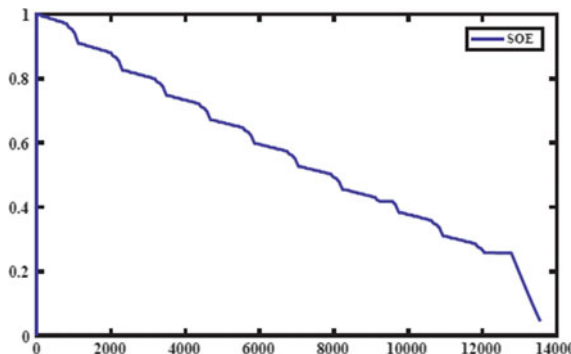


**Fig. 8.3** SOE estimation results under the NEDC load profile

## 8.2 State of Safety (SOS) Estimation

Fault diagnosis is key to ensuring battery safety. According to the BMS standard IEC/TR361431—1995, the BMS in EVs must have diagnostic functions, including ageing diagnosis and early warning of battery failures. The Chinese standard, QC/T 897—2011 has specified the list of compulsory and optional battery diagnosis and defined three levels of fault severity.

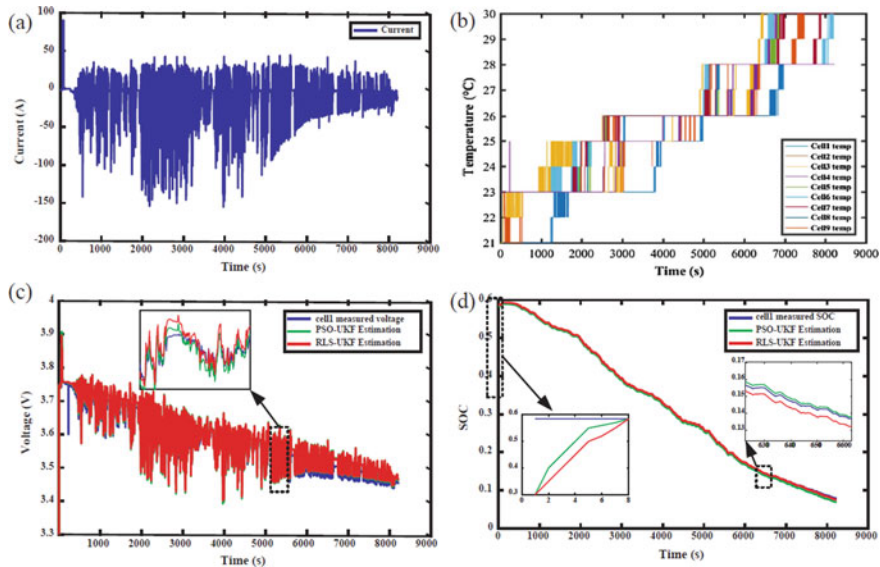


**Fig. 8.4** Drive cycle operating conditions: **a** current; **b** temperature of the cells; **c** voltage prediction of cell 1; **d** SOC estimation of cell 1

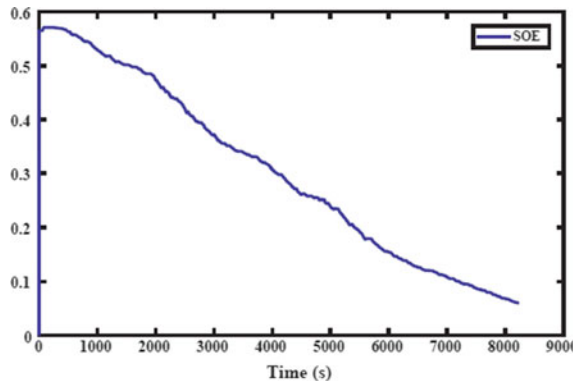


**Fig. 8.5** SOE estimation results under drive cycle operating conditions

The BMS needs to evaluate the battery's SOS and the fault level, which is key to battery monitoring. The thermal runaway is the major cause to severe battery accidents. Therefore, there is an urgent need for accurate SOS estimation methods for thermal runaway prediction. The main causes to thermal runaway include over-temperature, over discharge and internal short-circuit, etc. The boundary conditions of battery thermal runaway can be obtained by studying the mechanisms of battery overtemperature and internal short-circuit.

### 8.2.1 Thermal Runaway

Thermal runaway refers to rapid temperature rise of the battery due to a chain of exothermic reactions, which leads to over-temperature, fire or explosion. The thermal runaway of one cell in the battery pack can propagate to other cells if not detected or constrained in time.

The thermal runaway is caused by significantly higher heat generation than heat dissipation. The battery's thermal runaway is a positive feedback process: rising temperature causes more violent exothermic reactions which release more heat to further raise the temperature. Battery thermal runaway can be divided into three stages:

First stage: battery internal thermal runaway

When there is an internal short-circuit, external heating or high heat generation inside the battery under high current, which raise the battery temperature to around 90–100 °C, LiPF<sub>6</sub> starts to discompose. The chemical activity of charged graphite is high (close to Li metal), and the SEI layer at the surface of the negative electrode will decompose at high temperature. The exposed lithium inside the graphite will react with the electrolyte and binding materials, further raising the temperature to around 150 °C. The electrolyte will decompose which releases large amount of heat and produces PF<sub>5</sub>. PF<sub>5</sub> will further catalyze the decomposition reaction of the organic solvent.

Second stage: battery bulge

When the temperature rises to 200 °C, the positive electrode will decompose, releasing large amount of heat and gases, which further raises temperature. At around 250–350 °C, the negative electrode with intercalated lithium will react with the electrolyte.

Third Stage: thermal runaway and explosion

The positive electrode in charged state starts violent decomposition reactions, along with the vigorous oxidation reactions of the electrolyte, releasing huge amount of heat and gases. The battery then catches fire or explodes.

There are internal and external causes to battery thermal runaway. The internal causes include internal short-circuit due to manufacturing defects, lithium dendrite due to improper use, etc. External causes include mechanical abuse, electrical abuse and thermal abuse, etc. For example, external crushing or nail penetration can lead to battery short-circuit; and external short-circuit leads to huge heat generation inside the battery; excessive temperature causes SEI and positive electrode to decompose, etc.

#### (1) Thermal runaway triggered by over-temperature

The following reasons can cause over-temperature of the battery during operation: improper battery selection, over-current, insufficient heat dissipation due

to poor design of the thermal management system, external short-circuit, loss contact to busbar, etc. Therefore, there issues need to be addressed through proper design and battery management system. From the point of view of cell design, some materials can be used to prevent thermal runaway, such as self-cooling or flame-retardant electrolyte. In terms of the battery management system, the battery temperature can be monitored or predicted for early warning at different security levels.

(2) Thermal runaway triggered by over-charging

Over-charge can trigger thermal runaway. Aged battery packs have a high risk of over-charge of individual cells due to the high imbalances among cells. The cell-balancing method can be adopted to constrain the imbalance. Further, over-charge monitoring and protection mechanisms should be employed in the BMS to enhance thermal safety.

(3) Thermal runaway triggered by mechanical abuse

The battery pack design is key to improving the structure strength and reducing the risk of mechanical deformation of the battery pack. Crash sensors can also be used in the BMS in combination with the voltage, current and temperature sensors for detection and early warning of thermal runaway induced by mechanical abuse.

(4) Thermal runaway triggered by internal short-circuit

The battery internal short-circuit can be triggered by manufacturing defects and improper operations which cause lithium granulation, lithium plating and cell swelling. These processes are generally very slow and gradually build up in a couple of years, and it is difficult to repeat these processes, making onboard diagnosis and early-warning very challenging.

### ***8.2.2 Early Warning of Battery Failures***

The safety issues of EVs have attracted extensive attention of the SOCiety. The Ministry of Industry and Information Technology of the People's Republic of China has started formulating and revising safety standards for EV since 2016. One important objective is the early warning of battery thermal runaway, which can give passengers enough time to evacuate the vehicle.

Battery thermal runaway is usually accompanied by rapid changes of the measurable signals of the BMS, including voltage, current and temperature. Further, a large amount of gases is produced. Therefore, these measurable signals can be used for detection and early warning of battery thermal runaway.

The disadvantages of using battery external signals (voltage, current, temperature) for detecting thermal runaway include low response speed and low accuracy. Although sensors can be embedded inside the battery, it requires modification of the battery's manufacturing and packageing process, which is costly and time-consuming. Therefore, the model-based estimation techniques, gas detection and cloud-based algorithms have become the research hotspots for detection and early warning of battery thermal runaway.

### 8.2.2.1 Model-Based Internal State Estimation

The real-time estimation of the battery's parameters and internal states can be used for detecting thermal runaway. For example, the battery thermal model can be used to keep track of the internal temperature of the battery to predict the risk of thermal runaway. The battery internal pressure and temperature can also be monitored using pressure and thermal sensors. The cell imbalance can also be used to evaluate safety risk. However, these internal state estimation methods still cannot meet the vehicle's requirements in terms of reliability, accuracy and response speed.

### 8.2.2.2 Gas Detection and Analysis

In the early stage of the battery thermal runaway, the measurable signals including temperature, voltage and current, can very slowly, making it difficult for early detection and early warning, while the gases generated inside the battery, including electrolyte vapor dimethyl carbonate, diethyl carbonate and inorganic gases such as  $\text{CO}_2$ ,  $\text{CO}$  and  $\text{H}_2$ , can be detected using gas detection sensor for early warning of thermal runaway.

The comparison of the various detection methods for thermal runaway is given in Fig. 8.6, including thermal detection, voltage detection and gas detection. It shows that the gas sensors can be triggered much earlier than the voltage and temperature sensors. This early detection is vital to allow enough time for the passengers to evacuate the vehicle.

### 8.2.2.3 Cloud-Based Detection

Cloud-based data-driven analysis is another important technology for early-warning of battery thermal runaway. This method can be used in combination with the real-time monitoring and detection methods in the vehicle. The BMS data, such as the battery's voltage, current and temperature signals, can be uploaded to the cloud for risk analysis. A comprehensive system for early-warning of thermal runaway can be

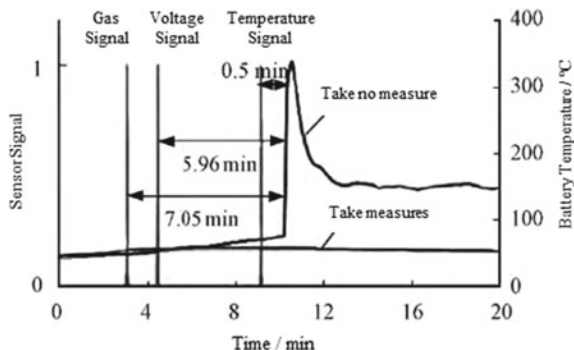


**Fig. 8.6** Comparison of early-warning methods for thermal runaway using temperature, voltage and gas detection

established, including vehicle-side early-warning methods, cloud-side early-warning methods, human-machine interface, and active intervention measures. The system can improve the safety of the vehicle and the passengers.

## References

- Cummings SR, Swartz SL (2017) Off-gas monitoring for lithium ion battery health and safety. In: Wright Patterson AFB: power sources committee meeting
- Feng X, Ouyang M, Liu X et al (2018) Thermal runaway mechanism of lithium ion battery for electric vehicles: a review. *Energy Storage Materials* 10:246–267
- Guenther C, Schott B, Hennings W et al (2013) Model-based investigation of electric vehicle battery aging by means of vehicle-to-grid scenario simulations. *Power Sources* 239:604–610
- Lai X, Zheng Y, Sun T (2018) A comparative study of different equivalent circuit models for estimating state-of-charge of lithium-ion batteries. *Electrochim Acta* 259:566–577
- Li X, Fan G, Pan K, Wei G, Zhu C, Rizzoni G et al (2017a) A physics-based fractional order model and state of energy estimation for lithium ion batteries. Part I: model development and observability analysis. *J Power Sources* 367:187–201
- Li X, Pan K, Fan G, Lu R, Zhu C, Rizzoni G et al (2017b) A physics-based fractional order model and state of energy estimation for lithium ion batteries. Part II: parameter identification and state of energy estimation for LiFePO<sub>4</sub> battery. *J Power Sources* 367:202–213
- Li X, Xu J, Hong J et al (2021) State of energy estimation for a series-connected lithium-ion battery pack based on an adaptive weighted strategy. *Energy* 214
- Liu X, Wu J, Zhang C, Chen Z (2014) A method for state of energy estimation of lithium-ion batteries at dynamic currents and temperatures. *J Power Sources* 270:151–157
- Ma JZ, Zhang JT (2020) Surface coating of electrocatalysts boosts battery performance. *Rare Met* 39:613–615
- Plett GL (2006) Sigma-point Kalman filtering for battery management systems of Li PB-based HEV battery packs: Part 1: Introduction and state estimation. *J Power Sources* 134(2):277–292
- Wang YB, Yang Q, Guo X, Yang S, Chen A, Liang GJ, Zhi CY (2021) Strategies of binder design for high-performance lithium-ion batteries: a mini review. *Rare Met*. <https://doi.org/10.1007/s12598-021-01816-y>

- Xia Y, Li T, Ren F, Gao Y, Wang H (2014) Failure analysis of pinch–torsion tests as a thermal runaway risk evaluation method of Li-ion cells. *J Power Sources* 265:356–362
- Zhang W, Shi W, Ma Z (2015) Adaptive unscented Kalman filter based state of energy and power capability estimation approach for lithium-ion battery. *J Power Sources* 289:50–62
- Zheng L, Zhu J, Wang G, He T, Wei Y (2016) Novel methods for estimating lithium ion battery state of energy and maximum available energy. *Appl Energy* 178:1–8

## **Part III**

# **Control Method**

# Chapter 9

## Passive and Active Balancing



### 9.1 Battery Pack Inconsistency Analysis

For battery pack in charge and discharge, the available capacity is limited by the cell with the least capacity. Due to the heterogeneities between cells in pack, the charge throughput of individual cells is different. Thus, cells in the pack are degraded differently. For battery pack of 18,650 cells in parallel, the difference of their available capacity can reach 3%. This difference accumulates with time and accelerates degradation of the battery pack. The difference could cause to overcharging, over discharging, and safety issues such as thermal runaway (Mwasilu et al. 2014; Jiangong et al. 2017).

The effect of heterogeneities between cells can be explained by barrel theory, as shown in Fig. 9.1.

The sources of heterogeneities between cells are mainly: production factor and use factor, as shown in Fig. 9.2. For production factor, the heterogeneities are generated during fabrication process and it is nearly impossible to eliminate all heterogeneities. For use factor, due to the fact that electrical parameters of the cells are different under dynamic loads and temperature, cell states are consequently different. The heterogeneities shall be eliminated by optimization of BMS.

#### 9.1.1 Production Factor

In the fabrication of Lithium-ion battery, many procedures are involved: mixing, coating, slitting, stacking, winding, packaging and electrolyte filling. Each procedure can influence the performance of Lithium-ion battery. Due to the fact of uncertainties during the fabrication, heterogeneities of cells always exist, even for cells of the same batches. Consequently, at beginning of life (BOL) cell parameters are different such as internal resistance, Lithium-ion concentration and separator thickness, etc.

**Fig. 9.1** Usable capacity of battery pack under inconsistency

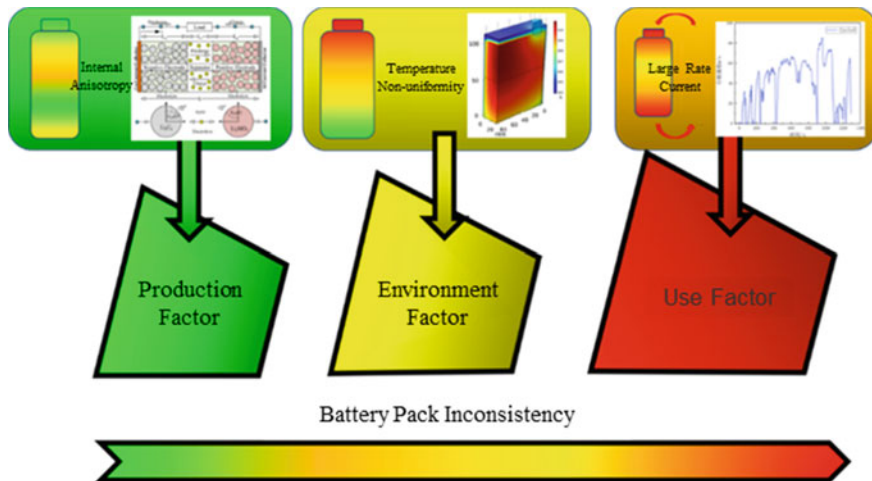
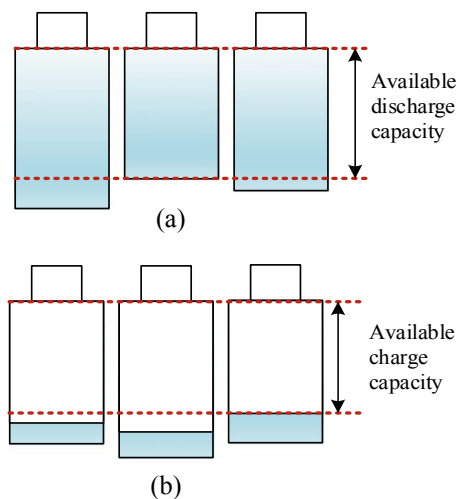


**Fig. 9.2** Inconsistency factors

### 9.1.2 Use Factor

Although the Lithium-ion batteries are comparatively uniform after selection in factory, the heterogeneities of cells are developed in practical usage and influence battery pack performance. The most significant use factors include charge/discharge rates and temperatures, etc.

### 9.1.2.1 Current Effect

The current (or C rate) affects the heterogeneities of cells by accelerating degradation of the cell of the least capacity. The overcharging and over discharging happen frequently for the cell of the smallest capacity, especially at high C rates. The degradation of cell is accelerated and promotes overcharging and over discharging, forming a positive feedback. The available capacity of the battery pack is therefore reduced. Moreover, the overcharging and over discharging would cause safety issues.

### 9.1.2.2 Temperature

Due to the heterogeneous internal resistances of cells, heat generations are different and there are thermal gradients within the battery pack. Temperature directly affects available capacity of cells. In general, cell degradation is faster at higher temperature. The cell with the higher temperature in the battery pack is degraded faster. The heterogeneous behavior of degradation reduces the battery pack lifetime and available capacity. The heterogeneous degradation is serious in working condition of low temperature.

### 9.1.3 Inconsistency Improvement

Although heterogeneities of cells cannot be eliminated totally, they can be controlled within safe range. For production factors, optimization on fabrication process would reduce heterogeneity. The optimization includes uniformity of raw materials (positive/negative electrodes and electrolytes, etc.) and processing precision (for current collector thickness and porosity of separator, etc.). Besides, produced cell classification in factory is an important precaution to avoid cells heterogeneities. For instance, by K-means clustering methods, the cells are classified according to OCV, internal resistance, capacity and self-discharging rate etc. to improve cells uniformity.

For heterogeneity of cells in use, cells are already assembled into battery pack and uniformity of cells have to be improved by methods such as battery balancing control. Other ways such as optimizing cell spacing for 18,650 cylindrical cells could also improve cells uniformity. For instance, spacing 5.5 mm would reduce heterogeneity to 13% (Shiqi et al. 2019). Such scheme could efficiently reduce cells heterogeneities.

Self balancing behaviors exist for cells in parallel in a battery pack due to the fact that voltages of individual cells tend to be uniform. In self balancing behavior, cells of different capacities inter charge/inter discharge themselves under low C rates. Self balancing is influenced by temperature, C rates and relaxation time at high SOC.

## 9.2 Balancing Management System

Inhomogeneities among battery packs can be reduced efficiently by balancing control. Hence, lifetime, safety and state of health for batteries are improved.

### 9.2.1 *Balancing System Architecture*

According to battery levels, the balancing control methods are categorized as: cell-cell, cell-module and module-module balancing. Among these methods, cell-cell balancing is the most basic and efficient. However, cell-cell balancing is not suitable for battery packs integrated by thousands of cells. Cell-module balancing is realistic and common. Module-module balancing is more complicated and requires balancing strategy with stability and reliability. Other methods such as module-cell are to be developed as well.

Until now, the mathematical models of balancing control are complicated and can be established in an easy way. Until now, balancing control models are mainly based on equivalent circuit models of battery cell. The common models include passive balancing, active balancing between cells, cell-module active balancing. These models are widely used to assist balancing design on BMS.

### 9.2.2 *Balancing System Classification*

In recent years, plenty of balancing control methods are developed. According to system structures, control methods are categorized as passive control methods and active control methods. According to the controlled variables, control methods are categorized as voltage control, SOC control and capacity control etc. For different control schemes, there are classic control, fuzzy control and model-based control. Passive controls are more common compared with active control. Balancing control systems are implemented in EV models such as BYD Qin, Roewe eRX5m Roewe ei5. The balancing control in the end stage of charging reduces the inhomogeneity of battery cells. Companies such as Infineon, Linear developed the chips for balancing control. Infineon TLE8001 chip can realize active and passive control. Linear LTC6802, LTC6804 also supports active control.

It has been shown that active/passive control reduces modules degradations (Wang et al. 2021). Until now, balancing control is mostly applied on static balancing such as the end stage of charging. Dynamic balancing needs to be further investigated. Efficiency of balancing control in full charge/full discharge condition is maximized (Kim et al. 2019). It is not necessary to apply balancing control on all conditions.

## 9.3 Balancing Circuit Topology

### 9.3.1 Passive Balancing

In passive balancing, the remnant capacity is consumed by the resistances and transferred into heat. In this way, the inhomogeneities within the cell is improved. Switch resistor is common in passive balancing.

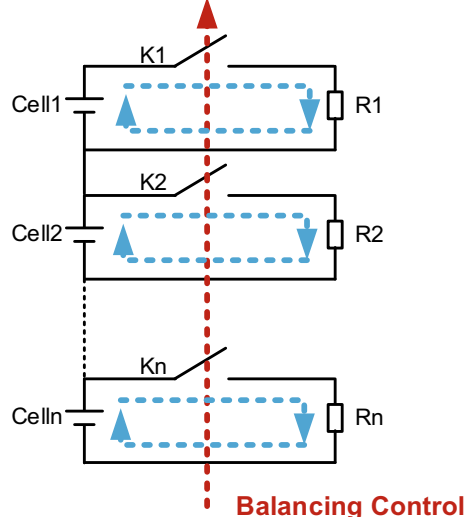
As shown in Fig. 9.3, the connection of resistors into circuits is determined by switches (semiconductors such as MOSFET). The heat generation rate follows Joules Law:

$$\dot{Q}_{dissipation} = I_{balance}^2 R \quad (9.1)$$

where  $\dot{Q}_{dissipation}$  is energy dissipation rate,  $I_{balance}$  is balancing current and  $R$  is balancing resistance.

Although remnant capacity is released from the cell with higher capacity, cell with lower capacity cannot be charged by the released capacity. The circuits in passive balancing is simple. The resistors can deplete capacity either in a continuous or pulsed way decided by the input signal. Passive balancing is commonly applied on EV models.

**Fig. 9.3** Circuit topology of switch resistive



For battery modules or small battery packs, passive balancing can satisfy the requirement to minimize inhomogeneity. For example, the unbalanced capacity of some type of cell is reduced from 1.21 to 0.82 Ah for degraded modules. However, for large EV, passive balancing is not efficient enough to balance the capacity inhomogeneity.

### 9.3.2 Active Balancing

In active balancing, energy is transferred between different battery cells by controlling the electrical circuits. Transfers between cell-module and module-module can be realized. Energy efficiency and balancing efficiency in active balancing is higher than in passive balancing. The active balancing technique is limited by circuits designs involving space occupancy, packageing, cost, balancing efficiency and reliability.

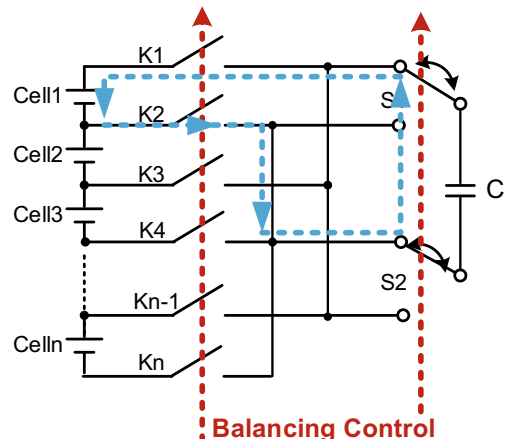
Until now, active balancing control are realized by elements such as capacitor, inductor and transformer where the energy is transformed.

#### 9.3.2.1 Capacitor-Based Balancing Topology

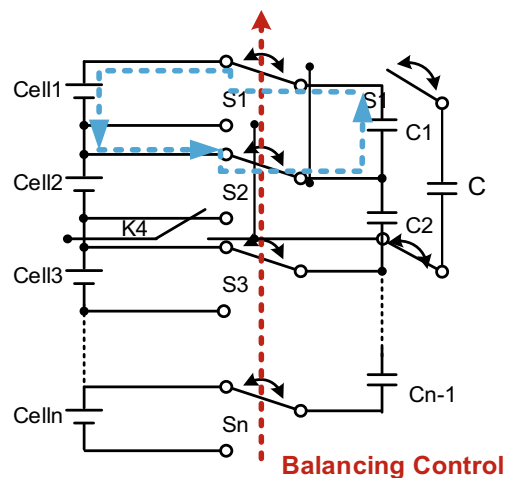
Active balancing based on capacitor is simple and low-cost but with high balancing time. The balancing efficiency can reach 90%. The main balancing circuits contain single capacitor, capacitor with switch and capacitor module with switches as shown in Figs. 9.4, 9.5 and 9.6.

Figure 9.4 shows capacitor-type circuits. The cells with either high or low capacity (or voltage) are chosen to be adjusted. By controlling the switch of the chosen cells, the capacity is transferred through capacitor.

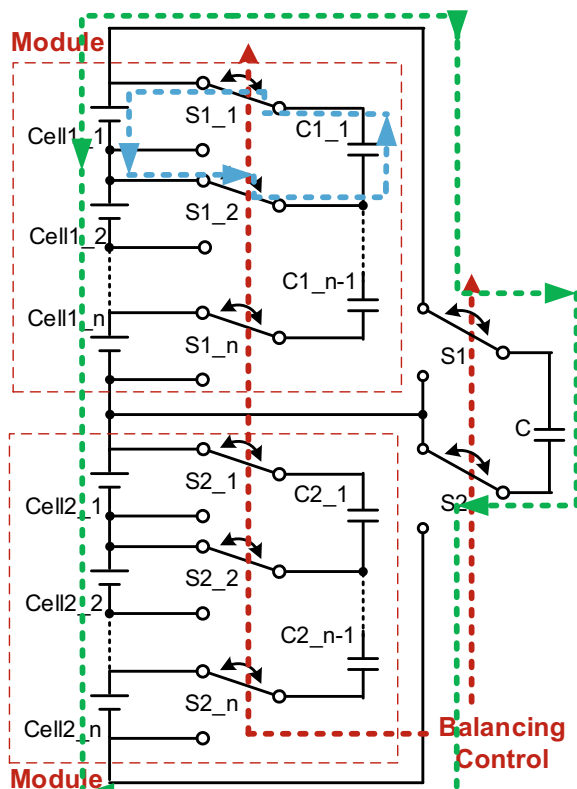
**Fig. 9.4** Circuit topology of single capacitor



**Fig. 9.5** Circuit topology of switched capacitor



**Fig. 9.6** Circuit topology of modular switched capacitor



The energy transfer within the capacitor is demonstrated here: Suppose E1 is the cell with higher capacity and cell E2 is of lower capacity. Switches K1 and K2 are closed initially. Switches S1 and S2 are initially turned towards upper position. At this stage, cell E1 transfers charge to capacitor. Capacitor is charged with positive charge at top and negative charge at bottom. The charging rate follows:

$$\dot{Q} = UI = CU \frac{dU}{dt} \quad (9.2)$$

In the equation, C is capacitance, U is terminal voltage of capacitor and I is current in capacitor. Then switches K2 and K3 are closed and switches S1 and S2 are turned downwards. Cell E2 is charged by capacitor.

Figure 9.5 shows circuits of capacitor with switches. Charge is transferred between cells through capacitors. This type of circuit is easy to control and of low cost. However, the balancing efficiency is low and it takes long time for cells to be balanced. Capacitor of double switches is of similar design. Two capacitors are used in charge transfer. The two capacitors reduce the balancing time to 1/4 of the circuit with one capacitor. But the structure of the design of two capacitors is more complicated.

Figure 9.6 shows capacitors in modules. Several switches are filled inside a battery module. Apart from charge transferred between cells, balancing between modules can be realized to reduce inhomogeneities inside battery packs.

### 9.3.2.2 Inductance-Based Balancing Topology

In this kind of balancing control, inductors are used as main elements to store and exchange charge. Charge transfer between cells, modules and packs is realized. The cost of this kind of balancing circuit is high and there exists energy loss due to magnetization. External capacitors are required as high frequency filters.

Figures 9.7 and 9.8 show the common circuits of inductors. In Fig. 9.7, single inductor transfers charge from cell of high capacity to the cell of low capacity. According to voltage difference between cells, inductors are charged or discharged by switches control. The balancing time is short for multiple cells.

The energy transfer for inductor circuits is illustrated here: Suppose cell E1 is of high energy and cell E2 is of low energy. S1 and S2 are initially switched off. Energy is transformed from cell E1 to inductor and the voltage direction follows right-hand rule. Then voltage potential at the top of inductor L is higher than the bottom. The energy transfer rate follows:

$$\dot{Q} = UI = IL \frac{dI}{dt} \quad (9.3)$$

where  $L$  is inductance and  $U$  is terminal voltage.

Later S2 and S3 are switched on. Cell E2 is charged by capacitor. Since the energy of inductor decreases with the decay of current, the stored energy will only stay for short time.

**Fig. 9.7** Circuit topology of single inductor

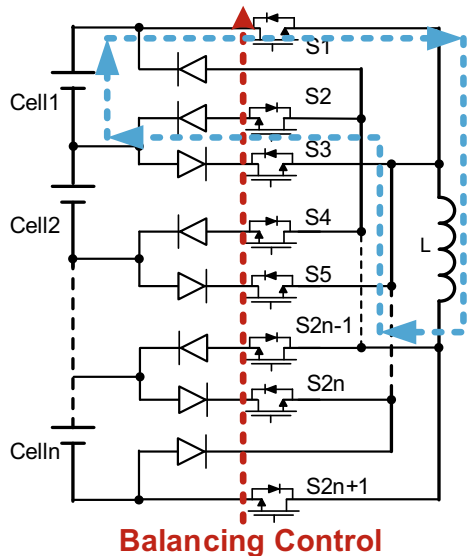


**Fig. 9.8** Circuit topology of multiple inductors

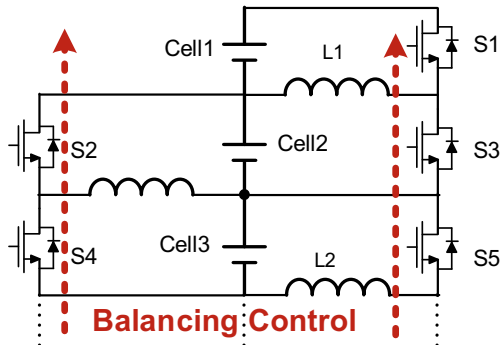
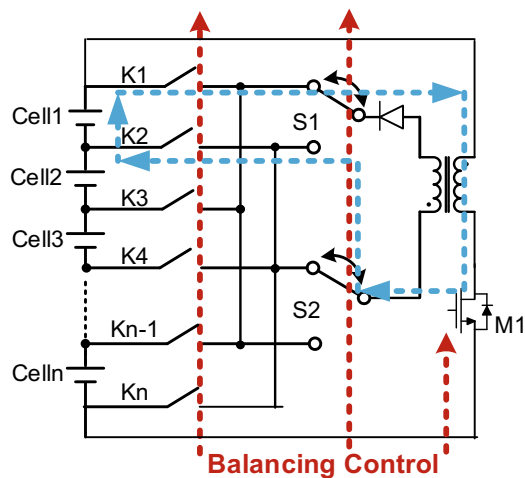


Figure 9.8 shows circuit of multiple inductors. Switches are controlled by PWM signal and the energy transfer among different cells. The energy from cells of high capacity is transferred to cells of low energy and the energy of the multiple cells is balanced. The energy is transferred in a single direction determined by the energy gradient. For the battery pack composed of many cells, the balancing time is long.

### 9.3.2.3 Transformer-Based Balancing Topology

In this balancing control, transformers are used as energy storage elements, including single winding transformers and multi-winding transformers.

**Fig. 9.9** Circuit topology of single winding transformer



Single winding transformer is also referred as switched transformer. Figure 9.9 schematically shows the circuit of single winding transformer. The transformers are controlled by switches. Energy is transferred from battery module to cells of low energy. The energy can also be extracted from cells of high energy and transferred to battery module. The required number of transformers is larger when there are more cells in series. Hence the circuit element occupies much space and cost is expensive.

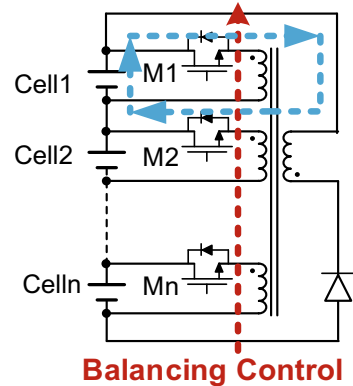
Single winding transformer is demonstrated as shown in Fig. 9.9. Assume cell E1 is of high energy and cell E2 is of low energy. Inductor follows counter clockwise spiral. K1 and K2 are initially switched off and S1 and S2 are connected to the up position. Cell E1 transfers energy to the single winding transformer. The voltage of the transformer follows right-hand rule. K2 and K3 are switched on, and S1 and S2 are connected to the bottom. Cell E2 is charged by the transformer. The transformer special occupancy is not limited by current. Hence the balancing efficiency can be improved by increasing balancing current.

Figure 9.10 shows circuits of multiwinding transformer. The transformer is composed of single primary coils and multiple side coils. Each primary coil is connected to a cell. The energy is transferred from cell to primary coil and the energy can also be transferred back to cell. The cost of this design high. It is difficult for this design to be integrated into battery packs.

### 9.3.2.4 DC/DC Converter-Based Balancing Topology

DC/DC balancing control is based on half bridge or whole bridge converters such as Buck, Boost, Buck-Boost and Cuk converters. In DC/DC balancing control, inductors and transformers can be used to store energy and DC/DC balancing control shares similar circuits. The precision of DC/DC balancing control is high with decent balancing efficiency, but the cost is high.

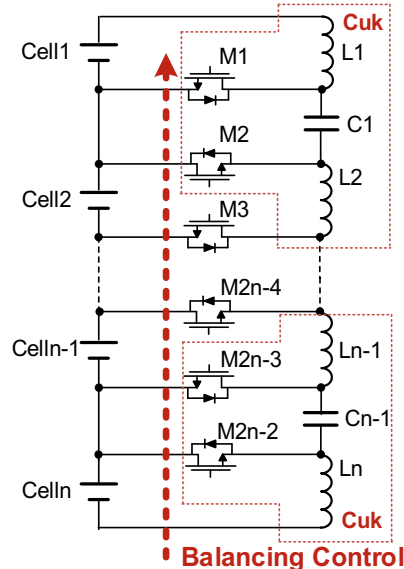
**Fig. 9.10** Circuit topology of multiwinding transformer



The advantage of DC/DC balancing control is that components are isolated from each other. If transformer is used, primary coils and side coils are isolated to improve balancing efficiency. Energy transfer circuits are also formed by side coils so that energy is transferred through battery modules.

Figure 9.11 shows Cuk structure where energy is transferred bi-directionally. Each cell is connected with two inductors in parallel. The inductors are controlled by MOS. Energy is transferred within cell. In the balancing period of Cuk circuit, energy is always transferred among the cells by capacitors or inductors when MOSFET is turned on or off. The main problem for Cuk circuit is that energy is only transferred between cells. The balancing efficiency will be affected when number of cells is

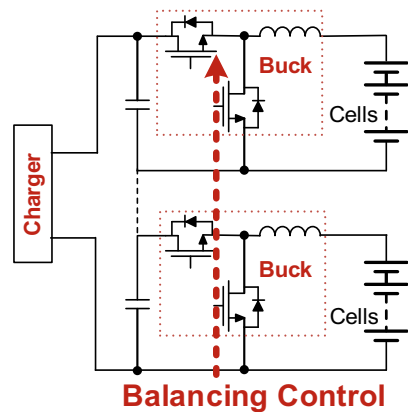
**Fig. 9.11** Cuk circuit topology



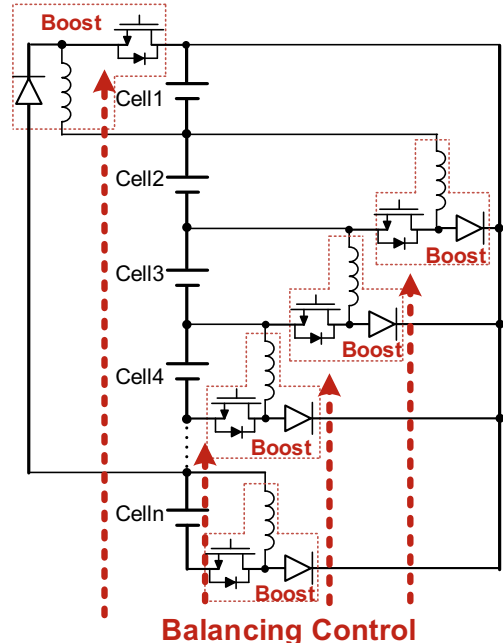
increased. The control precision of Cuk circuit is high but the cost is also high as there are many elements in the circuit. Figures 9.12 and 9.13 show Buck and Boost circuits, respectively.

Figure 9.14 shows a Buck-Boost circuit. The energy can be stored by DC/DC transformer and then transferred to the cell with lower capacity. Energy can be transferred bi-directionally in Buck-Boost circuit. The Buck-Boost circuit is simple with fewer elements. However, branch currents are superposed when several cells are

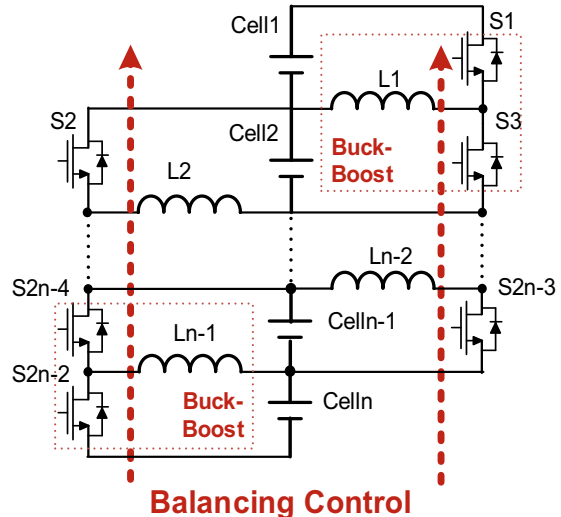
**Fig. 9.12** Buck circuit topology



**Fig. 9.13** Boost circuit topology



**Fig. 9.14** Buck-Boost circuit topology



discharged simultaneously, which make the system more instable. The Buck-Boost circuits can be implemented with bi-direction design. For Buck-Boost circuits, the balancing rate is fast. But the cost is high and design is complicated.

Flyback circuit is based on transformer. This type of circuit supports DC/DC transformer and DC/AC transformer, and is suitable for high power balancing control system. Flyback circuit avoids adopting elements of high inductance so that there is no voltage gap. The circuit is designed to transfer energy from cell of high capacity to the cell of low capacity efficiently and improve balancing efficiency.

### 9.3.2.5 Other Balancing Schemes

Passive balancing is faster while efficiency of active balancing is high. Combination of the two balancing controls can be a better solution. In multi-level hybrid balancing control, energy is transferred in cell-to-cell, cell-to-module and module-to-module level. The balancing rate is fast.

### 9.3.2.6 Balancing Methods Comparison

In passive balancing control, circuit is simple with easy implementation and low cost. But the balancing speed is slow. Due to the fact that remnant energy is transferred into heat, the heat rejection issue needs to be considered. It has been shown that (Omariba et al. 2019), passive balancing control reduce the capacity inhomogeneity and thermal inhomogeneity as well. But due to the heat generation of resistance, the temperature level is increased for passive balancing, while active balancing does not

suffer from the rise of temperature. Passive balancing is common in application for car manufactures such as Tesla and BYD.

In active balancing control, balancing rate is fast and energy loss is minimized. In constant current (CC) discharge/charge, active balancing control reduces inhomogeneities of capacity and resistance in a faster way, and maximize the battery lifetime. However, control strategy in active is more difficult than in passive control. Inductor circuits conduct balancing control bi-directionally with minimized energy loss. The balancing control by inductor circuits is limited by the control design complexity and implementation. In transformer circuits, primary coils and side coils are separated so that high power battery can be applied. The balancing rate and efficiency is ideal. The components occupy much space. This type of circuit is not widely adopted because cost of design is high, the control protocols are complicated and difficult in integration. Transformers based on DC/DC is a promising solution to balancing control due to its high efficiency and easy integration. However, the transformers based on DC/DC are limited by control protocols design.

### ***9.3.3 Summary of Balancing Topology***

Balancing control plays an important role in improving battery lifetime and discharge/charge performance. Developing balancing control system is significant in energy storage area.

The advantages and disadvantages of passive and active control are compared in Table 9.1.

## **9.4 Balancing Control Strategy**

In different balancing control protocols, control algorithms based on selected state variables are utilized to maintain the SOC inhomogeneities within a certain range. The studies on control protocols involve the selection of state variable and control algorithm development. Control protocols are affected by factors such as sampling accuracy, response characteristics, system robustness and hysteresis. Without suitable control protocols, the system may not be balanced or overbalanced and adverse effects arise such as energy loss, reduced lifetime and thermal runaway. Choosing correct state variables and robust algorithms for balancing control will improve balancing control performances.

**Table 9.1** Advantages and disadvantages of passive and active control

Balancing topology		Balancing time	System complexity	Control difficulty	Balancing efficiency	System volume	Total cost
Passive balancing topology		General	Low	Low	Low	Small	Low
Capacitance-type	Switched capacitor/single capacitor	Longer	Low	General	General	General	Low
	Double-layer capacitance-type	Shorter	General	General	High	Bigger	General
	Modular capacitance-type	Shorter	High	High	High	Bigger	General
Inductor/transformer-type	Inductor-type	Shorter	General	General	High	Big	General
	Multiwinding transformer-type	short	Higher	High	High	Bigger	High
DC/DC converter-type	Cuk-type	General	Higher	High	Higher	General	Higher
	Buck-Boost-type	Shorter	Higher	High	High	General	Higher
	Flyback-type	Shorter	General	High	High	Big	General

### 9.4.1 Balancing Control Variables

State variables play an important role in balancing control of EV batteries. A suitable state variable can reduce algorithm complexity and improve balancing efficiency. The selection of state variables is affected by: relation between target variable and SOC, difficulty in obtaining the target variable, sampling accuracy of target variable and time lag of the updating target variable, etc. Until now, the state variables for balancing control are mainly terminal voltage, capacity and SOC. Table 9.2 compares the features of using different state variables.

#### 9.4.1.1 Voltage-Based Balancing Strategy

For balancing control based on voltage, terminal voltage is collected from BMS during the battery discharge/charge cycling and is used to determine whether balancing control should be applied on the batteries. In this balancing control protocol, voltages are easily obtained and sampling frequency can be adjusted with no extra effort. However, voltage fluctuation can be serious under certain working conditions so that the batteries cannot be balanced or overbalancing happens.

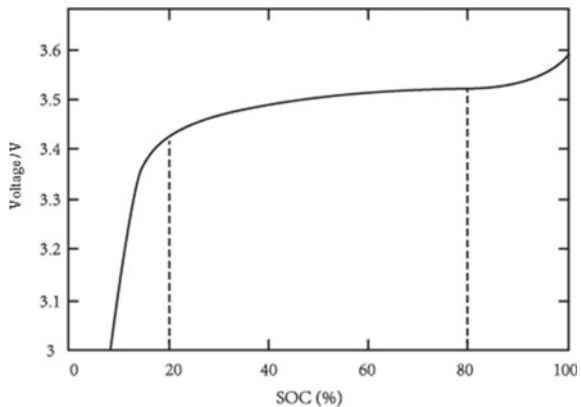
In balancing based on voltage, all batteries are controlled considering voltage, current and temperature to improve battery lifetime and solve safety issue arised from BMS design error. Balancing based on voltage is widely applied on batteries of NMC electrodes because the voltage is easily obtained with high accuracy. However, for batteries of LFP electrodes, variations in OCV-SOC curve are gentle especially in the SOC range between 20 and 80% (as shown in Fig. 9.15). The small change in OCV will cause severe SOC fluctuation. Moreover, in the stage in end of charge voltage difference between cells is smaller than the smallest precision in balancing control which is determined by the balancing resistance.

Balancing based on voltage is benefitted from the definite relation between OCV and SOC. However, real time OCV cannot be accurately measured as voltage

**Table 9.2** Comparison of the characteristics of each balancing variable

Balancing variable	Actual voltage	SOC	Battery capacity
Advantage	High sampling accuracy, fast sampling speed, simple control strategy	Accurately reflect system inconsistencies, prepare to characterize system status	Accurately reflect system inconsistencies
Disadvantage	There is a voltage plateau area. The balancing control accuracy is poor, and the phenomenon of over-balance and mis-balance is obvious	Complicated calculation method, poor accuracy, and poor real-time performance	Complicated calculation method, difficult to measure directly

**Fig. 9.15** Lithium iron phosphate battery of OCV-SOC graph



hysteresis exists. This balancing control protocol can be optimized by considering time lag of OCV or reducing relaxation time.

#### 9.4.1.2 SOC Estimation-Based Balancing

SOC is one of the most common parameters to show battery remained capacity. However, SOC cannot be measured directly and SOC estimation methods have to be applied such as Ah counting and model prediction.

Ah counting is base on the time integral of discharge/charge current. The complexity is simple but error is accumulated. For example, the error in current sensor would cause overall SOC estimation error. In Ah counting method, SOC estimation cannot be self-corrected.

For model prediction method, models are categorized into physics-based models and data-driven models. In physics-based models, online SOC estimation is conducted based on filter algorithms. There are less parameters in equivalent circuit models than electro-chemical models. For example, a first-order equivalent circuit model only contains two states and three parameters. The equivalent circuit model is frequently used in online SOC estimation as it can capture the dynamic characteristics of the battery cells well. In electro-chemical model, accuracy is high since they are based on the chemical reactions. But parameterization is difficult as there are plenty of parameters. There are Kalman filter, information filter and particle filter for model prediction. Kalman filter is widely used with decent computational cost in the process which involves inverting the matrices for several times. The accuracy is high (within 5%) and supports online estimation (Table 9.3).

Balancing based on SOC estimation is focused on the balancing control research area. There is competition of accuracy on SOC estimation and complexity. The complicated SOC estimation method will efficiently improve SOC estimation accuracy but reduce balancing efficiency as well. The accuracy for conventional SOC estimation method is relatively low. Developed SOC estimation method takes into

**Table 9.3** Comparison of SOC estimation methods

Algorithm name	Algorithm features	Complexity	Algorithm accuracy	Algorithm advantages and disadvantages
Information filter	Rely on the observed value to modify the filter model	Low	Low (error greater than 5%)	The algorithm is simple, and it can be rigorously proved the convergence of the algorithm, but it needs to rely on a large amount of sampling information
Kalman filter	Joint estimation using one-step forecast and innovation correction	Medium	Low (error approximately 5%)	The complexity of this algorithm is moderate, and it has good tracking ability for linear systems, but it cannot solve the problem of nonlinear estimation in the battery model
Extended Kalman filter	Approximate nonlinear equations using first-order Taylor expansion	High	Medium (error approximately 4%–3%)	The complexity of this algorithm is moderate, and it has a certain ability to solve the problem of nonlinear estimation. However, the high-order small items are discarded in the first-order Taylor expansion process, and there is a certain error. And it needs to calculate the differential in the process of algorithm realization, which increases the calculation amount of the algorithm

(continued)

**Table 9.3** (continued)

Algorithm name	Algorithm features	Complexity	Algorithm accuracy	Algorithm advantages and disadvantages
Unscented Kalman filter	Approximate calculation of nonlinear integrals using unscented transformation method	Medium	Medium (error approximately 3%)	The complexity of this algorithm is moderate, and it has a good ability to solve nonlinear problems. However, the algorithm has three parameters that need to be adjusted, which affect the accuracy of the algorithm
Cubature Kalman filter	Approximate calculation of nonlinear integral using cubature transformation method	Medium	High (error less than 3%)	This algorithm is moderately complex and has many variants. It has a rigorous mathematical derivation process, which can better ensure the convergence and accuracy of the algorithm
Particle filter	Using Monte Carlo sampling method to calculate nonlinear integral	Higher	High (error approximately 3%–2%)	This algorithm is complicated. The particle filter based on Monte Carlo sampling and sequence importance sampling method can effectively improve the estimation accuracy of nonlinear problems, but a large number of sampled particles are used in the calculation process, which greatly increases the calculation amount of the algorithm

account with considering electro-chemical reactions and thermodynamics. Neural network is suitable for application in SOC estimation and balancing control.

At present, the research focus of SOC estimation is on parameterization. The SOC estimation is affected by capacity fade and temperature etc. The error of SOC estimation can be severe if the above factors are ignored. Combined estimation method provides the solution but controversy exists for its application.

#### 9.4.1.3 Other Balancing Control Variables

In balancing control based on capacity, the control is designed to maximize the available capacity. Compared with control based on voltage, the control based on capacity shows the essence of balancing control system: to reduce the capacity inhomogeneity. The development of this control method is limited by capacity estimation. In discharge/charge working condition, the cell is affected by temperature, electrolyte concentration and discharge/charge current etc. Accurate capacity estimation cannot be realized with trivial effort and capacity inhomogeneity cannot be eliminated.

In balancing control based on internal resistance, internal resistance is set as control variable. The internal resistance is estimated and used to control balancing circuits. The resistance inhomogeneity represents cell inhomogeneity. Impedance, capacitive reactance or impedance angle are used as important parameters in this control protocol. The difference and deviation of internal resistance can be used to show the inhomogeneity of battery cells. However, internal resistance cannot be easily estimated with high accuracy. This control protocol will be developed with the help of online estimation techniques.

Balancing control can be based on battery module inhomogeneity as well. Estimation on battery module inhomogeneity is complicated. The common estimation methods include models based on equivalent circuits and electro-chemical analysis etc. Improving inhomogeneity estimation will benefit the balancing control protocol.

Control variable based on hybrid variable is an important direction of balancing control research. In this protocol, the advantages of the control protocols based on different state variables are combined to improve reliability of balancing control. One example is combining states of voltage and SOC.

#### 9.4.1.4 Summary of Balancing Control Variables

Until now the balancing control protocols of lithium-ion battery is mainly based on voltage and SOC. Balancing based on voltage is widely adopted due to its high sampling accuracy and easy implementation. However, voltage cannot accurately capture the remaining capacity. Polarization and voltage fluctuation is detrimental to balancing control accuracy. Balancing control based on SOC avoids the problem for voltage control protocol, but accuracy is limited by complexity. SOC protocol is one of the main research directions in balancing control.

Apart from voltage and SOC, internal resistance and remaining capacity are also used as state variables in balancing control. However, accuracy is limited due to the online estimation of the two variables.

### **9.4.2 *Control Strategy***

Selected parameters can be used as state variables in balancing control to judge when the balancing circuits are turned on. More balancing protocols based on mathematical methods are developed.

#### **9.4.2.1 *Battery Parameter Method***

The common parameters used in this method are maximum, average, variance and standard deviation. The logic is simple with easy implementation.

In balancing control protocol based on maximum value, maximum values are selected as state variables. Cells are discharged by balancing circuits based on this protocol. After one cell is fully discharged, all other cells are balanced to a unified level. This protocol is suitable to the situation where state variables are severely different. When the difference of state variables is small, pulses in discharge process will cause overbalancing and reduce balancing efficiency. Choosing maximum values as state variable is even worse as the maximum value cannot accurately represent battery states and individual cells can be overload. Therefore, this balancing protocol is frequently applied only to the stage in the end of charge when current is small.

In protocol of average value, average values of cells in series are selected as state variables for balancing control. Cells that need to be charged and discharged are decided in this protocol. This protocol can be easily implemented, but energy loss may happen as the cell of highest capacity and the cell of lowest capacity are separated far away. Block method can be combined to improve the efficiency of this balancing protocol.

#### **9.4.2.2 *Model Predictive Control***

In the protocol based on model prediction, optimization is iterated and the control variable is optimized in a limited prediction time domain. The protocol lies in the state at current time step and time domain in the future so that optimization can be conducted. This protocol is widely used in production industry. Although the accuracy is not high, the computational cost is lower than optimization algorithm and control efficiency is decent. It has been shown that this protocol will reduce possibility of overbalancing.

#### 9.4.2.3 Fuzzy Control Method

Fuzzy control protocol is based on artificial intelligence and combined fuzzy mathematics theories and fuzzy inference. Fuzzy control is among the advanced control protocols. In the situations where the variables to be controlled cannot be explicitly expressed, inference are conducted and the system is controlled after several rounds of optimization. However, the stability and robustness cannot be described in rigorous mathematics. In balancing control systems, stability and robustness are expressed by Hardware-in-the-loop (HIL) method. Fuzzy control is developed. In multi-input fuzzy control, input of voltage difference, voltage average, temperature, SOC, SOC difference and SOC average are used as state variables in balancing control and system is balanced by 4 fuzzy controllers.

#### 9.4.2.4 Neural Network Control

Neural network control protocol is more complicated than the above protocols. Data training has to be conducted. This protocol is developed in the past years. The balancing system is simplified as a non-linear control problem at first and multi-level neural networks are established for dynamic control. Neural network control can be combined with other control algorithm for better control performance.

#### 9.4.2.5 Summary of Balancing Control Strategy

Classic control protocols involve maximum value, average value. These protocols are widely adopted since the structures are simple with low complexity. However, noise and sampling error will cause overbalancing. Advanced balancing control such as PID, model prediction, fuzzy control and slider control are based on rigorous mathematical derivations so that accuracy and convergence, stability and robustness are satisfied. However, the algorithm is complicated and is difficult to be implemented into the vehicle balancing control system since the computational ability is limited. Combined control protocol is suitable for application, such as fuzzy-PI control protocol. With the development of implemented system, application of multi-core chip microcontroller, advanced control protocol can be widely applied into vehicle balancing control system.

### 9.5 Conclusion

The battery balancing control is developed with the deeper understanding of electrochemical reaction mechanism and improved parameterization methods. Control circuits, selection of state variables and balancing protocol are studied which will benefit the research in mechanism study of lithium-ion battery.

The lithium-ion battery balancing control system is designed to reduce inhomogeneities. In recent years, there has been improvement on theoretical study and application. However, a comprehensive protocol that involves balancing accuracy, rate, efficiency and complexity still needs to be developed. In the future, the research direction for balancing control can be:

Optimizing balancing circuits. The balancing control system will be based on structures with no energy dissipation. However, it is limited by the issues of complexity, spatial occupancy, implementation and cost. Microchips with fast speed, high efficiency and high-level integration are to be studied.

Selection of the best control variable. Classical balancing control protocols are widely applied in EV due to the features of high sampling accuracy, fast processing speed and easy logic. However, classical balancing control is not suitable for batteries of LFP electrodes. Until now SOC is mainly used as control variable, but is it limited by SOC estimation accuracy and updating frequency. With the deeper understanding of electro-chemical reaction mechanism, new balancing control based on sampling voltage or SOC will arise.

Innovate balancing control protocol. Balancing control protocols are developed such as fuzzy control and model prediction. However, unified standards are missing and issue of low reliability and low accuracy still limit the performance of this protocol. New control algorithms are to be developed and transferred to balancing control protocols.

## References

- Jiangong Z, Zechang S, Wei X et al (2017) Experimental investigations of an AC pulse heating method for vehicular high power lithium-ion batteries at subzero temperatures. *J Power Sources* 367:145–157
- Kim J, Oh J, Lee H (2019) Review on battery thermal management system for electric vehicles. *Appl Therm Eng* 149:192–212
- Mwasilu F, Justo JJ, Kim EK et al (2014) Electric vehicles and smart grid interaction: a review on vehicle to grid and renewable energy sources integration. *Renew Sustain Energ Rev*
- Omariba ZB, Zhang L, Sun D (2019) Review of battery cell balancing methodologies for optimizing battery pack performance in electric vehicles. *IEEE Access PP* (99):1–1
- Ou S, Xu H, Lin Z et al (2019) Light-duty plug-in electric vehicles in China: an overview on the market and its comparisons to the United States. *Renew Sustain Energ Rev* 112:747–761
- Wang S, Fan Y, Stroe DI et al (2021) Battery system active control strategies. *Battery Syst Model*

# Chapter 10

## Optimized Charging Management



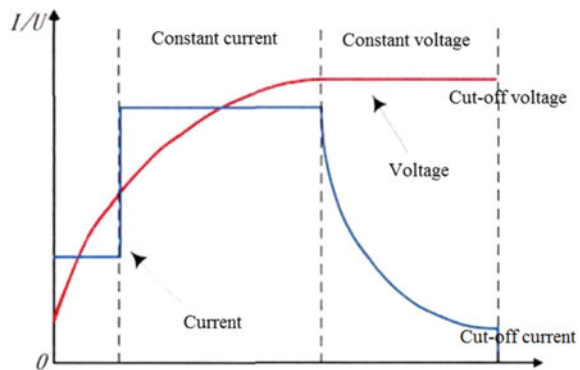
### 10.1 Background

The energy storage system of power battery is one of the significant aspects of electric vehicles. It determines the travel range and lifetime of electric vehicles. Lithium-ion battery is the ideal power battery due to its high energy density and long cycle lifetime, and has been studied comprehensively. Charging scheme optimization is a key research issue on lithium-ion battery as charging scheme and working condition influence the performance and lifetime of lithium-ion battery. At present, high power charging piles are widely utilized to meet the need of charging time reduction. Different charging schemes will lead to different battery charging performances. The optimized charging scheme will reduce charging time and energy loss, while increasing charged capacity and maintaining lifetime. The issue of energy loss during charging and charged capacity have been bottlenecks of development for electrical vehicle.

### 10.2 Charging Protocol

Until now, the charging protocols for electrical vehicle include constant current-constant voltage (CC-CV) charging, multi-stage constant-current charging and pulse charging.

**Fig. 10.1** Schematic diagram of constant current and constant voltage charging



### 10.2.1 Constant Current-Constant Voltage (CC-CV)

In constant current (CC) scheme, constant currents are maintained during the entire or partial process of charging. In constant voltage (CV) scheme, voltages are kept constant in the charging process.

In constant current–constant voltage (CC-CV) scheme, CC and CV schemes are combined. Figure. 10.1 schematically shows the current and voltage variation during the CC-CV scheme.

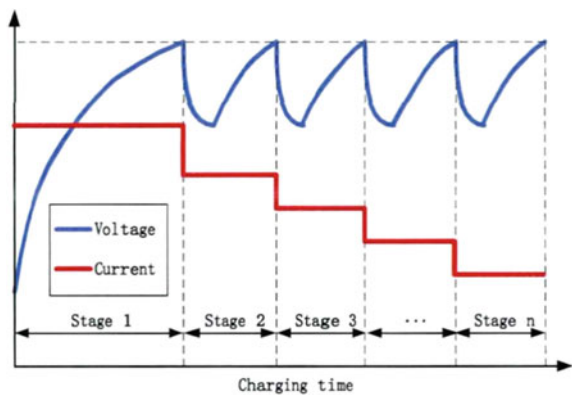
In the early stage of charging process, small C rates (e.g., 0.1C) are chosen according to battery voltage. As the voltage reaches the preset voltage, CC scheme is adopted. During this stage, current remains fixed and voltage keeps increasing. CV scheme starts when the voltage reaches the cutoff value. Voltage remains fixed and current keeps decreasing during this stage. As the charging current is lower than cutoff value, the whole charging is finished.

The CC-CV scheme is widely utilized since it combines the advantages of CC and CV schemes, and avoids their short comes (Ramos and Jabbari 2020). There has been comprehensive studies on the effect of constant current values, cutoff voltage values (Jiang et al. 2020).

### 10.2.2 Multi-Stage Constant-Current Charging

Multi-stage constant-current charging scheme is an optimized charging protocol based on CC scheme. The whole charging process include multiple constant-current stages. The current is changed to the value in the next CC stage when the voltage reaches the cutoff value, until the whole charging process ends. Figure. 10.2 representatively shows the current and voltage in the multi-stage constant-current charging scheme.

**Fig. 10.2** Multi-level constant current and voltage



In the multi-stage constant-current charging scheme, the current in each stage is generally lower than in the next stage. Otherwise, the voltage will hit cutoff value and the next stage is reached.

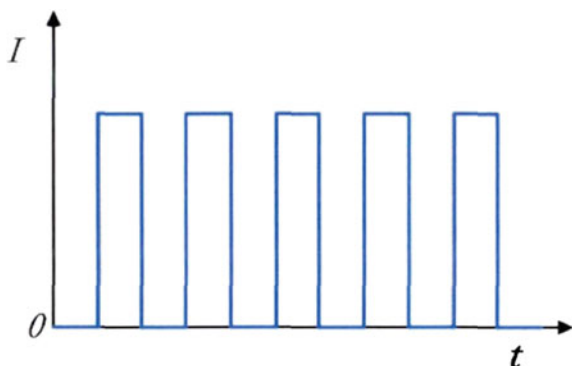
Multi-stage constant-current charging scheme has been comprehensively studied as this scheme suitably applies to the condition of current changes in the whole charging process (Keyser et al. 2017). However, this scheme suffers from problems of low charging speed and efficiency. The charging performances can be improved by different combinations of currents in all stages. Hence, how to optimize the currents in all stages leads to significant research questions.

### 10.2.3 Pulse Charging

In pulse charging scheme, currents or voltages are applied on the battery in a pulsing way. Between two adjacent pulses, there are relaxation or discharging to avoid the adverse effect of polarization. The charged capacity is kept increasing during the whole charging process. The charging is finished as the voltage reaches cutoff value. Figure 10.3 schematically shows current variation in pulse charging scheme.

Pulse charging scheme was applied mostly on lead-acid batteries to avoid the polarization effect. This scheme is developed for lithium-ion battery. Compared with the conventional schemes (e.g., CC-CV), current is maximized in pulse charging scheme while the concentration and Ohmic polarization are significantly reduced in each stage to facilitate the fast charging in the next stage. The pulse charging scheme is widely utilized due to the fact of reduced charging time, small temperature change and consequent lifetime maintaining.

**Fig. 10.3** Pulse charging current curve



### 10.3 Model-Based Charging Optimization Method

The key aspects in battery charging management include reducing charging time, prolonging cycling lifetime and improving stored energy. The three aspects are reviewed in this section.

#### 10.3.1 To Shorten the Battery Charging Time as the Optimization Goal

The application of lithium-ion battery to certain working conditions is significantly limited by the charging time.

At high charging currents, the chemical reactions within the lithium-ion battery become fast and are accompanied by side reactions, causing severe temperature rise. The charging current was optimized by electrochemical model (Klein et al. 2010). The characteristics in the lithium-ion battery are captured by considering lithium-ion concentration and voltage potentials in electrodes and electrolyte, molar flux of active material and temperature, etc., in electrochemical models. The charging time can be optimized by limiting maximum current, temperature and side reaction rates.

The charging time optimization can be realised by equivalent circuit models as well. In CC-CV charging scheme, although CC stage occupies 25% ~ 40% of the whole charging process, 75% ~ 80% of battery capacity is charged. The charging efficiency in CV stage is lower than in the CC stage. Therefore, CV stage can be adjusted in the CC-CV scheme (Hsieh et al. 2001). The FC-ASCC (fuzzy-controlled active state-of-charge controller) can optimize the charging protocol in CV stage.

The schematic of FC-ASCC is shown in Fig. 10.4. FC-ASCC steps in the CV stage and searches the most suitable current for battery charging. The optimized current generated by FC-ASCC replaces the current in the original CV stage. The whole charging process stops when the current hits the cutoff value.

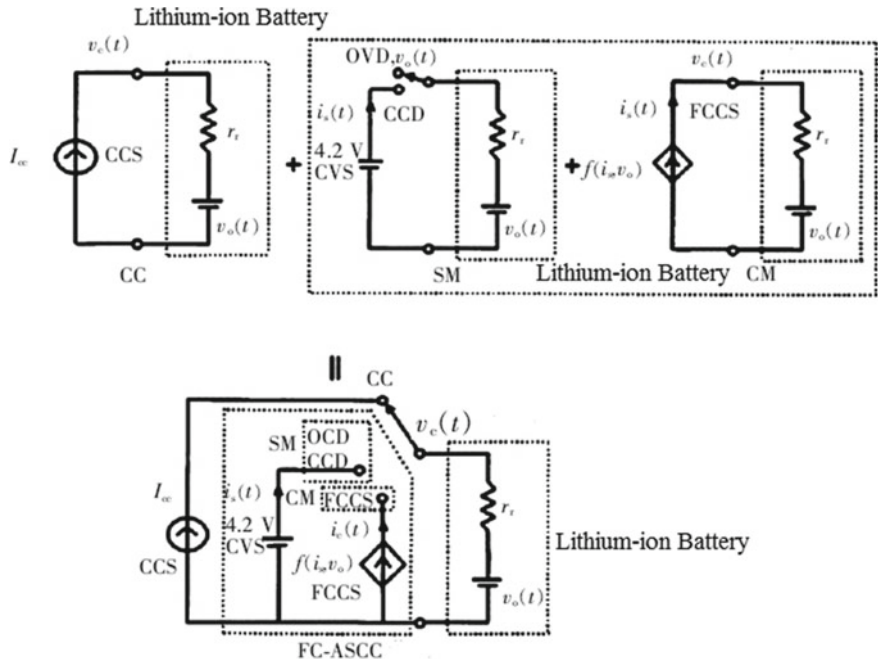


**Fig. 10.4** FC-ASCC schematic diagram

Furthermore, other charging current optimization methods based on non-linear model prediction, grey-predicted control, frequency control and taper-current control also improve charging efficiency in the CV stage.

### 10.3.2 To Extend the Battery Cycle Life as the Optimization Goal

Cycling lifetime has always been a bottleneck for the development of lithium-ion battery. The lifetime is relevant with the working condition and charging methods etc. Optimized charging technique considering the cycling lifetime is a significant aspect of the charging scheme.

In CC-DV charging, Different currents can be applied for the different stages of lithium-ion battery lifetime (Rahimian et al. 2010). The capacity fade is estimated by invoking capacity fade parameter in the single particle model. The dynamic response of the charging process is captured by the mathematical expression so that the optimization can be conducted to prolong lifetime. Through partial discretization method, the dynamic process is translated into nonlinear optimization using direct search (DS) and gen-etic algorithm (GA). Thus, the battery lifetime is prolonged.

### 10.3.3 To Improve Battery Storage Energy as the Optimization Goal

Stored energy (or energy density) of lithium-ion battery is considered the most significant on certain applications, which cannot be realized by CC-CV charging. Optimization charging protocols targeting at energy density is to be developed.

#### (1) Dynamic optimization based on electrochemical models

Based on electrochemical models, charging process can be controlled by monitoring the active material concentration in the chemical reactions. Aimed at maximizing energy density, the charging schemes are optimized by invoking the equations that describe dynamic responses (Methekar et al. 2010). Compared with CC-CV charging, charging current calculated by the dynamic optimization methods is nonlinearly decreasing with very low current near the end. In this situation, voltage reaches the cutoff value in a very long time and the stored energy is maximized.

#### (2) Optimization based on preset currents

Although the chemical reactions inside lithium-ion battery can be captured by electrochemical models, the accurate fundamental parameters are not easy to be obtained. Charging currents can be summarized from quantities of charge and discharge experiments under different working conditions so that a database is set up. The charging current is optimized based the database. The most obvious advantage of this optimization method is that the mechanism underlying the charging process is lumped into the training data, which makes the charging optimization method suitable for engineering applications. In a recent study, the charging process is divided into 5 constant-current sections where Ant Colony Optimization method was used (Liu et al. 2005). Compared with CC-CV charging, this method reduces charging time and improves cycling lifetime and efficiency.

## References

- Hsieh G, Chen L, Huang K et al (2001) Fuzzy-controlled Li-ion battery charge system with active state-of-charge controller. *IEEE Trans Industr Electron* 48(3):585–593
- Jiang L, Li Y, Huang Y et al (2020) Optimization of multi-stage constant current charging pattern based on Taguchi method for Li-Ion battery. *Appl Energ* 259
- Keyser M, Pesaran A, Li Q et al (2017) Enabling fast charging—battery thermal considerations. *J Power Sources* 367:228–236
- Klein R, Chaturvedi N, Christensen J et al State estimation of a reduced electrochemical model of a lithium-ion battery. In: Baltimore. IEEE, pp 6618–6623
- Liu YH, Teng JH, Lin YC (2005) Search for an optimal rapid charging pattern for lithium-ion batteries using ant colony system algorithm. *IEEE Trans Ind Electron* 52(5):1328–1336

- Methkar RN, Ramadesigan V, Braatz RD et al (2010) Optimum charging profile for lithium-ion batteries to maximize energy storage and utilization. *ECS Trans* 25(35):139–146
- Rahimian SK, Ragman SC, White RE (2010) Maximizing the life of a lithium-ion cell by optimization of charging rates. *J Electrochem Soc* 157(12):A1302–A1308
- Ramos ME, Jabbari F (2020) A decentralized, non-iterative smart protocol for workplace charging of battery electric vehicles. *Appl Energ* 272

# Chapter 11

## Thermal Management and Thermal Safety



### 11.1 The Effect of Temperature on Battery Performance

Temperature has a significant effect on capacity, impedance, maximum charge/discharge rate and degradation of lithium-ion battery. The thermal gradients will accelerate the inhomogeneity within the battery and are detrimental to battery performances. Generally, the effects of temperature on electrical vehicles are: (1) discharge performance is exasperated in low temperature, (2) degradation is accelerated in high temperature, (3) inhomogeneity can be increased and (4) safety reliability is reduced. Figure 11.1 schematically shows temperature relations with the above 4 aspects.

#### 11.1.1 Low Temperature

The available capacity of lithium-ion battery is significantly reduced in low temperature. On one side, the chemical reaction rates are slow. On the other side, low temperature would increase internal impedance. Compared with polarization impedance, Ohmic impedance is more sensitive to temperature. Consequently, the travel range of electrical vehicle can be reduced to 20%.

Figure 11.2 exhibits the voltage variation with discharge capacity under different temperature for a certain lithium-ion battery (Lei et al. 2015). It is clearly visible that discharge capacity is significantly reduced especially below 0 °C. The discharge capacity is reduced to 60% of the rated capacity at -30 °C. Hence, under low temperature, lithium-ion battery needs to be preheated to suitable temperature.

Under low temperature, the internal impedance is increased due to polarization. This makes the graphite potential closer to the value where lithium plating happens. To prevent piercing structures and consequent short circuiting, charging current and voltage have to be limited.

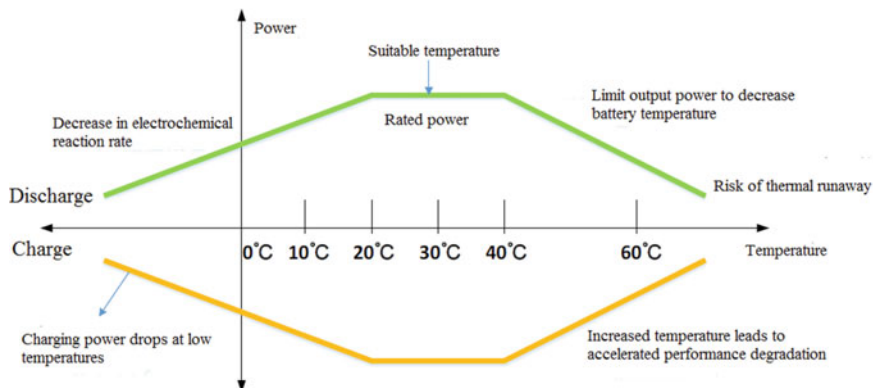
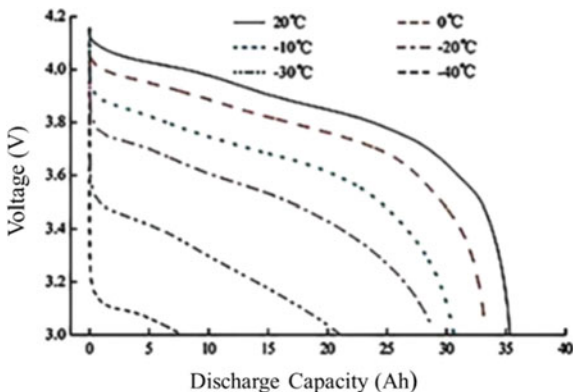


**Fig. 11.1** The influence of temperature on the temperature and safety of lithium-ion batteries

**Fig. 11.2** 10 A discharge curve of a certain lithium-ion battery at different temperature



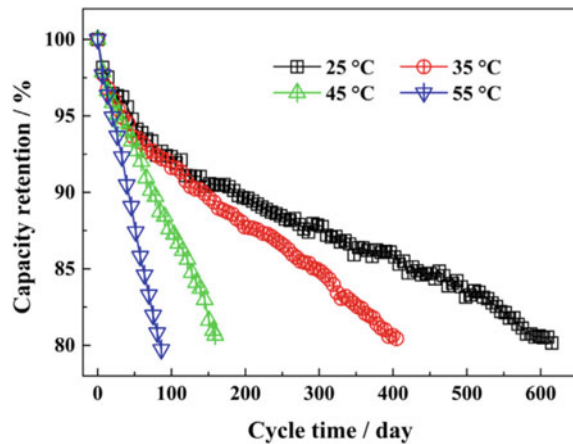
### 11.1.2 Higher Temperature

Electrochemical reactions are reversible inside lithium-ion battery. Temperature affects, reaction rates and higher temperature always accelerate the electrochemical reactions. However, as temperature is increased, polarization is also accelerated, and battery can be overcharged earlier. The active electrode materials can be decomposed at high temperature, cause irreversible structure damage and even explosion.

Figure 11.3 shows the capacity retention of LiFePO<sub>4</sub>/graphite battery at C/3 rate under different temperatures (25 °C, 35 °C, 45 °C and 55 °C). The cycling lifetime at 55 °C is 1/7 of lifetime at 25 °C (Sun et al. 2017).

Quantities of battery cells are needed in a electrical vehicle and the space for battery pack is limited. Hence the battery cells are densely arranged. Heat is generated during normal operation of charge/discharge. If the heat can not be dissipated efficiently, the cell temperature is high and may even causes thermal runaway.

**Fig. 11.3** The relationship between temperature and capacity



### 11.1.3 Temperature Difference

The temperature difference between battery cells would cause SoC inhomogeneity and hence available capacity loss. The capacity loss is increased as the temperature difference is increased. As shown in Fig. 11.4 (Yang et al. 2016), as the temperature difference is increased from 0 to 18 °C, the available capacity loss is increased from 19 to 22%. To maintain discharge performance and prolong life time, temperature difference should generally be kept within 5 °C.

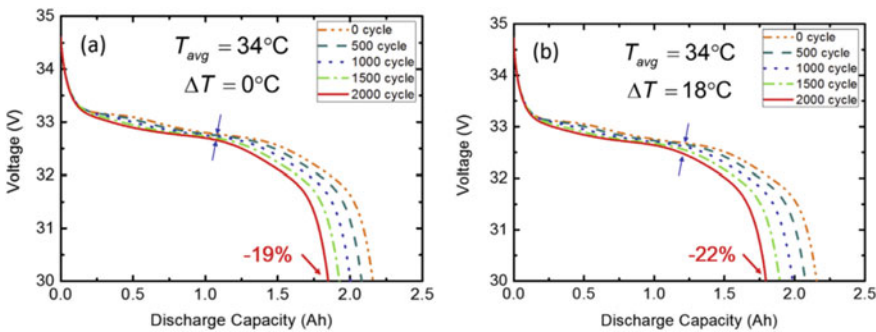


**Fig. 11.4** Battery cycle life under different temperature differences

## 11.2 Thermal Management Method

### 11.2.1 Low Temperature Heating Method

Under low ambient temperature, pre-heating is utilized to maintain a suitable temperature range for the battery. According to heat transfer paths, preheating is divided into internal heating, external heating and mixed heating (Safdar et al. 2020).

#### 11.2.1.1 External Heating

By external heating, power battery pack or module is heated externally through liquid/gas, heating plate, phase change material or Peltier.

##### (1) Gas heating

In gas heating, the battery is heated through gas. Forced air convection is common for gas heating. External fans blow air at temperature higher than battery and heat is exchanged between air and battery. The hot air is either generated either by heater or collected from motor or other electrical devices with high power. For hybrid electric vehicle, hot air can also be collected from engine.

Cost for gas heating is relatively low than other methods. Heating efficiency and uniformity can be improved by design of packaging, heating position and heating area.

##### (2) Liquid heating

Liquid heating is similar to gas heating in terms of the way heat is exchanged. However, heat conduction is faster in liquid heating due to the higher thermal conductivity in liquid than gas. In more complicated working conditions, liquid heating is better than gas heating for conventional thermal management requirements.

In liquid heating, heat is mainly transferred to battery pack through liquid. The battery modules can be configured with pipelines or immersed in liquid. For pipeline configuration, water, oil or coolant can be utilized as heating media. When the modules are immersed in heating liquid, short circuit is avoided by insulation.

The heat transfer between heating liquid and battery modules is determined by thermal conductivity, viscosity, density and flow velocity of liquid. The requirement for sealing and electrical insulation is higher in liquid heating than gas heating, making the battery pack design more complex and influencing reliability of the system.

##### (3) Plate heating

For plate heating, heat is generated by electrical heating device and transferred to battery cell in conductive way. Heating plate or film can be implemented

as heat source. The plate heating is slower than liquid heating and thermal gradients are induced.

(4) Phase change material

Phase change material (PCM) is of high heat capacity and frequently applied to thermal management system. Heat generated by battery is absorbed by PCM and stored by phase change in the melting process of PCM. In low temperature, heat is released in the solidification process of PCM so that battery is warmed. The low temperature is avoided by the fact that PCM temperature is maintained at solidification point.

The thermal conductivities of PCM is relatively lower than that of liquid. Adding graphite materials or carbon nanotubes to PCM will improve the thermal conductivities but increase cost as well.

(5) Peltier heating

When current flows through the thermoelectric device, heat is generated or absorbed as shown in Peltier effect. Heating or cooling can be realized by changing current in the Peltier element. The heating or cooling efficiency is controlled by adjusting current.

Until now, Peltier devices are applied on many electrical devices but not frequently on battery. The fabrication of thermal management system containing Peltier devices is complicated and the cost in design and usage is higher than other heating methods.

### 11.2.1.2 Internal Heating

For internal heating, Joules heat is generated when current flows through batteries with electrical resistance. The viscosity of electrolyte is usually higher in lower temperature, which increases the resistance in charge transfer. Under extreme circumstances, the electrolyte is even frozen. However, the increased resistance can be utilized to generate more heat so that the battery is maintained at suitable working temperature. According to the current direction, internal heating can be categorized as charging heating, discharge heating and pulsed current heating. The heating can also be divided into self heating and heating with external power.

(1) Charge heating

In charge heating under low temperature, the heat generation during the discharge process is used to recover the suitable temperature. Voltage is strictly limited to avoid overloading, hence the heating efficiency is affected.

(2) Discharging heating

Discharging heating can be used combined with external heating to improve heating efficiency. The energy loss during discharging heating increases with discharge time. There are requirements on loading. Discharging heating is limited as low SoC.

**Fig. 11.5** Self-heating structure of single battery

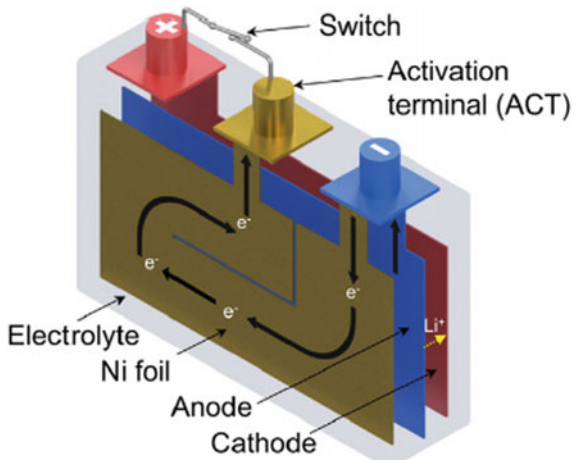


Figure 11.5 schematically shows the self heating structure of a battery. Nickel foils are implemented in battery. When the low temperature inside battery is detected, current is applied on Nickel foil. Along with heat generated by discharge, high heating efficiency is realized (Wang et al. 2016). However, this self heating structure will reduce the energy density.

### (3) Alternating current heating

Alternating current at controlled amplitude and frequency would heat the battery by the self resistance. Alternating current at high/low frequency would increase battery temperature in a short time but this is dependent on the facility.

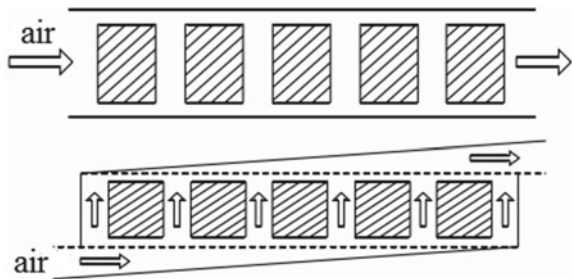
## 11.2.2 High Temperature Heat Dissipation Method

### 11.2.2.1 Air Cooling

Air cooling is one of the most simple ways of thermal management, with low cost and space limits. Natural cooling and forced convection cooling is common in air cooling. Cooling efficiency in forced convection cooling is high. Facilities such as pumps, fans, pipes are required in forced convection cooling hence cooling system is large and complex with high maintaining cost. There are direct and indirect cooling schemes in forced convection cooling. Compared with direct cooling scheme, indirect cooling scheme causes larger thermal gradients. Indirect cooling scheme is less utilized than direct cooling scheme (Shashank 2018).

Air cooling is adopted for Mazda Demio EV. Each battery module contains 2,018,650 cylindrical cells. There are 96 modules in series. The cooling system gets more complex as the number of cells increase. Air cooling scheme is also applied to electrical vehicle models such as Toyata Prius, Honda Insight, Nissan Leaf and

**Fig. 11.6** Serial ventilation and parallel ventilation



BYD F3DM, Nissan Leaf is configured with passive thermal management system that is rarely used in other models (Fig. 11.6). The battery pack is composed of 192 lithium-ion battery cells of 33.1 Ah each. There are 48 battery modules in series. Each battery module contains 4 cells (2 in series, 2 in parallel). The entire battery pack is thermally insulated from ambient circumstances. There is no liquid cooling or air cooling systems. For some cold regions, heating components are optional. The internal resistance of battery cell is reduced after cell design optimization, hence the heat generation is lowered down. Meanwhile, the thin structure of cell makes the heat difficult to accumulate. The complex active thermal management system could be avoided.

### 11.2.2.2 Liquid Cooling

In liquid cooling, battery is cooled by oil, water etc. Liquid cooling efficiency is higher than air cooling due to the larger heat capacity for liquid than air (Wakui et al. 2019).

The liquid cooling system is schematically shown in Fig. 11.7. The system contains two parts: (1) the coolant which is stored in pipes or water tank. The coolant can exchange heat with engine cooling system. (2) Frames with S-shaped cooling

**Fig. 11.7** Tesla liquid cooling system

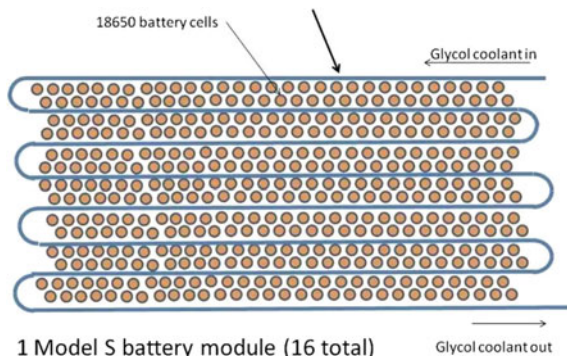


**Fig. 11.8** Volt cooling principle diagram

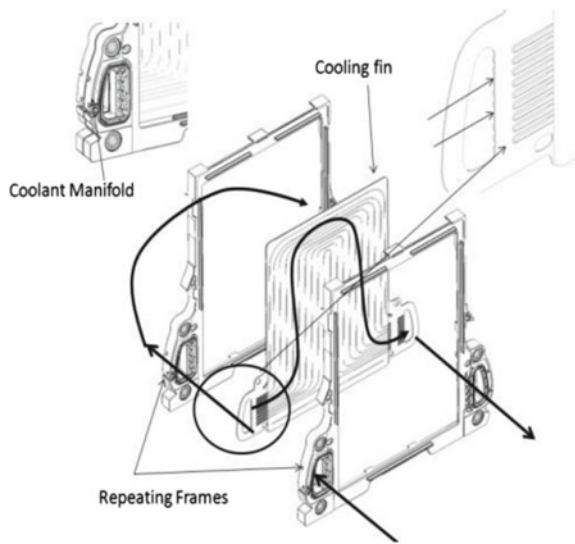


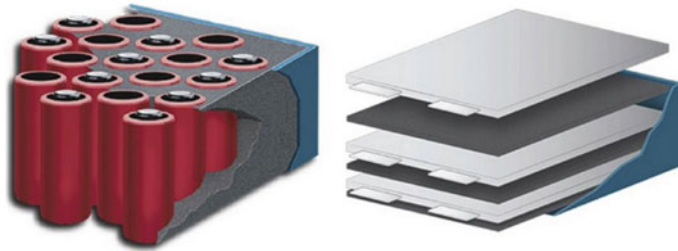
plate. Figure 11.8 shows the cooling system of GM Volt model where liquid cooling is applied. Cooling fins are implemented between cells.

### 11.2.2.3 PCM

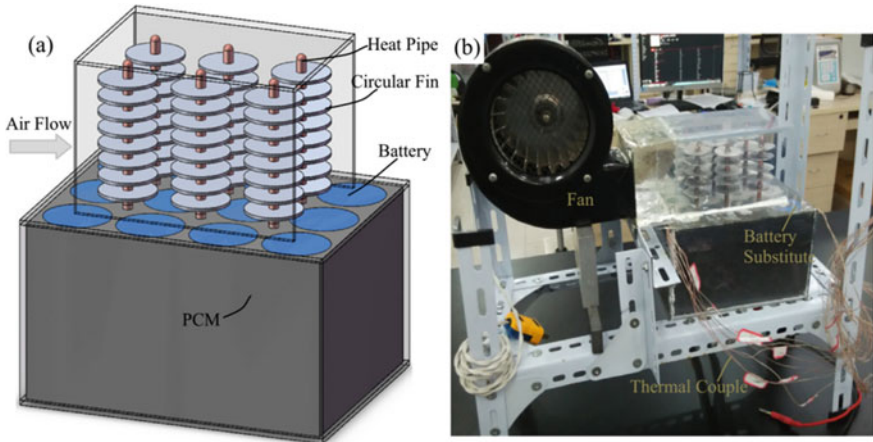
Cooling system based on PCM (Fig. 11.9) has been developed in recent years. Heat from battery is absorbed by PCM in phase change process. Since PCM application in thermal management was proposed by Professor S. Al-Hallaj from Illinois Institute of Technology, PCM has been developed and proved to be promising material for thermal management system.

PCM will absorb the heat generated by battery cells and maintain temperature as much as possible. As extreme heat is generated by battery, PCM absorbs the redundant heat. As the temperature is low and preheating is needed, PCM releases heat through phase change. Latent heat and phase changing point are the important indices (Killian et al. 2018).

Solid/liquid PCM is mostly based on paraffin and expanded graphite. PCM cools the battery without external facilities. However, PCM can absorb heat in a passive way. Under extreme conditions such as high temperature and high heat flux, entropy is depleted in a fast way and thermal management base on PCM fails. Mixed thermal management system is needed to improve the reliability in PCM cooling process. Figure 11.10 shows the mixed thermal management system. It contains heat pipes and circular fins so that heat is efficiently extracted in forced convection. Experimental results show that cooling efficient for this system is higher than that of air cooling. The mixed thermal management system maintains temperature below 50 °C and reduce thermal gradients.



**Fig. 11.9** Phase change thermal management system



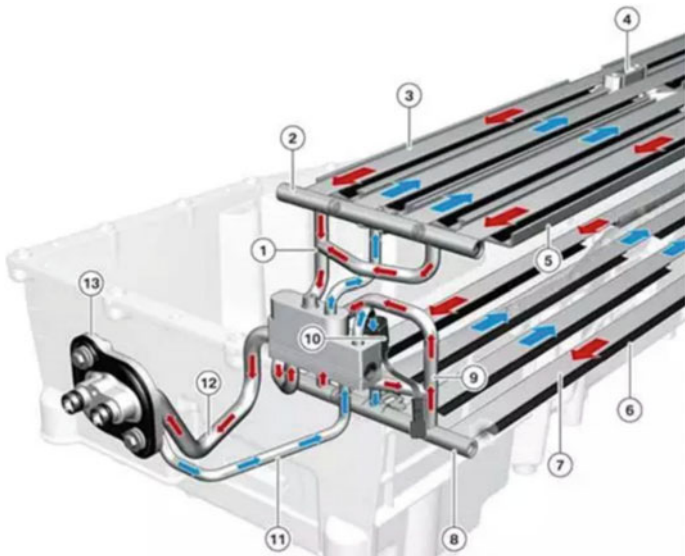
**Fig. 11.10** Phase change material and heat pipe cooling system

Figure 11.11 shows the cooling system for BMW i8 model. The coolant is R1234yf (European standard)/R134a (US standard). The coolant circuits contain two branches in parallel: one for vehicle interior cooling and the other for battery pack cooling. There are valves for both branches for controlling the cooling effect. The valve for battery pack cooling is controlled by voltage to adjust the coolant flow velocity.

### 11.3 Thermal Management Control Strategy

Compared with fuel cars, thermal management system for electrical vehicles covers more tasks and has more complicated structures. The thermal management has to be comprehensively designed considering the system integration, heat and power of whole vehicle.

One of the targets of thermal management system is to reduce temperature differences between battery cells while maintaining suitable working temperature



**Fig. 11.11** BMW i8 refrigerant circuit

range. Hence the discharge performance, lifespan and safety are improved. Thermal management system design requires the research on heat generation mechanism and thermal model.

### 11.3.1 Thermal Model

While thermal runaway is not considered, the heat generation can be captured by thermally coupled electrochemical models or equivalent circuit models (Zhu et al. 2019). This section discusses the heat generation for the two models.

#### 11.3.1.1 Electrochemical-Thermal Coupling Model

In thermally coupled electrochemical model, heat is lumped and weighted by different components of different thermal properties. Concentration of active material, voltage potential and electrochemical mechanisms are considered. 1D cell models are usually applied to model the electrochemical behaviors while 3D cell models are used to solve temperature distribution. The two types of models are coupled through heat generation and average temperature with decent modelling accuracy. Cell design optimization can be guided by the coupled models. The governing equations captures the parameters and fundamentals in electrochemical reactions inside batteries. Equations for charge and mass balance, Butler-Volmer and

Arrhenius type thermal activation are applied. These equations are derived by conservation laws. This chapter introduces electrochemical mechanisms and temperature-related Arrhenius equations and focus on heat generation and heat transfer, since electro-chemical models are discussed in other sections.

The electrochemical reactions inside battery are complex and most of these reactions are accompanied by heat generation. The heat generation includes reversible heat and side reaction heat. Generally, the fraction of side reaction heat is small and can be ignored compared with the reversible heat. Battery is inevitably polarized in the normal discharge/charge operation, including electrochemical polarization and concentration polarization. A fraction of heat involved in the polarization process is irreversible. Moreover, irreversible heat i.e. Joules heat is generated by Ohmic resistance from the jellyroll (for cylindrical cell)/battery stack (for pouch cell) and tabs. In side reactions, heat is generated in processes of SEI membrane decomposition, reaction between negative electrodes and electrolyte. Thermal runaway can be caused at high temperature or short circuiting due to mechanical stress. Hence side reaction can not be ignored. Large amount of heat can be generated in a short time and destroy the battery structure. The battery is vulnerable to failure and even explosion. Thermal runaway has to be monitored and avoided.

Heat generation in the discharge process is composed of (1) reversible heat from electrochemical reactions, (2) side reactions from processes of overcharge, self-discharge or electrolyte decomposition, (3) irreversible heat from mass transfer and (4) irreversible heat from internal resistance. The overall heat generation is obtained as:

$$Q_t = Q_r + Q_s + Q_p + Q_j \quad (11.1)$$

$$Q_t = q_t V \quad (11.2)$$

$$q_t = q_r + q_s + q_p + q_j \quad (11.3)$$

where  $q_t$  is overall heat generation rate,  $q_r$  is reaction rate,  $q_s$  is side reaction reaction rate,  $q_p$  is heat generation rate of polarization,  $q_j$  is irreversible heat generation rate and  $V$  is battery volume.

If generated heat from side reaction is ignored, the heat generation rate is:

$$q_r = a_s j T \frac{\partial U}{\partial T} \quad (11.4)$$

$$q_p = a_s j (\Phi_s - \Phi_e - U) \quad (11.5)$$

$$q_j = \sigma^{eff} \nabla \Phi_s \nabla \Phi_s + k^{eff} \nabla \Phi_e \nabla \Phi_e + k_D^{eff} \nabla \ln c_e \nabla \Phi_e \quad (11.6)$$

In the three equations above,  $a_s$  is surface-volume ratio with unit  $1/\text{cm}$ .  $j$  is current density with unit  $\text{mA}/\text{cm}^2$ .  $\Phi_s$  is voltage potential of electrodes surface with unit V.  $\sigma^{eff}$  is effective solid phase conductivity with unit  $\Omega^{-1} \text{ cm}^{-1}$ .  $k^{eff}$  is effective liquid phase ionic conductivity with unit  $\Omega^{-1} \text{ cm}^{-1}$ .  $c_e$  is electrolyte concentration with unit  $\text{mol}\cdot\text{cm}^{-3}$ .  $k_D^{eff}$  is effective liquid phase diffusional ionic conductivity with unit  $\Omega^{-1} \text{ cm}^{-1}$ . For current collector, only Joules heat is generated. For porous electrodes, the three types of heat are generated.

### 11.3.1.2 Electric-Thermal Coupling Model

The main electrochemical features of battery can be captured by equivalent circuit models. The common equivalent circuit models include Rint model, first-order, second-order and higher-order equivalent circuit models. The equivalent circuit model shown in Fig. 11.12 is described as

$$\left\{ \begin{array}{l} U_{ohm} = I_L R_o \\ \dot{U}_{p1} = \frac{I_L}{C_{p1}} - \frac{U_{p1}}{R_{p1} C_{p1}} \\ \dot{U}_{p2} = \frac{I_L}{C_{p2}} - \frac{U_{p2}}{R_{p2} C_{p2}} \\ U_L = U_{oc} - U_{p1} - U_{p2} - U_{ohm} \end{array} \right. \quad (11.7)$$

when discharge current is denoted as negative, the terminal voltage is

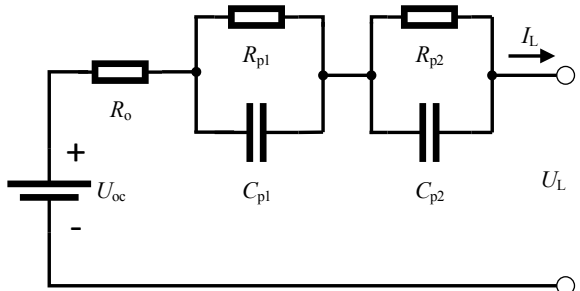
$$U_L = U_{oc} + U_{p1} \left( 1 - e^{-\frac{t}{\tau_1}} \right) + U_{p2} \left( 1 - e^{-\frac{t}{\tau_2}} \right) + I_L R_o \quad (11.8)$$

The heat generation rate is

$$Q_p = I^2 R_o \quad (11.9)$$

$$Q_j = I^2 R_o \quad (11.10)$$

**Fig. 11.12** Second-order RC equivalent circuit model



$$Q_r = IT \frac{dU_{ocv}}{dT} \quad (11.11)$$

### 11.3.1.3 Energy Conservation Thermal Model

The thermal model involving heat transfer and heat generation is assumed to be transient heat conduction process with time-variant heat generation rate. Based on energy conservation law, the partial differential equations (PDE) describing the thermal model are

$$\rho_k C_{p,k} \frac{\partial T}{\partial t} = \nabla \cdot (\lambda_k \nabla T) + q \quad (11.12)$$

where  $\rho_k$  is density,  $C_{p,k}$  is heat capacity. The first term on the right hand side is heat transfer.  $\lambda_k$  is thermal conductivity in the heat transfer direction. The second term  $q$  on the right hand side is heat source.

Boundary conditions and initial conditions are required to solve the PDE. In theory of heat transfer, ways of heat transfer are categorized as conduction, convection and radiation.

#### (1) Heat conduction

Heat conduction is more significant in the internal battery compared with convection and radiation. The transferred heat follows Fourier law

$$q_n = -\lambda_k \frac{\partial T}{\partial n} \quad (11.13)$$

where  $q_n$  is heat flux density with unit  $\text{J m}^{-2} \text{ s}^{-1}$ .  $\frac{\partial T}{\partial n}$  is temperature gradient in certain direction with unit  $\text{K m}^{-1}$ .  $\lambda_k$  is thermal conductivity in the same direction with unit  $\text{W m}^{-1} \text{ K}^{-1}$ . Thermal conductivities are different in different directions for battery cells.

#### (2) Convection

Convection is common at the boundary between battery cell and environment. Heat transfer in the way of convection is relevant with area and ambient temperature, and follows Newton's cooling law

$$Q_c = hA(t_w - t_f) \quad (11.14)$$

where  $Q_c$  is heat transferred in the way of convection,  $h$  is convection coefficient,  $A$  is area of interface between battery cell and environment,  $t_f$  is environment temperature. This equation is usually used as boundary condition.

Heat conduction and heat convection follow

$$-\lambda_k \frac{\partial T}{\partial n} = h(t_w - t_f) \quad (11.15)$$

In the different directions, the above equation is written as

$$\begin{cases} -\lambda_x \frac{\partial T}{\partial x} = h(t_w - t_f), x = 0, l \\ -\lambda_y \frac{\partial T}{\partial y} = h(t_w - t_f), y = 0, b \\ -\lambda_z \frac{\partial T}{\partial z} = h(t_w - t_f), z = 0, h \end{cases} \quad (11.16)$$

The initial temperature is

$$T(x, y, z, 0) = T_0 \quad (11.17)$$

### (3) Heat radiation

Heat transferred in the way of radiation is less compared with the way of conduction and convection. In most engineering applications, radiation heat can be ignored. However, for accurate thermal management on large format cell, radiation can not be ignored. The heat transferred in radiation can be described as Stefan-Boltzmann law

$$Q_{rad} = \varepsilon \sigma A (T^4 - T_s^4) \quad (11.18)$$

where  $Q_{rad}$  is radiation heat,  $\varepsilon$  is emissivity factor ( $\varepsilon$  is 1 for black body),  $\sigma$  is Stefan-Boltzmann constant ( $5.67 \times 10^{-8} \text{ W m}^{-2} \text{ K}^{-4}$ ),  $T_s$  is battery temperature with unit K.  $T$  is environment temperature.

For a thermal management system in good condition, the remained heat is calculated as

$$Q_b = Q_t - Q_c \quad (11.19)$$

where  $Q_t$  is total heat generation from battery cell,  $Q_c$  is convection heat (cooling or heating),  $Q_b$  is remained heat after convection cooling. Convection cooling is common utilized in thermal management.

### 11.3.2 Thermal Management Strategy

Concerning aspects of batteries in EVs involve safety, energy density, fast charging, deep discharging, cycling lifetime, self-discharging and cost. Breakthroughs can be achieved by conducting research on fundamentals of electrochemical reactions, such as characteristics of electrodes, electrolyte, binder and additives. Effective monitoring and management on batteries will improve the battery cell performances. Thermal management plays an important role in performances and lifetime of batteries. In

thermal management, batteries temperature is maintained at suitable range. The temperature gradients are reduced as well.

In thermal management schemes, there are classic control, fuzzy control and model-base control. Integrated thermal management involving battery packs, passenger compartment and other parts is the next concerning issue.

### 11.3.2.1 Classic Control

On/Off control and proportional–integral–derivative (PID) control are used in thermal management. The output status is either On or Off without any intermediate status. For example, in the case of heating, when temperature is lower than the bottom limit, status is triggered into On. Status is changed into Off as the temperature reaches top limit. Since output status is switched instantly when the limit value is hit, ‘hysteresis’ control is implemented to avoid frequent switching.

PID control uses integration and derivation to compensate for the system change. Compared with On/Off control, PID control more accurate and stable, so it is suitable for system with frequent changing.

### 11.3.2.2 Fuzzy Control

Fuzzy control is an algorithm that combines fuzzy mathematics and fuzzy inference in an empirical way. When the mathematical model of the controlled system can not be explicitly established, inference is conducted in fuzzy control algorithm to obtain control after several iterations of optimization.

Fuzzy control principles are chosen based on thermal effects. Internal battery temperature, temperature gradient, environmental temperature and charge/discharge modes can be set as input variables. The temperature of controlled body is the target. As a result, temperature fluctuation, temperature gradient and energy consumption are improved.

### 11.3.2.3 Model-Based Control

In recent years, model-based control applications are increasing. Model-based control predicts the effect of input variables according to the history information. Within a control period, the input at the moment is calculated considering its effect on the next time step. Thus, the input is corrected. Thermal management based on model prediction is expected to be combined with PID control algorithms.

## References

- Killian M, Zauner M, Kozek M (2018) Comprehensive smart home energy management system using mixed-integer quadratic-programming. *Appl Energy* 222(15):662–672
- Lei ZG, Zhang CN, Li JQ et al (2015) Preheating method of lithium-ion batteries in an electric vehicle. *J Mod Power Syst Clean Energy* 3(2):289–296
- Safdari M, Ahmadi R, Sadeghzadeh S (2020) Numerical investigation on PCM encapsulation shape used in the passive-active battery thermal management. *Energy* 193
- Shashank A (2018) Selection of thermal management system for modular battery packs of electric vehicles: A review of existing and emerging technologies. *J Power Sources* 400:621–640
- Sun S, Guan T, Shen B et al (2017) Changes of degradation mechanisms of LiFePO<sub>4</sub>/Graphite batteries cycled at different ambient temperatures. *Electrochim Acta* 237:248–258
- Wakui T, Sawada K, Yokoyama R et al (2019) Predictive management for energy supply networks using photovoltaics, heat pumps, and battery by two-stage stochastic programming and rule-based control. *Energy* 179(15):1302–1319
- Wang CY, Zhang G, Ge S et al (2016) Lithium-ion battery structure that self-heats at low temperatures. *Nature* 529(7587):515–518
- Yang N, Zhang X, Shang BB et al (2016) Unbalanced discharging and aging due to temperature differences among the cells in a lithium-ion battery pack with parallel combination. *J Power Sources* 306:733–741
- Zhu J, Knapp M, Darma M et al (2019) An improved electro-thermal battery model complemented by current dependent parameters for vehicular low temperature application. *Appl Energy* 248(15):149–161

**Part IV**

**Functional and Cyber Security**

# Chapter 12

## Functional Security



### 12.1 Introduction of ISO26262

#### 12.1.1 Background

With the extensive application of electrical devices, electronic equipment and programmable electronic devices in the field of automobile control, safety-related problems have become more and more prominent, brake failure, engine or gearbox control software failure and other automobile recalls frequently occur, not only to automobile enterprises caused huge economic losses, but also to people's lives and property security has brought serious threats.

The main reason is the failure of safety function of control system related to vehicle safety, especially the failure of vehicle electronic and electrical system. Therefore, the government, enterprises and consumers pay more and more attention to the functional safety of products, and have paid more attention to the design technology of product safety since 1989, the related technologies of electronic, electrical and programmable electronic safety control system are developed into a set of mature safety design technical standards. To this end, the International Electro technical Commission (IEC) promulgated in 2000 on electronic, electrical and programmable electronic systems functional security international standard IEC 61508. IEC 61508 has been widely adopted since its promulgation.

On the basis of IEC 61508, the standards of various industrial application fields have also been issued. However, IEC 61508, which originated from the process industry, is not entirely suitable for the automotive industry. With the wide application of safety-related electronic and electrical systems in automobiles, the automotive industry is demanding more and more functional safety standards for electronic and electrical systems. Therefore, on the basis of IEC 61508, the International Organization for Standardization (ISO), from November 2005, by the road vehicles technical committee (ISO/TC22), electronic and electrical sub-technical committee (SC3),

functional safety working group (WG16) and more than 30 automobile enterprises worldwide, after about six years, a functional safety standard for automotive electronic and electrical systems, ISO 26262, known as “Functional security of road vehicles”, was developed and promulgated in November 2011.

### **12.1.2 Goals**

The purpose of ISO 26262([ISO 2018](#)) is to improve the functional safety of automotive electronic and electrical products by pre-analyzing and evaluating potential hazards and risks in the product development and management processes. ISO 26262 also aims at risk reduction through the implementation of scientific safety technical measures, codes and methods, and the use of systematic testing, verification and validation of software and hardware, to enable the safety functions of electronic and electrical products to meet the requirements of the Automotive Safety Integrity Level within the safety life cycle, and to enhance the reliability of systems or products, to avoid excessive design and increase in costs, as well as the risk of system failure, random hardware failure, design defects. All of these enable the security functions of electronic systems in a variety of harsh conditions to maintain normal operation, to ensure the safety of motorists and pedestrians.

### **12.1.3 Scope and Content**

ISO 26262 is primarily targeted at specific safety-related electrical and electronic systems, including electronic equipment, electrical components and software components, installed on road vehicles (mass production passenger vehicles with a maximum total mass of 3.5 t or less).

One of the most difficult problems in automobile design is how to estimate the potential hazards and risks in advance and take appropriate measures to reduce them. ISO 26262 stipulates that “Hazard and risk analysis” must be performed at the beginning of development work. With the increase of system complexity and the application of software and electromechanical equipment, the risk of system failure and random hardware failure is increasing. ISO 26262 and its guidelines provide the requirements and processes for avoiding these risks. The road vehicle functional safety standard ISO 26262 is divided into 10 chapters, which regulate and require the whole life cycle of the product from the aspects of functional safety management, concept, system-level R & D, software and hardware R & D, production and operation, etc., and this allows the product to have its security features considered fairly well throughout its life cycle.

System security is achieved through a series of security measures. Security measures are implemented and applied to different levels of the development process

through various technologies (mechanical, hydraulic, pneumatic, electronic, electrical, programmable electronic, etc.). While ISO 26262 addresses the functional security of electrical and electronic systems, it also provides a security-related system framework based on other technologies:

1. The concept of automobile safety life cycle (management, development, production, operation, maintenance, scrap) and the necessary measures and methods in each phase are put forward;
2. According to the degree of security risk, the system or a part of the system is classified from A to D, and a method to determine the Safety Integrity Level based on risk analysis is proposed;
3. Use Safety Integrity Level to develop appropriate regulations and measures to avoid unreasonable residual risks;
4. Specification of verification and validation measures to ensure Safety Integrity Level are achieved;
5. Put forward the requirements related to the supplier.

So functional safety is influenced by development processes (including requirements specification, design, implementation, integration, verification, validation, and configuration), production processes, maintenance processes, and management processes.

#### ***12.1.4 Automotive Electronics, Electrical Products***

The standard covers a wide range of almost all automotive electronic and electrical products related to functional safety, including conventional and new energy vehicles, typical of which are shown in Table 12.1.

**Table 12.1** Typical products of conventional and new energy vehicles

Conventional vehicles	Powertrain: engine ECU, automatic transmission ECU, etc Chassis control: electric power steering anti-lock braking system, electronic hidden qualitative control system, traction control system, electronic brake force distribution, Emergency brake assist, intelligent parking auxiliary system, adaptive suspension control module, etc. Body electronics: keyless entry system, airbag electronic control, adaptive headlamp control module, lane departure warning system, seat belt pre-tightening system, driver drowsiness detection module, adaptive cruise control system, tire pressure monitoring system, etc.
New energy vehicles	Vehicle control system, motor control system, battery management system, charging system

### 12.1.5 *Introduction to the New Edition*

The development and promulgation of ISO 26262.2011 is a significant advance for the automotive electronics industry. Before the release of ISO 26262.2011, IEC 61508 was used as a standard for electronic and electrical parts industry, but there was no specific standard for automotive electronics. As IEC 61508 is a general standard, it is not suitable for some aspects of automotive electronics. The rapid development of automotive electronics has brought great challenge to IEC 61508, so it is very necessary to form specific standards for automotive electronics, in view of this, ISO 26262 emerged. Five years after the first edition of ISO 26262 was released, the International Organization for standards (ISO) evaluated it, refined it based on the first edition and formed a new version.

The motivation to update the ISO 26262 standard mainly comes from the experience accumulated in the application of the standard. In the actual application process, has discovered many may perfect place. As methods and technologies continue to improve, automakers will be allowed to apply process methods that are different from or even more efficient than the first version of ISO 26262. In addition, there is still room for improvement in language organization and expression. The update of the standards mainly includes:

Expansion of the scope of application: in the first edition, the scope of application was limited to passenger cars weighing not more than 3.5 tons. This extension is necessary and reasonable for a similar range of vehicles, so trucks, buses, and motorcycles are included in the second edition.

Semiconductor level supplement: Part 5 of ISO 26262.2011 for the hardware level requirements are more overall, it is difficult to take into account the semiconductor level, so the semiconductor level needs to be further explained.

## 12.2 ASIL Levels

In the ISO 26262 standard, when doing the function safety design to the system, a preliminary important step is carried on the hazard analysis and the risk assessment to the system, the system's hazards are identified and the risk Level, ASIL (Safety Automotive Integral Level, Automotive Safety Integrity Level), is assessed. ASIL has four grades: A, B, C and D, where A is the lowest and D is the highest. Then, at least one security objective is defined for each hazard. The security objective is the highest security requirement of the system. The security objective leads to the system-level security requirement, and then assigns the security requirement to the hardware and software. ASIL level determines the requirement of system security. The higher the ASIL level, the higher the requirement of system security, and the higher the cost of implementing security, which means the higher the diagnostic coverage of hardware and the more strict the development process, the corresponding development cost increases, the development cycle prolongs, the technical request

is strict. In ISO 26262, the ASIL decomposition, which can reduce the ASIL level to meet the security objective, can solve the difficulties mentioned above.

This section first introduces the hazard analysis in ISO 26262 and ASIL level determination in the risk assessment phase, then introduces the principle of ASIL decomposition, with examples to illustrate.

### ***12.2.1 Hazard Analysis and Risk Assessment***

When designing the function safety according to ISO 26262 standard, one should first identify the function of the system, and analyze all the possible function failure (Malfunction). If at any stage of system development a failure is identified that has not been identified at this stage, it is necessary to return to this stage for an update. Functional failures cause casualties in certain driving situations, such as low-light systems. One of the functional failures is that the lights are not expected to go out. If driving on a mountain road in the dark of night, the driver cannot see the road clearly, it could fall off a cliff and cause a car crash; if the malfunction occurred during the day, it would have no effect. So after the functional fault analysis, it is necessary to analyze the situation and identify the driving situation related to the fault, such as: highway overtaking, parking garage and so on. Analysis of driving scenarios should be considered from road types: such as national roads, urban roads, rural roads, road conditions: such as wet roads, ice and snow roads, dry roads; vehicle conditions: such as steering, overtaking, braking, acceleration, etc.; environmental conditions: such as: wind and snow, night, tunnel lights; traffic conditions: congestion, smooth, traffic lights; personnel: as passengers, pedestrians and other aspects.

The combination of a functional failure and a driving scenario is called a hazard event. Once a hazard event has been identified, the hazard level—ASIL—is assessed on the basis of three factors: Severity, Exposure, and Controllability. The severity refers to the degree of injury to drivers, passengers, or pedestrians, and the exposure rate refers to the probability of exposure to situations where system failure can cause harm. Controllability refers to the possibility that a driver or other person involved in danger can avoid an accident or injury. The classification of these three factors is given in Table 12.2.

ASIL levels are determined based on these three impact factors. Table 12.3 shows ASIL levels, where D represents the highest level, A represents the lowest level, and QM represents Quality Management, indicating that it is sufficient to develop the system or functionality according to the quality management system, regardless of any safety-related design considerations. After the hazard ASIL level has been determined, at least one safety objective is defined for each hazard as the basis for functional and technical safety requirements.

**Table 12.2** Severity, exposure rate, controllability classification

Severity		Exposure rate		Controllability	
S0	No harm done	E0	Not possible	C0	Completely manageable
S1	Mild to moderate injuriness	E1	Very low probability	C1	Easy to control
S2	Serious injury (with a chance of survival)	E2	Low probability	C2	Generally controllable
S3	Fatal injury	E3	Moderate probability	C3	Hard to control
		E4	High probability		

**Table 12.3** ASIL levels

Severity	Exposure rate	Controllability		
		C1	C2	C3
S1	E1	QM	QM	QM
	E2	QM	QM	QM
	E3	QM	QM	A
	E4	QM	A	B
S2	E1	QM	QM	QM
	E2	QM	QM	A
	E3	QM	A	B
	E4	A	B	C
S3	E1	QM	QM	A
	E2	QM	A	B
	E3	A	B	C
	E4	B	C	D

### 12.2.2 Examples of Hazard Analysis and Risk Assessment

This section illustrates the high-voltage safety risk assessment example for batteries (Zhu 2013). The power battery system is responsible for storing and supplying the electric energy to drive the vehicle and to supply the electric devices. The inner part of the battery system is mainly composed of the battery controller, the battery cell, the electrical elements and the structural elements, etc. The battery system communicates with the vehicle controller and charger externally, and the output of high-voltage DC supply to the motor and electrical components.

In the battery system, the functions related to high voltage safety include: Safety of BMS controller, high voltage interlock, collision switch, relay control/diagnosis and insulation monitoring. The ASIL level of each function is determined below.

(1) Overall function of BMS controller

Severity: if BMS is not functioning, there is no way to monitor the state of the high-pressure system, which could result in incorrect movements or loss of the ability to take appropriate protective measures, such as sudden disconnection of the high-pressure circuit and loss of power during high-speed driving, or it overcharges during vehicle charging and fails to protect, defined as severity S3. Exposure rate: high speed steering and charging combination can be considered an everyday event for electric vehicles, defined as exposure rate E4. Controllability: when turning at high speed, the steering system can work properly even if the vehicle loses power, and trained personnel should be able to rely on the vehicle's inertia to steer the vehicle out of the main lane. If the battery catches fire while the vehicle is charging, the driver should be able to escape by opening the doors and windows, with a controllability of C2, since the high voltage battery system will not affect the lock system.

(2) High voltage interlock

Severity: the high-voltage interlock switch is used to check the integrity of the high-voltage circuit and if the function fails, it may result in the exposure of the electrode with high voltage. People who do not take safety precautions may get electrocuted by contact with exposed poles or high voltage components, defined as severity S3. Exposure rate: users do not touch high pressure components, but only during maintenance and repair. Exposure rate is defined as E2, several times a year. Controllability: in both cases, a trained operator can prevent an electric shock by using basic protective equipment, hence the definition of controllability as C2.

(3) Collision switch

Severity: when the vehicle collides, the collision sensor will detect and send out a collision signal. It is necessary to cut off the high-voltage circuit at this time. If the function fails, it may lead to secondary danger, such as high-voltage short-circuit leading to battery fire and explosion; High voltage exposure causes an electric shock to the user, defined as the highest level of injury, S3. Exposure rate: since the detection and triggering of the collision signal are usually performed by the airbag sensor, the failure exposure rate is the same as that of the airbag trigger, defined as E1, with a low exposure rate. Controllability: to prevent external high-voltage circuits from short-circuiting after a collision, the battery management system is required to cut off the high voltage immediately upon detection of a collision signal, since the vehicle is already in a collision situation, the controllability of the vehicle is unpredictable and is designated here as C3 uncontrollable.

(4) High voltage relay control

Severity: the abnormal state of relay control cannot be closed, adhesion (cannot be cut off) and contact jumping, when the function failure, may cause the vehicle to lose power, high-voltage terminal clock live and high-voltage system heating, it may cause injury to a person in high speed driving or maintenance.

**Table 12.4** ASIL levels for each function

Function	Severity	Exposure rate	Controllability	ASIL levels
Overall function of BMS controller	S3	E4	C2	ASIL C
High voltage interlock	S3	E2	C2	ASIL A
Collision switch	S3	E1	C3	ASIL A
High voltage relay control	S2	E4	C2	ASIL B
Insulation detection	S3	E2	C1	QM

Severity is defined as S2. Exposure rate: daily parking, driving, charging, maintenance and so on will involve the action of the relay, the definition of exposure rate for E4, each driving will occur. Controllability: the relay can be diagnosed to confirm whether the failure, in the driving, charging and maintenance state can take control, defined as the controllability of C2, medium controllability.

#### (5) Insulation detection

Severity: failure of insulation detection may result in leakage of current in high voltage circuits, poorly insulated vehicles are still in use, and if a person is accidentally electrocuted, it may be life threatening. Severity is defined as S3. Exposure rate: taking into account that the high voltage circuit is normally shielded from the body and the low voltage circuit, and that the entire power battery system housing is connected to the body, there is no opportunity for normal use (driving, parking, charging) to contact the positive and negative electrodes at the same time, it is only possible to have simultaneous contact with the high voltage positive and negative terminals, defined as E2, several times a year, when disassembly maintenance is required. Controllability: the operator can prevent electric shock effectively through the corresponding equipment and tools during maintenance, which is defined as C1.

By comparing Table 12.3, the ASIL levels for each function are shown in Table 12.4.

Security objectives are also defined for each function. BMS functions: there are sufficient means to ensure the overall reliable operation of BMS, correct and timely monitoring of the system status and control of the high-voltage loop. High-voltage interlock: the high-voltage interlock function shall ensure that all high-voltage components are covered and the integrity of the high-voltage circuit is faithfully reflected, and the high-voltage output shall be cut off immediately if the high-voltage circuit is detected to be incomplete. Collision switch: ensure that in the event of a collision, can quickly and accurately cut off the high-voltage output. Relay control: the control and diagnostic logic should ensure that the relay is operating correctly as required and should respond in a timely manner in the event of abnormal action.

### 12.2.3 ASIL Decomposition Principle

Through the hazard analysis and risk assessment described in the previous section, we obtain the system's security objective and the corresponding ASIL level. From the security objective, we can deduce the security requirements in the development phase, and the security requirements inherit the ASIL level of the security objective. If a security requirement is decomposed into two redundant security requirements, the ASIL level of the original security requirement can be decomposed into two redundant security requirements. Because system failure occurs only when two security requirements are not met at the same time, the ASIL level of redundant security requirements can be lower than that of the original security requirements.

Of course, there are some restrictions on ASIL decomposition. If the two redundant security requirements are not independent, the ASIL level of the redundant security requirements will inherit the ASIL level of the original security requirements, unable to disintegrate. Independence means that two redundant security requirements do not affect each other and are not affected by the same factors, and that dependency Failure does not occur between them. There are two kinds of dependent Failure: Common Cause Failure and Cascading Failure. Common cause failure is the failure of two units due to common reasons, such as software replication redundancy, redundant units due to the same software bug cause both failure, in order to avoid the common cause failure, we use a variety of software design methods. Cascading failure refers to the failure of one unit leading to the failure of another unit, such as the failure of one software component to write to another software component's RAM, resulting in the failure of another software component's function, to control this cascading failure, we used memory management unit to detect illegal writes to RAM. Redundant security requirements that satisfy the independence requirement can be decomposed as shown in Fig. 12.1 by the ASIL decomposition principle given in chap. 9 of the ISO 26262 standard.

The decomposed ASIL level is followed by parentheses indicating the original ASIL level, such as Asil D level is decomposed into ASIL C (D) and Asila (D), because integration and verification of requirements are still based on their original ASIL level. ASIL decomposition can be performed in multiple phases of the security lifecycle, such as functional security concepts, system design, hardware design, and software design phases. And ASIL levels can be broken down several times, such as ASIL D being ASIL C (D) and ASILA (D), and ASIL C (D), which can be broken down into ASIL B (D) and ASIL A (D).

### 12.2.4 ASIL Decomposition Example

Suppose the function F, whose input signals are S1, S2, S3, which measure different physical quantities respectively, are independent of each other. After the logic operation in ECU, the trigger information is sent to the Actuator, the architectural schematic

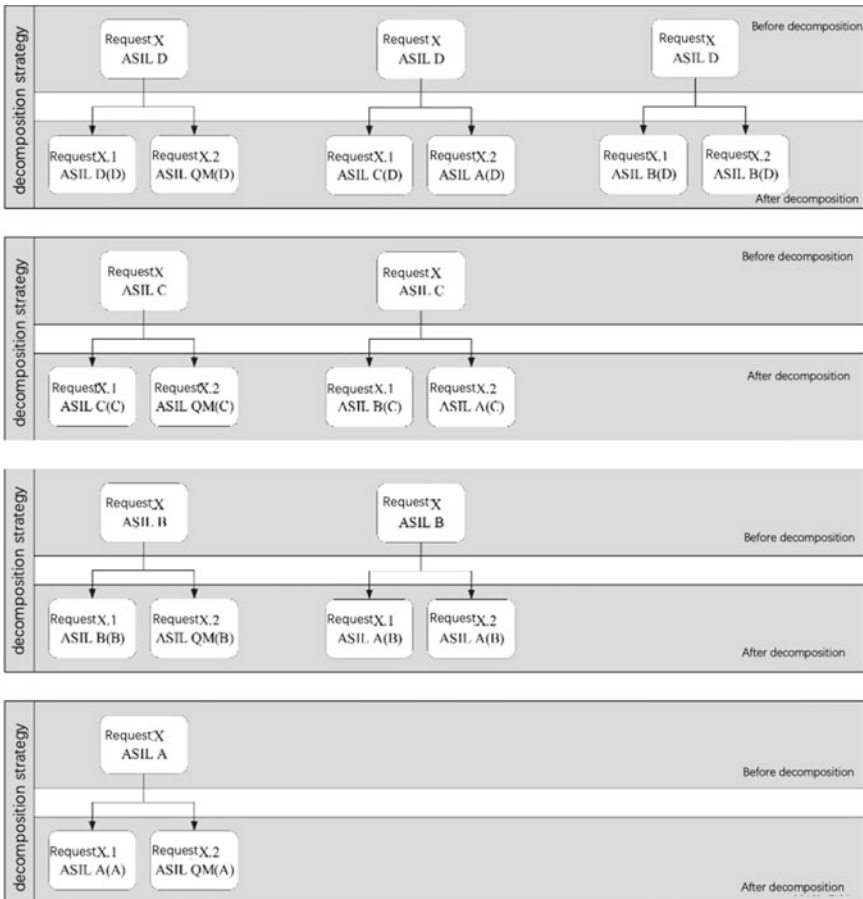


**Fig. 12.1** ASIL decomposition principle

of function F is shown in Fig. 12.2. Assuming that after hazard analysis and risk assessment, the ASIL level of function F is ASIL D, the security objective is to avoid unexpected trigger actuators. Then each part of function f inherits ASIL level, that

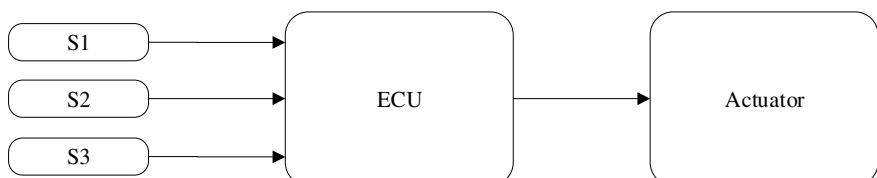


**Fig. 12.2** Functional F schematics

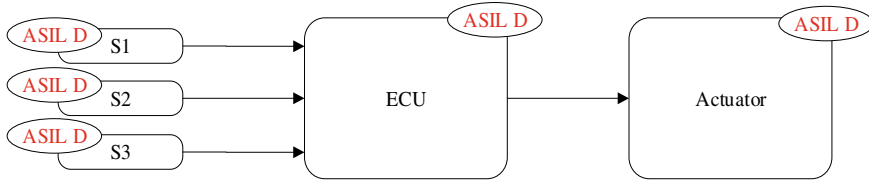


**Fig. 12.3** ASIL diagram of the distribution of grades on a functional F architecture

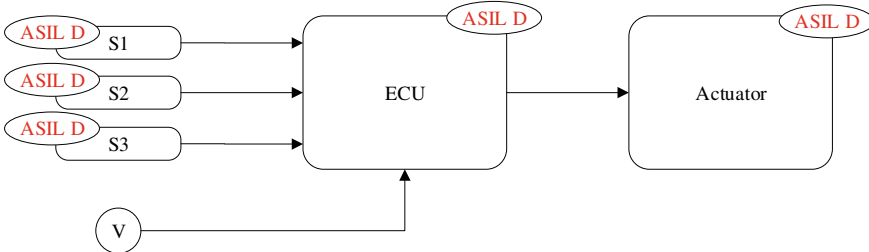


**Fig. 12.4** Architecture with security mechanisms in place

is, the sensor, ECU, and actuator all need to be developed according to ASIL D level, as shown in Fig. 12.3.

After further analysis, it is found that when velocity V is higher than the threshold value, the unexpected trigger actuator can cause danger. Then we add a security mechanism to the architecture of function F that does not allow the trigger to be triggered when the velocity v is detected to be greater than the threshold. Then the architecture of function F becomes as shown in Fig. 12.4.

The original ASIL level of function F can be decomposed into ASIL D (D) and QM (D) on these two requirements, which are redundant security requirements and meet security objectives, the ASIL level after decomposition is shown in Fig. 12.5.

The original sensors S1, S2 and S3 were developed according to QM, the speed sensors were developed according to ASIL D, the software in ECU, the original logic was developed according to QM, the logic of the security mechanism was

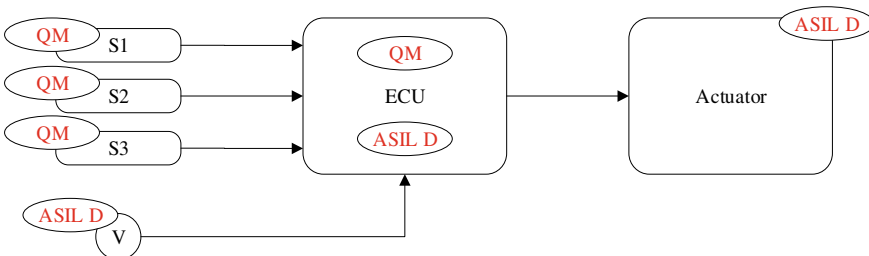


**Fig. 12.5** ASIL schematic of the decomposed architecture

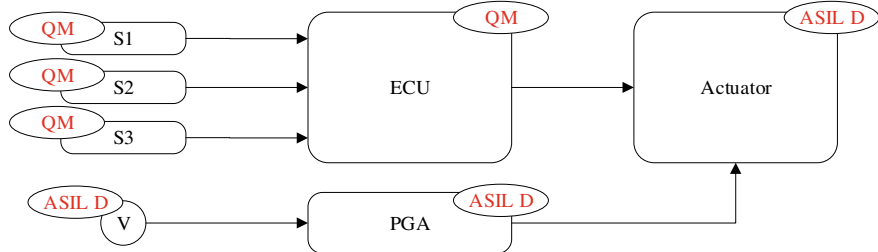


**Fig. 12.6** Improved ASIL architecture schematic after decomposition

developed according to ASIL D, the software of different ASIL levels existed in an ECU, in order to guarantee the independence of software and the non-interaction between them, it is necessary to consider the memory protection mechanism and the appropriate scheduling attribute to guarantee the independence of memory space and CPU time, which will increase a lot of software development costs. To further ensure independence, we chose a simple chip (such as the PGA, Programmable Gate Array) with a low cost to run the software in the security mechanism (Fig. 12.6). It is important to note that the PGA uses a separate power supply and clock.

After decomposition, the functional logic developed according to ASIL D is simple, which makes the development easier and the overall cost reduced.

## 12.3 Functional Security Development Process

The development process for ISO 26262 begins with a project definition. A project definition is a description of the project, which includes the project's functions, interfaces, environmental conditions, regulatory requirements, hazards, etc., it also includes other project-related functions, system and component-determined interfaces, boundary conditions, etc.

### 12.3.1 Concept Development

Determining the follow-up process based on whether the project is a new product development or an existing product change is called security lifecycle initialization. In the case of an existing product change, an impact analysis is performed on the product, and the results of the impact analysis determine which processes can be omitted throughout the life cycle.

After the security lifecycle is initialized, hazard analysis and risk assessment are performed first. This is the stage through which a project's ASIL level is determined. ASIL uses levels A, B, C, and D in the standard to specify ISO 26262 requirements

and security measures required for a project or unit to avoid unreasonable residual risks, as described in the previous section. Once the ASIL level of the project is established, all subsequent development processes and methods of the project are developed in accordance with the corresponding ASIL level, so this stage is critical in the overall process of functional security development.

In hazard Analysis and risk assessment, the exposure rate of the driving situation where the vehicle is, the controllability of the traffic participants and the severity of the damage to the traffic participants should be fully considered. The ASIL level of the project is determined by these three indicators, and the security objective is set for each risk, and the appropriate ASIL level is determined according to the ASIL level of the project. Security objectives should also consider the following: operating mode, fault tolerance time, security status, emergency operation time interval, and functional redundancy.

The next step in the functional security concept is to consider the basic architecture of the system, and to specify and refine the overall security requirements derived from the security objectives to the functional security requirements in each project element. At least one functional security requirement should be defined for each security objective, although a functional security requirement can cover more than one security objective, and each functional security requirement inherits the highest ASIL level from the relevant security objective, functional security requirements are then assigned to related items. For example, Table 12.5 defines two functional security requirements for the security objective.

In the previous section, we introduced the ASIL decomposition, in order to reduce the implementation cost of security objectives, but also a high ASIL security objectives can be decomposed into two separate security objectives of the lower level. Take the example of the SG1-precaution overplay in the article, which can be decomposed as shown in Fig. 12.7.

Systems and other technologies that go beyond boundary conditions can be considered as part of the functional safety concept. Requirements for the application of other technologies and external measures are not considered in 1S026262.

**Table 12.5** Define functional security requirements for security objectives

SG1: The cell in the battery pack should be prevented from over discharge		ASIL
FSR1.1	Battery SOC should be accurately estimated and communicated with other systems	C
	Description: The system is required to track the energy flow of the cell and react when the SOC of the battery pack exceeds the boundary of the range. In addition, if the SOC is out of range, it should communicate with other systems in the vehicle	
FSR1.2	If over discharge is detected, the current should be switched off within X ms	
	Description: in order to protect the cell from damage and prevent dangerous consequences, such as heat and fire, if an over discharge is detected, the system should cut off the current	

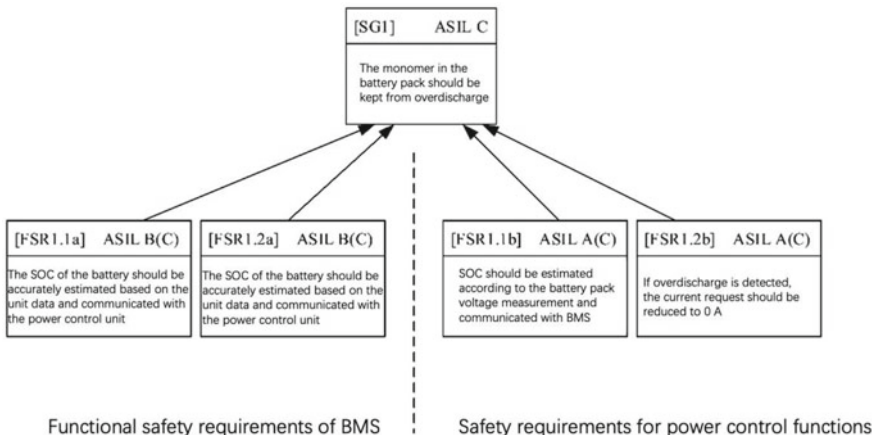


**Fig. 12.7** ASIL decomposition to prevent over discharge

### 12.3.2 System Level Development

With the specific security requirements in place, the technical security requirements specification can be derived from the security requirements, followed by system-level development. Figure 12.8 illustrates the structure and distribution of security requirements in the corresponding parts of ISO 26262.

The process of system-level development is a development process based on the V model. On the left side of the V model is “System-level product development start-up”, which updates the project plan and Security Plan according to the actual situation, and creates test plan, Validation Plan and evaluation plan. The next step is to clarify the specification of the technical safety requirements, which are derived from the functional safety requirements and the architectural design of the system or unit, in which the identification and control of system failures are described, and other system failure mechanisms, security state to achieve or maintain measures, warning and degradation measures, etc.

Technical security requirements should be defined in terms of functional security concepts, preliminary architectural assumptions for related items, and system characteristics such as:

- (a) external interfaces, such as communications and user interfaces, if applicable;
- (b) restrictions, such as environmental conditions or functional limitations;
- (c) system configuration requirements.

With the specification of technical safety requirements, it has entered the system design phase. The system design phase mainly completes these tasks: how to achieve the above security measures, further refine the system architecture, with the aid of security analysis of the security design verification (FMEA), clear hardware and

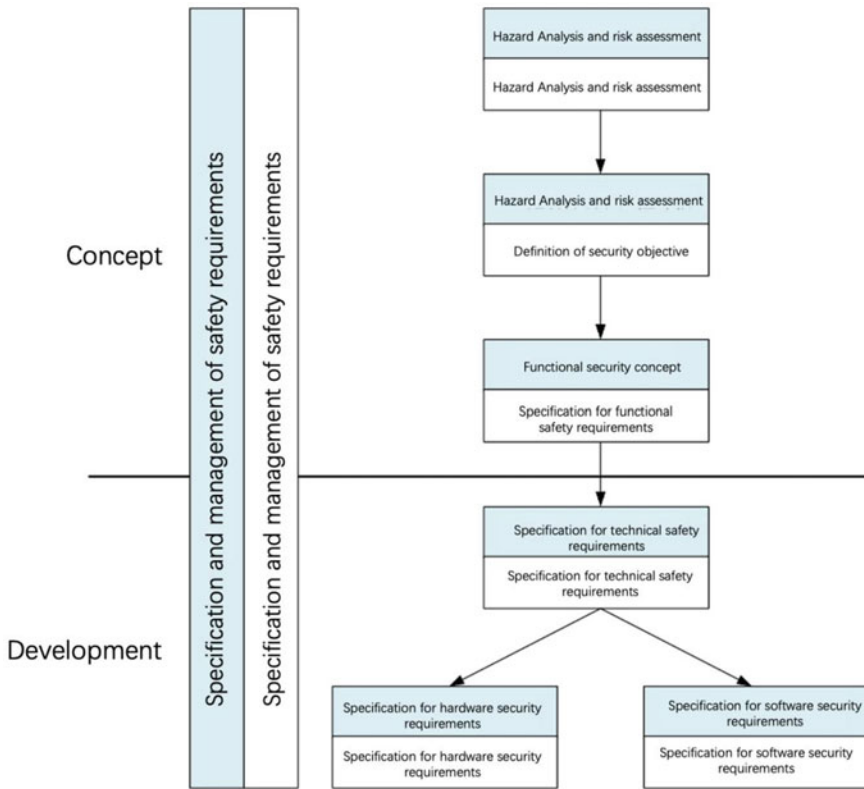


**Fig. 12.8** ISO 26262 structure and distribution of safety requirements in corresponding sections

software interface specifications. With regard to the realization of the technical security requirements, the following issues should be considered in the system design: 1. the verifiability of the system design; 2. the technical realization of the software and hardware; 3. the execution test capability in the system integration. The system and subsystem architecture should meet the technical security requirements of their respective ASIL levels, and each element should achieve the highest ASIL technical security requirements if a system contains subsystems with different ASIL levels, or security-related and non-security-related subsystems, they should be handled at the highest ASIL level.

In the system design stage, in order to avoid system failure, ISO26262 for different ASIL grade recommended different analysis methods, such as FMEA, FAT, etc. System failure due to internal or external causes shall be avoided or eliminated. To reduce systemic failures, it is advisable to apply trustworthy automotive system design principles, which may include:

- the reuse of trustworthy technology security concepts;

- (b) reuse of trustworthy design elements, including hardware and software components;
- (c) the re-use of reliable mechanisms for detecting and controlling failures;
- (d) reuse of trusted or standardized interfaces;

Hardware and software interface specifications are developed at the time of system design and are further refined at the time of hardware and software development. The hardware/software interface specification should specify hardware/software interaction, including the following attributes:

- (a) the operating mode of the hardware device and the relevant configuration parameters, the operating mode of the hardware device, such as: Default mode;
- (b) initialization, testing or advanced mode, configuration parameters such as: gain control, band pass frequency or clock divider;
- (c) ensuring the independence of units and supporting the hardware characteristics of the software partitions;
- (d) shared and dedicated hardware resources, such as memory mapping, registers, timers, interrupts, I/O port allocation;
- (e) hardware acquisition mechanisms such as serial, parallel, slave, master/slave;
- (f) each time series constraint that relates to the concept of technical security.

After the system design has entered the concrete hardware design and the software design stage. The process to the right of the V model for system-level development begins with project integration and testing. This is mainly to test whether the designed security functions meet the technical security requirements, each security requirement should be verified, and ASIL related test methods should be chosen. After the integration and testing of the project, safety verification will be carried out by in-house R&D engineers, the main purpose is to confirm whether the system design can fully achieve the initial safety goals and safety requirements at the vehicle level. Security confirmation is followed by a security assessment, which is generally conducted by a third party to verify that all work has been done correctly and completely and that the security level has met the ASIL requirements. After the security assessment is complete, the final stage is the product release. At this stage, production and Operation Plans and requirements for production, operation, service and disassembly of the product are required. Through these plans and requirements as well as rules and regulations, to ensure that the production and use of products to meet the functional safety requirements.

### ***12.3.3 Hardware Development***

After system-level development, hardware-level product development is also subject to the V model concept. The first step on the left side of the V model is the launch of hardware-level product development. This process is primarily about planning activities, planning and defining activities and supporting processes for this phase,

depending on the size and complexity of the project. Then, the hardware and software safety requirements are determined. The software and hardware safety requirements are derived from the technical safety requirements in the system phase.

The specification of hardware security requirements shall include every security-related hardware requirement, including the following:

- (a) the hardware security requirements and related attributes of the security mechanism for controlling the internal failure of the element hardware, which includes the internal security mechanism used to cover the associated transient failures (for example, transient failures due to the technology used);
- (b) hardware security requirements and related attributes of security mechanisms to ensure factor tolerance to external failures;
- (c) the hardware security requirements and the related attributes of the security mechanism to meet the security requirements of other elements;
- (d) hardware security requirements and related attributes of security mechanisms for detecting internal and external failures and transmitting failed information;
- (e) hardware security requirements with no defined security mechanism.

Hardware security requirements should be verified to provide evidence in accordance with the requirements of chaps. 6 and 9 of ISO26262-8. The hardware design can begin with a hardware functional block diagram, in which all elements and internal interfaces should be displayed. Then design and verify the detailed circuit diagram, and finally through deductive method (FTA) or induction method (FMEA) and other methods to verify the hardware architecture may appear fault.

According to the specification of hardware security requirement, hardware design should be carried out, including hardware architecture design and hardware detail design. The hardware architecture design should represent all hardware components and their relationships to each other, and implement the specified hardware security requirements. The relationship between hardware security requirements and hardware components should be clearly described. Fully reliable hardware components may be considered for reuse. When designing the hardware architecture, we should also consider the non-functional factors of the failure of security-related hardware components. For example: vibration, water, dust, EMI, etc. Hardware detail design refers to a design at the level of an electrical schematic diagram that shows the interrelationships between the components of a hardware component.

The next step is to calculate the hardware quantitative index, in the process of functional security development, there are three indicators can be quantified, namely single-point failure index, potential failure index and random hardware failure rate. The first two indexes represent the capability of the security function designed, and can be simply understood as the advantage and disadvantage of the security mechanism. The higher the index, the better the security mechanism designed. The last metric indicates the reliability of the hardware. The higher the metric, the more durable the security mechanism. For different ASIL grade products, the requirements for these three indicators are different, so at this stage we need to calculate the quantitative indicators to see if the corresponding ASIL grade requirements are met.

**Table 12.6** Common failure modes and coverage of battery pack voltage sensors

60% (Low)	90% (Medium)	99% (High)
Voltage too high, too low, out of range	Voltage too high, too low, out of range	Voltage too high, too low, out of range
The voltage is always constant	The voltage is always constant	The voltage is always constant
The voltage is always constant	DC voltage offset	The voltage measurements are unstable

Battery pack voltage sensor is a very important sensor for BMS system, so different failure modes of battery pack voltage sensor need to be analyzed according to different ASIL levels. Table 12.6 shows the failure modes that need to be covered for different coverage.

ISO 26262 recommends two alternative methods to assess whether the residual risk of violating security objectives is sufficiently low. Both methods evaluate the residual risk of violating the security objective caused by single point failure, residual failure and possible two-point failure. Multiple faults can also be considered if they appear to be related to security concepts. In the analysis, the coverage of the security mechanism is considered for residual and two-point faults, and the exposure duration is also considered for two-point faults. The first method includes the use of a probabilistic measure known as a probabilistic hardware failure probability PMHF (probability of random hardware failure), by using methods such as quantitative FTA or FMEDA (Failure Mode Effects and Diagnostic Analysis). The violation of the security objective under consideration is assessed by comparing this calculation to the target value. The second approach involves independent evaluation of each residual and single point failure and whether each double point failure results in a violation of the security objective considered, which can also be considered as a cut set analysis.

In the final stage of hardware design is hardware integration and testing, the main test design of hardware can achieve the expected function.

### 12.3.4 Software Development

The systematic failure of software is the main problem in the development of software functional security. In this subsection, the corresponding normative requirements are proposed for each phase of development activities, and the specific testing methods and contents for different ASIL level software development are proposed. The software development also follows the V model development, that is, the software architecture design, the unit design and the concrete code development are carried out at different levels from the requirements, and the corresponding integration and test work is carried out at each stage of the design development.

The software development process is similar to the hardware development, and the software architecture can be determined by the software security requirements and system requirements. Software architecture includes both static and dynamic aspects.

Static interface between the main and different software units:

- (1) the software architecture includes its hierarchy;
- (2) the logical sequence of data processing;
- (3) data types and their characteristic parameters;
- (4) external interfaces to software components;
- (5) external interfaces and constraints of the software (including architectural scope and external dependencies).

The dynamic aspect relates to:

- (1) functionality and behavior;
- (2) control flow and concurrent processes;
- (3) data flow between software components;
- (4) data flow time limits for external interfaces.

In the design of software architecture, the maintainability and testability of software should be considered. In the automotive industry, software maintenance should be considered throughout the product life cycle, as well as the simplicity of design testing for software architecture, which is an important aspect of ISO 26262, any design should also take into account the convenience of testing. To avoid a high level of complexity leading to systemic failures, ISO 26262 lists some recommended standards:

- (1) software hierarchy, high cohesion of software modules, limit the size of software modules;
- (2) the interface between software modules should be as few and simple as possible. This can be achieved by limiting the coupling of software modules;
- (3) the software scheduler should avoid using interrupts and, if they are used, consider the priority of the interrupts to ensure the execution time of the software unit.

There are many specific regulatory requirements on the software development, but the compliance check of these norms is actually not easy to operate. For both static and semantic code analysis, the code can be checked against specific specification standards (such as MISRA-C) with the help of specialized tools, which can help find all errors and non-conformities. And for some design rules, such as software architecture design should pay attention to hierarchy, high cohesion, low coupling. This kind of guidance requests, in the actual development, the developer is not easy to carry on the accurate appraisal to the development product. Here is a brief introduction to the industry more widely used architectural design standards and design ideas.

One of the most commonly used software Architecture design standards in automotive electronics is AUTOSAR (Automotive Open System Architecture).

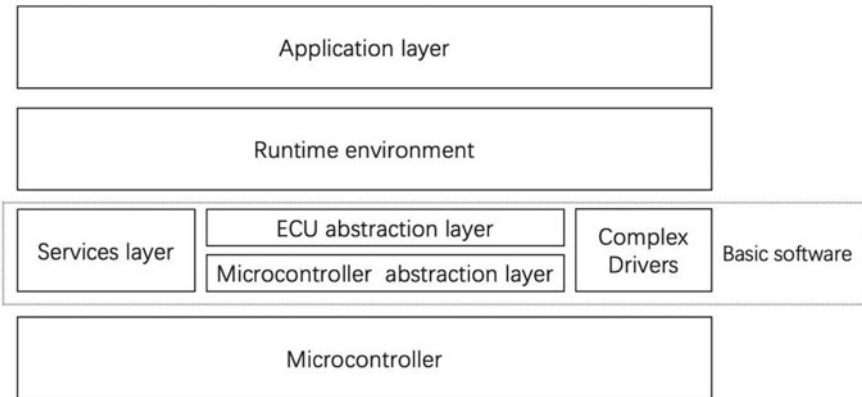


**Fig. 12.9** AUTOSAR architecture

AUTOSAR is an alliance of several OEMs led by BMW Europe in 2003 with Tier1, the goal is to develop a distributed, function-driven automotive electronics software development methodology and software architecture standardization solution for automotive electronics development. AUTOSAR uses a layered design to separate the hardware from the software. AUTOSAR architecture is shown in Fig. 12.9.

AUTOSAR successfully realizes the upper Application Software Layer and the lower hardware-based Basic Software Layer by using the RTE (Runtime Environment) as virtual bus. With AUTOSAR architecture design, the software development of application layer cannot be restricted by hardware ECU and get rid of the dependence on hardware. RTE brings together all the communication mechanisms provided by Autosar. Application software is divided into components. By system configuration, software components are mapped to the specified ECU, and the virtual connection between components is also mapped to CAN, FlexRay, MOST, etc. Software components communicate with RTE through pre-defined ports. Each software component is not allowed to communicate with each other directly. After encapsulating COM and other communication layer BSW in RTE layer, RTE + API is provided for upper application software.

The application layer can be isolated from the bottom layer by using AUTOSAR architecture in software development. The car factory or Tier 1 can focus on the application layer directly related to the product's functionality, creating features at the application layer that distinguish them from their competitors. For the middle layer and the bottom layer, it can be done by professional suppliers, and this part is becoming more and more similar. The middle and bottom layers are invisible to the user, and the garage can even use a common platform vendor for this part of the work, which is very helpful for cost and product maturity and stability.

## References

- ISO. Road vehicles- functional safety: ISO 26262:2018. ISO, Switzerland (2018)
- Zhu Y (2013) Power battery system high voltage functional safety concept based on ISO26262. Automob Parts 10:97–100

# Chapter 13

## Cyber Security



### 13.1 Overview of Automotive Cyber Security

With the in-depth integration of automobile manufacturing technology and new-generation technologies such as information and communication technology, the automobile industry is accelerating its development in the direction of electrification, intelligence, networking and sharing. In-vehicle electronic systems have become more and more complex, and have gradually equipped with networked communication functions, including communication with other vehicles, infrastructure, and access to the internet.

The reliability of system functional safety has always been the focus of research in the automotive field. While the active and passive safety capabilities of vehicles continue to increase, ISO 26262 also provides relevant guidance for the development of functional safety for vehicle and component manufacturers. However, the number of internal ECUs in automobiles has increased significantly. On the basis of traditional automobiles meeting daily transportation needs, modern automobiles, especially new energy automobiles, have been transformed into a large-scale intelligent mobile terminal. In this development process, a large amount of information transmission across multiple systems is involved. Once a cyber security incident occurs, it may have an extremely serious impact on property safety, personal safety and even national public safety. In recent years, while new energy vehicles have gradually become the development strategy of the automotive industry, the issue of automotive cyber security has become increasingly severe. As shown in Table 13.1 (360 Automotive Information Security Lab 2016, 2017, 2018), vehicle cyber security cracking incidents caused by various attack methods frequently occur.

In recent years, related research on cyber security has become an important topic and research hotspot in the automotive field. Therefore, the issue of cyber security is the top priority of the transformation, upgrading and development of the automobile industry. Only by realizing automobile cyber security can the healthy development of intelligent connected cars be guaranteed.

**Table 13.1** Main research or events of international automotive cyber security ([360 Automotive Information Security Lab 2016, 2017, 2018](#))

Time	Description of the research or event
2010	The University of South Carolina implemented an attack on the automobile tire pressure monitor system (TPMS)
	The University of Washington and the University of California San Diego (UCSD) controlled cars through physical contact
2011	At DEFCON, hackers used SMS to unlock Subaru Outback
	At USENIX, the University of Washington published an analysis report on the attack entrance of automobiles
2013	At DEFCON, the steering wheel, brakes and fuel tanks of the Ford Vuga and Toyota Prius were controlled through OBD-II
2014	At BLACKHAT, Miller and Valasek presented a research report that found security risks in many well-known automotive electronics systems
2015	Qihoo 360 Technology Co. Ltd stated that there are security vulnerabilities in the Tesla car application
	At USENIX, UCSD used OBD equipment to achieve remote control of the automobile
	At DEFCON, researchers demonstrated the control to open the Tesla door, start the automobile and drive away
	Qihoo 360 Technology Co. Ltd cracked BYD's cloud service
	At BLACKHAT, Miller and Valasek demonstrated the use of the Oday vulnerability in the Uconnect system to realize remote control of Jeep Cherokee cars by attacking IVI. This incident led to an emergency recall of 1.4 million cars
2016	Keen Security Lab of Tencent realized remote control of Tesla cars in a remote way without physical contact
	At DEFCON, Qihoo 360 Technology Co. Ltd demonstrated an attack on Tesla's autopilot system
2017	Subaru's IVI and various key systems had serious security design flaws
	Jay Turla built mazda_getInfo for Mazda IVI to automate the hacking process
	Keen security lab of Tencent cracked the code signing mechanism added by Tesla, showed the effect of Tesla light show, and designed the remote coordinated control of its multiple ECUs
	Qihoo 360 Technology Co. Ltd and Zhejiang University successfully conducted a dolphin sound attack test on in-vehicle voice assistants, and realized functions such as opening the sunroof, controlling air conditioning and navigation through ultrasound
2018	The data of more than 100 car factories including Volkswagen, Tesla, Toyota, Ford, and GM were leaked
	A relay attack on the keyless entry and start system of a car caused many vehicles to be stolen
	Tencent security research team conducted security analysis on various BMW models, found 14 general security vulnerabilities and applied for 7 CVE vulnerability numbers
	Kaspersky Lab discovered serious security vulnerabilities in a number of shared car apps

(continued)

**Table 13.1** (continued)

Time	Description of the research or event
	Mercedes-Benz was exposed with two CVE vulnerabilities
	Researchers discovered that a server operated by the manufacturer CalAmp was misconfigured
	security researchers from computes in the Netherlands can control the central screen, speakers, and microphones through loopholes in the IVI systems of Volkswagen Golf GTE and Audi A3 Sportback e-tron
	Tesla's keyless entry and start up system was exposed to a CVE vulnerability, numbered CVE-2018-16,806
	Vgate iCar 2 Wi-Fi OBD2 Dongle, a vehicle fault detection device, was exposed to a series of security vulnerabilities

Information security refers to preservation of confidentiality, integrity and availability of information. In addition, other properties, such as authenticity, accountability, non-repudiation and reliability can also be involved (Ma et al. 2019).

As shown in Table 13.2 (Ma et al. 2019), foreign research on the cyber security of intelligent networked vehicles started earlier. Relevant institutions in developed countries such as the United States, Japan, and the European Union, as well as authoritative organizations and societies such as ISO/TC22, SAE, have all conducted relevant research on the formulation of information security standards for in-vehicle embedded systems. However, there is still a lack of safety standards and regulations recognized by the industry.

Among them, the Japanese Information-technology Promotion Agency (IPA) issued the automotive cyber security guidelines in 2013. A defined automobile cyber security model called IPA Car is shown in Fig. 13.1 (National Information Security Standardization Technical Committee, 2018). This guide has made a systematic arrangement of possible ways to attack automobile systems, cyber security countermeasures for different automobile functional modules and so on.

SAE J3061 is the first guidance document on the cyber security of automotive electronic systems in the world. System Cybersecurity is the state of a system that does not allow exploitation of vulnerabilities to lead to losses, such as financial, operational, privacy, or safety losses. System safety beyond regulatory requirements is the state of a system that does not cause harm to life, property, or the environment. The two domains are also related in that there is some overlap between the elements of system safety engineering and the elements of system Cybersecurity engineering, but the elements are not identical between the two engineering disciplines.

In recent years, the Chinese government and relevant departments have also recognized the importance of vehicle cyber security. The vehicle cyber security has become an important measure to guide automobile strategies. On the one hand, relevant departments are committed to the research on the testing and evaluation system and the automobile information standard policy, and successively released *Equipment Manufacturing Standardization and Quality Improvement Plan, Mid and Long-term Development Plan of the Automobile Industry, Guideline for Developing National*

**Table 13.2** The formulation of foreign automotive cyber security standards and policies (Ma et al. 2019)

Country/organization	Standards/policies/regulations	Main content
European Union	E-safety vehicle intrusion protected applications (EVITA)	The project (2008–2011) aims to design, validate and prototype vehicle network architectures to prevent tampering with security-related components and protect sensitive data from attacks
	Preparing secure vehicle-to-X communication systems (PRESERVE)	The goal of this project (2011–2015) is to design, implement, and test a secure, scalable V2X security subsystem that provides security and privacy protection measures for V2X communications that are close to practical applications
EU authorized ETS、CEN/ISO	ITS security architecture	The technical specifications include security application layer services, security management, error reporting, and HSM security requirements, as well as related security technical specifications (TS)
Japan	Vehicle information security guide	From the perspective of automobile reliability, the guide defines an automobile cyber security model called IPA CAR through the analysis of attack methods and approaches to automobile security, and proposes automobile life cycle security protection measures
America	Federal automated vehicles policy	The policy divides the safety deployment tasks of highly autonomous vehicles into four parts: self-driving vehicle performance guidelines, state policy models, current regulatory methods, and new regulatory tools and powers
	Automated driving systems 2.0: a vision for safety	The guide recommends that automobile manufacturers take measures to deal with cyber threats and cyber vulnerabilities, and conduct cyber security assessments of vehicle auxiliary systems

(continued)

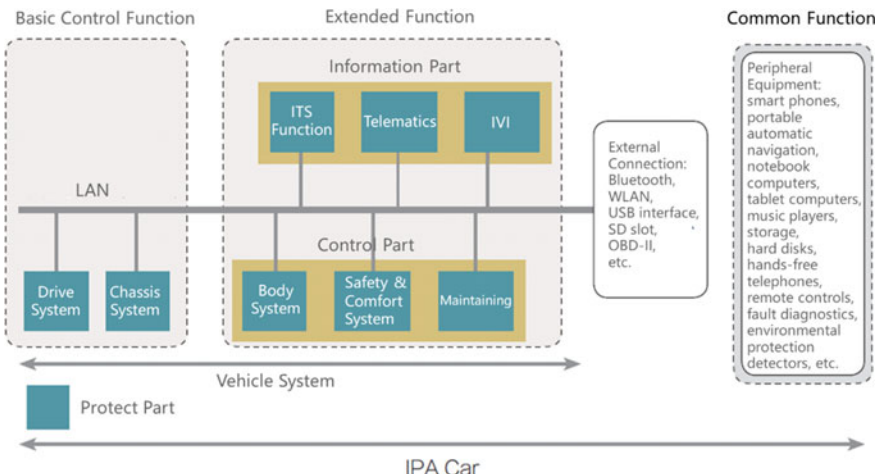
**Table 13.2** (continued)

Country/organization	Standards/policies/regulations	Main content
	Cybersecurity best practices for modern vehicles	The guidance document of the intelligent connected vehicle mainly includes general cybersecurity guidance, automotive industry cybersecurity guidance, vulnerability/vulnerability exploitation/security incident response process, and basic vehicle cybersecurity protection measures
Britain	The key principles of cyber security for connected and automated vehicles	The eight key principles include top-level design, risk management and evaluation, product after-sales service and emergency response mechanism, overall security requirements, system design, software security management, data security, and flexible design
Germany	Road traffic Law—eighth amendment	The law stipulates in principle the scope of the definition of autonomous driving, the responsibilities and obligations of drivers, and the recording of driving data. It also stipulates the boundaries of rights and obligations for all stakeholders in autonomous driving, and proposes the direction of government supervision
	Self-driving code of ethics	As the first ethical code for the autonomous driving industry in the world, it establishes rules for the ethics and value issues arising from autonomous driving by determining priority principles in the areas of road safety, travel convenience, personal protection and utilitarianism, personal rights or property rights, etc
ITU-T	X.1373	It uses appropriate security control measures to provide a software security update program between the remote update server and the vehicle, and defines the security update process and content recommendations
SAE	SAE J3061	To provide a cybersecurity process framework and guidance to help organizations identify and assess cybersecurity threats and design cybersecurity into cyber-physical vehicle systems throughout the entire development lifecycle process

(continued)

**Table 13.2** (continued)

Country/organization	Standards/policies/regulations	Main content
ISO/TC22	ISO/SAE 21434	This document specifies requirements for cybersecurity risk management for road vehicles, their components and interfaces, throughout engineering, production operation, maintenance, and decommissioning

**Fig. 13.1** Automobile cyber security model (IPA Car) (National Information Security Standardization Technical Committee, 2018)

*Internet of Vehicles Industry Standard System (Intelligent & Connected Vehicle)* and other documents to standardize and guide the healthy development of cyber security in the automotive industry. On the other hand, various Chinese standardization organizations such as TC114, TC260, TC268, CCSA, TIAA, CAICV, are also actively promoting the development of relevant standardization, and have successively issued *White Paper for Cybersecurity of Intelligent and Connected Vehicle*, *Guideline for Cybersecurity Protection of Internet of Vehicles (DIS)*, *Information Security Technology-Cybersecurity Guide for Automotive Electronics Systems*, *White Paper for Cybersecurity of Internet of Vehicles*, *White Paper for Standardization of Automotive Electronics Cybersecurity* and so on (Ma et al. 2019).

The *White Paper for Internet of Vehicles* (China information and Communication Research Institute 2018) issued by CAICT in 2018 puts forward development suggestions for strengthening cyber security protection and building a comprehensive, efficient and reliable security management system. Some of its main purposes include: strengthening the connected vehicles' protective capabilities of cyber security in

each link of device-channel-cloud, strengthening the classification management and access control of Internet of Vehicles data throughout the lifecycle, improving the identity authentication system in the process of vehicle development, production and use, production and use System, and building a multi-party linkage, information sharing, real-time and accurate operation security service platform. The *White Paper for Standardization of Automotive Electronics Cybersecurity* (National Information Security Standardization Technical Committee, 2018) categorizes the main cyber security risks currently faced by intelligent and connected vehicles into six levels, including basic components, key software and hardware devices, internal communication buses, vehicle operating systems and applications, external terminals, and cloud service platforms. In the follow-up of this chapter, the security threats, protection and other technologies related to cyber security will be introduced from three aspects: in-vehicle communication, new energy vehicle charging and remote communication.

## 13.2 Cyber Security for In-Vehicle Communication

Ensuring the cyber security of in-vehicle communication is the key to the cyber security protection of intelligent and connected vehicles. The vehicle's internal system consists of a variety of vehicle network buses. The vehicle network is responsible for the interaction of internal electronic control unit (ECU) information. As shown in (Fig. 13.2 China Automotive Engineering Society 2017), many ECUs communicate with each other through different vehicle network buses.

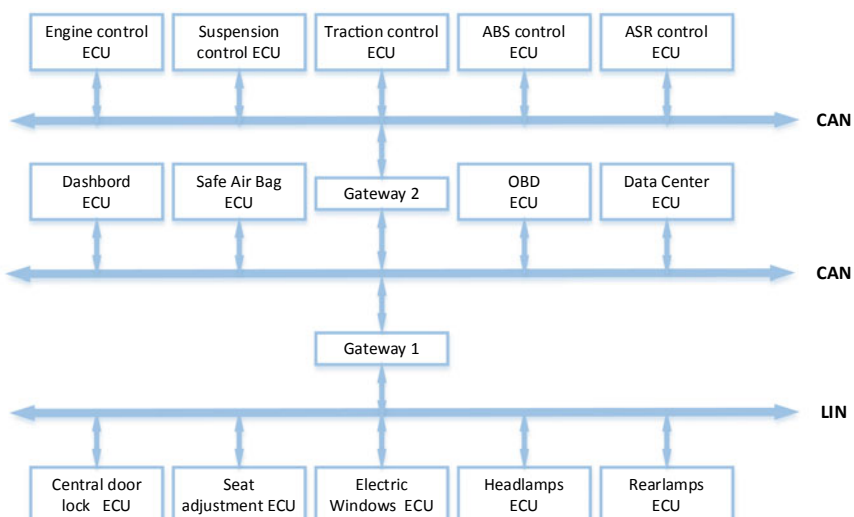


Fig. 13.2 Transmission of in-vehicle network (China Automotive Engineering Society 2017)

However, due to the application in a relatively closed environment and the limited computing power of sensors, the adopted in-vehicle network communication protocol security protection measures are weak. So, in-vehicle network cannot resist attacks by the attackers on sensor information collection, attack message construction, message protocol analysis, message replay and so on. Many ECU units in the vehicle are connected through the vehicle network bus (such as CAN, LIN). If the attackers break into the in-vehicle network, they can operate the ECU at will, or send a large number of error messages to cause the bus to fail, which in turn causes the ECU to fail. This shows that the security of the in-vehicle communication system is extremely important.

### ***13.2.1 In-Vehicle Network***

At present, the in-vehicle network bus is represented by CAN, LIN, FlexRay and MOST. As shown in Table 13.3 (Yu 2016), they play different roles in the corresponding field of the vehicle network with their respective advantages.

Controller Area Network (CAN) was developed by the German company BOSCH, which is famous for its research and production of automotive electronic products. Because of its outstanding reliability and effectiveness, CAN has become a standardized serial communication protocol, and it is widely used in automobile internal control system. Local Interconnect Network (LIN) is widely used in low-speed buses because it is cheap and easy to implement. The FlexRay bus is dedicated to supporting important safety wire control technology. It uses a time trigger mechanism to provide low latency and high-speed transmission. Media Oriented System Transport (MOST) is a data bus technology designed to meet the special needs of infotainment applications. Although FlexRay and MOST are outstanding in their respective application systems, their characteristics determine that they cannot become a general vehicle network standard like CAN bus. Therefore, as the backbone bus of the vehicle network, the security of the CAN bus is directly related to the security of the vehicle.

### ***13.2.2 CAN Bus Communication Protocol***

Data frame is used to transmit information between ECUs on the in-vehicle CAN bus. The ECU broadcasts a data packet with a specified ID to the network, and other ECUs on the network can optionally accept or respond to the message based on the ID. According to the length of the message identifier, the CAN bus protocol is divided into the standard CAN2.0A and the extended CAN2.0B. The standard CAN2.0A has an 11-bit identifier while the CAN2.0B extends 18 bits on the basis of CAN2.0A. As shown in Fig. 13.3 (Yu 2016), the CAN 2.0B is compatible with the CAN 2.0A standard frame format and extended frame format.

**Table 13.3** A list of in vehicle network bus (Yu 2016)

Bus	LIN	CAN	FlexRay	MOST
Scope	Low-level subnet	Lightweight real-time system	Complex real-time system	Interactive multimedia and telematics
Application	Door lock, temperature control, electric window, rain sensor, etc	ABS, ADAS, engine control, transmission	BBW, steering, shifting and emergency system	Entertainment, navigation, information services, mobile office
Architecture	Single-control	Multiple-control	Multiple-control	Multiple-control
Access control	Polling	CSMA/CA	TDMA, FTDMA	TDMA, CSMA/CA
Shift mode	Synchronous	Asynchronous	Synchronous/asynchronous	Synchronous/asynchronous
Bit-rate	20 k bit/s	1 M bit/s	10 M bit/s	24 M bit/s
Redundancy	No	No	Yes	No
Protection	Checksum Check bit	CRC Check bit	CRC Bus monitor	CRC System service
Physical layer	Single-wire	Two-wire	Optical fiber/two-wire	Optical fiber

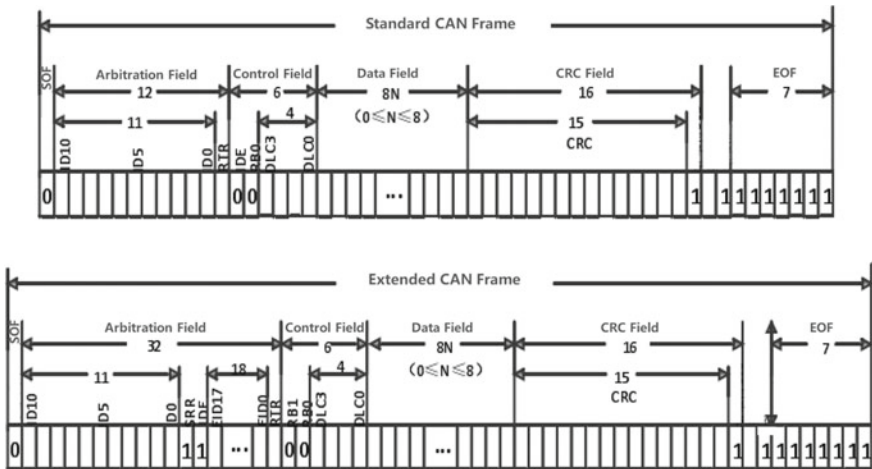


Fig. 13.3 The data frame format of CAN 2.0A and CAN2.0B (Yu 2016)

The CAN bus data message consists of the following parts: A 1-bit start of frame (SOF). A 11-bit standard frame ID or a 29-bit extended frame ID. A 1-bit identifier extension bit (IDE) indicates whether it uses extended format. A 6-bit control field indicates that it is followed by the length of the data in the data field. A data field can carry 0–8 bytes of data. The data field is followed by a 16-bit CRC field, a 2-bit ACK field, and a 7-bit end of frame (EOF) field. In addition, CAN2.0B also defines three different types of message: remote frame, error frame and overload frame.

Among all frame types of CAN bus, there are five frame types that can effectively communicate.

- (1) Data Frame: used for data transfer between nodes.
- (2) Remote Frame: used to ask for the transmission of data frame with the same identifier from another node on the CAN bus. It is composed of six parts: start of frame field, arbitration field, control field, CRC field, response field and end of frame field. The remote frame can be regarded as a special data frame. It does not contain data field and the RTR filed inside the arbitration ID is put in recessive, while the RTR field in the data frame is dominant.
- (3) Error Frame: when an error is detected, the node sends out an error frame. It contains two parts: error flag and error delimiter. The error delimiter consists of 8 recessive bits. The error flag is determined by different error types. The active error flag has 6 dominant bits, and the passive error flag has 6 recessive bits.
- (4) Overload Frame: the receiving node informs the sending node that it is not ready to receive. It consists of an overload flag and an overload delimiter. The overload flag has 6 dominant bits, and the overload delimiter has 8 recessive bits.

- (5) Inter-frame Space: used to separate the data frame and the remote frame from the previous frame. However, no inter-frame space is inserted before overload frames and error frames.

Among them, the data frame and the remote frame are named by the same ID. Even if they have the same ID, the priority of the data frame is higher than the remote frame when the bus conflicts. The CRC field provides error detection during transmission, which is also the only security check mechanism in the CAN protocol. However, this verification mechanism is far from enough in the context of intelligent and connected vehicle.

### **13.2.3 CAN Bus Cyber Security Vulnerability**

At present, with the rapid development of intelligent and connected vehicles, the number of external communication interfaces of vehicles has increased sharply, and external devices frequently communicate with the electronic systems in the vehicle. These external communication interfaces not only provide the driver with better comfort and functionality, but also provide the attackers with more portals for malicious attacks on the vehicle bus network. As a result, more and more cyber security risks are gradually exposed to people's vision.

Since 2013, the famous white hat hackers Charlie Miller and Chris Valasek have successively published research reports about automotive cyber security issues at the world's top security conferences. Whether it is a direct connection for an attack or a remote attack through a vulnerability in the in-vehicle infotainment system, it sends a forged command message from the CAN bus to the ECU node in the car to realize the remote control of the car.

The CAN bus is currently the most widely used in-vehicle network technology. Initial design of CAN bus based on the requirement of control system has no cyber security protection mechanism and means. With the emergence of automotive cyber security issues, the attackers penetrate the on-board CAN bus network connected to the key control unit through the external access interface, and then send malicious attack messages through the CAN bus network. This interferes with the working conditions of the vehicle and seriously endangers the personal, property and information security of the vehicle driver, passengers and traffic participants. Therefore, studying the cyber security of the in-vehicle CAN bus network has very important theoretical value and practical significance. The following is an analysis of the main cyber security vulnerabilities of the vehicle CAN bus (Liu 2019; Peng 2019).

- (1) Lack of adequate message authentication mechanism

The CRC field in the CAN bus frame format is the only security authentication mechanism. But it can only provide error detection in the transmission process. There is no message authentication for message sending

and receiving to ensure data confidentiality, message integrity, availability, authenticity, non-repudiation and data freshness.

(2) Lack of data encryption mechanism

The design of the CAN bus protocol has a broadcast feature. Once the CAN message is sent, it is broadcast to all nodes on the CAN bus. The attackers can use monitoring devices such as CANTest and USB-to-CAN to monitor CAN messages at will. Due to the lack of a data encryption mechanism for CAN messages, the CAN messages monitored by the attackers can crack the messages through reverse analysis and other methods. And then the attackers inject new messages on the CAN bus to control the vehicle, so that the integrity and authenticity of the messages cannot be guaranteed.

(3) Lack of identity authentication mechanism

The frame format specified by the CAN bus protocol does not include the identity authentication field, or even any source identifier field. Therefore, any hijacked node on the CAN bus or an attacked node connected to the outside can be faked into other nodes, and send malicious control information to the control unit on the bus. This seriously threatens the cyber security of the CAN bus.

(4) Lack of segmentation and border defense

The CAN bus network lacks necessary network segmentation and does not isolate or protect key ECU nodes. All networks are connected to each other. The attackers can connect to any node of the CAN bus network, and monitor data and maliciously control the entire CAN bus.

(5) The vulnerability of CAN

The CAN bus uses the CSMA/CA arbitration mechanism. It arbitrates according to the priority of the message ID, and provides the possibility for the attackers to perform a denial of service attack (Dos) on the bus. The attackers can make the ECU unable to send and receive message data normally by attacks such as flooding and replay. It can even paralyze the entire CAN bus. In addition, the attackers can also disconnect the ECU from the CAN bus by sending a malicious error frame message.

(6) Weak authentication of ECU firmware refresh

At present, when ECU firmware is refreshed, most cars still lack identity authentication or use authentication technologies such as weak passwords. Therefore, the attackers can illegally reprogram the ECU with the new firmware.

(7) Problem of information leakage

By initiating a session through OBD-II, the attackers can grasp vehicle operating information, and then replay or tamper with the information, and ultimately trigger information leakage.

### 13.2.4 CAN Bus Attack Methods

The ECU in the vehicle is directly or indirectly connected to the CAN bus through a gateway. The attackers can access the CAN bus entrance through any ECU that interacts with the outside of the vehicle. The attackers can discard, tamper with, and eavesdrop on the information that has been sent to the CAN bus, and then perform spoofing attacks between the source node and the target node, as well as denial of service attacks and replay attacks. The main attack methods of the CAN bus are as follows (Yu 2016):

(1) Message discard

By controlling the gateway in the CAN bus network, the attackers can obtain all the messages on the CAN bus connected to the gateway. The gateway is usually responsible for data exchange between multiple CAN bus networks. The attackers can delete or not forward certain key message data, so that ECUs that require these key messages cannot complete normal functions. When the attackers control an electronically controlled terminal node and turn off its bus transceiver, it can cause the node to go offline and even lose a certain function of the vehicle.

(2) Message tampered

By invading or intercepting a certain gateway in the CAN bus, the attackers can tamper with the message data forwarded from the gateway. The tampered message data does not look different from the normal message. But the wrong information may cause very serious consequences on the vehicle.

(3) Message eavesdropped

The attackers can steal bus messages through any ECU in the vehicle or a monitoring device connected to the CAN bus. Once the key or private information is sent on the CAN bus, it may be read by the attackers. Since the CAN bus does not have any encryption means, once the attackers monitor the bus network through an intrusion node, they may get all the data on the bus.

(4) Spoofing

For the purpose of consuming the processor resources of the ECU, the attackers can send an error message or a diagnostic message after invading any node, so that the ECU on the CAN bus can respond. The remote frame of the CAN bus, as a special data frame, can make the ECU receiving the message respond to the message data with the same ID. The attackers deliberately fill in the wrong CRC check code to force the ECU that receives the message data to discard the message or send an error frame, which consumes ECU processor resources.

(5) Denial of service (DoS) attack

The attackers can send high-rate flooding messages to the network where they are located by controlling any ECU. Because the CAN bus uses priority arbitration, messages using a high priority ID can always preempt bus resources.

Sending a large number of high-priority messages at a high frequency has always occupied bus resources. The CAN bus is paralyzed because the nodes on the network cannot send messages.

(6) Replay attack

Replaying CAN messages is a common method in the reverse analysis of automotive CAN bus protocols. Different functional messages on the CAN bus are sent to the bus in a fixed cycle. To realize the control of a specific function, it is necessary to replay the message sequence when the function is running normally. In order to maliciously control certain functions of the vehicle, the attackers take a series of actions. Firstly, they control any ECU in the vehicle or a monitoring device connected to the CAN. Furthermore, they record the message sequence used by a specific function when the function is running normally. Finally, they replay the sequence to deceive the target system when launching the attack.

### **13.2.5 CAN Bus Protection Measures**

The most basic requirement for the security of communication information in the vehicle is the confidentiality, freshness, integrity, authenticity and availability of CAN bus information. The cyber security protection mechanism of the CAN bus mainly includes data encryption, message verification, identity authentication, anti-replay attack. The following is an introduction to several key technologies of the above-mentioned protection mechanisms.

#### **13.2.5.1 Data Encryption—Advanced Encryption Standard (AES)**

Advanced Encryption Standard (AES) is a block encryption algorithm released by the National Institute of Standards and Technology (NIST) in 2001. This standard, used to supersede the Data Encryption Standard (DES), is currently one of the most popular algorithms in symmetric key encryption in the world.

The AES encryption algorithm uses a symmetric block cipher system, the block length is fixed at 128 bits, and the key length is 128, 192, and 256 bits. Depending on the key length, the number of rounds of encryption is also different. The AES encryption algorithm has compact coding, simple design and can resist many types of attacks. The AES encryption process operates on a  $4 \times 4$  byte matrix, termed the state. And its initial value is a plaintext block (the size of an element in the matrix

is one byte in the plaintext block). When encrypting, each round of AES encryption cycle (except the last round) includes four steps (Ministry of Industry and Information Technology of the People's Republic of China 2018):

(1) The Add Round Key step:

Each byte of the state is combined with a byte of the round key using bitwise XOR. Each sub key is generated by a key generation scheme.

(2) The Sub Bytes step:

A non-linear substitution step where each byte is replaced with another according to a lookup table.

(3) The Shift Rows step:

A transposition step where the last three rows of the state are shifted cyclically a certain number of steps.

(4) The Mix Columns step:

A linear mixing operation which operates on the columns of the state, combining the four bytes in each column.

In the last encryption cycle, the Mix Columns step is omitted and replaced by another Add Round Key step.

The main process of AES algorithm is shown in Fig. 13.4, taking the key length of 128 bits and the encryption rounds of 10 as an example. Firstly, the 128-bit plaintext is grouped to obtain a  $4 \times 4$  plaintext state matrix as the input of the algorithm. Furthermore, the key matrix is selected to perform an Add Round Key step on the plaintext state matrix, and then 10 rounds of round function encryption are performed. The steps of round function encryption are Sub Bytes, Shift Rows, Mix Columns, and Add Round Key. The last round of Mix Columns not only not improve security, but reduce the speed of the algorithm. Therefore, this round of discarding the Mix Columns step. The decryption algorithm is still 10 rounds. Since the four rounds of the algorithm are all reversible transformations, the decryption process uses the same key as the encryption process to reverse the encryption operation for each round. In practical applications, the data encryption of the CAN bus usually combines the advantages of multiple encryption algorithms.

### 13.2.5.2 Message Verification–Message Authentication Code (MAC)

Message Authentication Code (MAC) is used to ensure the integrity and authenticity of data. MAC is essentially a Hash function with a key. The input parameters are messages and keys of any length. It outputs a short data block with a fixed length of  $n$  bits as an authentication code. When in use, the sender sends the message and the generated authentication code to the receiver, and the receiver performs the same operation on the received message with the same key as the sender to obtain a new authentication code. And the receiver compares the received authentication code with the calculated authentication code. If the two are equal, then:

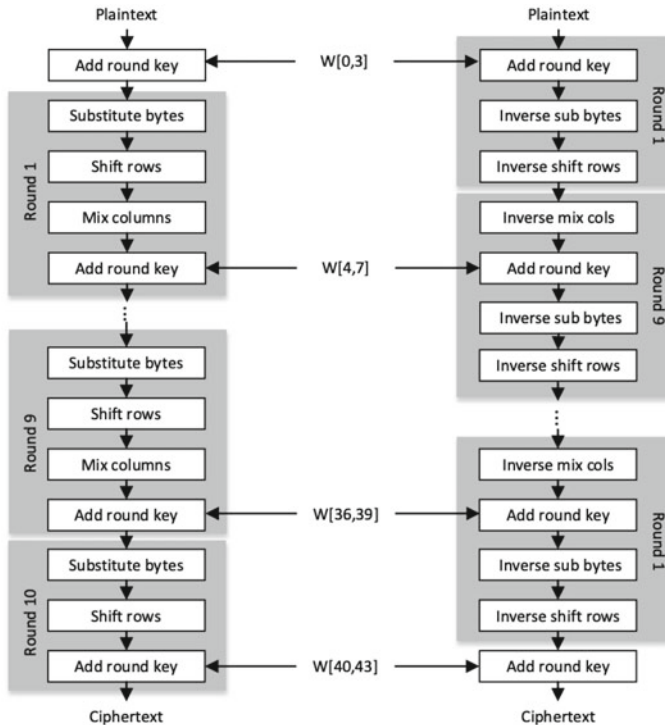


**Fig. 13.4** The main process of AES

- (1) The message is tampered with.

If the attackers tampered with the message, the authentication code calculated by the receiver will not be equal to the received authentication code, because the attackers cannot change the corresponding authentication code.

- (2) The message comes from the real sender.

Because the other parties do not know the key, it is impossible to forge the correct authentication code.

At present, there are mainly two types of MAC algorithms, namely, the Cipher-based Message Authentication Code (CMAC) and the Hash-based Message Authentication Code (HMAC). The essence of the CMAC algorithm is a block cipher algorithm based on CBC. At present, the data processing complexity of the widely used Hash functions such as MD5 and SHA series algorithm is generally lower than that of block cipher algorithms such as AES and IDEA algorithm. Therefore, the efficiency of HMAC is better than CMAC (Zhang 2018).

### 13.2.5.3 Identity Authentication

The identity authentication technology occupies an absolute core position in traditional cyber security. It prevents the attackers from impersonating the identity of user to achieve malicious access to useful resources. The identity authentication technology has different classification methods from different angles. From a technical perspective, it is mainly divided into static authentication, dynamic password authentication and so on.

Static authentication refers to the realization of identity authentication by entering the account password. This certification process is simple and easy to understand. However, if the password is intercepted by the attackers during the transmission of the CAN bus, the attackers will successfully invade the bus network and cause serious consequences. Therefore, the security factor of static authentication is not very high.

Dynamic password authentication is an authentication method with a higher security factor than static authentication. It, also known as one-time password authentication, can resist most of the attacks faced by static authentication to improve security, because its passwords are changed regularly. Most of the current dynamic authentication methods are two-factor authentication. The two factors of the algorithm's seed key and uncertainty factor ensure the use value of the password.

Dynamic password authentication mainly includes event synchronization-based dynamic passwords, time synchronization-based dynamic passwords, and Challenge/response-based asynchronous dynamic passwords.

#### (1) Event synchronization-based dynamic passwords

Using the sequence of events as an uncertain factor. And the corresponding dynamic password is generated through an algorithm. Among them, the choice of uncertain factors generally comes from the event counter.

#### (2) Time synchronization-based dynamic passwords

Using time as an uncertain factor. Time means that the time on the user and server side remains the same. However, due to disturbances and delays, time deviations occur. It is difficult to ensure time synchronization.

#### (3) Challenge/response-based asynchronous dynamic passwords

After the user sends an authentication request, firstly, the server generates a different challenge code each time and sends it to the user. Then, the user and the server use the same algorithm to calculate the challenge code. Finally, it is judged whether the authentication is passed by comparing whether the calculated values at both ends are the same.

In the practical application of the CAN bus security protection, challenge/response-based asynchronous dynamic passwords is mainly used. It not only avoids the risk of inaccuracy caused by time parameters and counter counting, but also is not affected by fluctuations caused by poor network environment. Therefore, it significantly improves the effectiveness of identity authentication (Wu 2018).

### 13.2.5.4 Anti-Replay Attack—IEEE1588 Time Synchronization Protocol

The main protection mechanism of replay attacks is to check the time stamp of the message during the communication process in order to ensure the freshness of the information. Each node on the CAN bus has its own clock system. The node ECU periodically exchanges the information of time with higher precision through the network to synchronize the clocks of each node. Synchronization is divided into time synchronization and frequency synchronization. A frequency synchronized system is not necessarily time synchronized, but the frequency of a time synchronized system must be synchronized.

High-precision time stamp is a means to prevent replay attacks. Time synchronization refers to the process of making the time between the slave clock and the master clock consistent, that is, taking a certain ECU as the “clock reference”, and other ECUs update the local ECU time stamp parameters by receiving the time stamp information of the ECU. Since operations on the network can cause delays, such as transmitting data, receiving and sending data, encryption and decryption. It is necessary to correct the delay caused by transmission.

The time synchronization protocol of IEEE1588 protocol is shown in Fig. 13.5 (Luo et al. 2019). By calculating the time delay and offset, the deviation of the message sent time and the received time is obtained. Thus, according to the calculated time deviation, the ECU that needs to synchronize the time corrects the received time stamp parameter (Luo et al. 2019).

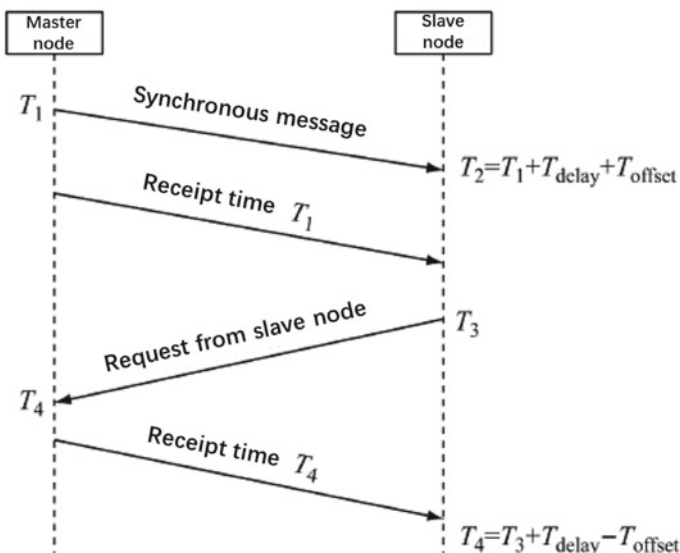


Fig. 13.5 IEEE 1588 clock synchronization mechanism (Luo et al. 2019)

The calculation formulas of the delay time ( $T_{delay}$ ) and the offset time ( $T_{offset}$ ) are as follows:

$$T_{delay} = \frac{(T_2 - T_1) - (T_3 - T_4)}{2}$$

$$T_{offset} = \frac{(T_2 - T_1) + (T_3 - T_4)}{2}$$

where,  $T_1$  is the sending time of the master node,  $T_2$  is the receiving time of the slave node,  $T_3$  is the sending time of the slave node,  $T_4$  is the receiving time of the master node.

### 13.3 Cyber Security for Charging

With the continuous development of the new energy vehicle industry, cyber security issues in the charging process of new energy vehicles have received more and more attention. In December 2015, the Standardization Administration, the National Energy Administration, the Ministry of Industry and Information Technology of the People's Republic of China, the Ministry of Science and Technology of the People's Republic of China and other departments issued the newly revised five national standards for electric vehicle charging interfaces and communication protocols, including GB/T 18487.1–2015 *Electric vehicle conductive charging system—Part 1: General requirements* and GB/T 27930–2015 *Communication protocol between off-board conductive charger and battery management system for electric vehicle* in Beijing. At present, some of China's national standards, such as the DC interface of electric vehicle charging pile, control guide circuit, and communication protocol, are listed as the world's four major DC charging interface standards alongside the United States, Europe and Japan. China's influence in the field of international charging and replacement has been significantly improved (Zhang 2018).

Among them, according to GB/T 27930–2015 *Communication protocol between off-board conductive charger and battery management system for electric vehicle* and *Communication protocol between electric vehicle on-board charger and AC charging spot*, the communication network between the charger and the electric vehicle BMS adopts CAN2.0b communication protocol. It consists of two nodes: the charger and the BMS.

#### 13.3.1 The Overall Process of Charging

As shown in Fig. 13.6, the whole charging process includes six phases: physical connection complete, power-on with low voltage auxiliary, charging handshake

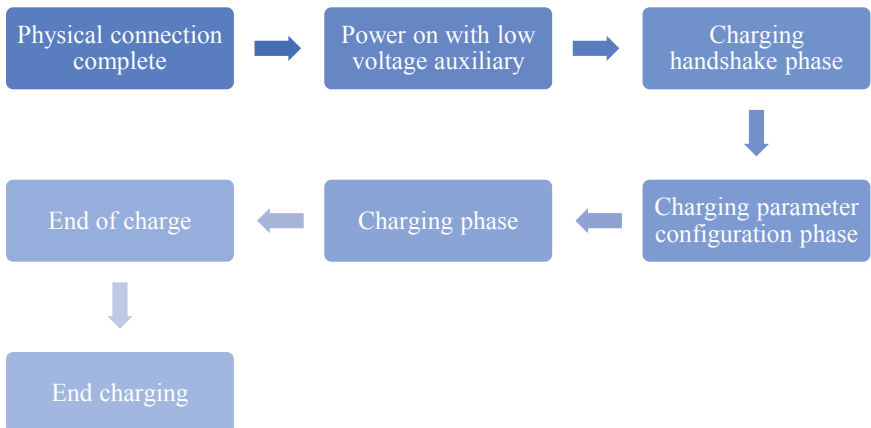


**Fig. 13.6** The overall process of charging

phase, charging parameter configuration phase, charging phase and end of charge. In each phase, if the charging spot and BMS do not receive the message of the other party or do not receive the correct message within the specified time, it is judged to be a timeout (timeout refers to the failure to receive the complete or correct data packet of the other party within the specified time). The timeout is 5 s unless otherwise specified. When timeout occurs, the BMS or the charger will send the specified error message and enter the error processing state (State Grid, China energy construction group Guangdong Electric Power Design Research Institute Co., Ltd., 2015).

### 13.3.1.1 Low-Voltage Auxiliary Power-On and Charging Handshake Phase

The charging handshake phase is divided into the handshake start phase and the handshake identification phase. When the charger is physically connected to the BMS and powered on normally, turn on the low-voltage auxiliary power supply, enter the handshake start phase to send handshake messages, and then perform insulation detection. After the insulation monitoring is completed, the handshake identification phase will be entered. Both parties will send identification messages to determine the necessary information of the battery and the charger. The message in the charging handshake phase should meet the requirements shown in Table 13.4 (State Grid, China energy construction group Guangdong Electric Power Design Research Institute Co., Ltd., 2015).

**Table 13.4** Message classification in the charging handshake phase (State Grid, China energy construction group Guangdong Electric Power Design Research Institute Co., Ltd., 2015)

Message code	Message description	PGH (Dec)	PGN (Hex)	Priority	Length byte	Message cycle ms	Source address-destination address
CHM	Charger handshake	9728	002600H	6	3	250	Charger-BMS
BHM	Vehicle handshake	9984	002700H	6	2	250	BMS-charger
CRM	Charger identification	256	000100H	6	8	250	Charger-BMS
BRM	BMS and vehicle identify message	512	000200H	7	41	250	BMS-charger

### 13.3.1.2 Charging Parameter Configuration Phase

In the charging parameter configuration phase, the charger sends a message of the maximum output capacity of the charger to the BMS. And the BMS judges whether charging can be carried out according to the maximum output capacity of the charger. The message in the charging parameter configuration phase should meet the requirements shown in Table 13.5 (State Grid, China energy construction group Guangdong Electric Power Design Research Institute Co., Ltd., 2015).

**Table 13.5** Message classification in the charging parameter configuration phase (State Grid, China energy construction group Guangdong Electric Power Design Research Institute Co., Ltd., 2015)

Message code	Message description	PGH (Dec)	PGN (Hex)	Priority	Length byte	Message cycle ms	Source address-destination address
BCP	Charging parameters of power battery	1536	000600H	7	13	500	BMS-charger
CTS	The charger sends time synchronization information	1792	000700H	6	7	500	Charger-BMS
CML	Maximum output capacity of charger	2048	000800H	6	8	250	Charger-BMS
BRO	Ready state for battery charging	2304	000900H	4	1	250	BMS-charger
CRO	The output ready state of the charger	2560	000A00H	4	1	250	Charger-BMS

### 13.3.1.3 Charging Phase

After the charging configuration phase is completed, the charger and BMS enter the charging phase. During the entire charging phase, the BMS sends charging requirements to the charger in real time, and the charger adjusts the charging voltage and charging current accordingly to ensure the normal progress of the charging process. The charger and the BMS send their respective state of charge to each other in the charging process, and the BMS sends specific status information of the power battery and information such as voltage and temperature to the charger as required. BMV, BMT, and BSP can be selectively reported, and the charger does not make a message timeout judgment for them.

The BMS judges whether to end the charging, based on whether the charging process is normal, whether the battery state reaches the charging end condition set by BMS itself and whether it received the charging suspension message from the charger (including the specific reason for the suspension, the message parameter value is all 0 and the untrusted state). The charger judges whether to end the charging, based on whether the charging stop command is received, whether the charging process is normal, whether the set charging parameter value is reached and whether it received the charging suspension message from the BMS (including the specific reason for the suspension, the message parameter value is all 0 and the untrusted state). The message in the charging phase should meet the requirements shown in Table 13.6 (State Grid, China energy construction group Guangdong Electric Power Design Research Institute Co., Ltd., 2015).

### 13.3.1.4 The End of the Charging Phase

At the end of the charging phase, the BMS sends the charging statistical data during the entire charging process to the charger, including the starting SOC, the ending SOC, and the lowest and highest values of battery voltage. After receiving the charging statistics data of the BMS, the charger sends information such as output power and accumulated charging time to the BMS, and finally stops the output of the low-voltage auxiliary power supply. The message in the end of the charging phase should meet the requirements shown in Table 13.7 (State Grid, China energy construction group Guangdong Electric Power Design Research Institute Co., Ltd., 2015).

### 13.3.1.5 Error Message

During the entire charging phase, an error message is sent when the BMS or the charger detects an error. The message of error should meet the requirements shown in Table 13.8 (State Grid, China energy construction group Guangdong Electric Power Design Research Institute Co., Ltd., 2015).

**Table 13.6** Message classification in the charging phase (State Grid, China energy construction group Guangdong Electric Power Design Research Institute Co., Ltd., 2015)

Message code	Message description	PGH (Dec)	PGN (Hex)	Priority	Length byte	Message cycle	Source address-destination address
BCL	Battery charging requirements	4096	001000H	6	5	50 ms	BMS-Charger
BCS	The total charge status of the battery	4352	001100H	7	9	250 ms	BMS-Charger
CCS	The charging status of the charger	4608	001200H	6	8	50 ms	Charger-BMS
BSM	Status information of power battery	4864	001300H	6	7	250 ms	BMS-Charger
BMV	Single power battery voltage	5376	001500H	7	Unknown	10 s	BMS-Charger
BMT	The temperature of the power battery	5632	001600H	7	Unknown	10 s	BMS-Charger
BSP	Reserved message of power battery	5888	001700H	7	Unknown	10 s	BMS-Charger
BST	BMS aborted charging	6400	001900H	4	4	10 ms	BMS-Charger
CST	Charger aborted charging	6656	001A00H	4	4	10 ms	Charger-BMS

**Table 13.7** Message classification at the end of the charging phase (State Grid, China energy construction group Guangdong Electric Power Design Research Institute Co., Ltd., 2015)

Message code	Message description	PGH (Dec)	PGN (Hex)	Priority	Length byte	Message cycle ms	Source address-destination address
BSD	BMS statistical data	7168	001C00H	6	7	250	BMS-charger
CSD	Charger statistical data	7424	001D00H	6	8	250	Charger-BMS

**Table 13.8** Error message classification (State Grid, China energy construction group Guangdong Electric Power Design Research Institute Co., Ltd., 2015)

Message code	Message description	PGH (Dec)	PGN (Hex)	Priority	Length byte	Message cycle ms	Source address-destination address
BEM	BMS error message	7680	001E00H	2	4	250	BMS-charger
CEM	Charger error message	7936	001F00H	2	4	250	Charger-BMS

### 13.3.2 Cyber Security Protection During Charging

#### 13.3.2.1 Charger-BMS

According to the main function or communication rate, the CAN bus on vehicle is divided into several different CAN networks. But the CAN between the charger and the BMS consists of only two nodes: the charger and the BMS. In addition, GB/T 27930–2015 *Communication protocol between off-board conductive charger and battery management system for electric vehicle* and *Communication protocol between electric vehicle on-board charger and AC charging spot* clearly stipulates the CAN message classification, message priority, data length, communication process and others between charger and BMS.

Therefore, the cyber security protection during the charging process of the charger and the BMS is essentially the same as the cyber security protection for CAN bus. In order to better resist the possible attacks on the CAN bus, Chinese researchers (Li 2016; Qin 2017; Yang 2017) have conducted research on related technologies such as CAN bus defense detection. They have proposed methods such as installing protocol filters and statistics-based (like information entropy) or machine learning-based (like Decision trees, support vector machines) CAN bus anomaly detection. In addition, aiming at the research on the security of the management between charging spots and electric vehicles, the scholar (Huang et al. 2018) proposed a security model for the decentralized management of electric vehicle charging piles called LNSC (Lightning Network and Smart Contract) to improve the information security of transactions between electric vehicles and charging spots, which is based on the blockchain ecosystem.

#### 13.3.2.2 Infrastructure of Charging Spot

Charging spots are an important infrastructure for the operation of new energy electric vehicles. The input terminal of charging spot is directly connected to the AC grid. And the output terminal of charging spot is equipped with a charging plug, which can charge various electric vehicles according to different voltage levels. The network which is composed of charging spot is known as Spot Networking.

At present, many Spot Networking solutions are carried in traditional Ethernet or wireless transmission networks. The user can perform operations such as the corresponding charging method, charging time, and cost data printing by swiping the card on the human-computer interaction interface provided by the charging spot.

In the process of data transmission by charging spot network, it is faced with malicious threats such as interception, stealing, tampering, deciphering, impersonation, passive attack. The cyber security problem of Spot Networking cannot be underestimated. The PLC circuit of the charging spot control module is connected to the management system through Ethernet, and the internal network of the charging spot basically does not take any safety protection measures. If the attackers invade the spot network through the Internet, they can modify the charging data, such as charging voltage, charging amount, which will cause the loss of users and vehicles (China Automotive Engineering Society 2017).

Combined with the actual situation of extensive construction of charging spots in China, researchers have conducted related explorations on the lack of cyber security protection capabilities of electric vehicle charging spot infrastructure. Based on the analysis of information security requirements from the aspects of physical security, network topology security and others, researchers (Mo 2012) have designed a cyber-security protection architecture for communication network of charging stations. On the basis of considering the cost and reliability requirements of charging facilities, researchers (Zhao et al. 2011) propose a security strategy for data communication. Aiming at the problem that the data transmitted in the charging pile communication is easy to be illegally tampered with, researchers (Zhao et al. 2013) have designed a charging spot device for electric vehicles that can guarantee data confidentiality.

## 13.4 Cyber Security for Remote Communication

Vehicle remote communication refers to the realization of intelligent information exchange and sharing, control of the central control door-lock system, over-the-air download (OTA) and other functions through the network connection between the vehicle to X (pedestrian, vehicle, infrastructure, cloud, etc.). The main body of the communication scene is the two ends and one cloud, and road side infrastructure are supplemented. The objects of communication scenarios include intelligent and connected vehicle, mobile intelligent terminal, cloud service platforms and others. As shown in Fig. 13.7 (China information and Communication Research Institute 2017), the communication scenarios involve four types: Vehicle to Cloud communication, Vehicle to Vehicle communication, Vehicle to Pedestrian communication, and Vehicle to Infrastructure communication.

Vehicle to Cloud (V2C) communication: The vehicle communicates with Internet of Vehicles service platform through cellular networks, satellite communications and others so that it can transmit vehicle data and accept instructions from the service platform.

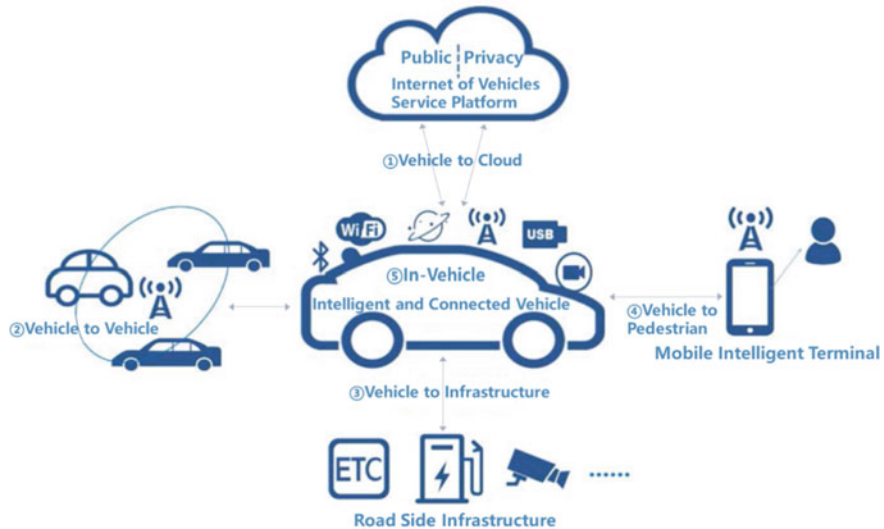


**Fig. 13.7** The scenes of vehicle remote communication (China information and Communication Research Institute 2017)

**Vehicle to Vehicle (V2V) communication:** The vehicle communicates information with neighboring vehicles through LTE-V2X and 802.11p.

**Vehicle to Infrastructure (V2I) communication:** The vehicle communicates with road side infrastructure through LTE-V2X, 802.11p, radio frequency identification and other technologies.

**Vehicle to Pedestrian (V2P) communication:** The vehicle communicates information with the user's mobile intelligent terminal through WiFi, Bluetooth or cellular mobile communication.

### 13.4.1 *Cyber Security Threats of Remote Communication*

#### 13.4.1.1 **The Main Threats of V2C Communication Are Communication Protocol Cracked and Man-In-The-Middle Attacks**

V2C communication occupies an important position in the security of the Internet of Vehicles and has become the main method of Internet of Vehicles attacks. The main threats of it are man-in-the-middle attacks and others. The attackers hijack the T-BOX session and monitors communication data through pseudo base stations, DNS hijacking and other means. On the one hand, it can be used to crack the communication protocol. On the other, it can steal sensitive vehicle data, such as vehicle identification number (VIN) and user account information. In addition, after cracking the

protocol, the attackers combined with session hijacking can implement illegal control of the vehicle's power system based on the man-in-the-middle forge protocol. In January 2015, a security researcher from Germany ADAC attacked BMW Connected Drive based on a man-in-the-middle. He used a pseudo base station to reverse the communication control protocol and then forging control instructions to unlock the door, which attracted people's attention (China information and Communication Research Institute 2017).

#### **13.4.1.2 The Main Threat of V2V Communication is Malicious Nodes**

In the future application scenarios of the Internet of Vehicles, direct-connected V2V communication will become an important way for road condition information transmission and roadblock warning. In the Internet of Vehicles, connected vehicles face the problem of frequent access and withdrawal of nodes. At this stage, in the management of LTE-V2X network access and exit, the secure access control of vehicle nodes cannot be effectively implemented, and the isolation and punishment mechanism for untrusted or out of control nodes has not been established yet. Therefore, the LTE-V2X trusted network environment has outstanding security risks. Once the malicious node invades, the attackers can influence and destroy the authenticity of the V2V communication message by blocking, forging, tampering with or replaying attack, which can affect the transmission of road condition information (China information and Communication Research Institute 2017).

#### **13.4.1.3 The Main Threats of Short Distance Communication Are the Cracking of Protocol and Authentication Mechanism**

With the wide application of multiple wireless communication technologies and interfaces, vehicle nodes need to deploy multiple wireless interfaces to realize the connection of WiFi, Bluetooth, 802.11p, LTE-V2X and other networks. The cracking of protocol and authentication mechanism in short-distance communication has become the main threat at present. By cracking authentication passwords such as WiFi and Bluetooth, the attackers can access in-vehicle network through WiFi or Bluetooth that obtain internal data information of the vehicle or conduct penetration attacks (China information and Communication Research Institute 2017).

### **13.4.2 V2C Communication Security Protection Strategy**

At present, the security protection of remote communication in vehicles is mainly aimed at V2C communication, which mainly focuses on strengthening access control and carrying out abnormal traffic monitoring.

### **13.4.2.1 Strengthen Vehicle-Mounted Access Control and Implement Sub-Domain Management for Reducing Security Risks**

The current intelligent and connected vehicles are usually equipped with two APNs to access the network. APN1 is responsible for the communication of the vehicle control domain (Clean Zone), which mainly transmits vehicle control commands and sensitive data. The other end of the communication is usually the private cloud platform of the vehicle manufacturer, which has a high level of security. APN2 is responsible for the communication of the information service domain (Dirty Zone), which mainly accesses public Internet infotainment resources. The other end of the communication may be the public cloud platform of the vehicle manufacturer or the third-party application server. Applications in the IVI system, such as news, entertainment, broadcasting, usually communicate through APN2. The vehicle control domain and information service domain adopt an isolated method to strengthen security management. The first is network isolation. APN1 and APN2 networks are completely isolated, so that two security domains with different security levels are formed to avoid unauthorized access. The second is the isolation of the in-vehicle system. The control units and non-control units of the in-vehicle network are security isolated, and a stronger access control strategy is implemented for the control units. The third is data isolation. Data storage devices of different security levels are isolated from each other, and the system is prevented from accessing multiple networks at the same time to avoid data cross propagation. The fourth is to strengthen the control of network access. The vehicle control domain can only access the IP addresses in the trusted whitelist to avoid interference from the attackers. Some models of the vehicles have also restricted the access address of the information service domain to strengthen network management and control (China information and Communication Research Institute 2017).

### **13.4.2.2 Build the PKI and Communication Encryption-Based Credible V2C Communication**

At present, enterprises generally attach importance to communication encryption. Some manufacturers build PKI systems based on soft encryption to build more convenient V2C communications. The specific protective measures taken include: The first is digital certificate-based identify authentication. The traditional V2C communication is authenticated by binding PIN, which can easily be bypassed by forgery. The current more complete method is PKI-Based identity authentication. When the intelligent and connected vehicle starts to communicate for the first time, the cloud platform issues a trusted certificate and writes it into the in-vehicle security chip for V2C communication. It is important to ensure that only certified vehicles can communicate with the private cloud. At the same time, based on PKI technology, the cloud platform has the function of certificate revocation and update. The second is digital certificate-based transmission encryption. After the intelligent and connected vehicle obtains the trusted certificate, the subsequent communication uses the certificate for key

negotiation and encrypts the communication data. The encryption protocol usually adopts HTTPS application layer encryption or SSL, TLS transmission layer encryption, which increases the difficulty of eavesdropping and cracking by the attackers and ensures communication security.

#### **13.4.2.3 Improve the Security Protection Capabilities of the Internet of Vehicles by Monitoring Abnormal Traffic on the Network Side**

This solution is deployed by operators. At present, a Chinese company has carried out a pilot application. It uses abnormal traffic monitoring to monitor the process of the Internet of Vehicles business, and provides security monitoring & early warning and emergency response services, which are specifically divided into two aspects: monitoring & early warning and network control (China information and Communication Research Institute 2017):

(1) Monitoring & early warning:

It is customized monitoring services to detect security events. It provides traffic monitoring optimization, abnormal traffic alarms, historical data retention and other functions.

(2) Network control:

It includes defining protected IP addresses/ranges, preventing peer-to-peer communications, and interrupting abnormal IP communications with the help of firewalls and intrusion detection system.

#### **13.4.3 Application of FOTA Security Technology in Vehicle System**

Firmware Over-The-Air (FOTA) refers to the provision of firmware upgrade services for devices with networking capabilities through cloud upgrade technology. In-vehicle electronic devices, such as T-BOX, IVI system, or other ECUs that require upgrades, usually use FOTA to upgrade their firmware systems after networking.

##### **13.4.3.1 Module Composition and Function**

Traditional FOTA solutions, including software supplier, OTA service platforms, and in-vehicle terminal upgrade programs, are easily exploited by the attackers due to lack of security mechanisms. Therefore, the secure FOTA solution adds a security service platform and terminal OTA security components to the original architecture. The specific functions of each component are as follows (National Information Security Standardization Technical Committee, 2018):

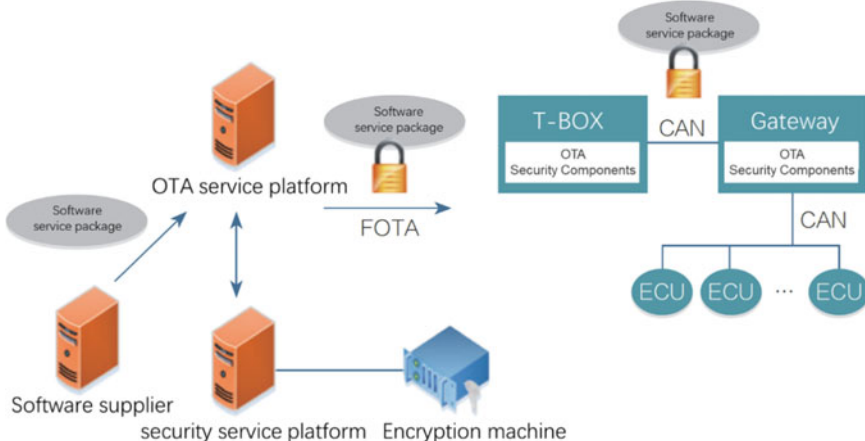


**Fig. 13.8** Logic diagram of FOTA (National Information Security Standardization Technical Committee, 2018)

- (1) Software supplier: The publisher of the original firmware upgrade package.
- (2) Security service platform: It provides security services for the OTA service platform, including key certificate management services, data encryption services, digital signature services.
- (3) OTA service platforms: It provides OTA services for vehicle terminals.
- (4) OTA security component of the terminal: It verifies the legality of the upgrade package and adapts to the security upgrade process (Fig. 13.8).

#### 13.4.3.2 Threat Analysis

There are mainly transmission risks and service package tampering risks in the FOTA process. In the transmission process of the terminal downloading the service package, the attackers can use network attack methods, such as man-in-the-middle attack, sending the tampered and forged service package to the vehicle terminal. If the terminal lacks a verification mechanism in the upgrade process, the tampered service package can successfully complete the upgrade process, achieving the purpose of malicious programs such as tampering with the system, implanting rootkit. The attackers may also unpack the service package to obtain some available information such as loophole patches. Due to the exposure of critical information in the service package, the service package increases the risk of being attacked (National Information Security Standardization Technical Committee, 2018).

### 13.4.3.3 Application of Security Technology

Security FOTA usually protects from three stages: service package release, service package transmission, and terminal upgrade. In order to resist the attackers' reverse analysis and tampering attacks on the upgrade package, the OTA server can increase the deployment of security servers and provide security infrastructure, such as key generation and management, digital encryption, digital signatures. The reinforcement function of the service package is implemented based on the security server, and finally the OTA server releases the reinforced service package. The basic functions of the security server can be implemented with software solutions or the deployment of hardware encryption machines.

In order to ensure the security of the upgrade package transmission process, a security transmission tunnel is built between the OTA server and Vehicle information system to achieve mutual identity authentication and transmission encryption.

The terminal system adds an upgrade package verification mechanism before the upgrade process to decrypt and verify the legality of the upgrade package. Only after the verification is passed can it enter the upgrade process. There are some reasons that the implementation of FOTA security solutions on the terminal needs to consider specific system conditions: The diversity of in-vehicle systems, differences in operating systems and large differences in hardware performance. Therefore, it is very important to find a balance between the security level and the support capability of the target system (National Information Security Standardization Technical Committee, 2018).

## References

- 360 Automotive information security lab (2016) Automotive information security annual report.  
<https://skygo.360.cn/2017/04/12/2016-skygo-annual-report/>
- 360 Automotive information security lab (2017) Automotive information security annual report.  
<https://skygo.360.cn/2018/04/03/icv-cybersecurity-annual-report-2017/>
- 360 Automotive information security lab (2018) Automotive information security annual report.  
<https://skygo.360.cn/2019/03/20/2018-security-report/>
- China automotive engineering society, Beijing university of aeronautics and astronautics, Bangbang security research institute. Intelligent network vehicle information security white paper (2017).  
[https://www.bangcle.com/articles/detail?article\\_id=508](https://www.bangcle.com/articles/detail?article_id=508)
- China information and communication research institute. Networking security white paper (2017).  
[http://www.caict.ac.cn/kxyj/qwfb/bps/201804/t20180426\\_158472.html/](http://www.caict.ac.cn/kxyj/qwfb/bps/201804/t20180426_158472.html/)
- China information and communication research institute. Vehicle networking white paper (2018).  
[http://www.caict.ac.cn/kxyj/qwfb/bps/201812/t20181218\\_190858.html/](http://www.caict.ac.cn/kxyj/qwfb/bps/201812/t20181218_190858.html/)
- Huang X, Xu C, Wang P et al (2018) LNSC: a security model for electric vehicle and charging pile management based on blockchain ecosystem. IEEE Access 99:1–1
- Li D (2016) Research on vehicle information security control system. Jilin Agricultural University, Changchun, pp 8–9
- Liu Y (2019) Research on security protocol based on CAN bus network on vehicle. Jilin University, Changchun

- Luo F, Hu Q, Liu Y (2019) CAN-FD bus based vehicle network security communication. *J Tongji Univ (nat Sci Ed)* 47(03):386–391
- Ma C, Liu T, Shi P (2019) Literature review on automobile information security. *Equip Maintenance Technol* 2:25–28
- Ministry of industry and information technology of the people's Republic of China, NXP Semiconductors (China) Management Co., Ltd. (2018 October 12) Network security technology and application of intelligent interconnected vehicle. Publishing House of Electronics Industry, Beijing
- Mo P (2012) Research on information security of electric vehicle charging station. North China Electric Power University, Beijing, pp 44–45
- National information security standardization technical committee, information security assessment standards working group. White paper on standardization of automotive electronic network security (2018). <https://www.tc260.org.cn/front/postDetail.html?id=20180416001525>
- Peng J (2019) Research on information security and detection technology of networked automotive CAN bus. Tianjin University of Technology, Tianjin
- Qin Z (2017) Research on a vehicle network security protection mechanism. Chengdu University of Information Engineering, Chengdu, pp 5–6
- State Grid, China energy construction group Guangdong Electric Power Design & Research Institute Co., Ltd. (2015) Communication protocol between on-board conductive charger and battery management system of electric vehicle: GB/T 27930-2015. China Standard Press, Beijing
- Wu S (2018) Research on identity authentication method based on CAN bus network on vehicle. Jilin University, Changchun
- Yang H (2017) Research on attack and defense detection technology of CAN bus based on intelligent network vehicle. Tianjin University of Technology, Tianjin, pp 40–41
- Yu H (2016) Research on network vehicle information security and CAN bus anomaly detection technology. Jilin University, Changchun
- Zhang B (2018) Research and implementation of information security protection technology for charging pile of distributed electric vehicle. Harbin Institute of Technology Harbin
- Zhao X, Liu Z, Chen J et al (2011) Data Communication Security Strategy for electric vehicle charging facilities. *Power Syst Autom* 35(9):92–94
- Zhao B, Cen W, Zhai F et al (2013) Control device of charging pile for electric vehicle with safety protection function. *Appliances Energ Eff Manage Technol* 16:53–57

## **Part V**

# **Application and Perspective**

# Chapter 14

## Vehicle Applications



As the most important energy storage system of electric vehicle, all kinds of available batteries, such as lead acid battery, nickel metal hydride battery and lithium-ion battery, have been used in electric vehicles. Among them, Li-ion battery has many advantages such as high energy density, long cycle life, low self-discharge rate, good safety performance and environmental friendliness, at present, it has become the most widely used type of power battery in electric vehicle, which can be divided into lithium iron phosphate, lithium manganese oxide, lithium nickel oxide, ternary (nickel–cobalt–manganese mixture or nickel–cobalt–aluminum mixture) according to the cathode material system. The anode materials used are mainly graphite, carbon materials and lithium titanate; according to the shape, there are three kinds of cylindrical, prismatic and pouch cells, but the pouch cells presents the fast rising tendency (Xiong et al. 2020).

In China, the battery of electric vehicle has formed two main application trends, the pure electric passenger vehicle mainly uses the high energy density three-component battery, the commercial vehicle mainly uses the safety and the service life good lithium iron phosphate battery. At the same time, in response to the requirements of vehicle mileage, battery enterprises are constantly increasing the energy density of the battery cell, in which the ternary system mainly uses increasing the content of nickel to increase the energy density of the material, at present, domestic enterprises are gradually transitioning to the use of NCM811 or NCA as positive and negative electrode materials, with the technical route of graphite or silicon–carbon negative electrode. It is expected that the unit mass specific energy of the battery can reach the target of 300 Wh/kg, Ningde Times New energy development of the battery mass energy density of 302 Wh/kg, cycle life has reached 1000 times.

However, the basic characteristics and working principle of the lithium-ion battery determine the low voltage and small capacity characteristics of the cells. Generally, the rated working voltage of the lithium-ion battery is 3.2–3.8 V, and the unit capacity ranges from a few ampere hours to several tens of ampere hours, can not meet the power source requirements of electric vehicles. Therefore, in the vehicle application,

often by hundreds of thousands of individual batteries in series-parallel form power battery pack to meet the vehicle voltage, capacity and power requirements (Hossain et al. 2021).

## 14.1 Composition of Power Battery System

The power battery system is a kind of energy storage device used to provide energy for the driving of electric vehicle. Besides the power battery as the energy carrier, it also includes the Battery Management System (BMS), the voltage, current and temperature sensors, smoke sensors, thermal management systems, high and low voltage wire harnesses or connectors, switching devices (relays, fuses, MSD, etc.), mounting assemblies (brackets, pallets, bolts, etc.), upper and lower boxes, auxiliary assemblies (seals, rubber pads, heat conducting gasket sealants), etc., as shown in Fig. 14.1.

It is usually necessary to complete the design and layout of battery module, battery management system, thermal management system, high voltage system, etc., the power battery system has the advantages of good safety, high specific energy, high specific power, high temperature adaptability, long service life, strong installation and maintenance, and low comprehensive cost.

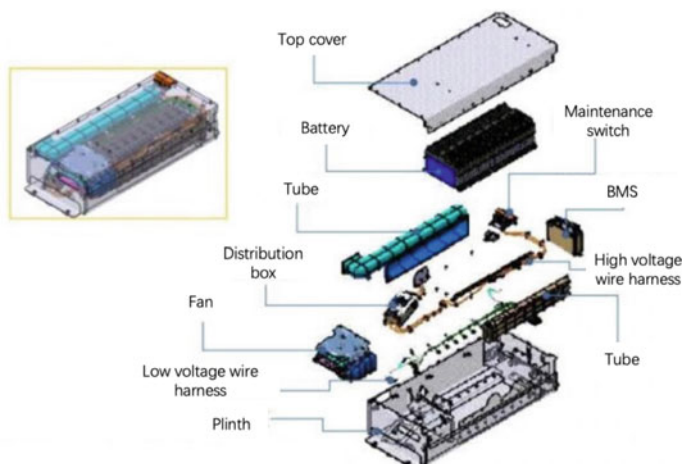


**Fig. 14.1** Power battery system composition

## 14.2 Power Battery Pack

Most of the existing power battery system adopts three-level structure, that is, cell level, module level, system level, as shown in Fig. 14.2. First, multiple cells are combined into modules according to different series-parallel connection modes, and then a certain number of modules are combined into a battery system, the battery module includes a single cell, a fixed frame, an electrical connection, a temperature sensor, a voltage detection circuit, etc.. In addition, in order to improve the energy density of the system more effectively, some enterprises have begun to carry out the modular design of the power battery system, such as CATL has launched the power battery system based on the CTP technology. However, at present, the main body of the market still takes modularization as the development direction of power battery system.

Batteries and power battery systems of different shapes and sizes have a matching degree. For the irregular battery case, the cylindrical battery can make full use of the space and has more advantages than the square battery and the flexible battery case, while the flexible battery case has higher requirements for the module design, and the square battery case is more suitable for the regular battery case, such as electric passenger cars, logistics vehicles commonly used in the standard box. Figures 14.3, 14.4 and 14.5 correspond to different cylinder, square and package manufacturer schemes from cell to system efficiency scatter plot.

From the scatter plot, it can be seen that the group efficiency of the battery system with three kinds of cells is scattered because of the difference of the box shape, module structure and manufacturer, but the group efficiency of square cell is the highest among the three kinds of cells. Although the specific energy of flexible package cell is higher in the same material system, the efficiency of package cell from cell to system does not show great advantage because some structural elements are needed to be applied.



**Fig. 14.2** Three-stage structure of power battery

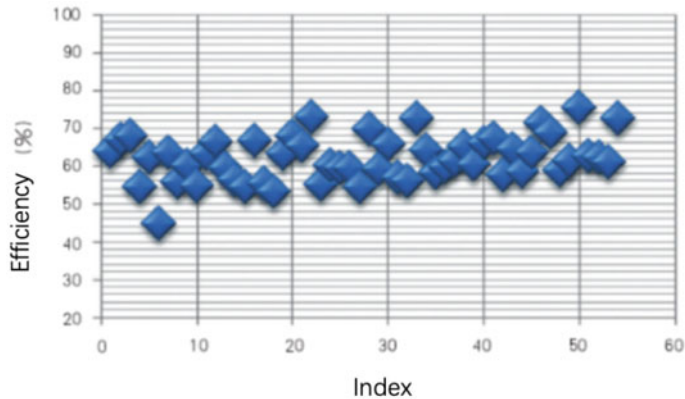


**Fig. 14.3** Scatter plot of group efficiency of cylindrical cell system

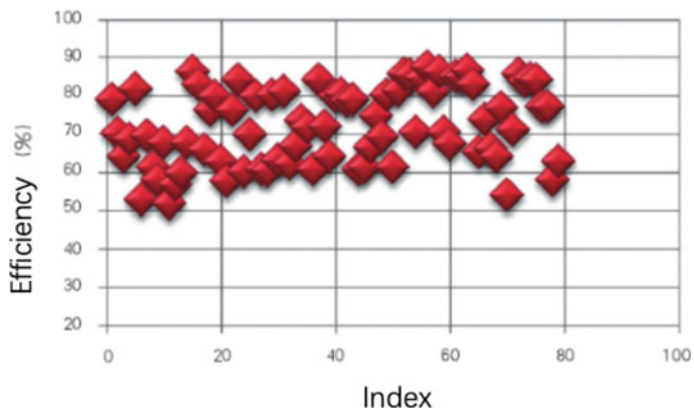


**Fig. 14.4** Group efficiency statistics of square cell system

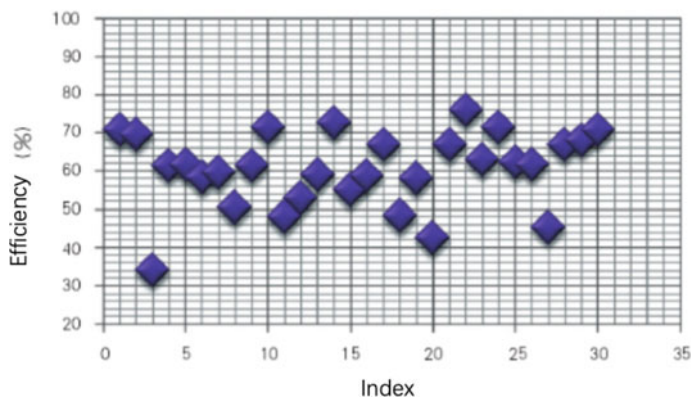


**Fig. 14.5** Group efficiency statistics of flexible battery system

Therefore, in order to further improve the efficiency of clustering, it is necessary to improve the clustering approach:

(1) Optimization design of module

The module mainly consists of electric core, bus bar, fixed electric core, heat conduction glue and other parts. Most of the structural parts are made of aluminum alloy or plastic material, the material used in the module has been selected as a less dense material, so there is little room for material improvement in the module. Module structure is difficult to change, to further improve the efficiency of module group, it is necessary to reduce the weight of each structure. One way is to replace them with higher capacity cells and reduce the number of cells. For example, the Tesla Model 3 uses a cylinder 21,700 instead of a cylinder 18,650, the number of cells in the battery system has been reduced by 30%, and the number of welded fittings has been reduced accordingly. The other method is to increase the size of the module in order to increase the number of cells, so that the weight of the components distributed to each cell is reduced and the group efficiency of the module is improved.

(2) Reduce the system hierarchy

The battery case can not be canceled because of its safety and load-bearing functions, but the module level can be canceled and the battery case is designed as a large module. The design of large module has the characteristics of large capacity, specific energy and less structural parts. For example, the battery systems of two domestic SAIC Roewe and BYD passenger cars are all connected in series with three-element batteries with a capacity of more than 100 Ah. The efficiency of the battery box system with this design is more than 80%, and the maintenance is convenient in the later stage, the information monitored by BMS can be found easily.

(3) Overall arrangement to improve the utilization of system space

Through the overall arrangement to improve the battery box space utilization, the box as far as possible inside the full battery. In order to increase the number of battery cells, the first choice of battery cells and battery boxes is to meet the relevant standards of the automobile industry at home and abroad, such as the German VDA standard, so that the battery cells and battery boxes have the highest matching degree, to achieve longer range.

## 14.3 Lightweight of Battery Pack

### 14.3.1 *Lightweight Design Approach for Battery Systems*

When the energy density of the battery increases slowly, the lightweight design of the power battery system is a very effective way to increase the mileage and reduce the cost of the system.

The lightweight design of power battery system is mainly divided into limit design and lightweight material application. The thin-walled structure of the battery case is designed by CAE simulation technology, and the design is strengthened at the load-bearing part, and the material thickness is thinned as far as possible at the non-load-bearing part. CAE technology has the capability of static strength, mode, vibration, impact, extrusion and so on. With this technology, topology optimization and shape optimization can be realized, it is necessary to know the critical value of the battery case clearly. The critical value not only meets the product performance requirements, but also meets the processing and assembly process requirements.

The application of the new material has obvious effect on the weight reduction of the system. At present, there are two kinds of light weight materials: light alloy materials and composite materials. Aluminum, magnesium and titanium alloys are light alloy materials with small volume weight, which can effectively reduce the body mass and improve the mileage of electric vehicles.

Aluminum alloy has the advantages of light weight, good corrosion resistance and recyclability, so aluminum alloy is still the main material for lightweight application of battery case. Aluminum alloy battery box manufacturing mainly die-casting, extrusion, welding, stamping four processes, which die-casting and welding strength is higher, generally used for the battery box; The aluminum alloy box with die-casting technology can be 10–30% lighter than the traditional battery box. The stamping and welding aluminum box is usually used in the upper cover of battery bag. Magnesium is lighter than aluminum, and only two thirds as dense. Magnesium alloy has high specific strength, good impact resistance and good damping capacity, but the stamping process of magnesium alloy is not mature enough, resulting in very high manufacturing cost. Although titanium alloy has excellent comprehensive properties, the main factor that restricts its development is its high price.

Composite materials have the advantages of high strength, low density, good corrosion resistance and easy processing and molding, and are gradually replacing metal materials. The application of composites in automobile industry mainly includes glass fiber reinforced plastics and carbon fiber reinforced plastics. Due to the cost factor, the composite materials used in the battery case are relatively common materials, such as glass fiber reinforced plastic, modified resin, etc. The density of FRP is only 1.6 g/mm<sup>3</sup>, so the effect of using composite material is obvious. But the ductility of FRP is poor and brittle, generally used in the upper cover of battery pack, the application of molding process, can be compared with traditional battery pack upper cover weight of about 38%.

### 14.3.2 Trends in Lightweight Battery Systems

Improving the specific energy of Li-ion power battery is still the core of the lightweight battery system. By 2020, the industrialization of power cells with a mass specific energy density of over 300 Wh/kg has made a substantial breakthrough. Using lithium rich manganese based solid solution, high capacity lithium-ion battery anode, and high voltage resistant electrolyte, the specific energy density can be increased to 400 lithium-ion battery. Driven by the high specific energy requirement of new energy, more and more battery enterprises and vehicle enterprises invest in the research of new battery technology, high specific energy and high safety become the important technical direction of power battery.

In order to meet the need of long-distance driving, the integrated design of battery system and electric vehicle chassis has become an important development direction of battery system lightweight. The first-generation t-shaped and i-shaped structures, the second-generation earth-shaped and field-shaped structures, have been transformed into the third-generation integrated platform, which has the advantage of transferring part of the weight of the battery pack to the chassis, not only can the system be lightweight, but also can greatly reduce the cost of battery pack.

## 14.4 Application of BMS

As the main energy supply device of electric vehicle, the power battery system is one of the most important parts of the electric vehicle, and has become the key part of the development of electric vehicle, it has a very important influence on the driving range, power, economy and life of electric vehicle, and has become the most expensive part of electric vehicle. Therefore, reasonable and effective management and use of power battery system, for electric vehicles, is of great significance (Xiong et al. 2018; Li and Zhao 2021; Hu et al. 2019).

As one of the components of the power battery system, the battery management system is an important bridge connecting the on-board power battery system and the electric vehicle. Its main function is to monitor and manage the batteries of the power battery system safely and effectively, to improve the efficiency of power battery system, to prevent overcharge, overdischarge, short circuit, overtemperature and other abusive working conditions. For electric vehicle, the effective control of charge and discharge of battery pack by this system can increase the range, prolong the service life, reduce the running cost, and ensure the safety and reliability of battery pack application.

At present, BMS Enterprises which are led by battery enterprises and main machine factories occupy half of the market of passenger car, and few third-party BMS Enterprises can compete with it. Specifically, the top 10 new energy passenger vehicle models in 2018 are Beiqi EC series, BYD Qin, Chery EQ1, BYD Company E5, BYD Song Dm, BYD Tang, Jianghuai iEV6E, Byd Yuan Ev, Rongwei ei6, Jiangling E200. There are a total of 12 BMS enterprises supporting these ten best-selling passenger car models, specifically: Ningde Times, BAIC New Energy, BYD Company, Anhui Guibo Xinneng, Chery New Energy, Yineng Electronics, Huating Power, Shanghai Jieneng, Jiangling New Energy, Funeng Technology, Ha Guangyu, Thor technology. From the point of view of the main body, the main body of BMS is: main plant BMS, Power Battery BMS, BMS PACK plant BMS and third-party BMS. According to the statistics, BMS, which is led by the main engine plant and the Power Battery Enterprises, together account for 77% of the total number of production and sale models in the top ten. It can be seen that BMS, which is led by the main engine plant and the power battery enterprises, occupies the mainstream of the domestic passenger vehicle market, among them, BMS has the largest share in the main plant, and mainstream power battery enterprises such as Ningde Times, Funeng Technology and HA Guangyu are also involved in the field of BMS, which is conducive to deepening their cooperation with the main plant.

Foreign companies BMS have done relatively good, Liandian, the mainland, Delfaut, AVL and FEV, and so on, now are basically in accordance with the AUTOSAR architecture, as well as ISO26262 functional safety requirements to do, in general, software functions more, reliability and accuracy are also high (Zhu 2013; ISO 2018).

## References

- Hossain L, Hannan M, Karim TF et al (2021) Intelligent algorithms and control strategies for battery management system in electric vehicles: progress, challenges and future outlook. *J Clean Prod*  
 Hu X, Feng F, Liu K, Zhang L, Xie J, Liu B (2019) State estimation for advanced battery management: key challenges and future trends. *Renew Sustain Energy Rev* 114  
 ISO (2018) Road vehicles—functional safety: ISO 26262:2018. ISO, Switzerland  
 Li S, Zhao P (2021) Big data driven vehicle battery management method: a novel cyber-physical system perspective. *J Energy Storage* 33

- Xiong R, Zhang Y, Wang J, He H, Peng S, Pecht M (2018) Lithium-ion battery health prognosis based on a real battery management system used in electric vehicles. *IEEE Trans Veh Technol* 9545:1–11
- Xiong R, Pan Y, Shen W et al (2020) Lithium-ion battery aging mechanisms and diagnosis method for automotive applications: recent advances and perspectives. *Renew Sustain Energy Rev* 131
- Zhu Y (2013) Power battery system high voltage functional safety concept based on ISO 26262. *Auto Parts* 10:97–100

# Chapter 15

## Battery Digital Twin



Digital twin is a technology which integrates multi-physics, multi-scale, multi-subject attributes, has the characteristics of real-time synchronization, faithful mapping and high fidelity, and can realize the interaction and fusion between the physical world and the information world. With the concept of digital twin shop put forward, the potential application of digital twin in intelligent manufacturing has obtained more and more attention. Digital twin is to create a corresponding “virtual world” in cyberspace by digitizing all elements of the physical world, such as people, objects and events, the result is that the physical world in the physical dimension and the virtual world in the information dimension coexist and blend with each other. This is to create virtual models for physical objects in a digital way, to simulate their behavior in the real world. Digital twin is the result of accelerating breakthroughs in information technologies such as control, sensing, networking, big data and artificial intelligence, especially the development of IoT. IoT technology feeds back the parameters of the physical world to the digital world through sensors, making simulation verification and dynamic adjustment possible.

Digital twin is the necessary way to the development of digitalization. Digital twin was first used in the industrial field, especially in the field of large-scale equipment manufacturing. By setting up a digital twin production system that integrates all manufacturing processes, realize from product design, to production planning, and then to the implementation of the whole process of digital manufacturing. This digitalization takes innovation, efficiency, and effectiveness to a whole new level.

With the development of information technology and the coming of the internet of everything, there is a clear trend that the physical world and the corresponding digital world will form two systems, which will develop in parallel and interact with each other.

As Fig. 15.1 shows, everything in the future can appear as digital twin, meaning that each will be divided into two parts: an entity that exists in the physical world, and a digital twin of an entity that exists in the digital world. The twin is the virtual image of the entity, representing the entity and mapping the entity's every move. Anything

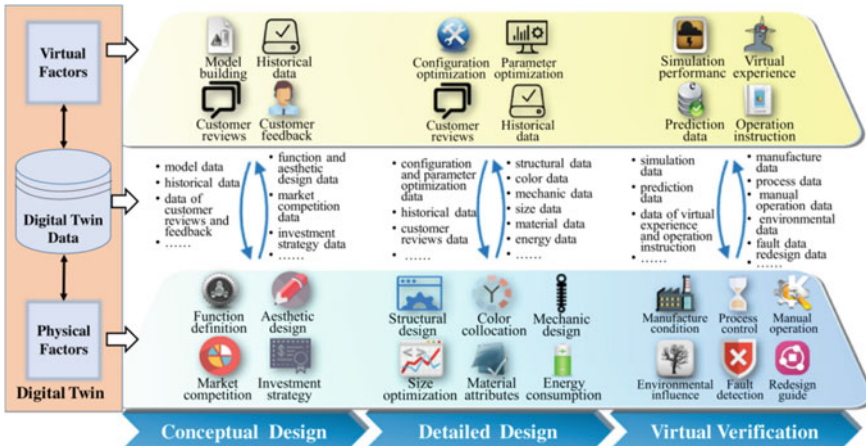


**Fig. 15.1** Concept of digital twin design

in the physical world can be checked and tracked in the digital world. In essence, the Digital World exists in order to serve the physical world, and the physical world becomes more beautiful because of the digital world. These twins are the inevitable result of the digital tide, the only way and the ideal state of digitalization. If the physical world is a factory, the corresponding digital world can be seen as a digital twin factory. If the physical world is a city, the corresponding digital world is a digital twin city. From point to line, from line to surface, based on digital identification, automatic perception, network connection, intelligent control, platform services and other powerful technical capabilities, the digital model can emerge completely, as a twin running parallel with the physical world.

Today's digital technology is constantly changing every business. In the future, all enterprises will become digital companies, which not only requires enterprises to develop products with digital characteristics, but also means to change the whole process of product design, development, manufacturing and service by digital means, and to connect the enterprise's internal and external environment through the digital means.

With the shortening of product life cycle, the strengthening of product customization, and the establishment of cooperative ecological environment with upstream and downstream, enterprises have to take digital means to accelerate product development, improve the effectiveness of development, production, services and improve the enterprise's internal and external environment openness.

This digital transformation can be very difficult for traditional industrial enterprises, as it is a far cry from the traditional, experience-based design and manufacturing concepts that have been used for decades. Designers may no longer need to rely on the development of actual physical prototypes to validate design ideas, or complex physical experiments to verify the reliability of products, it is possible to

predict production bottlenecks without small-scale trial production, or even to gain insight into the operation of products sold to customers without going to the site.

This approach, which will no doubt run through the entire product life cycle, will not only accelerate the product development process, improve the efficiency and economy of development and production, more effective understanding of product usage and help customers avoid losses, more accurate will be the real use of the customer feedback to the design side, to achieve effective product improvement. And all of these, need the enterprise to have the complete digitization ability, but among them the foundation, is digital twin.

## 15.1 Concept of Digital Twin

Digital twin, as the name suggests, refers to the physical world objects, through digital means to build a digital world identical entity, thereby achieving the understanding of physical entities, analysis and optimization.

### 15.1.1 *History of Digital Twin*

In 2002, Dr. Michael Grieves first proposed the concept of digital twin in an article published in 1998. He believed that data from a physical device could be used to construct a virtual entity and subsystem in the virtual (information) space that could represent the physical device, and this connection is not one-way and static, but throughout the life cycle of the product.

Obviously, this concept not only refers to the design stage of the product, but also extends to the manufacturing and service stage. However, due to the limited digital means at that time, the concept of digital twin is only stuck in the design stage of the product, a prototype of a physical device is represented by a digital model.

Since then, the concept of digital twin has expanded to include analog simulation, virtual assembly, and 3D printing, and after 2014, as internet of things, artificial intelligence, and virtual reality technologies continue to evolve, more and more industrial products and equipments have the characteristics of intelligence, and the digital twin has gradually expanded to the complete product cycle stage including manufacturing and service, and constantly enriched the form and concept of digital twin (Fig. 15.2).

### 15.1.2 *Different Forms of Digital Twin*

Digital twin technology runs through different stages of the Product life cycle, and it coincides with the philosophy of Product Lifecycle Management. It can be said that

## A New Class of Digital Twin



Fig. 15.2 Origin of digital twin

the development of digital twin technology extends PLM capabilities and concepts from the design phase to the full lifecycle.

The digital twins take the product as the main line, and introduce different elements in different stages of the life cycle, forming different stages of performance. Figure 15.3 shows the digital twin-driven product design concept.

### 15.1.2.1 Digital Twins at Design Stage

In the stage of product design, digital twin can improve the accuracy of design and verify the performance of product in the real environment. This stage of digital twin includes the following functions:

**Digital model design:** One should use CAD tools to develop a product virtual prototype to meet the technical specifications, accurately record the various physical parameters of the product, and display them in a visual way, and finally test the accuracy of the design through a series of verification means to;

**Simulation:** Through a series of simulation experiments with repeatable, variable parameters and acceleration, the performance and performance of the product under different external environments are verified, and the adaptability of the product is verified at the design stage.

For example, in the automotive design process, Dassault Systèmes has helped companies including BMW, Tesla, and Toyota use their CAD and CAE platforms 3D Experience because of the need to save energy and reduce emissions, accurate aerodynamics, fluid acoustics analysis and simulation, data analysis and simulation in the shape design, greatly improving the flow linearity and reducing air resistance.

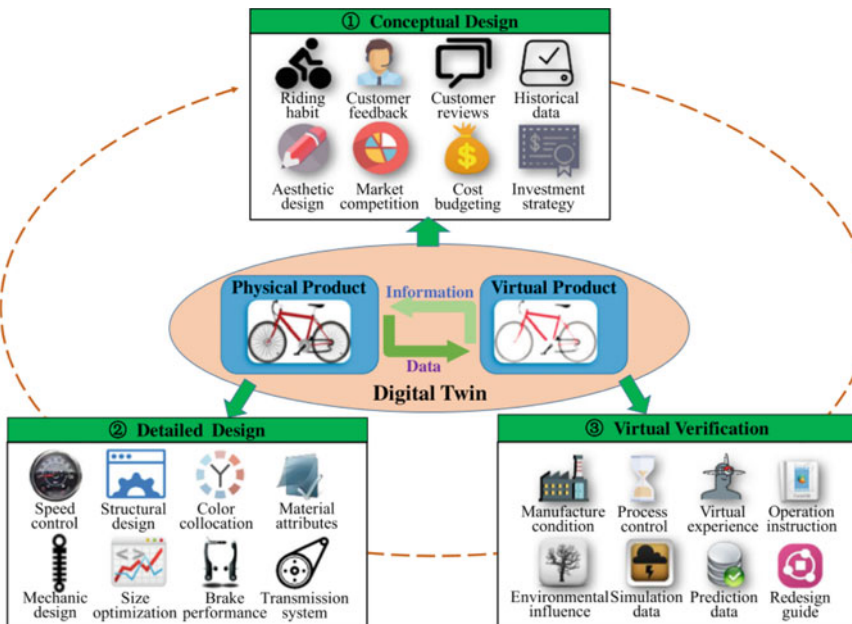


Fig. 15.3 Origin of digital twin (Tao et al. 2018)

### 15.1.2.2 Digital Twin at the Manufacturing Stage

In the manufacturing stage, the use of digital twin can speed up the time of product introduction, improve the quality of product design, reduce the production cost and improve the speed of product delivery.

The digital twin of the product stage is a highly collaborative process, a virtual production line constructed by digital means, the digital twins of the product itself is highly integrated with the digital twins of production equipment, production process and other forms to achieve the following functions:

**Production process simulation:** Before the product is produced, the production process under different products, different parameters and different external conditions can be simulated by means of virtual production, to achieve capacity, efficiency and production bottlenecks and other issues in advance, to speed up the process of new product introduction;

**Digital production line:** the integration of the various elements of the production phase, such as raw materials, equipment, process formulations and process requirements, in a tightly coordinated production process by means of digital means, and in accordance with established rules, automatic completion of different conditions under the combination of operations to achieve automated production process, while recording the production process of various types of data for follow-up analysis and optimization to provide a basis.

Key indicators monitoring and process capability assessment: through the collection of real-time Operation Data of various production equipment on the production line to achieve the visual monitoring of the entire production process, and through experience or machine learning to establish key equipment parameters, test indicators monitoring strategy, to violation of the strategy to deal with the abnormal situation in a timely manner and adjust to achieve stable and continuous optimization of the production process.

### 15.1.2.3 Digital Twin at the Service Stage

As the internet of things matures and sensor costs fall, many industrial products, from large equipment to consumer products, use a large number of sensors to capture the environment and working conditions of the product during its operational phase, and through data analysis and optimization to avoid product failure, improve the user experience of the product. This stage of digital twin can do the following:

Remote monitoring and predictive maintenance: by reading the real-time parameters of sensors or control systems of intelligent industrial products, building visual remote monitoring and giving the collected historical data, a hierarchical health index system of components, subsystems and the whole equipment is constructed, and trend prediction is realized by using artificial intelligence. Based on the prediction results, the maintenance strategy and spare parts management strategy are optimized, reduce and avoid the loss of customers due to unplanned downtime;

Optimization of customer production targets: for many industrial customers who need to rely on industrial equipment to achieve production, the rationality of industrial equipment parameter setting and adaptability in different production conditions, often determine the quality of the customer's product and delivery cycle. And industrial equipment manufacturers can build up experience models for different application scenarios and different production processes through massive data collection to help their customers optimize parameter configuration in order to improve their product quality and production efficiency.

Product feedback: by collecting real-time running data of intelligent industrial products, manufacturers of industrial products can gain insight into customers' real demand for products, not only can help customers to speed up the introduction cycle of new products, avoid product failure caused by wrong use, improve the accuracy of product parameter configuration, but also can accurately grasp customer needs, avoid R & D decision-making mistakes.

### 15.1.3 Key Features of Digital Twin

Digital twin technology is to create the corresponding dynamic and high simulation digital model of physical entity (system) in the special data closed loop driven by directional multidimensional heterogeneous data, to provide object-specific active or

responsive services in different contexts. Physical objects have information equivalence. Human intelligence can extract effective information from physical objects to meet specific needs. Digital twin is a tool for managing complex information in a data visualization way, representing and maximizing the information value of twin objects in a model language, so as to provide a real-time, efficient and intelligent service scheme for individuals, organizations and even systems. The Beihang team (Tao et al. 2018) developed the digital twin model from the original three-dimensional structure to the five-dimensional structure model based on years of research in intelligent manufacturing services, manufacturing IOT, manufacturing big data, etc., these include physical entities, virtual models, service systems, twin data, and connections.

Physical entity is an objective existence, it usually consists of various functional subsystems (such as control subsystem, dynamic subsystem, execution subsystem, etc.). Various sensors are deployed on physical entities to monitor their environmental data and operational status in real time.

Virtual model is a faithful digital image of physical entity, which integrates and merges four-layer models of geometry, physics, behavior and rules. The physical model analyses the physical properties such as current, voltage and temperature, and the behavioral model responds to external driving and disturbance. The rule model can model the rule of physical entity, and make the model have the functions of evaluation, optimization, prediction, evaluation and so on.

The service system integrates evaluation, control, optimization and other information systems to provide intelligent operation, accurate management and reliable maintenance services based on physical entities and virtual models.

The twin data includes the related data of physical entity, virtual model, service system, domain knowledge and its fusion data, and is continuously updated and optimized with the production of real-time data. twin data is the core driver of digital twin.

The connection connects the above four parts in two ways so that the data can be transmitted in real time effectively, and the real-time interaction can be realized to ensure the consistency and iterative optimization among the parts.

### 15.1.3.1 Virtual-Real Symbiosis

According to the level of technology integration, the development of digital twin technology can be divided into three stages (Alam and Saddik 2017): virtual-reality connection, virtual-reality fusion and virtual-reality symbiosis. In the period of virtual-real connection, digital twins appear in the form of digital model, and the data exchange between model and physical entity is carried out manually. The Digital twin in the virtual-real fusion period is more called Digital Shadow, which uses data collection techniques such as Internet of things and big data analysis to update the virtual model parameters dynamically corresponding to the real-time state of physical entities, but the virtual side can not transmit data to the physical side actively. The third stage is the high-order form of digital twin, combining with the Digital Thread technology, the virtual entity and the corresponding intelligent system (twin objects)

in the future can complete the two-way self-flow of data, in the whole life cycle, virtual-reality symbiosis, the ultimate form of fusion between virtual and reality, is realized. Physical entities are optimized by virtual-real interactive feedback, multi-dimensional data fusion analysis and decision-making iteration, so as to promote the efficient coordination of all stages in real activities.

#### **15.1.3.2 High Virtual Simulation**

At present, the transmission rate of 5G network and the real-time rendering ability of computer are greatly improved, which makes digital twin technology able to provide high simulation virtual objects. For example, in the industrial application scenario, structural engineers and styling engineers have different viewing requirements for the same twin object at different stages, the presentation of twin objects should also be flexible. The authenticity of the model refers to the relationship between the factual information and its token under the guidance of a specific goal, that is, the greater the degree of correlation with the factual information needed by the goal, the higher the authenticity of the model. Therefore, the Digital Twin technology based on General Digital Twin, with the help of the function of situational awareness, for different user needs, to provide the corresponding high-fidelity special model.

#### **15.1.3.3 High Real Time Interaction**

Digital twin technology emphasizes the collection and interpretation of underlying real-time multidimensional data, but the human-computer interface presents mainly the simulation model of physical objects, in the form of models, data visualization, etc., human-computer “Communication” is one of the characteristics of digital twin technology. As MBSE (Model-based System Engineering) becomes more and more popular in the industry, digital twin technology will be combined with immersion technology, and the systems Engineering will become more and more popular, it combines interactive technologies such as wearable devices, augmented reality glasses, virtual reality and even brain computer interfaces to provide a full range of information sensing experiences.

#### **15.1.3.4 Insight**

With the continuous enhancement of big data collection and analysis technology, the improvement of artificial intelligence algorithms and computing power, virtual entities in digital twins are also beginning to generate knowledge through “Learning”, a new paradigm of knowledge, skills and experience: distributed and symbiotic knowledge space based on digital twin technology may also emerge in the future. Under the development background that all things can be twins, all things will also have the attribute of “Wisdom”, and human beings will be in the living space of

wisdom. In the case of a human being as a twin, knowledge can be transferred to a virtual avatar using digital twin technology, which in turn can be learned through continuous simulation training, interaction with the ontology, etc., to provide insight into different situations.

### ***15.1.4 Meaning of Digital Twin***

Since the concept was put forward, digital twin technology has been evolving rapidly, which has greatly promoted the design, manufacture and service of products (Rasheed et al. 2019).

(1) Easier and more conducive to innovation

Digital twin maps the properties of physical devices into virtual space by means of digital design tools, simulation tools, internet of things, virtual reality, etc., to form a detachable, replicable, transferable, modifiable, erasable, repeatable digital image, which greatly speeds up the operator's understanding of the physical entity, it can make many operations, such as simulation, batch copy and virtual assembly, which can not be completed because of physical conditions and must depend on real physical entities, become accessible tools, it inspires people to explore new ways to optimize design, manufacturing, and service.

(2) More comprehensive measurements

As long as it can be measured, it can be improved. This is an unchanging truth in industry. Whether it is design, manufacture or service, it is necessary to measure all kinds of properties, parameters and running state of physical entity accurately in order to realize accurate analysis and optimization.

However, traditional measurement methods have to rely on expensive physical measurement tools, such as sensors, acquisition systems and detection systems, in order to obtain effective measurement results, and this will undoubtedly limit the coverage of measurement, for many can not directly collect the measured value of the indicators, often powerless.

And digital twin technology, with the help of Internet of things and Big Data Technology, through the collection of limited physical sensor indicators of direct data, and with the help of large sample base, through machine learning to infer some indicators can not be directly measured.

For example, we can use the historical data of lubricating oil temperature, winding temperature, rotor torque and so on, and use machine learning to construct different fault feature models and infer the health index of generator system indirectly.

(3) More comprehensive analysis and forecasting capabilities

The existing product life cycle management, rarely able to achieve accurate prediction, so often can not be hidden under the surface of the problem in advance to predict.

Digital twin can combine data acquisition, big data processing, and artificial intelligence modeling and analysis of the Internet of things to achieve the assessment of the current state, the diagnosis of problems in the past, and the prediction of future trends, and give the results of analysis, simulation of various possibilities to provide more comprehensive decision-making support.

#### (4) The digitization of experience

In the traditional industrial design, manufacture and service fields, experience is often a vague and difficult to grasp form, it is difficult to take it as the basis for accurate decision. One of the key advances in digital twin is the ability to digitize previously unpreserved expertise and provide the ability to preserve, copy, modify and transfer it.

For example, for various fault features in the operation of large-scale equipment, the historical data of sensors can be trained by machine learning into digital feature models for different fault phenomena, and combined with the records processed by experts, it can be used to form the basis of accurate judgment of equipment fault state in the future, and can enrich and update the feature library for different new forms of fault, and finally form an autonomous intelligent diagnosis and judgment.

With the emergence and application of new technologies such as cloud computing, artificial intelligence, blockchain and quantum computing, the digital twin using Open architecture (or loose standards) has become very dynamic. The digital twin is built on the Model-Based Systems Engineering (MBSE), but with the continuous development of the technology, the professional division of labor is gradually formed. The Systems Engineering of the digital twin is based on the Model-Based Systems Engineering, some enterprises put some complex technology into the market after packaging, greatly promoting the development of the digital twin market. Beihang, Guangdong University of Technology and Tsinghua University are active in the field of digital twins, and have made some achievements (Fig. 15.4).

At present, the Ministry of Industry and Information Technology (MIIT) is promoting the industrial internet strategy. MIIT focuses on the industrial internet system and is divided into three core parts: network, platform and security, from physical assets to perceptual control, digital models and decision optimization, the business applications are finally formed. Digital twins drive the closed loop of data optimization. In addition, the Industry 4.0, the digital twin research center, and the digital twin lab are exploring the connection.

As a new paradigm or method, digital twin has great potential, but its connotation and scope are still uncertain, especially the definition of digital twin model is not clear. It can be divided into general model and special model according to the category of the model, and the special model is still the focus of current research, it also includes the development of specialized models.

In addition to parts measurement and quality control, additive manufacturing, design and work process, and system management, these specific projects also include applications in biomedical and petroleum engineering. The tools and techniques for developing the special model are diversified, including general industrial software, special industrial software, simulation platform and self-developed tools,

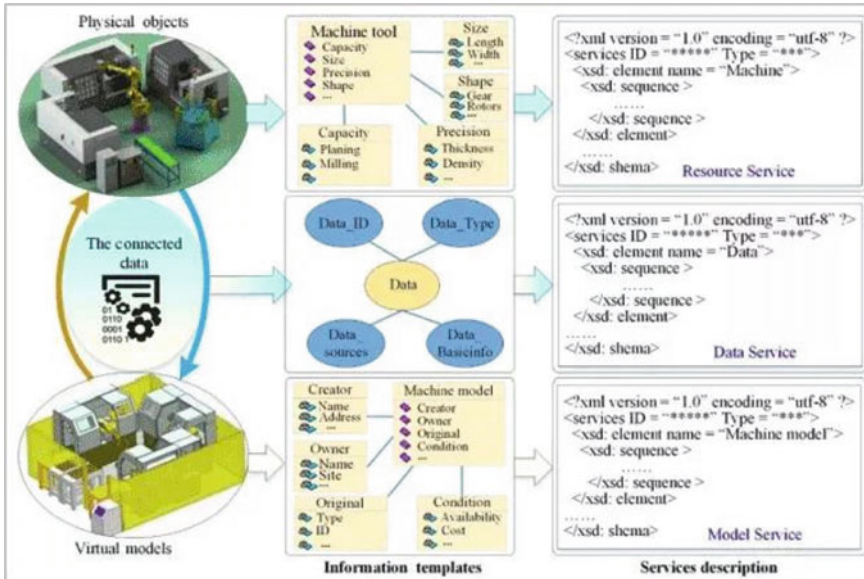


Fig. 15.4 Digital twins designed by Professor Tao Fei of Beihang University

etc.. The object of study of digital twin general model is not a specific item, but how to express model controlled elements as a set of general objects and the relationship between them, this provides a consistent approach to the management and communication of controlled elements across different environments.

The research of digital twin general model is mainly divided into concept research and realization method of general model. From the macro perspective of product life cycle management, to the description of system behavior, such as General System Behavior and system reconfiguration, and then to the specific workflow, conceptual research is carried out, such as design method, product configuration management, manufacturing system, manufacturing process, the research content is more divergent, there is no special hot spot.

As for the realization of the digital twin universal model, it mainly studies the construction of the modeling language, the exploration of the model development method, the use of specific tools, the implantation of the metamodel idea and the exploration of the model algorithm. The digital twin model is one of the core areas of digital twin research, its future research will focus on how to reduce the external characteristics and internal attributes of different digital twins to integrated, interactive and extensible models, it is convenient to realize the information flow between the physical world and the digital world more efficiently, thus realize the universal application of the digital twin, and then support the construction of CPS (network physical space) and CPPS (network physical production system). Therefore, the next step of digital twin model research is how to interface with standard reference architecture, such as Germany's Industry 4.0, Rami4.0, and China's IMSA On the need to

establish a unified description of digital twin models and establish consistent conclusions, in order to standardize the independent development of the established models, so as to improve the interoperability and scalability of the model. Otherwise, with the expansion of the scale of the system, the efficiency of the model will decrease obviously, and the research of the digital twin model in China needs the support of the domestic professional industrial software and the modeling software urgently.

## 15.2 Digital Twin in BMS

In view of the problems existing in the existing technology, it is difficult to solve the problems and feasible solutions with comprehensive modeling, algorithm, theory and so on. Because cloud computing platform has advanced computing and model simulation capability, the whole life cycle battery management system based on digital twin is an important solution in the future.

The solution of full lifespan battery management system based on digital twin is to establish digital twin system by coupling physical entity with virtual entity, using the twin cloud data platform to analyze the physical and virtual entities in real-time through the method of rolling optimization, the data of the twin clouds are processed by the cloud computing system to obtain the state and control strategy of the entity battery and the Twin Virtual Battery, and interact with the BMS system of the terminal, the whole life cycle management of battery pack is realized.

In the digital twin system of the battery management system, physical entity refers to the power battery pack in the real world, and virtual entity refers to the digital model of the power battery pack in the virtual simulation cloud environment, the twin cloud data platform is a cloud data storage, analysis and transmission system, based on the Advanced Cloud Computing Platform as a cloud data processing system, a large database and a data analysis platform, the high-speed CAN bus communication or wireless communication is used to realize the data interaction between the simulation system and the real system, and the simulation control strategy is fed back to the terminal BMS to realize the cloud control solution based on the high-precision model.

At present, according to the function and structure, the power battery group generally includes three levels: cell level, module level and system level. Single cell level model is built for single battery, which can monitor, forecast and maintain single battery, and module level model is used to analyze and optimize the consistency and aging characteristics of module battery. For the whole battery system, system-level model can be constructed to describe the interaction and coupling relationship between each module model and cell model, so as to analyze and predict the evolution of the whole system.

Based on the multi-level cell-module-system model, the real-time parameters obtained by BMS in the cloud data platform can predict the whole life cycle of the battery, and feedback to terminal BMS to control and further optimize the state of the battery. The building process of digital twin simulation model mainly includes geometric configuration, macroscopic attribute construction, microscopic

scale attribute construction, dynamic attribute updating, historical data association and so on, geometry includes, but is not limited to, shape, size, position, assembly relationship, etc.. It can be used in 3D modeling software to improve the rendering effect of detail level Macroscopical attribute construction includes but is not limited to physical attribute, parameter constraint, parameter characteristic of physical model, including but is not limited to fluid, battery, electrochemistry, thermodynamics etc. The construction of micro-scale attributes includes, but is not limited to, the characteristics of ion motion in different particle sizes and different spatial scales Dynamic attribute updating includes, but is not limited to, the analysis of time-varying, dynamic and performance degradation of virtual system using state machine, Markoff chain and neural network The Association of historical data includes, but is not limited to, the optimization process of producing invisible knowledge by adopting new rules of process mining system such as depth learning and consistency analysis.

The twin cloud data platform is the driver of the digital twin system, performance in the system specifications, functions, performance, relations and other physical elements of the data and reflect the system operation, real-time performance, environmental parameters, sudden disturbances, such as dynamic process data, the data are collected by sensors, embedded system, data acquisition card, and the simulation data of process simulation, behavior simulation, process verification, evaluation, analysis and prediction are carried out by the model, including algorithms, models, data processing methods, algorithmic data, including such standard data as expert knowledge, industry standards, rule constraints, inference, common algorithm bases and model bases, etc., by fusing physical real-time data with multi-spatio-temporal correlation data, historical data, standard data and other information data, information physical fusion data is obtained, which reflects more comprehensive and accurate information and realizes information sharing and value-added.

The full lifespan battery management system solution based on digital twin can support the deep integration of digital twin and New IT technology, and can advance through the linkage with New IT. At the same time, it can provide support for the multi-dimensional and multi-space–time scale model, information physics fusion data and so on needed in the process of digital twin application, and realize the whole life cycle management of power battery pack, it provides the necessary intelligent service support for different battery requirements in electric vehicle field, and has good adaptability and data mobility (Fig. 15.5).

### ***15.2.1 Multi-Scale/Dimension Design of Battery Based on Digital Twin***

The wide and extensive application of lithium battery has stimulated the demand for high performance lithium battery with high energy/power density, cycle stability under thermal and mechanical abuse condition. The comprehensive understanding of the lithium batteries and rational multiscale design from application terminal

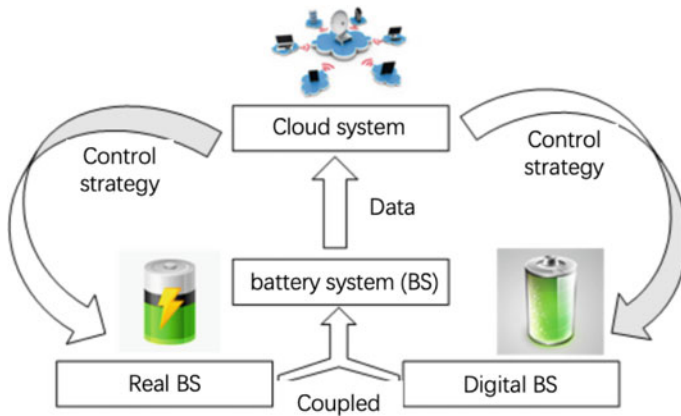


**Fig. 15.5** Digital twin battery system based on battery management

(e.g., EV, mobile electric devices) are required for the satisfaction of such increasing demand to intrinsic material properties. Figure 15.6 demonstrates the multi-scale processing and simulation from system design to material properties.

1. System control. The stable energy/power output, reliability and controllability of the lithium battery system under different abuse operating condition still remain challenging despite the great improvement for the past decades. The practical application of lithium batteries in various electrical power system not only reply on the realization of the single battery performance but also the battery monitoring and control. Thousands of lithium batteries (cell) make up the array of battery module (pack). The battery management system ensures the stable and reliable operation of the whole module. It is challenging but imperative to monitor the

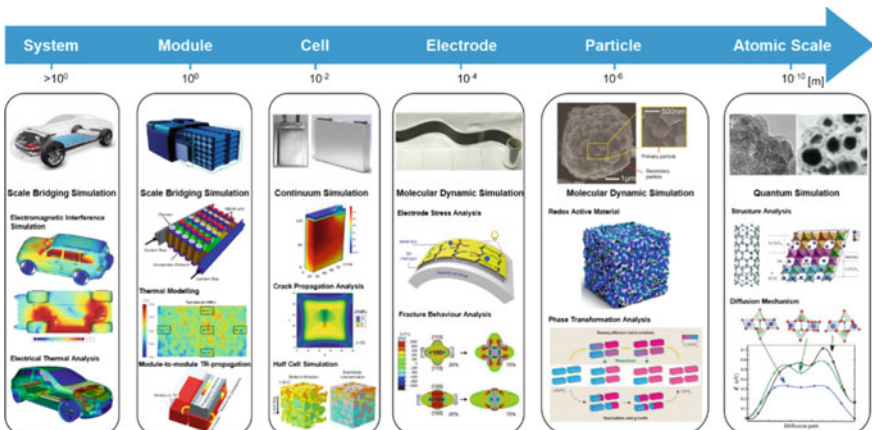


**Fig. 15.6** Multi-scale processing and simulation from system design to material properties

single cell state to prevent safety issues such as thermal runaway and predict the longevity of the whole system based on the single cell performance.

2. Electrode. Ideal electrodes provide sufficient ionic and electronic conducting path to ensure fast rate performance, robust mechanical stability to resist volume change. The rate performance is greatly influenced by the electrode microstructure and morphology, for example the aligned electrode structure with less tortuosity will contribute to the fast interfacial ionic diffusion, whereas sacrificing volumetric energy density. The chemical composition of the electrode is also important, such as highly conductive carbon to accelerate electron transfer, highly adhesive binder to provide mechanical support. To increase the mass energy density, the none-active material including current collector, binder, conductive carbon should be rationally reduced.
3. Particle scale. The physical/chemical properties (including morphology characteristics, specific surface, particle size, crystallinity, etc.) of the electrode particle have significant influence on reaction and charge transfer on the electrode surface, determining the cycling stability and rate performance. The surface impurities and the exposure of high valance state transition metal with high catalysis will aggravate the interfacial decomposition of electrolyte on the cathode surafce. The random crystallographic orientation of the primary cathode particles will lead to significant anisotropic volume change, resulting in potential crack formation and severe electrolyte decomposition, which will be mitigated in single-crystal cathode. Lithium de-solvation takes place on the electrode surface before the lithium ion could intercalate into electrode host, where the local solvation structure and interaction toward electrode surface can greatly influence the rate performance. While on the anode surface, the electrolyte will be reduced to form solid electrolyte interface (SEI) preventing the further electrolyte decomposition.
4. Atomic scale. Considerable efforts have been devoted to optimizing the electrochemical performance of the electrode material. The intrinsic crystal structure of the lithium ion host and the atomic local interaction determines the capacity of the cathode and anode materials. To increase the specific energy density, the equilibrium voltage of the lithium ion intercalation is expected to be increased as much as possible within the stable electrochemical window of the electrolyte. The increased lithium concentration within the lithium-host materials will trigger the structural evolution such as phase change leading to the evolution of equilibrium voltage which is called the voltage profiles. The typical characters of voltage profiles can help to analysis the structural evolution and also serve as data for battery diagnose. The elevated power density of lithium batteries relies on the ionic mobility within the electrode materials which is called the rate capability. The ionic mobility is determined by the energy barrier to insertion/extraction of the lithium ions into/from the lithium-host structure of the electrode materials. Better understanding of the ion migration pathway will help to enhance the power density performance. Safety and stable operating of the lithium ions under different current and temperature conditions has been greatly valued. The enhancement of cycle stability depends on the intrinsic thermal

stability of electrode materials, the structural tolerance for reversible lithium de/insertion, interfacial stability to resist electrolyte decomposition. Combination of atomic experimental characterization and computational investigation with high throughout and accuracy is essential to develop high performance energy material and discover the in-depth reaction mechanism.

To meet the ever-increasing energy density and safety demand of lithium batteries, the comprehensive and in-depth understanding from atomic physical/chemical properties, multi-scale characterization of reaction and degradation mechanism, to macro scale system designs should be integrated with experimental and computational exploration.

### ***15.2.2 Modeling of Battery System Based on Digital Twin***

Aiming at the performance and test object of battery system, dynamic system modeling is carried out, the battery is represented by the virtual-real symbiosis of physical system and virtual system, and the virtual-real symbiosis of virtual system has the following changes:

Visual Presentation: the state parameter is visualized by the state parameter data; In-situ characterization is the change from time measurement to in-situ characterization; Two-way Drive: from only measuring physical quantities to virtual-real symbiotic data two-way drive change; The adjustment mode changes from passive response to adaptive active control based on virtual-real interaction; The management mode changes from state detection to life-cycle state prediction based on virtual-real synchronous mapping.

Based on the new design, debugging and operation mode of the control system under the digital twin, it is necessary to make some breakthroughs in the following aspects (Wu et al. 2020):

1. The interface interaction needs to solve the problem of driving interaction and state feedback between the model and the control system so as to realize the seamless interaction between the digital twin and the control system
2. Based on the physical properties and dynamic characteristics, the control simulation realizes the behavior simulation of digital twin model driven by control data, which is the real description of physical equipment.
3. Autonomous decision-making is based on massive, timely and multi-dimensional data of digital twin model, which breaks through the local optimal restriction of traditional relying on common data training set, and solves the validity and accuracy of control self-decision-making from the data source.

### 15.2.2.1 Application Scenario Analysis: Intelligent Health Management Strategy

Intelligent Health Management based on digital twins has completely changed the “Black Box” state of power battery system operation under the traditional mode. It has realized the realistic perspective monitoring, the accurate fault warning based on multi-dimension feature and its fusion, the continuous iterative optimization of running state and the accurate verification of maintenance strategy, etc., it provides an effective way for the healthy management and reliable operation of power battery system (Schmuck et al. 2018; Cheng et al. 2017).

Power battery system entities and their virtual models run simultaneously, producing twin data that not only includes real-time sensing data such as temperature, voltage, and current, it also includes the simulation data of ohmic resistance, reaction polarization factor, solid–liquid diffusion factor, positive and negative active materials, and the fusion data obtained by multidimensional data processing and fusion. Driven by twin data and virtual model, intelligent health management application service for power battery system is implemented to ensure its healthy operation. Among them, the condition monitoring service enables the operation and maintenance personnel to observe the actual operation state of the power battery system through the high fidelity virtual model, through real-time comparison and interaction with the current desired state defined by the virtual model, the health state of the virtual model is evaluated from seven levels: excellent, good, qualified, warning and so on.

### 15.2.2.2 Application Scenario Analysis: Fault Diagnosis Services

The multi-dimensional features of power battery system, such as entity feature, virtual model feature and fusion feature, are taken into account in fault diagnosis service to accurately warn the high temperature, over-voltage and over-current hazards of power battery system.(Frank 1990; Hong et al. 2019) The optimal operation service makes use of the real-time interaction between the entities of the power battery system and its model to realize the iterative optimization of the cell, module, system and operation parameters, so as to keep the power battery system running under the optimal condition. Based on the high fidelity virtual model, the service process of fault diagnosis of power battery system is simulated, and the 3D operation instruction is formed to improve the accuracy of diagnosis.

### 15.2.2.3 Application Scenario Analysis: Thermal Runaway Warning

With the rapid development of electric vehicles, high-capacity, high-energy-density, fast-charging power batteries result in a wide range of temperature distribution. As a result, there are safety issues with batteries, such as life aging, accelerated degradation and stability deterioration due to increased heat generation rate. (Bernardi et al.

1984; Wang et al. 2018) In the current research results, there are three main types of methods for battery management system to realize fault alarm: threshold-based judgment method, physical model-based judgment method and data-driven model-based judgment method. The threshold-based judgment method mainly implements the judgment of undervoltage, overvoltage, and overheating phenomena and provides alarms. The physical model-based judgment method establishes a physical–chemical model to realize early warning based on the internal electrochemical mechanism of the battery. The data-driven model-based judgment method achieves early warning by processing a large amount of battery operating condition data through advanced deep learning neural network algorithms.

With the latest developments in cloud computing and the proliferation of big data, machine learning approaches have begun to provide valuable insights that can drive adaptive control of battery thermal management systems (BTMS) and improve performance. Smart battery management systems are a critical enabling factor for energy storage systems with high power output, higher safety and longer life.

Cloud-based BTMS provides multi-scale insights using network hierarchies and interactive network (CHAIN) frameworks that allow for more advanced and efficient algorithms to implement state estimation, thermal management, cell balancing, and other functions of traditional BTMS systems.

#### 15.2.2.4 Application Scenario Analysis: Reflection Between Macroscopic Parameters and Microscopic Mechanism

Multi-scale models can be developed that incorporate microscopic simulation data for effective ion diffusivity, electronic conductivity, and interfacial electrochemical kinetics, and the formation of solid electrolyte interface (SEI) into a macroscopic homogeneous model at the cell scale. Battery charging and rate performance, as functions of both applied current and cell temperature, could reflect the material chemistry, morphology, and constructed architecture. Material design and the manufacturing process can be optimized with the assistance of multi-scale characterizations to satisfy the performance requirements of EVs such as power output and endurance mileage. Figure 15.7 shows multi-scale battery processing of battery materials and systems. There is the angstrom structure at the nano to micro scale at the bottom, as well as thousands of cells in series and parallel at the macro scale.

CHAIN demonstrates a closed-loop approach to reveal the mapping between the microscopic mechanism of materials and macroscopic performance of battery systems, suggesting optimization of battery design and manufacturing in return for artificial intelligence technology and cloud computing.

The coupling relationships of multi-physical fields should be specifically revealed and taken into consideration during real-time modeling in order to obtain a precise picture for the mapping relationships between external operating conditions and internal mechanisms. However, there is a lack of refined and implementable models through which to understand the electrochemical reactions nondestructively. Multi-physical modeling lies not solely in LiBs but also in other energy-storage fields such

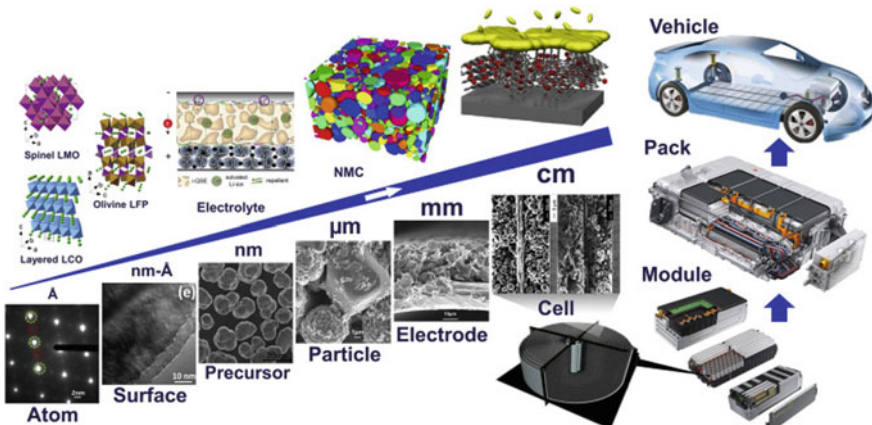


**Fig. 15.7** CHAIN: multi-scale processing from battery materials to system control

as fuel cells and solar power, requiring a similar CHAIN solution for full-lifespan management.

The perception of nano- and micro-materials and macroperformance requires sensors with high sampling accuracy and refined models to generate multi-dimensional, multi-state, and multi-factor hierarchical data, which is fundamental to evaluating the operating states of battery systems nondestructively, as well in diagnosing certain cell flaws that could possibly arise from assembly. There is also a lack of high-precision detection methods and tools for further research.

## References

- Alam K, Saddik A (2017) Digital twin architecture reference model for the cloud-based cyber-physical systems. *IEEE Access* 5:2050–2062
- Bernardi D, Pawlikowski E, Newman J (1984) General energy balance for battery systems. *Electrochim Soc Ext Abs* 84–2(1):164–165
- Cheng X-B, Zhang R, Zhao C-Z, Zhang Q (2017) Toward safe lithium metal anode in rechargeable batteries: a review. *Chem Rev* 117:10403–10473
- Frank PM (1990) Fault diagnosis in dynamic systems using analytical and knowledge-based redundancy: a survey and some new results. *Automatica* 26:459–474
- Hong J, Wang Z, Chen W, Wang L (2019) Multi-fault synergistic diagnosis of battery systems based on the modified multi-scale entropy. *Int J Energy Res* 43:8350–8369
- Rasheed A, San O, Kvamsdal T (2019) Digital twin: values, challenges and enablers, 1–31
- Schmuck R, Wagner R, Höpfl G et al (2018) Performance and cost of materials for lithium-based rechargeable automotive batteries. *Nat Energy* 3:267–278
- Tao F et al (2018) Digital twin-driven product design, manufacturing and service with big data. *Int J Adv Manuf Technol* 94:3563–3576

- Wang Y, Gao Q, Wang G, Lu P, Zhao M, Bao W (2018) A review on research status and key technologies of battery thermal management and its enhanced safety. *Int J Energy Res* 42:4008–4033. <https://doi.org/10.1002/er.4158>
- Wu B et al (2020) Battery digital twins: perspectives on the fusion of models, data and artificial intelligence for smart battery management systems. *Energy and AI* 1:100016

# Chapter 16

## Cloud Battery Management System



An intelligent battery management system is a crucial enabler for energy storage systems with high power output, increased safety and long lifetimes. With recent developments in cloud computing and the proliferation of big data, machine learning approaches have begun to deliver invaluable insights, which drives adaptive control of battery management systems (BMS) with improved performance. Yang's Group proposed a general framework utilizing an end-edge-cloud architecture for a cloud-based BMS, with the composition and function of each link described. Cloud-based BMS leverages from the Cyber Hierarchy and Interactional Network (CHAIN) framework to provide multi-scale insights, more advanced and efficient algorithms can be used to realize the state-of-X estimation, thermal management, cell balancing, fault diagnosis and other functions of traditional BMS system. (Yang et al. 2020, 2021).

### 16.1 Electric and Electronic Architecture

With the rapid development of electronic information technology and changing consumer trends, vehicles are becoming more and more complex. Throughout the history of the automobile, mechanical systems have been considered the primary cause of this complexity, however, the complexity of electrical and electronic components is progressively increasing. Automotive electrical and electronic architecture is a collection of electrical and electronic system principal design, central electrical box design, connector design, electrical and electronic distribution system design for the whole vehicle as a whole electrical and electronic solution. The automotive electrical and electronic architecture integrates sensors, ECUs, wiring harnesses, and electrical and electronic distribution systems to achieve the overall configuration and functionality of the vehicle (Fig. 16.1).

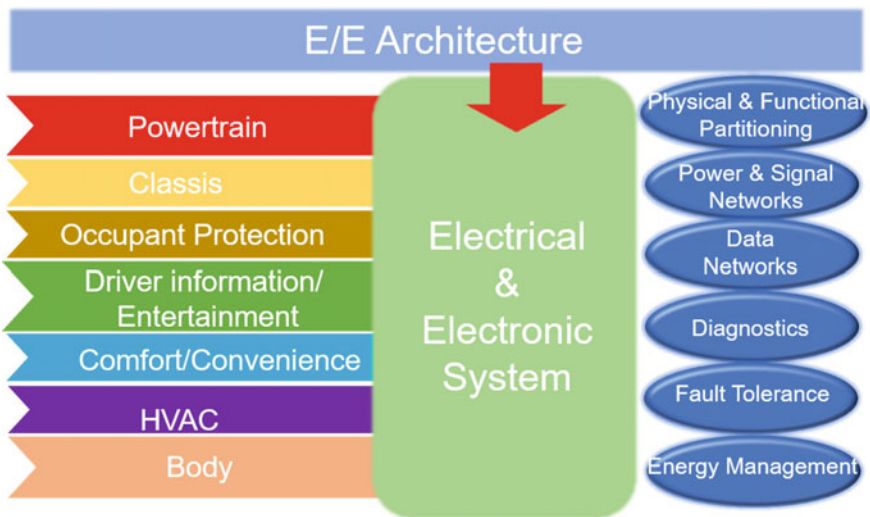


**Fig. 16.1** Framework of electric and electronic architecture

Most of the car companies are still in the stage of distributed architecture, and a small number of car companies appear the concept of sub-domains. The current control system of the whole vehicle is centered on the ECU, and each function corresponds to one or more ECUs, such as the heating unit ECU, multimedia system ECU, etc. With the increasing complexity of functions and the number of ECUs, some car companies have divided ECUs into domains according to body, chassis, power, infotainment, etc. on the other hand, they have realized cross-functional connections through central control gateways to enhance the collaboration of each component.

With the continuous development of cloud-based control technology, the following trends will emerge in the electrical architecture of automotive electronic. Upgrade of automotive electronic and electrical architectures from decentralized to more centralized multi-domain control; Software development and in-vehicle Ethernet are key factors in the transformation of EEA (Electrical/Electronic Architecture).

## 16.2 Cloud Platform and Service

Based on CHAIN framework, the cloud platform and service enable hierarchical cloudification of heterogeneous infrastructure, improving operational efficiency through unified management while reducing operating costs. The resulting benefits, including data-driven value, cloud-based performance improvement, and management optimization structure, are unreachable under the traditional management technology development models. At present, the BMSs mostly developed by different

battery manufacturers are basically separate, self-contained, and decentralized systems, resulting in inefficient utilization of the substantial data collected by a multiple sensor.

To address these issues thoroughly, the cloud battery management system provides a hierarchical comprehensive service that integrates infrastructure, software platforms, and applications (Fig. 16.2) based on CHAIN framework. By multiple sensors such as current–voltage sensors and thermocouples, multi-scale and multi-dimensional hierarchical data are regularly uploaded to the CHAIN platform via 5G and other communication technologies, hosted by three different entities: the data owner, the data user, and the cloud server. CHAIN consists of four layers of service architecture: Infrastructure as a Service (IaaS), Platform as a Service (PaaS), Software as a Service (SaaS) and Data as a Service (DaaS). IaaS provides services about computing, storage, security, and other fundamentals of infrastructure, allowing availability for the consumer to control the operating system. (Muzaffar et al. 2017) PaaS offers modular services such as big data analysis, Internet of Things platform, artificial intelligence platform driven by algorithms of a decision tree, logistic regression, reinforcement learning, and support vector machine, among others. In this context, Ethernet and IP-based routing enable the link between the vehicle electronics and superior control services. (Botta et al. 2016) SaaS can be accessed by potential users under permission at any time from anywhere with any device, establish multi-scale models (molecules, monomers, packs, and connected vehicles), and directly offer software application services to enterprise users. (Iranpour and Sharifian 2018) DaaS means that any service related to data could occur in a centralized location, such as aggregation, data quality management, data cleansing, etc., making the data available to different systems and users.

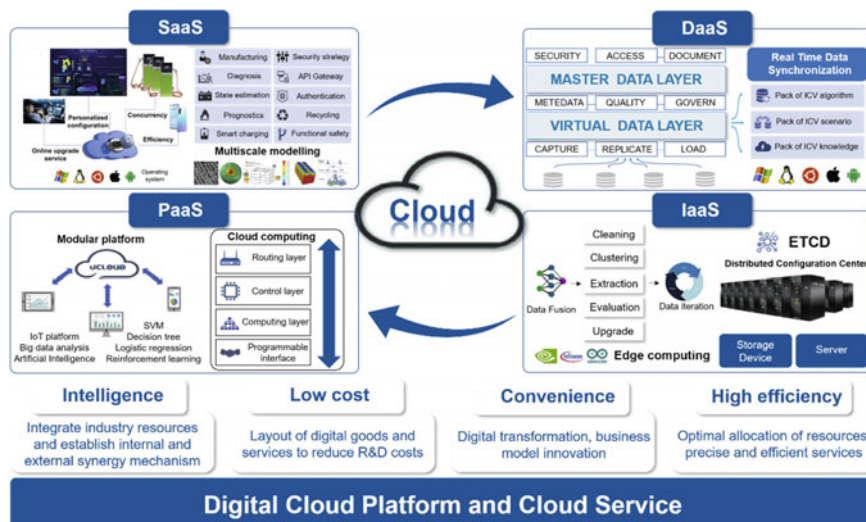


**Fig. 16.2** Framework of cloud platform and service

Basically, relevant operations should be subjected to the security authentication license before transmission to prevent security leakage. All levels of service will be equipped with a security authentication gateway and the corresponding security devices. Controlled access is ensured with authentication protocols and by providing granular level access, which in turns helps to share the required data precisely. Consequently, extracted hierarchy data have to be shared, stored, and accessed with the help of controlled secure keys. Through mutual authentication the transmission of data in the whole system is two-way: the upstream data from the sensors and historical database should be filtered step by step to obtain the specific format for the algorithm and model training, while the downstream data from the cloud platform contains optimized information about the configuration, function, application, parameters, and guiding the actual controls at the basic equipment end.

Voluminous variant data tend to be highly intricate on account of data provenance. In addition, the correlations between the vast volume of data are complex, which is the trigger for computational complexity of the cloud computing; therefore, research into data complexity and regularity, as well as the theoretical model of data distribution, are crucial for further application. As the core of CHAIN realization and the prerequisite for interactional cloud management, the intelligent processing of data involves many disciplines, such as probability theory, statistics, approximation theory, convex analysis, and algorithm complexity theory. For example, heuristic algorithms (Mohanty et al. 2017) provide better results in terms of makespan and average resource utilization; round robin algorithms and data preprocessing such as data fusion and iteration can be done in the data resource pool. Overall, cloud computing has many characteristics such as on-demand self-service, broad network access, resource pooling, elasticity, and measured service.

With the CHAIN framework, the cloud battery management system could approach that the state-of-the-art chemistries formatting brand new cells will be developed to achieve higher capacities than projected on today's material roadmaps. At pack level, the capacity fading pattern of different batteries can be driven by data analysis of CHAIN, which can also be applied for further evaluation of the behaviors and lifetime under various operating conditions. Additionally, the fast charging strategy can be iteratively optimized according to the full-lifespan degradation process and inconsistency of performance. Similarly, an active balancing strategy and thermal management of battery modules or cells can be adjusted, effectively improving the performance of the system.

In terms of vehicles, functional safety is akin to the immune system of the human body with respect to the detection of potential danger, whereby protection or error correction is essential in providing mitigation measures. In short, the ultimate goal of functional safety is to ensure battery system safety with the implementation of cloud battery management system, whereby threats, vulnerabilities, and risks in information security in automobiles are predictable in advance.

## 16.3 Cloud Battery Management System Framework

With the advent of cloud computing, access to more computationally intensive software and data storage/access can be achieved anywhere with an internet connection. This allows for devices to deliver functionality that would normally only be possible with high end hardware and also the analysis of aggregated big data sets. (Li et al. 2020) This connection between the physical and virtual world is often enabled by framework consisting of end, edge and cloud elements, the application of digital twin technology can better monitor battery states and improve battery performances. (Tao and Qi 2019) When combining this digital twin and with deep learning approaches, complex detection, prediction and optimization functions can be achieved which is difficult with traditional BMSs. A cloud-to-things framework is shown in Fig. 16.3, and consists of four subsystems: end, edge, cloud and knowledge.

### 16.3.1 End Sensing

Data acquisition depends on the sensing hardware capabilities of local end. Typical data types collected from BMSs include: current, voltage, time, location, ambient temperature, cell temperature and communication address of cell or module. Key decisions include the sampling frequency, where a higher resolution allows for greater fidelity of the data but at the cost of large data sets which need to be transmitted,

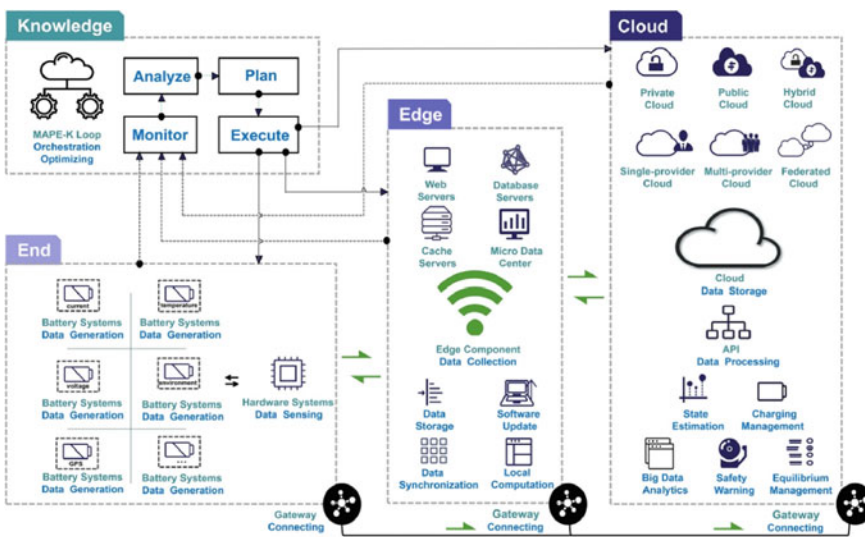


**Fig. 16.3** A cloud to things framework which consists of four subsystems: end, edge, cloud and knowledge

stored and processed. The specification of data resolution will also define the hardware elements to be implemented, many different micro-controllers exist, though the Raspberry Pi is one of the most widely used devices which can provide good computing, sensing and connectivity. This connectivity allows for system architectures such as mesh network clusters to be formed, in which nodes form connection with as many other nodes as possible in a dynamic and non-hierarchical form to efficiently transfer data. These can be centrally managed by a nominated controller or distributed to improve the overall performance. Mist computing, whereby processing of data occurs at the extreme edges of a network, can be implemented on a Raspberry Pi independently without communication with edge or cloud, which reduces communication requirements. Clearly, various IoT frameworks have been developed for other connected devices and the ideal structure of energy storage applications yet to be matured.

### ***16.3.2 Edge Computing***

In some cases, monitoring and estimation functions are time critical, such as monitoring overcharge and overdischarge of cells, and when compounded by bandwidth limitations, edge computing functionality is the most computationally efficiency structure to reduce cloud load. Edge computing embeds electronic devices which communicates and interacts with the battery systems that are monitored and controlled remotely. Here, this edge computing framework consisting of web servers, database servers, cache servers and micro data centers to ensure the reliability and fluency of the functions.

Having a stable network connection for data transmission is very important for effective real-time data transmission between the battery system and the digital twin. In order to improve the reliability of the whole system, the functions at each point in the operation process should be run locally. Then, data transmission, local update, data synchronization and local computing functions can be all realized in the edge computing.

To ensure higher accuracy, computationally intensive analysis requiring large amounts of data can be run in the cloud, with model parameters later being updated. This might include cloud-based training of neural network models from locally collected data, with weights and biases for these models being then loaded onto the edge computing nodes for state estimation which can be used to more effectively mitigate degradation. An example of this advanced functionality might be in the case of battery fast charging, where lithium plating is one of the key degradation modes. Various strategies exist for avoiding this plating, where the driving force is when the anode potential drops below 0 V vs Li/Li<sup>+</sup>. In commercial cells, it is generally not possible to measure the anode potential directly, however various authors have suggested state-estimation approaches to monitor the anode potential and regulate the current to avoid plating. However, these overpotentials change over the lifetime of operation and therefore, having a digital twin approach would allow for a more accurate representation of anode potential during lifetime use.

For data transmission, the cell data will be sent to the edge nodes through the end nodes using approaches such as on CAN (Controller Area Network) protocol. Processing of this data can then be done by using programs such as Python. The end component is also responsible for sending the generated data to the cloud with TCP/IP and Message Queuing Telemetry Transport (MQTT) protocols; ensuring its security and privacy.

### ***16.3.3 Cloud Computing***

Cloud computing is a type of distributed computing. It decomposes a large data processing program into numerous small programs. These small programs are processed and analysed through a system composed of multiple servers. The results will then be returned to the user. Due to the limited storage and computing capacity of edge devices, complex data processing is generally not possible. While, cloud computing with almost unlimited storage and processing capacity can realize the scalability and real-time data analysis of IoT devices. By coupling accurate algorithms, cloud connected BMSs can realize the functions such as state estimation, life prediction, adaptive control and safety early warning. It can also combine collected data and similar data sources with advanced deep learning algorithms to improve these functions. Cloud BMSs can set a variety of Application Programming Interface (APIs) to connect with Python, Structured Query Language (SQL), etc. to upgrade its functions. The data will be finally connected to the user interface for visualization and will be fed back to the server for remote disaster recovery, which can also further calculate the data.

Compared with end and edge computing, cloud computing provides more durable data storage and more powerful computing resources. However, each element is required in this framework. Here, the end device is needed to collect the battery temperature, voltage and other information in real time. This is sent to the permanent storage area in the cloud computing layer for evaluation and data mining. Moreover, latency is not a concern for cloud computing. In terms of persistent storage, cloud storage is preferred as it is usually cheaper and more reliable than edge and fog computing. Cloud computing itself can be divided into private, public, hybrid, single provider, multi-provider and joint cloud systems. Each cloud framework will have different performance metrics such as response time.

### ***16.3.4 Knowledge Repository***

For processing and actioning insights from the collected data, a control schema known as the monitor-analyze-plan-execute over shared knowledge (MAPE-K) loop is one of the most promising routes for automatic and self-adaptive control, which was introduced by IBM. This MAPE-K loop is an orchestration process nominating

almost all orchestration optimization techniques from the monitor to the executor. In this process, a monitor collects observed metrics ranging from application-level to system-level and hardware-level data in real time and updates the latest status of the whole system for the analysis phase. The analyser is responsible for data analysis with insights leveraged from the use of machine learning methods. The planner given the optimization technique, decides on the adaptation of the application and underlying resources. For example, the load balancer decides where to offload the incoming task, either to end or to edge cloud layers to balance the load. Finally, the executor is authorized to implement the decision which can handle such actions through a gateway. The knowledge repository consists of all the monitored data and activities of the loop components in MAPE-K to optimize overall performance.

## 16.4 Cloud Battery Management System Module and Function

### 16.4.1 Cloud Control Method

LIBs have been widely used in energy storage, electric vehicles, 3C devices and other related fields. However, one of the obstacles hindering the future development of battery technology is how to accurately evaluate the battery SOX (SOC, SOH and SOP), which affects the entire lifespan of battery usage (Fig. 16.4).

When the electric vehicle is running, the real-time vehicle will collect a large number of data, such as the voltage, current, temperature, system SOX cycle number

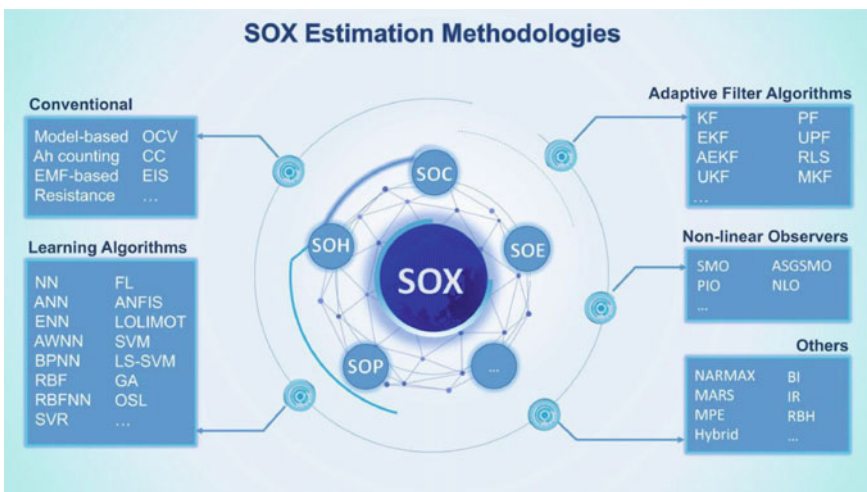


**Fig. 16.4** Categorization of SOX estimation methodologies

of the single battery, etc., as well as insulation, under-voltage, over-voltage, consistency and other fault information; as well as vehicle speed, acceleration, location and other driving data information. Besides, it's not enough to assess battery health comprehensively through the state of health alone, the brand-new health evaluation indicator-state of nonlinear aging (SoNA) could be utilized to explain the nonlinear aging phenomenon. The health evaluation indicator could be utilized to build a complete LIB full-lifespan grading evaluation system and integrates multi-scenario data collection, multi-dimensional data-based grading evaluation and cloud management functions. Cloud after massive data analysis, combined with thermal management model and cloud fine model, it can judge the health status and temperature distribution of the battery, and realize the real-time parameter identification of the vehicle model, so as to realize more accurate vehicle end control.

On the other hand, the cloud platform can also set BMS parameters which are more suitable for the real vehicle characteristics, and can set the operating parameters of the battery system such as SOP and charging mode more effectively, to improve battery system performance and life. At the same time, the cloud system can also provide information to the vehicle, for the driver to provide more energy-saving, safe driving.

#### ***16.4.2 Thermal Runaway Early Warning Method***

Safety is an important problem that restricts the scale application of electric vehicle, especially lithium-ion power battery. The safety performance of power battery is closely related to material system, cell design, thermal management, application conditions and so on.

In recent years, most of new energy vehicles have adopted high energy density power battery system. The reliability of power battery decreases under the conditions of charging, mechanical shock, flooding and so on. The main types of new energy vehicle fire accidents include: one is spontaneous combustion in normal driving; two is spontaneous combustion in collision; three is spontaneous combustion in static state; four is spontaneous combustion in charging; five is spontaneous combustion in water immersion (extreme environment), etc. The causes of vehicle fire accidents include system failure, single failure, electrical failure and ignition, etc.

System failures include the failure of contactors, BMS and other components, as well as thermal runaway of the power battery system caused by mechanical impact. The accidents of single cell fault are mainly caused by the bad consistency of single cell, leakage of liquid, short circuit and so on. The failure of electrical system is mainly caused by the bad contact of wire harness or plug-in, contact piece or terminal, which leads to short circuit, heat and fire. The external ignition accident is mainly caused by the external heat source of the whole vehicle.

With the rapid growth of new energy vehicles, the safety accident of power battery has become one of the key bottlenecks restricting the rapid development of new energy vehicles, and it also seriously threatens the personal safety of passengers. If

we can realize the remote safety warning of new energy vehicle based on cloud data set model, it will play a great role in improving the safety and reliability of new energy vehicle.

Based on the thermal management method of the power battery system controlled by the cloud, the full lifespan model of the power battery unit is established by the electrochemical-thermal-mechanical coupling method, which is used to simulate the evolution of the dynamic characteristics of the battery during the charging and discharging. The thermal cloud maps of the solid battery pack system are calculated in real time based on the online computing mode of the cloud analysis system, and then the temperature predictions are made. The thermal management control strategy is formulated, and fed back to both the physical and digital systems. Then the thermal management control strategy is optimized on-line according to the data transmitted by the battery system to realize the next time thermal management control strategy formulation.

The cloud security early warning model is a digital twin system based on the massive data sent by new energy vehicles to the cloud platform and coupled with the cloud refinement of battery units, modules and system models, the long-term and short-term safety risk level of the battery system is determined by analysing the working condition, status and consistency of the battery in the cloud in real-time.

#### ***16.4.3 Cloud Big Data Analysis***

Big data mining refers to the mining of huge potential information and knowledge from the large amount, multiple types, fast dynamic cycles and low value density of big data, and providing it to customers in form of services. In contrast to traditional data mining, it also aims to mine valuable information and knowledge. However, in the context of technological development, there are differences in the data environment faced by big data mining as well as in the breadth and depth of mining.

With the increasing demand for lean management of traditional lithium batteries, the traditional BMS is facing many challenges. The state of Li-ion battery is subject to multiple influences during the whole life cycle, and it is difficult to have one model to characterize all its changes. Big data-based cloud-end collaborative management strategy could monitor and manage batteries while uploading battery operation data to the cloud layer in real time. For non-smoothly changing, multidimensional massive battery data, the nearly unlimited storage capacity and computing power of cloud-based servers are utilized. The big data analysis model is built based on machine learning method, continuously iterating to match the latest state of the battery management parameters and wirelessly delivering, thus realizing more powerful cloud-based collaborative management, whole life cycle management and personalized management of lithium batteries.

Cloud-end state collaborate estimation: Realize high noise immunity, low error, high robustness and fast convergence of battery state of charge (SOC), state of energy

(SOE), state of power (SOP), state of health (SOH), remaining usable life (RUL) and other battery state collaborate estimation in the cloud layer to improve battery application experience and extend battery life.

Cloud-based full time equalization: To address the overall performance degradation and health deterioration caused by the inconsistency of large-capacity battery packs, the charging curves of each single cell are fitted based on massive data in the cloud, and then the capacity differences between the single cells are calculated and the equalization time is estimated accurately. The control command is sent to the terminal module for equalization through the server, which improves the efficiency by more than 80% compared with the traditional BMS equalization.

Active safety management in the cloud. Based on path planning, ambient temperature, real-time road conditions and other multi-source information, the battery charging and discharging power management strategy and thermal management (heating or cooling) strategy are adjusted in real time at the edge side of the cloud platform to ensure safe and reliable operation of the power battery system. Based on the cloud data, the battery input and output characteristics and the evolution trajectory of battery performance under different working conditions are tracked to establish a battery whole life cycle fault diagnosis mechanism. The cloud platform is utilized to assist in high-voltage circuit contact resistance trend judgment and battery system thermal field change analysis is executed to provide timely warning and intervention for battery subhealthy state.

#### ***16.4.4 Full Life Cycle Management***

The power battery system equalization management system based on cloud control is a digital battery system model which is matched with the solid battery system in the cloud and coupled into a digital twin system, by analyzing the inconsistency of battery capacity and its future development trend in the cloud, a reasonable control strategy is formulated and transmitted to the BMS in the BMS for controlling the BMS, in order to achieve the management of battery charge inconsistency and control the future direction of the development of inconsistency.

At present, solid battery system can be divided into cell-cell equalization system, module-module equalization system and system-system equalization system according to the energy flow direction of equalization system. Cell-cell equalization system refers to the equalization operation between individual batteries in the same battery module. The function of this part includes voltage monitoring, temperature monitoring, electric quantity monitoring and fault monitoring. After receiving the equalization control strategy, the unit-unit equalization system can balance the battery, the equalization current and the equalization time according to the strategy. Module-module equalization system refers to different modules in the same battery to achieve balanced operation. According to the balance strategy of the cloud analysis system, the unit in the module is balanced at the same time so that the balance process between module and module can be realized. System-system equalization

system refers to the balanced operation between battery module and battery pack. According to the selected balance strategy, the energy transmission process between the battery and the battery is controlled to realize the balance function.

The simulation-based digital battery system is to establish the virtual simulation model of the battery system according to the macroscopic or microscopic mathematical and physical laws. The model includes geometric model, macroscopic physical law, microscopic physical law, dynamic response, historical data and so on. The geometric model means that the geometry of the digital battery system in the 3D and the connection and fastening are identical to the solid battery system; The macroscopic physical laws include but are not limited to the fluid mechanics method, heat transfer method, electrochemistry principle, circuit principle, etc. The microscopic physical laws include but are not limited to the Molecular dynamics, etc. Dynamic response refers to the dynamic response of the digital battery system to the mechanical state (such as stress), thermal state (heat generation power and heat transfer of the battery), electric state (polarization characteristics of the battery, charge-discharge characteristics, etc. Historical data refers to the digital battery system inherits all the historical data of the entity battery system, and realizes data mining based on the data.

There is a rolling optimization process between the solid battery system and the digital battery system, that is, the current inconsistency of the solid battery system and the future inconsistency of the digital battery system are analyzed by the computation of the cloud analysis system, thus, the equalization control strategy is formulated according to the current inconsistency and the future inconsistency, and it is sent to the BMS system in the battery system by signal transmission to update the system control strategy, the BMS is based on the updated equalization control strategy to achieve the equalization control of the real battery system, in order to reduce the inconsistency of the current battery system and the disturbance of the inconsistency of the future battery system, at the same time, the digital battery system also depends on the system control strategy provided by the cloud analysis system for system state evolution, which is used for the next time system inconsistency prediction process.

## 16.5 Future Task and Perspective

BMS mainly performs the work of monitoring, management, protection and communication, among which monitoring requires the collection of voltage, temperature and other data with the help of wires, and also requires modules to complete the aggregation of data and communication. Therefore, the BMS must have a local physical counterpart. Cloud BMS should be considered whether the calculation is put into the cloud, that is, the numerical calculation (SOC, SOH), the management calculation (equilibrium, thermal management) with the help of cloud computing power.

For new energy vehicles and intelligent vehicles, based on historical operating conditions and real-time data collected in the past, the cloud-based big data platform analyzes, diagnoses and warns of battery failures, realizes 7 \* 24 h online tracking,

and pushes safety warnings through the APP for possible abnormalities in the battery system to achieve 2 h advance prediction of key failures such as smoke, fire and explosion. With the increase in vehicle access and use of time growth, cloud BMS failure prediction and life prediction model can also continue to optimize the model parameters to improve the prediction accuracy.

V2G describes the two-way interaction between electric vehicles and the grid. When the on-board battery needs to be charged, the current flows from the grid to the vehicle; when the EV is not in use, the on-board battery delivers the remaining controllable power back to the grid system. With the maturity of the technology of smart grid and active distribution network and the perfection of power market mechanism, intelligent two-way charging and discharging is expected to be realized. Big Data technology covers the whole data life cycle management process from information generation, collection, storage, transformation, integration, mining, analysis, calculation, presentation, application and maintenance. Based on historical and real-time data from traffic and charging stations, the cloud BMS analyzes users' travel and charging demand, and on this basis, it performs charging load prediction, V2G potential assessment, station-level and regional-level energy management strategy formulation, etc. By mining the vehicle's driving conditions characteristics, the entire vehicle power and economy changes are predicted combined with the vehicle's driving history data. Design algorithms or parameters to regulate cooling strategy, energy recovery strategy, and discharge strategy to extend the range of a single charge and life cycle, so that the potential of V2G is exploited to realize energy interconnection and new business development.

## References

- Botta A, De Donato W, Persico V, Pescape A (2016) Integration of cloud computing and internet of things: a survey. *Futur Gener Comput Syst* 56:684–700
- Iranpour E, Sharifian S (2018) A distributed load balancing and admission control algorithm based on fuzzy type-2 and game theory for large-scale SaaS cloud architectures. *Futur Gener Comput Syst* 86:81–98
- Li W, Rentemeister M, Badeda J, Jöst D, Schulte D, Sauer DU (2020) Digital twin for battery systems: cloud battery management system with online state-of-charge and state-of-health estimation. *J Energy Storage* 30:10155, ISSN 2352-152X, <https://doi.org/10.1016/j.est.2020.101557>
- Mohanty S, Patra PK, Mohapatra S, Ray M (2017) MPSO: a novel meta-heuristic for load balancing in cloud computing. *Int J Appl Evol Comput* 8. <https://doi.org/10.4018/ijaec.2017010101>
- Muzaffar AW, Mir SR, Anwar MW, Ashraf A (2017) Application of model driven engineering in cloud computing—a systematic literature review. *ACM Int Conf Proc Ser* 7–12
- Tao F, Qi Q (2019) Make more digital twins. *Nature* 573(7775):490–491
- Yang S et al (2020) CHAIN: cyber hierarchy and interactional network enabling digital solution for battery full-lifespan management. *Matter* 3:27–41
- Yang S et al (2021) Implementation for a cloud battery management system based on the CHAIN framework. *Energy and AI* 5:100088